Andreas Sæter Bøe

Experimental investigations on fire
performance of the engineered wood
products cross-laminated timber and
I-joists

Doctoral thesis

NTNU
Norwegian University of
Science and Technology

Andreas Sæter Bøe

Experimental investigations on fire performance of the engineered wood products cross-laminated timber and I-joists

Thesis for the Degree of Philosophiae Doctor

Trondheim, April 2024

Norwegian University of Science and Technology
Faculty of Engineering
Department of Civil and Environmental Engineering

NTNU
Norwegian University of
Science and Technology

Abstract

The building industry has, in recent years, more frequently used different engineered wood products, like cross-laminated timber (CLT), glue-laminated timber and I-joists. The increased popularity is due to the many advantages of building with wood, like the possibility of prefabrication, the low carbon dioxide footprint, the easy handling and mounting of wood, and the aesthetic look.

Conversely, when building with wood, additional combustible mass is introduced into the buildings. Given that these wooden products are exposed (i.e., visually present), they would produce pyrolysis gases when subjected to a fire and thus have an impact on the fire dynamics.

For over a decade, different research groups have conducted compartment fire experiments with exposed CLT. Most of those experiments have been conducted in relatively small compartments with small ventilation openings. Thus, the role of the exposed CLT is better understood in small compartments than in large. Small compartments with exposed CLT could be relevant for certain buildings. However, CLT is used in a variety of different rooms, including open-plan offices, lobbies, canteens, dwellings, kindergartens, schools, etc. In other words, the great variation in the use of CLT, including room size, geometry, and orientation, challenges the current understanding of how exposed CLT affects a fire.

The main focus of this thesis has been to increase the knowledge of the fire behaviour in large compartments with exposed CLT. The methodology consisted of conducting two large-scale (95 m^2) compartment fire experiments. In the first experiment, named #FRIC-01, the ceiling was exposed, while in the second experiment, #FRIC-02, both the wall and the ceiling were exposed. The compartment had four open window openings along one wall, which caused a well-ventilated compartment. The fuel load density was representative of an office building (352 MJ/m^2) and was represented by a continuous wood crib on the floor. These experiments aimed to better understand how two different configurations of CLT affect the fire dynamics, including fire spread inside the compartment, external flames, charring rate of CLT, decay phase, self-extinguishment of flames and delamination.

In both experiments, the ignition of the CLT ceiling triggered a clear change in the fire dynamics, in which flames spread under the ceiling and caused a strong radiative heat flux to the wall and the wood crib. The increased radiative heat flux effectively preheated the wood crib (and the wall in #FRIC-02) and led to a significantly faster spread across the wood crib than before the CLT was ignited.

In #FRIC-01, a new behaviour was observed, in which the flames in both the ceiling and of the wood crib travelled back and forth three times. As such cycles have not been reported earlier, we have named them *flashing waves*. Three such waves were observed before the fire was fully developed in the fourth wave. Despite retraction of the flames, the wood crib fire grew larger after each wave, contributing to a significantly faster fire spread rate than before the CLT ceiling ignited. In total, it took 13 minutes from ignition of the ceiling until the fire was fully developed. After a few minutes of intense burning, the flames in the ceiling started to extinguish, and over a period of 11 minutes, all flames in the ceiling were extinguished.

This occurred while the wood crib was still burning. No reignition was observed within a total duration of four hours.

In #FRIC-02, the contribution of having CLT exposed in both a wall and the ceiling was clearly seen. From ignition of the CLT ceiling, it took only 91 seconds before the entire compartment was burning. The fire spread was dominated by the rapid flame spread under the ceiling and upper part of the wall first. This caused a strong radiative heat flux to the wood crib and the other parts of the wall. The fire spread rate after ignition of the ceiling was 15 m/min across the ceiling and 11.7 m/min across the wood crib, corresponding to a fire growth rate faster than the ultrafast fire growth rate defined by Eurocode 1 (EN 1991-1-2).

During the most intense burning phase, large external flames emerged mainly out of one window. For some period, the flames covered almost the entire window opening, reached above the facade wall (5.2 m), and extended about 3 m horizontally from the window. The flames effectively reduced the inflow of air through that window, resulting in more air being supplied through the other windows. This imbalance in air supply contributed to large temperature variations throughout the compartment. These non-symmetrical external flames are believed to be mainly due to the wind coming diagonally from behind the corner of the compartment, but also due to the very rapid fire spread. The characteristic behaviour of the external flames was successfully reproduced in a CFD simulation when similar wind conditions as in the experiment were considered. This strengthens the hypothesis that the non-symmetrical external flames were influenced by the wind conditions.

After 10 minutes of intense burning, the gas temperatures started decaying, and also with this CLT configuration (wall and ceiling exposed), the flames of the CLT self-extinguished. About 50 minutes after the start of the decay phase, multiple small flames appeared at the surface of both the CLT wall and ceiling. Within 10 minutes, all combustible surfaces were burning again, corresponding to a second flashover. The temperatures were, for a short period, almost as high as after the first flashover. After that, the fire intensity varied strongly over the next 100 minutes but continued to burn until it was manually extinguished after almost 3 hours. This ongoing fire can be explained by the build-up of the CLT with thick (40 mm) outer layers and thin (20 mm) intermediate layers and the use of a regular PUR adhesive known to cause delamination.

A side topic of this thesis has been to study the charring of I-joists in light timber framed assemblies with combustible insulation. In recent years, there has been increased interest in combining I-joists with new combustible insulation products, like wood fibre and cellulose insulation. However, as there is no available design model for calculating the load-bearing capacity of this combination when exposed to a fire, the outspread of this combination has been limited.

This part of the research was aimed at producing experimental data to better understand the charring of I-joists and the recession rate of combustible insulation when these products are combined. This data could later be used to develop or validate design parameters for combustible insulation.

Through five experiments, a combination of I-joists with different flange sizes and different combustible insulation types (wood fibre, cellulose and phenolic foam) were exposed to the

standard fire curve (ISO 834) in a medium-scale furnace. Thermocouples were embedded into and outside of the flanges and used to determine the charring rate of the I-joist and the recession rate for the insulation. After exposure, the final char depth and the remaining cross-section were measured.

The charring rates were compared against calculated values based on the design model for rectangular cross-sections in the current Eurocode 5 (EN 1995-1-2) and the new model for I-joists in the draft of the new Eurocode 5 (prEN 1995-1-2).

Compared to those models, the charring rates were mainly on the conservative side. The charring rates decreased with increasing flange size and were comparable for the flanges of solid wood and laminated veneer lumber (LVL).

Overall, the combustible insulation protected the I-joists well, and the recession rates were lower than values reported for glass wool insulation. The lowest values were obtained by cellulose- and wood fibre insulation. Due to few repetitions, the results must be considered as indicative. Still, the results strongly indicate that biobased, and thus more sustainable, insulation types deserve a great market share in the future.

Altogether, the experimental work in this thesis has contributed to improved knowledge of both CLT and I-joists and could be considered a small but important step towards a more sustainable and fire-safe building sector.

Sammendrag

I løpet av de siste årene har byggeindustrien i større og større grad tatt i bruk moderne treprodukter, deriblant massivtre, også kjent som krysslaminerte treelementer (KLT), limtrebjelker og I-bjelker. Årsaken til den økende populariteten er blant annet muligheten til å prefabrikere elementer, materialenes evne til å binde opp CO_2, at de er enkle å jobbe med, og ikke minst at eksponert tre gir et pent estetisk uttrykk.

På den annen side, når man bygger med tre tilfører man en ekstra mengde brennbart materiale inn i bygget. Dersom trematerialene som benyttes er eksponert, det vil si er synlige, vil de produsere brennbare gasser hvis de utsettes for en brann, som vil gi en påvirkning av branndynamikken.

I mer enn et tiår har ulike forskningsgrupper gjennomført brannforsøk for å forstå hvordan eksponert KLT påvirker en brann. Hovedandelen av de gjennomførte eksperimentene har vært utført i nokså små rom med små ventilasjonsåpninger, og kunnskapen om hvordan KLT bidrar til brannutvikling er derfor bedre i små rom enn store. Små rom med eksponert KLT vil være relevant for enkelte typer bygg, men i dag benyttes KLT i en rekke andre romkonfigurasjoner, som kontorbygg, oppholdsrom, kantiner, leiligheter, skoler og barnehager m.m. Med andre ord benyttes nå KLT for bruksområder, inkludert romstørrelse, geometri og konfigurasjon, som strekker seg langt forbi forståelsen vi har om hvordan eksponert KLT påvirker en brann.

Hovedfokuset i denne doktoravhandlingen har vært å øke kunnskapsgrunnlaget om hvordan en brann utvikler seg i store rom med eksponert KLT. Metoden for å innhente ny informasjon har vært ved å gjennomføre to storskala (95 m^2) brannforsøk. I det første forsøket, kalt #FRIC-01, bestod taket av eksponert KLT, mens i det andre forsøket, #FRIC-02, bestod både taket og en vegg av eksponert KLT. Testrommet hadde fire store åpne vinduer langs en vegg, som bidro til at rommet var godt ventilert. Den spesifikke brannenergien tilsvarte et kontorbygg (352 MJ/m^2) og ble representert av en lang kontinuerlig trekrybbe plassert på gulvet. Målet med forsøkene var å bedre forstå hvordan to ulike konfigurasjoner med KLT påvirker branndynamikken, deriblant intern brannspredning, eksterne flammer, forkullingshastigheten til KLT, nedkjølingsfase, selvslokking av flammer og delaminering.

I begge forsøkene førte antennelse av taket til en tydelig endring i branndynamikken, der flammer spredte seg under taket og førte til en kraftig varmestråling mot veggen og trekrybben. Den økte varmestrålingen bidro til en effektiv forvarming av trekrybben (og veggen i #FRIC-02), og førte til en vesentlig raskere brannspredning langs trekrybben i forhold til før taket antente.

I #FRIC-01, ble det observert en brannspredningsmekanisme som ikke tidligere har blitt beskrevet. Etter antennelse av taket spredte brannen seg raskt, men trakk seg etter kort tid tilbake. Ettersom dette fenomenet ikke har blitt rapportert tidligere, har vi valgt å kalle disse syklusene: *flashing waves*. Brannen gjennomgikk tre slike bølger før brannen i den fjerde bølgen spredte seg til den andre enden og ble værende. Til tross for at brannen trakk seg tilbake i hver bølge, ble brannen i trekrybben kraftigere etter hver bølge noe som bidro til en betydelig raskere brannutvikling enn før taket antente. Totalt tok det 13 minutter fra antennelse av KLT i taket til brannen var fullt utviklet i hele rommet. Etter et par minutter

med intens brann begynte flammene i taket å slokne, og var fullstendig sloknet i løpet av 11 minutter. Dette skjedde mens trekrybben fortsatt brant. Etter hvert brant trekrybben opp, og ingen reantennelse ble observert i løpet av en total testtid på fire timer.

I #FRIC-02 ble effekten av å ha både taket og en vegg eksponert tydelig. Fra taket ble antent, tok det kun 91 sekunder før hele rommet var overtent. Brannspredningen ble dominert av flammer som spredte seg under taket og langs øverste del av veggen. Disse flammene bidro med en kraftig varmestråling ned mot gulv og vegg, som bidro til at brannen også spredte seg langs trekrybben og nedre del av veggen. Etter antennelsen av taket spredte brannen seg under taket med en gjennomsnittlig hastighet på 15 m/min, mens spredningen langs trekrybben var 11.7 m/min. En slik brannutvikling tilsvarer en raskere utvikling enn den ultraraske brannutviklingskurven definert i Eurokode 1 (EN 1991-1-2).

I den mest intense fasen av brannen oppstod det store ekstern flammer, primært ut av ett vindu. For en kort periode dekket flammene nesten hele vindusåpningen, strakk seg omtrent 3 m horisontalt ut fra vinduet og nådde høyere enn fasadeveggen på 5.2 m. De store flammene bidro til å blokkere tilførselen av luft gjennom det vinduet, og luft ble istedenfor tilført gjennom de andre vinduene. Denne ubalansen i lufttilførsel bidro til store temperaturforskjeller i rommet. Årsaken til de store flammene primært ut gjennom et vindu var sannsynligvis knyttet til vindforholdene, der vinden kom skrått bakfra i forhold til testrommet, men også på grunn av den veldig raske brannspredningen. En FDS-simulering av brannen klarte å gjenskape disse forholdene når liknende vindforhold som på testdagen ble lagt til i simuleringen. Dette bidrar til å styrke hypotesen.

Etter omtrent 10 minutter med intens brannen begynte temperaturene å avta, og også med denne KLT-konfigurasjonen (eksponert vegg og tak) sloknet flammene på vegg og tak av seg selv. 50 minutter etter at nedkjølingsfasen hadde startet, oppstod det plutselig nye flammer på både vegg og tak, og i løpet av 10 minutter var rommet fullstendig overtent igjen, et fenomen kjent som sekundær overtenning. Temperaturene var for en kort periode nesten like høye som under den første overtenningen. Deretter varierte brannens intensitet kraftig over de neste 100 minuttene. Det brant fortsatt godt da brannen ble manuelt slokket etter nesten tre timer. Den vedvarende brannen kan forklares ved oppbyggingen av KLT elementene, der de ytre lagene var tykke (40 mm), mellomlagene var tynne (20 mm), og det ble benyttet en ordinær limtype (PUR) som er kjent for å gi delaminering.

Et sidetema i denne doktoravhandlingen har vært å studere hvordan I-bjelker forkuller når de blir beskyttet med brennbar isolasjon. I senere tid har det vært økt interesse for å kombinere I-bjelker med nye typer av brennbar isolasjon, deriblant trefiber og celluloseisolasjon. Utbredelsen av denne kombinasjonen er likevel svært begrenset ettersom det ikke finnes noen designmodell for å beregne gjenværende bærekapasitet for en I-bjelke beskyttet med brennbar isolasjon som utsettes for en brann.

Målet med denne delen av avhandlingen, har vært å fremskaffe eksperimentelle data for å bedre forstå hvordan en I-bjelke forkuller og hvordan brennbare isolasjonstyper forbrenner, når disse produktene er kombinert. Disse dataene kan senere benyttes til å utvikle eller validere designparametere for brennbar isolasjon.

Gjennom fem forsøk ble I-bjelker med ulike flensstørrelser kombinert med ulike typer av brennbar isolasjon (trefiber, cellulose og fenolskum) eksponert for en standard brannkurve (ISO 834) i en mellomstor ovn. Termoelementer ble installert inni og utenpå flensene for å bestemme forkullingshastigheten til I-bjelken og forbrenningshastigheten til isolasjonen. Etter forsøkene ble det gjort målinger av gjenværende tverrsnitt.

Forkullingshastighetene ble så sammenlignet mot verdier beregnet fra den eksisterende designmodellen for rektangulære tverrsnitt i Eurokode 5 (EN 1995-1-2), og mot den foreslåtte nye modellen for I-bjelker i den kommende utgaven av Eurokode 5 (prEN 1995-1-2).

Sammenlignet med disse modellene var forkullingsverdiene hovedsakelig på konservativ side. Forkullingshastigheten ble redusert med økende størrelse på flensen og det var liten forskjell om flensen var laget av heltre eller LVL (laminated veneer lumber).

Generelt ble I-bjelkene godt beskyttet av brennbar isolasjon, og forbrenningshastighetene til isolasjonen var lavere enn verdier oppgitt for glassull. De laveste verdiene ble målt for trefiber og celluloseisolasjon. På grunn av få repetisjoner, bør resultatene anses som indikative. Likevel indikerer resultatene tydelig at biobaserte, og dermed mer miljøvennlige, isolasjonsprodukter fortjener en større markedsandel i fremtiden.

Overordnet har det eksperimentelle arbeidet i denne avhandlingen bidratt med økt kunnskap om både massivtre og I-bjelker, og kan betraktes som et lite, men viktig steg videre mot en mer bærekraftig og brannsikker bygningssektor.

Preface

The subsequently presented doctoral thesis was conducted at the Norwegian University of Science and Technology (NTNU), Department of Civil and Environmental Engineering (IBM) under the supervision of Professor Anne Steen-Hansen, Senior Research Scientist Kathinka Leikanger Friquin at SINTEF Community and Professor Ivar S. Ertesvåg at Department of Process Engineering (EPT). The experiments were conducted at RISE Fire Research in Norway as part of the Fire Research and Innovation Centre (FRIC). FRIC was established in spring 2019. The aim of the centre is to increase the knowledge within fire safety to make optimal decisions and develop better solutions that provide increased fire safety in buildings. FRIC is led by RISE Fire Research in Trondheim, with NTNU and SINTEF as research partners. FRIC has partners from public organisations, fire safety consultants, producers and suppliers of building products and building installations, and property development and management. The research centre is funded by all partners, in addition to funding from the Research Council of Norway, program BRANNSIKKERHET, project number 294649. Read more at www.fric.no.

From the beginning of my PhD, I was determined that challenges related to cross-laminated timber (CLT) and fire safety should be my main area of interest. This is a topic that has caught my interest since 2015 when I witnessed a full-scale CLT compartment experiment of a student dwelling, where I observed that having exposed combustible surfaces truly changes the fire dynamics of a compartment fire.

My thesis is also an example, among others, that the intended path of a PhD does not always follow the plan. Just a few months into my PhD, I was recommended to join a research project studying I-joists and combustible insulation. Despite having chosen CLT as my main topic, this was considered a valuable opportunity as I could gain experience on a somewhat related topic and assist in doing the experiments, analysing the data and being a co-author of the paper. However, due to unforeseen events, the foreign researchers were hindered from conducting the experiments. I then ended up leading the project and carrying out the experiments. As I also took several courses in this period, the time window to conduct the experiments was relatively narrow. I, therefore, had to rely on the experimental setup the other researchers had prepared. After conducting the experiments, I also ended up doing the post-measurements, the analysis and writing most of the paper. In total, this part ended up taking a lot more time than I had foreseen. Although it did not change the main focus of my PhD, it certainly cost me time that I could have spent on more advanced analysis of the CLT experiments. On the other side, these experiments gave me valuable insight into charring of wood, design models and proper techniques for measuring the charring rate by thermocouples, which was useful in the CLT experiments.

In my PhD, I have received valuable input and help of different kinds from many people. Although not all of those who have helped me are explicitly mentioned, I am grateful for each contribution. Still, a few people have played a larger role in assisting and guiding me and deserve to be mentioned.

First, I want to thank my supervisors: Anne, Kathinka and Ivar. You have always been available, shared your expertise and experience, and asked critical questions. Combined, you

"Something can only be 'sustainable' if you have addressed the hazards and don't flirt with a future ban."

Danny Hopkin

Contents

List of publications

Peer-reviewed journal publications

Andreas Sæter Bøe, Kathinka Leikanger Friquin, Daniel Brandon, Anne Steen-Hansen, Ivar S. Ertesvåg, *Fire spread in a large compartment with exposed cross-laminated timber and open ventilation conditions: #FRIC-01 – Exposed ceiling,* Fire Safety Journal, Volume 140, no. 103869, 2023, ISSN 0379-7112, DOI: https://doi.org/10.1016/j.firesaf.2023.103869

Andreas Sæter Bøe, Kathinka Leikanger Friquin, Daniel Brandon, Anne Steen-Hansen, Ivar S. Ertesvåg*, Fire spread in a large compartment with exposed cross-laminated timber and open ventilation conditions: #FRIC-02 – Exposed wall and ceiling,* Fire Safety Journal, Volume 141, no. 103986, 2023, ISSN 0379-7112, DOI: https://doi.org/10.1016/j.firesaf.2023.103986

Andreas Sæter Bøe, Katrin Nele Mäger, Kathinka Leikanger Friquin, Alar Just*, Experimental Study of the Charring of I-Joists and Recession of Combustible Insulation in Light Timber Frame Assemblies with Comparison to Eurocode 5*, Fire Technology, 2023, DOI: https://doi.org/10.1007/s10694-023-01464-x

Submitted manuscript

Lei Jiang, Andreas Sæter Bøe, Tian Li, *Numerical simulation of fire spread in large-scale open CLT compartment,* 2023.

Additional publications

Andreas Sæter Bøe, Kathinka L. Friquin, *Travelling fires in compartments with exposed cross-laminated timber surfaces*, World Conference on Timber Engineering 2023 (WCTE 2023), Oslo, Norway, 2023. (Conference proceedings / Oral presentation)

Andreas Sæter Bøe, Kathinka L. Friquin, *Travelling fires with exposed CLT surface. Planning of full-scale test*. Nordic Fire and Safety Days, Lund, Sweden, 2022. (Conference proceedings / Oral presentation)

Andreas Sæter Bøe, Katrin N. Mäger, *Charring of wooden I-joists in assemblies with combustible insulation*. Nordic Fire and Safety Days, electronic conference, 2021. (Oral presentation)

List of acronyms and abbreviations

CFD	Computational fluid dynamics
CLT	Cross-laminated timber
FDS	Fire Dynamics Simulator
FLD	Fuel load density
HHV	Higher heating value
HRR	Heat release rate
HRRPUA	Heat release rate per unit area
LVL	Laminated veneer lumber
LHV	Lower heating value
MLR	Mass loss rate
MUF	Melamine urea formaldehyde
PT	Plate thermometer
PUR	Polyurethane
TC	Thermocouple

List of symbols

σ	Stefan Boltzmann constant	[W/m^{2}K^4]
T_{PT}	Temperature measured by plate thermometer (PT)	[K]
T_g	Gas temperature	[K]
h_{PT}	Convective heat transfer coefficient for the PT	[W/m^{2}K]
ε	Emissivity	[-]
k_{PT}	Thermal conduction coefficient for the PT	[W/m^{2}K]
C_{PT}	Heat capacity of the PT	[J/m^{2}K]
$\dot{q}''_{inc}$	Incident radiative heat flux	[W/m^2]
$\dot{Q}$	Heat release rate	[W]
$\dot{m}$	Mass loss rate	[kg/s]
ΔH_C	Net heat of combustion	[MJ/kg]
χ	Combustion efficiency	[-]
H_v	Heat of evaporation	[MJ/kg]
m	Mass of moist wood	[kg]
m_0	Mass of dry wood	[kg]
w	Moisture content based on the dry value of wood	[-]
f	Moisture content based on the moist value of wood	[-]
A_V	Area of ventilation openings	[m^2]
H_V	Height of ventilation openings	[m]
A_T	Total area of enclosure surfaces, including the opening areas	[m^2]
ϕ	Porosity factor	[cm]
A_{CS}	Cross-sectional area of the vertical shafts in the crib	[cm^2]
A_S	Surface area of wood exposed to air	[cm^2]
s	Spacing between wood crib sticks	[cm]
b	Thickness of a single wood stick	[cm]

Part I – Thesis Background

1 Introduction

1.1 General background

The building and construction sector was in 2021 responsible for approx. 34% of energy use and 37% of energy and process-related CO_2 emissions, of which 9% of the emissions were related to manufacturing building materials and products like steel, glass and cement [1]. To reach the climate goals [2], emissions must be drastically reduced in the coming years. One approach to lower the emissions of the building sector is to replace energy-demanding materials like steel and concrete with a more sustainable alternative, namely wood. Wood has the ability to sequester carbon during the lifetime of the building and even longer if the wood can be reused. However, part of the gain could be zeroed out if the wood is transported long distances, for example, from Europe to the USA.

For centuries, wood has been used as a building material, but most houses have been restricted to just a few floors. This building height limitation has been due to restrictions in building regulations and practical challenges, such as the quality of wood beams [3]. However, in the last years, wood has had its renaissance, and several new products have entered the market, e.g., cross-laminated timber (CLT), glue-laminated timber, I-joists and several others classified as engineered wood products. The implementation of performance-based design in many countries has opened up for building high-rise wooden buildings. Examples of such high-rise buildings around the world are "Haut" (73 m) in the Netherlands [4], "Ascent" (87 m) in the USA [5] and "Mjøstårnet" (85 m) in Norway [6]. In addition, prescriptive solutions for low and mid-rise buildings have made wood a mainstream alternative to steel and concrete in some countries [7].

Furthermore, building with wood has lately become many architects' preferred choice, as such buildings are appealing and have an aesthetic look. From a construction point of view, CLT is popular as elements are prefabricated, making the construction process more effective. Moreover, CLT is easy to work with, and the working conditions are cleaner and less noisy than building with steel and concrete. At last, it has been found that people working or living in wooden buildings experience increased well-being and satisfaction, indicating that exposed wood may induce positive health effects [8, 9].

In general, when introducing new products or using existing products in a new way, there is a potential to introduce new fire risks or change the severity of existing risks. For a safe implementation of wood-based products into the market, fire safety engineers must know the limitations of such products and to what extent they differ from the products they replace. However, due to all the new areas where wood is used, the knowledge base is not entirely up to date to understand all the consequences wood may lead to regarding fire safety.

In this PhD, the focus has been to gain new experimental data on how two different wooden construction materials behave in fire. The main topic was how exposed CLT affects the fire dynamics of a large, well-ventilated compartment. A side-topic has been to study charring rates of I-joists and recession rates of different types of combustible insulation when these two products are combined.

1.2   CLT - background

Build-up and properties

CLT, or cross-laminated timber elements, are prefabricated engineered wood products used as load-bearing elements in walls and floors, see Fig. 1. A CLT element comprises an odd number of layers, typically 3, 5 or 7, where adjacent layers have a 90° orientation to each other and are held together by an adhesive. There are several different adhesive types, including phenol resorcinol formaldehyde (PRF), polyurethane (PUR), melamine urea formaldehyde (MUF), and emulsion polymer isocyanate (EPI). The choice of adhesive strongly depends on the wood species [10]. The two most common ones used for CLT are PUR and MUF [11].

Fig. 1 Building under construction where load bearing CLT elements are used in walls and floors. Openings for windows and doors have been cut out during production.

Due to the build-up, CLT elements have high strength and stiffness, which make them suitable for tall buildings which need more stabilising due to wind. Furthermore, the use of CLT has shown promising behaviour when exposed to earthquake loads [12].

Another favourable property is the light weight of CLT compared to steel and concrete. The lower weight will reduce costs related to the foundation work for certain buildings.

Ignition and self-extinction of CLT

When wood is heated, a pyrolysis process occurs, which decomposes the long polymer chains found in wood to inert and combustible gases, liquid tars and inorganic ash [13]. To burn, the long polymers must be decomposed into smaller units that can exist in the gas phase. To ignite the wood and cause a stable flame, a sufficient amount of combustible gases must be continuously provided to the surface of the wood. Piloted, i.e., assisted, ignition is known to occur around 10-13 kW/m^2, while non-piloted ignition requires exposure to an external heat flux of 25-33 kW/m^2 [13]. While burning, a thicker and thicker char layer forms on the burning surface. This layer acts as an insulating barrier between the fire and the unburned wood behind the char layer and consequently reduces the charring rate [14].

Self-extinction of CLT has been reported in several experiments with both regular PUR adhesives and heat-resistant ones [15-19]. Regarding self-extinction, there are two definitions. The first considers self-extinction as cessation of flames, while the second considers cessation of both flames and smouldering combustion. In most experiments, authors are referring to the first definition.

To sustain flaming combustion of the CLT after the char layer has formed, the CLT depends on an external heat flux, like heat from burning combustibles or a burning surface (e.g., CLT wall or ceiling). This threshold has been found to typically range between 30-45 kW/m^2 [20, 21], corresponding to a surface temperature of 600-700 °C. High heat flux levels could be maintained over a long period if several exposed surfaces are present and provide re-radiation between each other. Hence, the number and orientation of CLT surfaces are relevant to whether self-extinguishment of flaming combustion would occur or not [16-18, 22].

Despite most published papers only consider the self-extinguishment of flames, the occurrence of smouldering should not be neglected. In several experiments, it has been observed that smouldering may go on for hours after the visible flames have died out [23]. If no mitigation measures are undertaken, ongoing smouldering might cause a post-collapse of structural elements or transition back to flaming combustion [24-26]. The heat flux threshold for sustaining smouldering is suggested to be 5-6 kW/m^2 and an airflow over the surface of maximum 0.5 m/s [27].

Delamination and second flashover

For several years, it has been known that the adhesive loses its adhesive properties when heated, resulting in the outermost layer detaching from the layer behind [17, 22]. This phenomenon is known under several names, including delamination, glue-line integrity failure, and premature char-fall off. In this thesis, the term delamination is used to describe this phenomenon.

Delamination would cause fresh wood to be exposed to the fire and is typically recognised by a significant increase in gas temperatures and heat release rate and will often cause a prolonged fire duration [17]. This phenomenon is often called a second flashover.

To overcome this problem, extensive research has been conducted to develop adhesives with better heat-resistant properties [28]. In the American standard (ANSI/APA PRG320) [29], a

new method is designed for evaluating adhesives. To be classified as a heat-resistant adhesive, delamination cannot occur within a four-hour full-scale compartment fire test, and a bench-scale test must be passed.

Although glue products are now available with better heat-resistant properties, many producers of CLT still use adhesives known to lose their bonding strength at elevated temperatures and thus are likely to cause delamination [30]. This might seem counterintuitive when the consequence of using such adhesives is known. However, this production method is more cost-efficient than producing the elements with an improved adhesive.

With a non-heat-resistant adhesive, the key factor to avoid delamination is that the glue-line temperatures are kept below the critical level where the adhesive loses its stickability. Several factors affect whether this could happen, including the fuel load density and fire duration, layer thickness, ventilation conditions and orientation and number of exposed CLT surfaces.

External flaming

When building with wood, additional combustible mass is introduced into the buildings. Given that these wooden products are exposed (i.e., visually present) or become exposed during the fire, they will affect the fire dynamics as they release pyrolysis gases when heated. A known consequence of having exposed CLT is the presence of larger external flames [17, 31-33] due to production of combustible gases from the CLT. Nonetheless, the increase of the external flame with exposed CLT has been reported to be less for compartments with medium and large openings than previously observed in compartments with small openings [34]. Furthermore, a compartment with a high variable fuel load density seems to be less sensitive to the effect of exposed CLT, as the percentage increase of combustible gases from a CLT surface becomes lower than for a similar compartment with a lower fuel load density [35].

A large external flame could pose a significant threat to spreading the fire to the facade (if combustible), the floors above, or an adjacent building.

Travelling fires

Most of our understanding of compartment fires has originated from experiments with relatively small compartments with small openings. A fire in such a room is typically assumed to grow locally until a sufficient gas layer is created, which is hot enough to spontaneously ignite remaining combustibles. In large compartments, a fire would typically behave like a travelling fire with a distinct leading and trailing edge. In such a fire, the thermal field is divided into two regions: the near field and the far field. The near field is where the fire is physically present, while the far field is represented by locations remote from the flames that not yet have been ignited but are still subjected to increased temperatures and heat fluxes [36].

A travelling fire can be divided into three distinct modes of fire spread, given by the flame front (V_S) and burnout (V_{BO}) velocities [37]. Burnout is here considered as the extinction of visible flames.

- Mode 1 ($V_S/V_{BO} \rightarrow \infty$) – a very rapid spreading fire that may lead to a flashover.
- Mode 2 ($V_S/V_{BO} > 1$) – a growing fire.
- Mode 3 ($V_S/V_{BO} \approx 1$) – a steady moving fire.

The burnout velocity has a weak dependence on external radiation. In contrast, the flame front velocity is strongly influenced by the heat and radiation feedback from the smoke layer and the enclosure geometry [37].

For many years, travelling fire experiments were primarily conducted with non-combustible surfaces, like the TRAFIR experiments [38], the Edinburgh travelling fire experiments [39], X-ONE [40], X-TWO [41] and the Tisova fire experiment [42]. In most travelling fire experiments, Mode 2 and Mode 3 have been the dominant modes, and the transition to Mode 1 has occurred relatively late, 24 min, 45 min, and 237 min after ignition [43].

The influence of combustible linings on travelling fire experiments has just recently been put on the agenda. In the Malveira experiments with a size of 21 m x 4.7 m x 2.5 m [44], 60% of the ceiling consisted of a combustible cork layer. It took four hours for the fire to spread to this area. However, after reaching the cork layer, the fire spread across the rest of the room in minutes.

In a series of reduced-scale experiments with a size of 2.2 m x 0.8 m x 0.4 m, the effect of having a CLT ceiling was studied, and it was concluded that an exposed CLT ceiling would effectively increase the fire spread rate compared to a non-combustible ceiling [45].

The Code Red experiments [23, 46, 47] were the first to explore in large scale how an exposed CLT ceiling would influence the fire spread. The compartment was 34.3 m x 10.3 m x 3.1 m and had a floor area of 352 m^2. The ceiling was fully exposed in CodeRed #01 [23] and #02 [46], while Code Red #04 [47] had a partially exposed ceiling. CodeRed #03 [48] tested the effect of a water mist system with success. A continuous wood crib with a fuel load density of 374 MJ/m^2 per wood crib area represented the variable fuel load. This corresponds to a fuel load density of 169 MJ/m^2 per floor area and is lower than for most other experiments on travelling fires, which typically have been around 420 MJ/m^2, the suggested design value for offices in Eurocode 1 [49]. The opening factors were 0.071 m$^{1/2}$ and 0.039 m$^{1/2}$ for CodeRed #01 and #02, respectively. The opening factor (OF) is defined through Eq. (1):

$$OF = \frac{A_V \cdot H_V^{1/2}}{A_T} \qquad (1)$$

where A_V is the area of the ventilation openings, H_V is the height of the openings and A_T is the total area of the enclosure surfaces, including the opening areas [49].

The fire development of those experiments clearly showed that the presence of an exposed CLT ceiling significantly changes the fire spread and fire dynamics of a compartment fire. This was evident through the fast fire spread across the room, 5 and 8 minutes [46] in CodeRed #01 and 02, respectively, compared to 12 minutes in X-ONE [40] and 22 minutes in X-TWO [41], which were similar experiments concerning size, ventilation conditions and fuel

package but without the CLT ceiling. The fire spread rate after ignition of the ceiling was approx. 160 mm/s (9.0 m/min) for Code Red #01 and #02.

Results from another large-scale experiment performed in Canada have recently been published [50]. The compartment had an L-shaped geometry with a floor area of 204 m^2. The ceiling and 35% of the wall area were exposed. Ten openings were present along the L-shaped outer wall with an opening factor of 0.12 m$^{1/2}$. Where most travelling fire experiments have used a continuous wood crib to represent the moveable fuel load, this experiment instead used mock-up furniture, which better mimics an actual office. The FLD was 362 MJ/m^2 per floor area. Also here, the fire spread rapidly after ignition of the ceiling. Within 2 minutes, the fire had spread to the end of the ceiling, while the entire room was burning within 3 minutes. The fire spread across the ceiling after CLT ignition was approx. 140 mm/s (8.4 m/min), whereas the fire spread rate across the variable fuel was approx. 100 mm/s (6 m/min).

New CLT buildings often have large open-plan spaces and large windows, and it is natural to consider them as objects relevant for travelling fires. Although the recent experiments have provided unique and relevant knowledge about travelling fires with exposed CLT, the setups are not necessarily relevant for all types of CLT buildings as key parameters like the floor size, ceiling height, opening factor, fuel load density, and number and area of exposed CLT surfaces could be different. Furthermore, there is a complete lack of data on travelling fire experiments that compare how the fire develops with different CLT configurations.

Also, when considering that 70% of all CLT fire experiments had a floor area less than 25 m^2, 86% less than 50 m^2, and 86% had window openings corresponding to a ventilation-controlled fire [51], it is undoubtedly a need for more knowledge on large compartments with different exposed surfaces and different opening factors.

1.3 I-joists - background

CLT has many supporters but also some opponents. A common claim is that CLT is not sustainable enough as it uses too much wood [52]. A wooden alternative that overcomes this claim is the wooden I-joist. This engineered wood product has reduced the material use to a minimum but still offers better structural properties than similar-sized rectangular members of solid wood [3] and could be used as a structural element in both walls and floors. However, its strength is not in the same range as CLT, and it is thus not a direct competitor to CLT. Instead, it could be considered a material-efficient wooden alternative for low-rise buildings and combined with steel, concrete or CLT in taller buildings to lower the material consumption.

An I-joist is built up of two flanges with a web in-between, see Fig. 2. The flanges are normally made either of solid wood or laminated veneer lumber (LVL), whereas the web is 8-10 mm thick and made of hard fibreboards or particleboards. The flanges are typically 39-47 mm thick, while the width is provided in different sizes, typically 45-97 mm.

Despite their great strength, I-joists are vulnerable to losing their load capacity when subjected to fire due to their slim cross-section. In fact, they are likely to fail when the web is burned through, even if the bottom flanges are partly remaining [53].

Fig. 2 An I-joist comprises two flanges and a web in between. Here, the flanges are made of solid wood and the web of oriented strand board (OSB). The length of the I-joists is normally much longer than in the image.

With the focus on building more sustainable, several bio-based insulation products have entered the market in recent years, and there has been increased interest in combining I-joists with new combustible insulation products, like wood fibre and cellulose insulation.

However, combining bio-based insulation with I-joists is more complicated than using stone wool. Stone wool is non-combustible, and the charring and the heat transfer occur mainly through the non-protected side of the flange and could be treated as one-dimensional. The design model for rectangular members in the current Eurocode 5 [54] can be used for this combination or other developed models for I-joists and mineral wool [55-57].

Conversely, a combustible insulation would be consumed when exposed to fire or heat. As the insulation gets consumed, the flanges become exposed on the lateral sides, and the charring of the flanges can no longer be treated as a one-dimensional process.

Design models for I-joists have only been developed for stone wool and glass wool [55-57], i.e., no combustible insulation products, like wood fibre, cellulose, and phenolic foam insulation, are included in the models.

In the final draft of the new Eurocode 5 [58], a new design model for I-joists is proposed based on the work of Mäger et al. [55, 56]. However, the design parameters are derived from experiments with rectangular members, not I-joists. Hence, design parameters for combustible insulation derived from experiments with I-joists are still missing, and predicting the charring of I-joists is not possible based on the currently available design parameters.

In order to increase the use of I-joists and combustible insulation, a solid knowledge base is needed on how the different combustible insulation behave when subjected to a fire, and design parameters for the different types must be derived based on experiments combining I-joists and combustible insulation.

1.4 CLT - Aim of the research and methodology

1.4.1 CLT experiments

Background for doing large-scale experiments

Although not many large-scale travelling fires with exposed CLT have been conducted, they have revealed that the current understanding of fire dynamics and fire spread in large open-plan compartments with exposed CLT is limited. These experiments have demonstrated that the flame spread rates could be many times higher than rates found in compartment experiments without exposed combustible surfaces, which in general have been ≤ 1 m/min [59-63]. Such rapid fire spread rates are typically not accounted for in European design standards [49]. However, a fast flame spread rate is a parameter that affects several aspects of the fire safety strategy, including available time for evacuation and the size of the fire when the fire brigade enters the building, which in turn influences what extinguishing tactics that are available.

According to these recent findings, expanding our knowledge on how exposed CLT affects fire spread and safety in large open-plan spaces is essential. This includes gaining a better understanding of the feedback mechanisms between combustible surfaces and variable fuel load, as well as how this interaction affects fire dynamics, spread, duration, external flaming and decay phase.

Small- and medium-scale experiments are cost-effective and can be used to explore and study qualitative aspects of CLT behaviour in compartment fires. However, as Liu and Fischer [51] point out, large-scale experiments are important to verify small- and medium-scale results to assess the findings at realistic scales. Furthermore, several review papers have highlighted a general lack of data from large-scale experiments [31] and especially large-scale experiments with exposed CLT [51, 64, 65].

In other words, many aspects remain unstudied at full scale for compartments with exposed CLT. Furthermore, the experiments performed to date have:

- had an ignition package strong enough to cause flame impingement on the ceiling, which is a less probable scenario for compartments with high ceilings and smaller ignited items.
- had relatively small openings, which have facilitated a large accumulation of smoke gases under the ceiling before ignition and during the flame spread.

- studied the effect of an exposed ceiling, but never considered the combination of a fully exposed wall and ceiling.

To increase the knowledge of this topic and address the shortcomings addressed above, two large-scale CLT compartment experiments for two different configurations of exposed CLT surfaces have been conducted. The first experiment, #FRIC-01, had exposed CLT in the ceiling, while the second experiment, #FRIC-02, had exposed the ceiling and one wall.

Aim

The CLT experiments aimed to better understand and gain knowledge on how two different configurations of CLT affect the fire dynamics in a large compartment, including fire spread and travelling fire behaviour, temperature distribution inside the compartment, self-extinction of flaming combustion, external flames, charring behaviour and delamination of CLT, and the decay phase.

Methodology

The methodology consisted of gaining new knowledge from two large-scale compartment experiments with different exposed CLT surfaces and open ventilation conditions, see Fig. 3. The compartment had an oblong shape, ideal for observing the travelling fire behaviour. Several methods were used to describe the fire and measure the effects of the exposed CLT, including analysis of video recordings, measurements of the temperatures and heat fluxes inside the compartment and at the facade, measurements of the charring rates of the CLT, calculation of the heat release rates for the variable fuel and CLT, and post-measurements of the final char depth of the CLT.

The method and main results of the experiments are described in Section 2.1.1 and 2.1.2.

Fig. 3 Photo of the CLT compartment with exposed CLT ceiling. This is of the #FRIC-01 experiment with only the ceiling (not shown) exposed.

1.4.2 CFD simulations of CLT experiments

After completion of the experiments, a CFD simulation of the #FRIC-02 experiment was conducted.

Aim

The CFD simulations aimed to explore whether the key findings of #FRIC-02, i.e., the CLT compartment experiment with both the wall and the ceiling exposed, could be reproduced in a simulation, including the rapid fire development and the non-uniform external flames.

Methodology

The simulations were performed with the Fire Dynamics Simulator (FDS) [66]. The model was built based on the experimental setup of #FRIC-02. The FDS "simple pyrolysis model" was applied to model the fire spread with an ignition temperature and a prescribed burning rate, i.e., heat release rate per unit area. The main results were then compared against results from #FRIC-02, including fire spread rate, temperatures, mass loss rate, heat release rate, velocities through window openings and incident heat flux to the facade.

The method and main results of the experiments are described in Section 2.1.3.

1.4.3 Learning from a real incident – a large compartment with exposed wood

Background

During my PhD-period a fire broke out in a school gym at Lambertseter school in Oslo, Norway. This fire caught my attention due to the rapid fire development, the large amount of exposed wood on the surfaces, and the shape that was to some extent similar to the #FRIC-01 and -02 geometry with large windows along one wall. As pointed out above, there is a limited understanding of how fires develop in large compartments with exposed wooden surfaces due to the few experiments conducted. However, there are regularly actual fires which could have taught us a lot, if those were 1) properly investigated and 2) the findings had been shared with the public. Unfortunately, this is too seldom done.

Thus, this case was considered a relevant scenario to increase the understanding of how a fire might develop in a large compartment with exposed wooden surfaces.

Aim

Draw learning points from an actual fire related to the overall topic of fire development in a large compartment with exposed wooden surfaces.

Methodology

The main methodology consisted of interviewing the fire brigade that intervened in the fire and getting key information about the building geometry and material choice.

The case is discussed in Section 5.3.

1.5 I-joists - Aim of the research and methodology

Aim

The main aim of these experiments was to gain experimental data on charring rates of I-joists and recession rates for different types of combustible insulation. The data is intended to be used to determine design parameters for I-joists and combustible insulation in the future.

Methodology

The methodology consisted of gaining new knowledge through furnace experiments run according to the standard time-temperature curve [67]. The test specimen was a light timber frame assembly built up of I-joists, and the cavity completely filled with insulation. A gypsum board type F [68] was attached on the fire-exposed side, and a fibre board on the non-exposed side. Five experiments were performed in total, in which two different I-joist types (flanges of solid wood and LVL) with three different flange sizes and four different types of combustible insulation (phenolic foam, wood fibre batt, wood fibre loose-fill and cellulose loose-fill) were combined.

Charring rates of flanges and recession rates of the insulation were found by TCs embedded into and attached to the surface of the flanges. Post-measurements were used to determine the final char depth and residual cross-section. The measured charring rates were then compared against the existing model for rectangular cross-sections (EN 1995-1-2:2004 [54]) and the upcoming model for I-joists (prEN 1995-1-2:2021 [58]).

2 Main results

2.1 Paper overview and contribution of the candidate

The primary research output of this thesis is composed of three papers, all of which are published in peer-reviewed journals in the fields of fire safety and fire engineering. A fourth manuscript is submitted to a peer-reviewed journal, and some unpublished results from the CLT experiments are presented in this thesis.

Papers I and II describe the results of the two large-scale compartment fire experiments with exposed CLT and open ventilation conditions. The papers are strongly linked and should be read in order. Paper III is a submitted manuscript which comprises a simulation of the first ten minutes of the experiment described in Paper II.

Paper IV is an independent paper and is not directly related to the other three. The paper describes the results from five experiments where two different I-joist types are combined with four types of combustible insulation. This work was performed together with researchers from Tallinn University, Estonia.

The main results from each paper are presented in the subsequent sections.

2.1.1 Paper I
Title: Fire spread in a large compartment with exposed cross-laminated timber and open ventilation conditions: #FRIC-01 - exposed ceiling

Authors: Andreas Sæter Bøe, Kathinka Leikanger Friquin, Daniel Brandon, Anne Steen-Hansen, Ivar S. Ertesvåg

Contribution of the PhD-candidate:

I had the leading role in all parts of generating the paper, including literature review, planning of the experimental setup, ordering of materials and instrumentation, rigging and execution of the experiments, post-measurements, data management and analysis, and writing the paper. In the rigging of the experiments, I had valuable help from technicians at RISE Fire Research. Still, I was actively involved in all parts of the preparations, including building the facade walls, assembly of the CLT elements, building the wood crib, preparing the instrumentation, and setting up the cameras. In addition, I took the initiative to find extra funding for the experiments outside the original budget. The co-authors contributed with valuable suggestions and discussions both in the planning phase and analysis phase, and critical reviews and editing of the manuscript.

2.1.2   Paper II
Title: Fire spread in a large compartment with exposed cross-laminated timber and open ventilation conditions: #FRIC-02 - exposed wall and ceiling

Authors

Andreas Sæter Bøe, Kathinka Leikanger Friquin, Daniel Brandon, Anne Steen-Hansen, Ivar S. Ertesvåg

Contribution of the PhD-candidate:

Same as for Paper I.

2.1.3   Paper III (submitted manuscript)
Title: Numerical simulation of fire spread in large-scale open CLT compartment

Authors: Lei Jiang, Andreas Sæter Bøe, Tian Li

Contribution of the PhD-candidate:

I devised the idea, made a draft FDS model, and provided several relevant research papers for modelling the wood crib. I also provided data from #FRIC-02 to validate the results and was involved in editing the paper.

2.1.4   Paper IV
Title: Experimental study of the charring of I-joists and recession of combustible insulation in light timber frame assemblies with comparison to Eurocode 5

Authors: Andreas Sæter Bøe, Katrin Nele Mäger, Kathinka L. Friquin, Alar Just

Contribution of the PhD-candidate:

The idea, concept and test matrix were mainly planned by my co-authors and primarily by the researchers from Tallinn, as they had conducted similar experiments already. However, I was the main contributor to the rigging of the experimental setup, execution of the experiments, post-measurements and analysis of results. All authors were involved in the writing and editing of the paper, whereas I did the core of the work.

2.1.5   Data access
Raw data from the experiments can be downloaded through the NTNU Open Research Data repository:

- Paper I   [69].
- Paper II [70].
- Paper IV [71].

2.2 Paper I – Fire spread in a large compartment with exposed cross-laminated timber and open ventilation conditions: #FRIC-01 - exposed ceiling

This section summarises the method and the most important results of Paper I. Further details of the method are described in Paper I, and additional details are provided in Section 3 of this thesis.

2.2.1 Method

The following description is summarised from the method chapter in Paper I [72].

Compartment

"The compartment in the experiment was built of CLT elements in three walls and the ceiling, while the fourth wall was almost entirely open with four large openings. The CLT elements in the roof rested on the three CLT walls. They were supported on the fourth wall by a 140 mm × 315 mm glulam beam resting into a pre-cut hole in the CLT end walls and supported by three aerated concrete columns. The inner geometry of the compartment was approx. 18.8 m × 5.0 m x 2.5 m (L x W x H). A sketch of the compartment is given in Fig. 4.
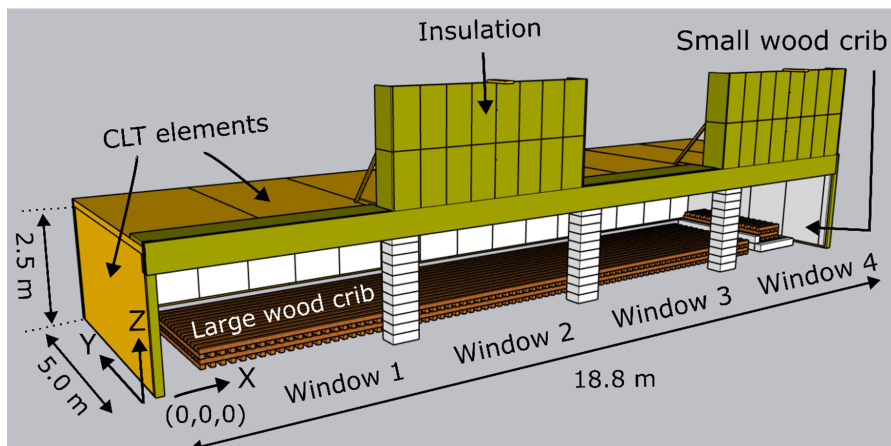

Fig. 4 Sketch of the CLT compartment. X, Y and Z describe the location of TCs, PTs, etc. Origo is on the floor to the left of the compartment in the opening.

The beam and the three columns in the window wall created four openings of 4.25 m width and 2.20 m height, with a total opening area of 37.4 m2. This corresponds to an opening factor of 0.18 $m^{1/2}$ when calculated according to Eq. (1).

The CLT elements in the back wall and ceiling were 140 mm thick and made of 5 layers (40-20-20-20-40 mm), while the end walls were built of 80 mm thick CLT with three layers (30-20-30 mm). The wood in the elements was Norwegian spruce, and the glue between the layers was a regular polyurethane adhesive named Loctite HB-S, an adhesive that lacks a demonstrated resistance against glue-line integrity failure.

The density of the CLT elements was approximately 484 kg/m³ with moisture content (dry value) of 12.8% ± 0.3% (standard deviation, n = 48) measured with a moisture meter.

The ceiling was exposed, in total 89 m². The walls were protected by two layers of 15 mm thick fire-rated gypsum boards Type F. The outer gypsum board layer was shifted with a half board width to the innermost layer to avoid continuous joints leading directly into the wood.

The glulam beam and edges of the CLT at the front wall were protected with two layers of 25 mm thick ceramic fibre insulation. The outer layer was shifted half a width to avoid overlapping joints. The outer layer covered approx. 100 mm of the exposed CLT ceiling along the glulam beam.

The experiment was performed outdoors. On the day of the experiment, the weather was cloudy, with negligible wind and no precipitation. The temperature at the start of the experiment was 15 °C and gradually increased to 20 °C during the experiment."

Wood crib

"The variable fuel load in the compartment was represented by a long continuous wood crib, 15.5 m x 2.8 m x 0.2 m, and a smaller wood crib, 1.0 m x 2.8 m x 0.2 m. The small crib was placed on a scale 0.2 m higher than the large crib. The large and the small cribs are hereafter referred to as one unit, "the wood crib". The wood crib contained wood sticks with a cross-section of 50 mm x 50 mm, stacked horizontally on top of each other in four layers, where the sticks in each layer were perpendicular to the previous layer. The sticks laid perpendicular to the crib length were 2.8 m, while the parallel ones were 4.3 m long. The average moisture content was 14.5%, with 13% ± 0.8% (standard deviation, n = 20) and 16% ± 0.6% (standard deviation, n = 20) for the short and long sticks, respectively. The wood used was Norwegian spruce, with an average density of 486 kg/m³ ± 40 kg/m³ (standard deviation, n = 25). The distance between the sticks was 50 mm, which gave a crib porosity factor of 0.19 cm (see Eq. (2) in Section 3.3). The porosity factor is related to the ratio of the mass flow rate of air to fuel inside vertical shafts of a crib, expressed through dimensions of the crib [73]. 0.19 cm corresponds to the open regime, where the crib burning is not controlled by the porosity (spacing between the sticks) but rather by the thermal feedback from the compartment and the geometry of the wood crib [73]. The total mass of the crib was 2065 kg, determined by weighing all sticks. This corresponds to a fuel load density of 353 MJ/m² (per floor area) when using a net heat of combustion of 16.0 MJ/kg (see Section 3.5 for calculation)."

Ignition

"Ten aluminium metal trays with dimensions 150 mm × 220 mm × 50 mm (L × W × H) were positioned at 70 mm distance to each other directly below the edge of the wood crib at the left end of the compartment to get a uniform fire across the width of the crib. The first stick of the bottom wood crib layer was removed to make room for the trays to be positioned with 50 mm of the tray directly below the crib. Each tray was filled with 0.5 L of heptane, with a total amount of 5.0 L."

Instrumentation and measurements

Temperatures were measured with 120 thermocouples (TC) of type K 1.5 mm and 24 plate thermometers (PT). The incident heat flux was calculated based on Eq. (10) in Section 3.6.3.

Termination of the experiment

From ignition, the fire was allowed to burn freely until four hours, at which it was manually extinguished by water.

Post-flashover measurements

After the CLT elements had cooled down, the final char depth was measured for five of eight CLT elements.

2.2.2 Main results
Late ignition and slow initial fire spread

In #FRIC-01, the wood crib was ignited by 5.0 litres of heptane. Due to local draft conditions, the heptane fire was tilted away from the wood crib, and just 5 cm of the wood crib was burning with tiny flames when the heptane burned out at approx. 3 minutes. Hence, the wood crib fire developed from a very small fire and grew slowly for the first 20 minutes (Fig. 5). After 22 minutes, the end of the wood crib started burning out, and the size of the fire did not grow any further. The fire had spread to 1.5 m along the crib when the ceiling above the wood crib fire ignited at 32.5 minutes. The average fire spread rate along the wood crib in this period was 54 mm/min, which is close to the fire spread of many previous travelling fire experiments with non-combustible surfaces [38, 44]. The fire spread rate for this period gives a good indication of how the fire would have developed if the ceiling was not present or at a height where it had not been ignited. The slow ignition of the ceiling could be explained by the initial small fire, the flames not impinging on the ceiling and high window openings that effectively ventilated out the hot smoke.

Fig. 5 It took 32.5 minutes before the ceiling was ignited. This image is taken from ca. 20 minutes. This fire spread to 1.5 m before the ceiling was ignited but did not grow larger in size as the first part of the crib was starting to burn out from this point.

Flashing waves and fast fire spread

The ignition of the ceiling marked a clear change in the fire dynamics where the wood crib fire increased in flame height, became more intense and started spreading rapidly under the ceiling, see Fig. 6. The flames in the ceiling caused a strong radiative heat flux towards the wood crib. The irradiation from the ceiling enlarged the existing fire and effectively preheated the unignited wood crib. This contribution thus accelerated the fire spread along the crib. The flames in the ceiling spread to about ¾ of the length of the compartment before it retracted. Following the retraction, the wood crib fire also retracted a little, but the size of the wood crib fire was larger than before the ignition. Three such cycles, or *flashing waves* as we have called them (see Fig. 7), occurred before the fire was fully developed in the fourth wave at 45.5 minutes and did not retract. Despite retraction of the flames after each wave, the wood crib fire grew larger after each wave. The acceleration of the fire spread across the wood crib is recognised in the distinct shift in the fire spread rate before and after ignition of the ceiling, 54 mm/min to 1.2 m/min. A more detailed overview of the fire spread is given in Fig. 8, which shows an exponential increase in the fire spread rate after ignition of the ceiling.

Fig. 6 Flame spread under the ceiling shortly after ignition of the CLT ceiling in #FRIC-01. The image was taken at 33 minutes.

Fig. 7 In the third flashing wave, the fire spread to cover the entire wood crib and ceiling before it retracted shortly after. Time (hh:mm:ss).
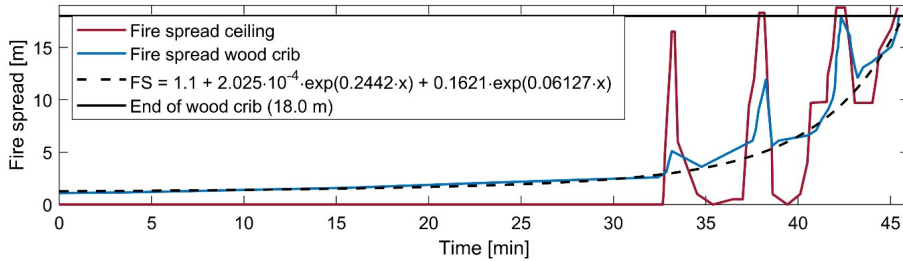
Fig. 8 Fire spread across wood crib and ceiling.

Temperature and heat release rate

The first peak in Fig. 9 originated from the heptane fire. After the extinguishment of the heptane fire, the temperatures rapidly decayed. After 9 minutes, the temperatures started increasing again due to the development of the wood crib fire and increased steadily until a plateau was reached between 22 and 33 min, which corresponds well with the almost constant fire base area, i.e., the burning area of the crib, for this period as the first part of the crib was burning out with a similar pace as the wood crib fire was spreading forward.

After 32.5 min, the ceiling spontaneously ignited. Temperatures increased along the entire ceiling but to a higher level near the ignition point and lower at longer distances. The highest recorded temperatures on the back wall near the wood crib fire (positioned at X = 3.0 m) were 476 °C and 670 °C at heights of 1.1 m and 2.4 m, respectively. At a height of 2.4 m, the corresponding maximum heat flux was 78 kW/m² and stabilised at 40 kW/m² until the next wave. At a height of 1.1 m, the maximum heat flux was 15 kW/m² before it reduced to approximately 10 kW/m² and then slowly increased to 20 kW/m² before the second wave.
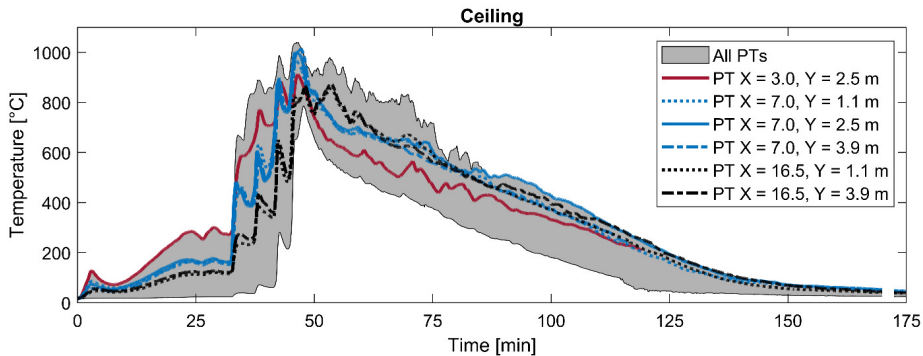
Fig. 9 Temperatures measured by plate thermometers (PT). The grey area represents the range of temperatures measured at all the installed PTs at the wood crib (facing upwards), at the wall (facing outwards) and in the ceiling (facing downwards).

The 2nd flashing wave started at 37 min and followed the same behaviour as the 1st wave. There were considerable temperature variations in the compartment during this period, with part of the compartment fully burning and the other part having temperatures close to ambient

temperatures. The 3rd flashing wave started at 42 minutes and led to the entire compartment burning, see Fig. 7. The 4th wave occurred shortly after the end of the 3rd and led to a stable burning fire in the entire compartment. The highest temperatures were reached at 45–46 min, with the peak temperature of 1040 °C.

Fig. 10 Image of the fully developed fire in #FRIC-01. Image from 47 minutes.

The CLT surface behind the two layers of gypsum boards on the back wall reached a maximum temperature of 106 °C during the fire. At the glue line, 40 mm deep, the maximum temperature was 67 °C. The highest temperatures for different depths into the wood were measured at 125–140 minutes, i.e., more than 75 minutes after the most intense phase of the fire. After 300 minutes, the temperatures in the fire-exposed layer (0–40 mm) were almost uniform, at approximately 55 °C.

The total heat release rate (HRR) was estimated to have a maximum value of 41 MW. The peak contribution of the CLT ceiling was approximately the same as the peak for the wood crib (~20 MW), as seen in Fig. 11. From the ignition of the ceiling, the HRR developed with a growth rate between the fast and ultrafast t^2-curve defined in Eurocode 1 [49].
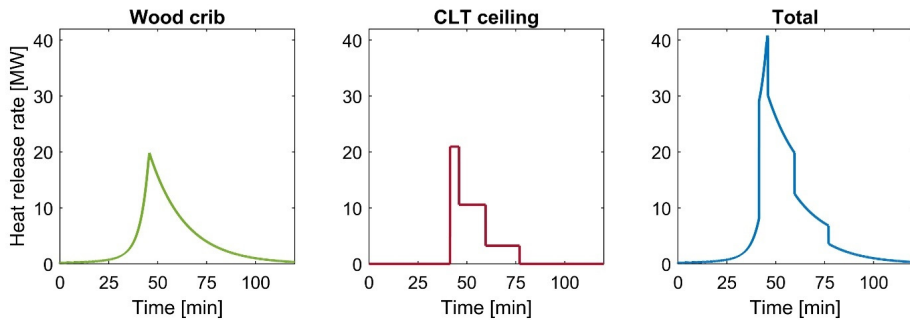
Fig. 11 Heat release rate for the wood crib, CLT ceiling, and total (wood crib + CLT).

The HRR was estimated based on the mass loss rate multiplied by the net heat of combustion of the wood and a combustion efficiency of 0.8. The mass loss rate (MLR) of the wood crib was based on the real MLR of a part of the crib measured by a scale to find a HRR per unit length of the crib. The HRR per unit length was then integrated over the entire wood crib based on the fire spread across it. The MLR of the CLT ceiling was based on an estimated charring rate based on the propagation of the 300 °C isotherm through the wood found by embedded TCs at 10, 20, 30 and 40 mm into the CLT.

External flames

External flames emerged out of the window openings during the flashing waves and for a few minutes after the flashover. Temperatures and heat fluxes to the facades were measured by TCs and PTs, and given in Fig. 12 and Fig. 13. The highest temperatures and heat fluxes were measured during the 3rd and 4th flashing waves, although the duration was short. The maximum PT temperatures at the façade were 440–445 °C, 550–600 °C and 660–680 °C at 0.8, 1.8 and 2.8 m height, respectively, above the window opening. From flashover (45.5 min) and until the flames of the CLT had extinguished (61 min), the incident heat fluxes were gradually reduced from approx. 50 to 10 kW/m^2, 40 to 6 kW/m^2 and 37 to 5 kW/m^2 for 0.8, 1.8 and 2.8 m above the window opening, respectively.
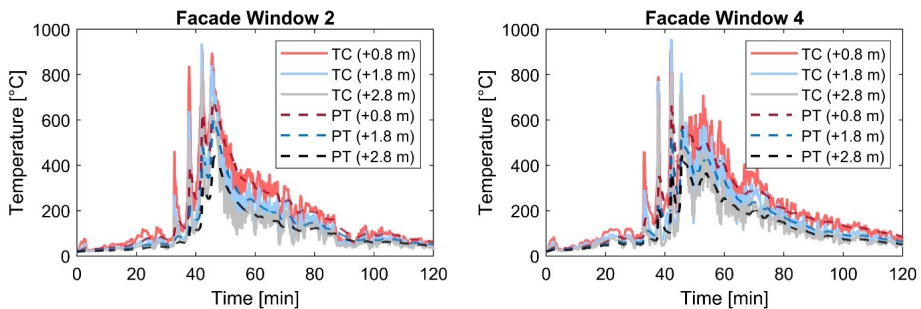

Fig. 12 Temperatures measured by TCs and PTs at the façades above Windows 2 and 4. +0.8, 1.8 and 2.8 m are the locations above the window opening. The TCs are not

corrected for any radiation exposure and might deviate slightly from the real gas temperature.
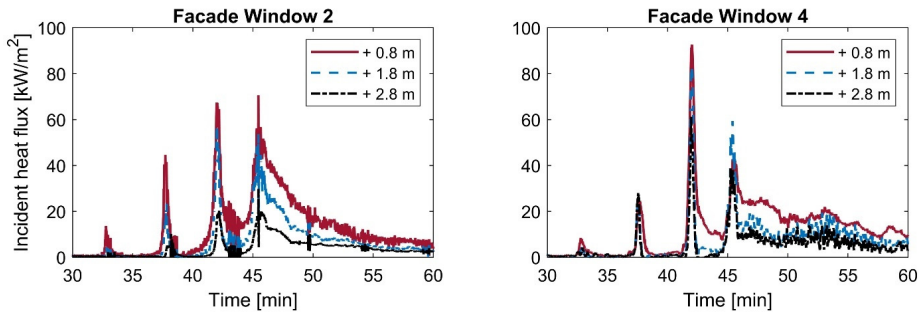

Fig. 13 Incident heat fluxes were calculated based on TCs and PTs at the façades above Windows 2 and 4 from Eq. (10). +0.8, 1.8 and 2.8 m are the locations above the window opening.

Self-extinction of flames in the CLT

The fire burned intensely for a few minutes (Fig. 10) before the flames in the ceiling started to extinguish from the ignition side of the compartment at 50 minutes. At 61 minutes, all flames in the ceiling were extinguished, while the wood crib was still burning. Upon extinguishment of the CLT, the temperatures in the compartment dropped rapidly, and the wood crib fire burned out. The compartment was observed until a test duration of 4 hours. No reignition was observed, but some local hot spots were observed with an infrared camera.

The decay phase was initiated by a sudden drop in temperatures and continued with the extinction of flames in the ceiling. During the extinction of the CLT, the oxygen concentration was 16–17% of the exiting smoke gases. The temperatures below the ceiling were 695–705 °C, corresponding to an incident heat flux of 49–52 kW/m2. During the extinguishment of CLT, the average compartment temperature dropped from 910 °C to 650 °C.

The decay phase then continued almost linearly over the next 90 min, with an average temperature decay rate below the ceiling of 7.1 ± 0.5 °C/min. The difference between the minimum and maximum compartment temperatures during most of the post-flashover and decay phase was between 200 and 400 °C.

Fig. 14 Self-extinguishment of the flames in the CLT ceiling when the wood crib was still burning.

Delamination

During the experiment, several lamellas had been partly delaminated, i.e., they were visually detached from the layer behind, and some were hanging down. From visual inspection, the layer behind was mainly discoloured, not charred, and the char depth had not reached through the loose lamellas in most places, see Fig. 15. Despite such partial delaminations at several locations, no reignition was observed during the decay phase when the delamination happened.

The maximum temperature measured at the glue-line, i.e., 40 mm depth, was 194 °C and was reached around 120 minutes. It seems likely that the delamination also occurred approximately at this time. A supporting argument is the discolouration of the second layer, which is known to occur around 200 °C. This is close to the measured temperatures at the glue line. The gas temperature below the ceiling at 120 min was approx. 220 °C and declining. This low temperature is insufficient to cause ignition of the fresh wood and explains why the charring did not continue into the second layer and caused a reignition.

Fig. 15 The image shows partial delamination where several lamellas are partly loose, and some are hanging down. The second layer was mostly discoloured, not charred, which indicates that the temperature at delamination was around 200 °C or lower.

Non-uniform charring

The charring rate was initially high but was reduced significantly for each subsequent 10 mm into the CLT. The charring rates for 0–10, 10–20 and 20–30 mm into the wood were 2.23, 1.13 and 0.35 mm/min, respectively. The average final char depth was 26 mm ± 4 mm standard deviation (n = 250) with an average charring rate of 1.1 mm/min. The charring was least pronounced at the ignition end of the compartment (24 mm) and the most pronounced from the centre and towards the other end (29 mm), see Fig. 16. Also, a few mm increased charring was observed close to the back wall.

BACK WALL

	0.2	0.7	1.2	1.7	2.2		5.0	5.5	6.0	6.5	7.0		9.8	10.3	10.8	11.3	11.8		14.5	15.0	15.5	16.0	16.5		16.8	17.3	17.8	18.3	18.8	AVG
4.8	21	27	24	22	24		31	27	24	22	24		30	32	33	33	32		33	32	33	30	29		29	26	25	25	27	28
4.3	22	25	22	19	27		22	25	22	19	27		24	30	32	36	27		25	28	27	30	28		30	29	23	22	27	26
3.8	23	23	24	25	29		23	23	24	25	29		27	33	32	28	26		25	32	29	30	33		29	27	24	23	25	27
3.3	27	24	25	22	29		27	24	25	22	29		27	33	27	32	27		25	32	34	32	31		29	28	22	23	25	27
2.8	26	29	22	22	26		26	29	22	22	26		30	30	30	28	26		38	35	36	29	32		30	30	24	24	28	28
2.3	30	26	26	20	27		30	26	26	20	27		28	28	30	32	28		29	30	28	28	31		27	28	25	23	23	27
1.8	25	27	24	22	23		25	27	24	22	23		21	30	32	31	30		27	29	28	28	31		26	27	25	25	21	26
1.3	22	23	20	22	25		22	23	20	22	25		22	24	28	32	26		26	30	33	29	26		24	24	21	22	22	24
0.8	24	22	20	22	21		24	22	20	22	21		19	25	27	27	20		23	31	25	26	25		23	22	21	23	21	23
0.3	20	21	22	24	22		20	21	22	24	22		28	26	26	32	24		40	27	30	31	25		22	26	24	26	24	25
AVG	24	25	23	22	25		25	25	23	22	25		26	29	30	31	27		29	31	30	29	29		27	27	24	23	24	

IGNITION SIDE (vertical label on left)
Y / X (coordinate axis lower left)
WINDOW WALL

Fig. 16 Final char depth [mm] measurements of CLT wall elements. X and Z represent compartment coordinates in meters.

2.3   Paper II – Fire spread in a large compartment with exposed cross-laminated timber and open ventilation conditions: #FRIC-02 - exposed wall and ceiling

This section presents a short summary of the method and the most important results of Paper II [74]. Further details of the method are described in Paper II, with additional details in Section 3 of this thesis. Some additional results are presented in Section 2.6.

2.3.1   Method

The experimental setup was identical to #FRIC-01 except for the following changes summarised from the method chapter in Paper II [74]:

Exposed CLT

In #FRIC-02, both the ceiling (89 m^2) and the back wall (47 m^2) had exposed CLT, while in #FRIC-01, only the ceiling was exposed.

Ignition package

"14 metal trays (150 × 220 × 50 mm) were positioned on the floor next to the wood crib on the left end. The trays were filled with 0.7 L of heptane in each and positioned 70 mm from each other. The two first bottom sticks of the crib were removed and put on top of the crib, so there were four stick layers at the beginning of the crib as well. The trays were rotated by 90° compared to in #FRIC-01, and 150 mm of the trays were positioned under the wood crib."

Compared to #FRIC-01, 14 instead of 10 trays were used, and each was filled with 0.7 L of heptane instead of 0.5 L. Hence, the surface area of the heptane trays was increased by 40%, and the heptane amount was increased from 5.0 L to 9.8 L. Also, the trays were positioned 100 mm further under the wood crib.

A discussion of the change in the ignition package is given in Section 3.4.

Wind conditions

During the #FRIC-01 experiment, there was negligible wind, while during #FRIC-02, there was a wind of 2 m/s with gust velocities from 5-8 m/s coming diagonally from behind the corner of the compartment close to Window 4.

2.3.2   Main results

Fire development

In #FRIC-02, ignition of the ceiling happened earlier compared to #FRIC-01. This was caused by a 40% larger surface area of the heptane and the heptane trays positioned more under the wood crib, which resulted in more of the wood crib being involved in the initial fire. Due to the larger ignition package, the ceiling ignited at 01:42 (mm:ss), and the wall closest to the wood crib fire ignited at around 2 minutes. Due to the different sizes of the ignition package, the ignition times of the ceiling are not comparable.

After the ignition of the ceiling, the fire spread rapidly under the ceiling and the upper part of the wall, which caused intense radiation to the unignited parts of the wall and wood crib. At

02:20, the flames were covering approx. one-fourth of the ceiling, while the wood crib fire had not grown any larger. However, from then on, the development happened very fast, and the entire compartment was burning at 03:13, see Fig. 17.

Hence, it took only 91 seconds after ignition of the ceiling before the fire was fully developed. This corresponds to an average fire spread rate of 11.7 m/min. Interestingly, the spread rate developed exponentially, see Fig. 18. This can easily be observed by comparing the fire development across the wood crib, where it took 81 seconds (after ceiling ignition) to travel across the first half of the wood crib and only 10 seconds to travel the second half. This indicates that the average fire spread rate could have been even faster in a longer compartment.

Fig. 17 From ignition of the ceiling, the fire spread across the room in just 91 seconds. Time (mm:ss) after the start of the experiment.
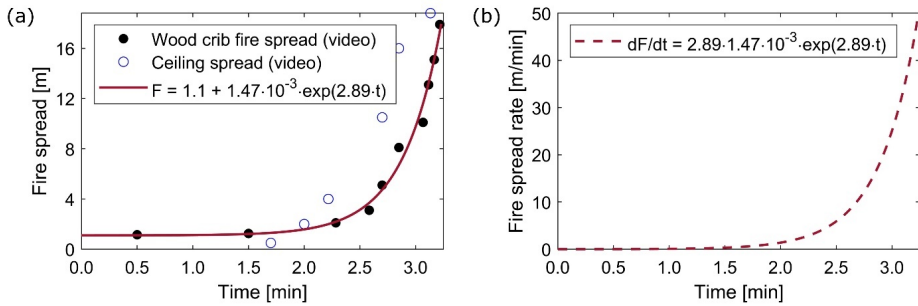
Fig. 18 (a) Fire spread across the wood crib and the ceiling. (b) Estimated fire spread rate across the wood crib.

After a period of intense burning, the temperatures started decaying after approximately 12 minutes, and the visible flames at the CLT back wall and ceiling started extinguishing from the ignition side. At 16 minutes, all the flames of the CLT were visually gone. This happened while the wood crib was still burning.
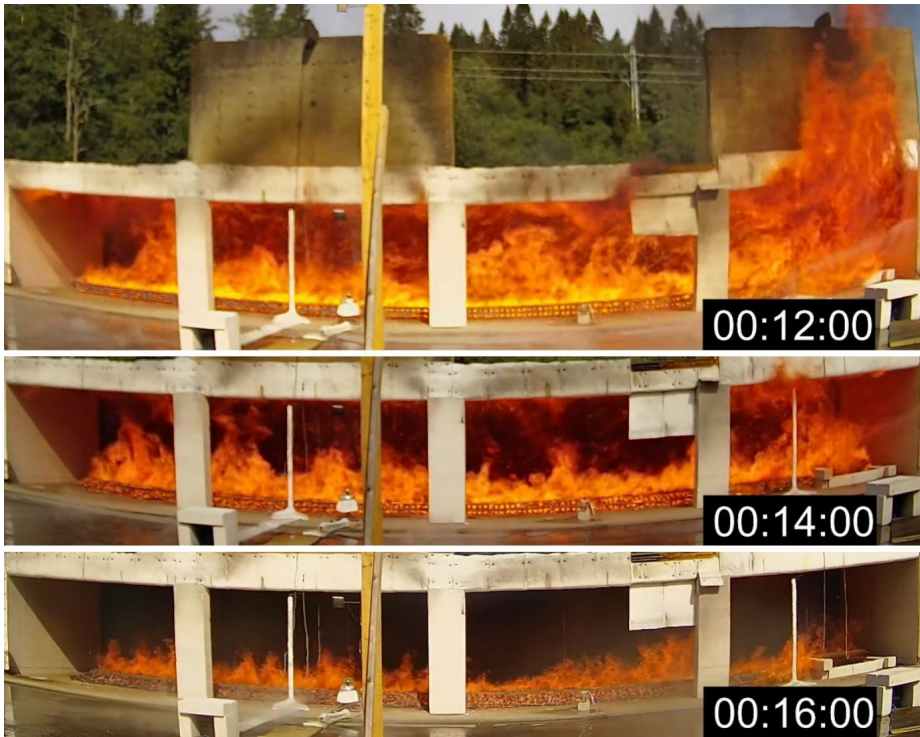

Fig. 19 Self-extinguishment of the flaming combustion of the CLT. Time (hh:mm:ss) after the experiment started.

From 66 minutes, small flames appeared spontaneously in several locations at the wall and in the ceiling. In the next minutes, more flames appeared, and the existing flames grew larger. At 76 minutes, almost the entire compartment was burning again, including the originally charred and self-extinguished first layer, see Fig. 20.

Fig. 20 Development of the second flashover. Time as hh:mm:ss.

The most intense burning phase lasted just a few minutes. After that, the intensity varied due to the delamination of the subsequent layers, as seen in Fig. 21. The fire was manually extinguished at 175 minutes. The temperatures had, at this time, an increasing trend (Fig. 25), and the fire showed no signs of being close to self-extinguishment at this time.

The ongoing fire with varying intensity after the second flashover can be explained by the

- thin (20 mm) intermediate layers of the CLT and the use of an adhesive that lacks a demonstrated resistance against glue-line failure.
- The natural variation in the mass loss rate of wood, in which the rate initially is high but decreases due to the formation of a char layer at the surface.
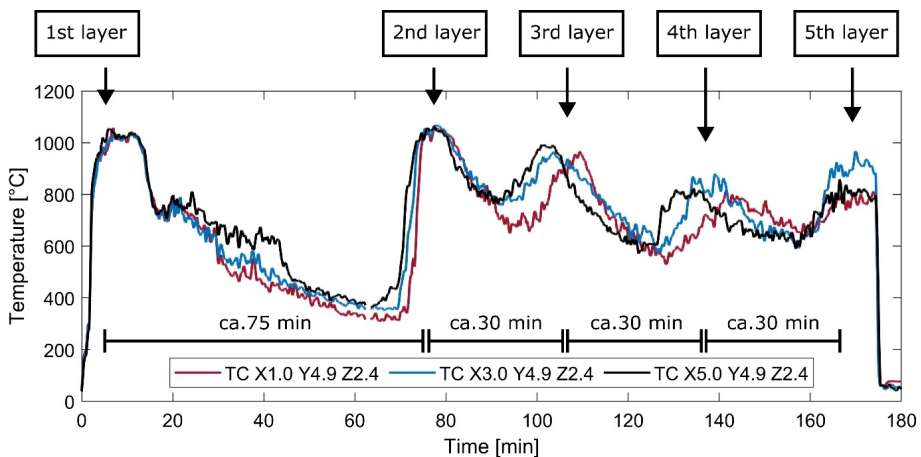

Fig. 21 Gas temperatures 100 mm from the back wall at three different locations. The peaks correspond to the burning of the different layers in the CLT wall.

External flames and non-symmetrical air supply

Another characteristic of #FRIC-02 was the large, non-symmetrical external flames. Both visually and confirmed through temperature measurements, the external flames were significantly larger through Window 4 (Fig. 3) than the other windows, see Fig. 22. For some period, the flames out of Window 4 filled the entire height of the window opening, extended several meters out from the facade and reached well above the top of the facade wall, which was 5.2 m above the ground and 3 m above the window soffit. The largest flames occurred shortly after flashover and had a maximum HRR estimated to be 66 ± 20 MW based on a relation between the flame volume and the HRR [75].

As flames occupied a large fraction of the window area, this effectively reduced the inflow of air through that window. Instead, the air was supplied through the other windows. This difference in air supply caused a large temperature difference throughout the compartment. In the area inside Window 4, almost uniform temperatures were measured. Conversely, through Window 2 a distinct temperature gradient was measured from the window opening towards

the back wall. Generally, the highest temperatures were close to the end walls, while the lowest were in the centre of the compartment.

The reason for the non-symmetrical external flame and air supply was suggested to be caused by the wind coming diagonally from behind the right corner, i.e., next to Window 4, see Fig. 22. This would cause an underpressure outside of Window 4, which drags smoke and flames out of this window. In contrast, the other windows were more shielded from this effect by the compartment itself. A CFD study (Paper III) was able to reproduce these non-symmetrical flames when similar wind conditions as on the test day were implemented into the model.

Fig. 22 Image of #FRIC-02 after 3.5 minutes. The external flame covered almost the entire opening of Window 4 directly after flashover, whereas the external flames from the other windows were relatively small.

That the external flames were larger from Window 4 than the other windows, was evident also through the temperature and heat flux measurements, as shown in Fig. 23 and Fig. 24. The highest temperatures were measured above Window 4 between 3 and 9 min with peak PT temperatures of 1020 °C, 865 °C and 720 °C at 0.8, 1.8 and 2.8 m above the window soffit. The exposure to the facade was also significant during the second flashover but lower than during the first flashover.
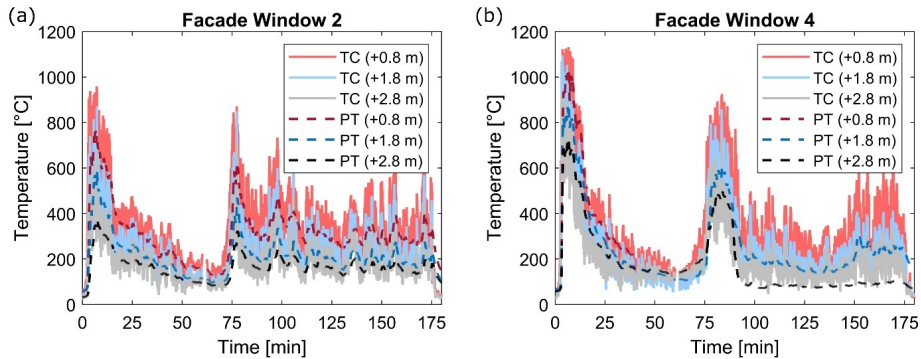
Fig. 23 Temperatures measured by TCs and PTs at the façades above Windows 2 and 4. +0.8, 1.8 and 2.8 m are the locations above the window opening. The TCs are not corrected for any radiation exposure and might deviate slightly from the real gas temperature.

The heat flux above Window 4 was at its maximum between 3 and 9 min, with heat flux levels fluctuating between 125 and 175 kW/m^2 0.8 m above the window. The maximum 30-s moving average was 156, 96 and 67 kW/m^2 for heights 0.8, 1.8 and 2.8 m above the window opening, respectively. At +0.8 m height, the maximum 30-s averaged value occurred at 6 min, while the maximum value for +1.8 and + 2.8 m occurred at 3.5 and 4 min, respectively. This confirms that the largest flames lasting 30 s were present shortly after flashover, although short-lived large flames were present also later. In comparison, the values above Window 2 were significantly lower, with a 30-s average of 64, 34 and 12 kW/m^2.

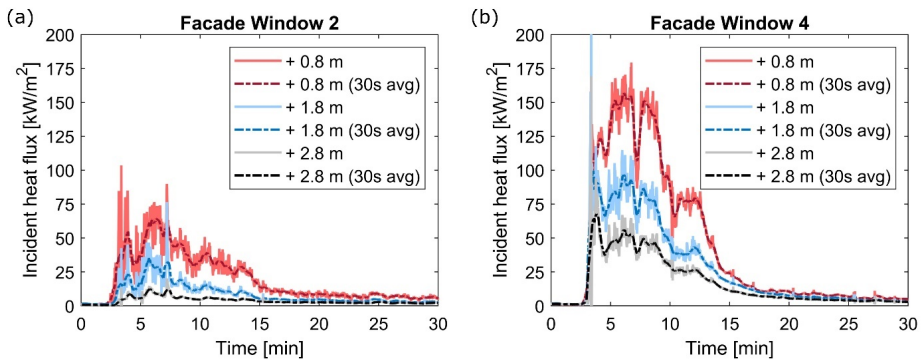**Fig. 24 Incident heat fluxes were calculated based on TCs and PTs at the façades above Windows 2 and 4 from Eq. (10). +0.8, 1.8 and 2.8 m are the locations above the window opening.**

Temperatures and heat release rate

Due to the fast fire spread rate, the temperatures increased rapidly in the entire compartment, and after 4 minutes, all PT temperatures had increased to 700–1000 °C. The peak

temperatures were reached at 7 min, with temperatures between 1010 and 1172 °C for all PT locations.

At 12–18 min, the temperature dropped from 1135 to 810 °C for the maximum PT measurements and from 924 to 575 °C for the minimum PT measurements. The decay rate of the compartment temperatures in this period was 52 ± 10 °C/min on average. The extinguishment of flames at the CLT wall and ceiling started from the left end and was extinguished completely between 14 and 16 min. Visible flames extinguished at temperatures (PTs) between 805 and 845 °C and an incident heat flux of 70–84 kW/m². This is higher than the suggested critical heat flux of 43.6 ± 4.7 kW/m² reported from bench-scale testing [21].

From 18 minutes, a slower decay phase started with an average decay rate of 5.7 °C /min. Before the initiation of the second flashover, the temperatures in the compartment had cooled down for about an hour. The temperatures measured by PTs below the ceiling and on the back wall were 386–490 °C, while the gas temperatures were 430 – 445 °C.

During the most intense burning in the second flashover (76-80 min), the temperature reached approx. 1050 °C. After this intense burning phase, the temperature varied considerably but remained above 550 °C below the ceiling and 500 °C by the wall until the fire was manually extinguished at 175 minutes. The fire reached its minimum phase at approx. 128 min with all PT temperatures below 585 °C, corresponding to an incident heat flux of 19–28 kW/m².
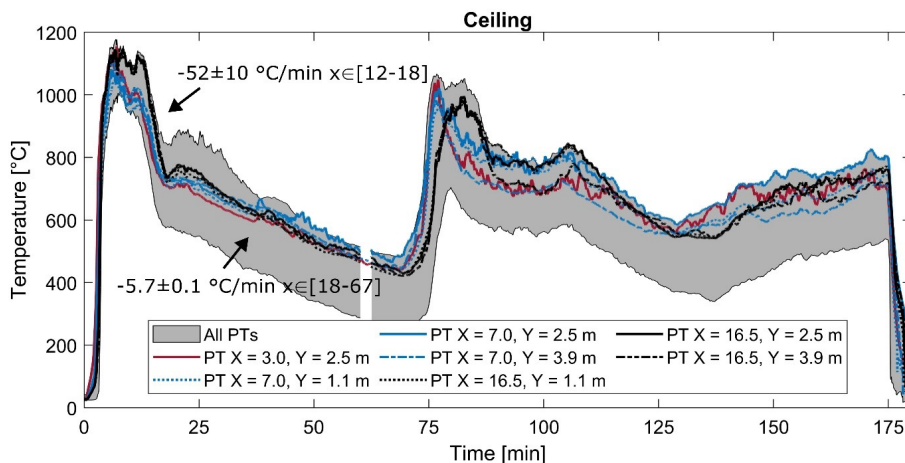

Fig. 25 Temperatures measured by plate thermometers (PT). The grey area represents the range of temperatures measured at all the installed PTs at the wood crib (facing upwards), at the wall (facing outwards) and in the ceiling (facing downwards).

Large temperature variations were seen in the compartment, and a particular difference was present at the end of the compartment inside Window 4 compared to the other windows, see Fig. 26. Inside Window 4, the temperatures were almost uniform as little air was provided through this window. Inside the other windows the temperature distribution was more affected by the supplied air through the lower parts of the window openings.

The total heat release rate (HRR) in #FRIC-02 had an estimated peak of 73 MW. The development of the HRR was faster than the ultrafast fire growth rate curve in Eurocode 1 [49] with a fire growth rate constant, t_α, of 27 s vs. 75 s.
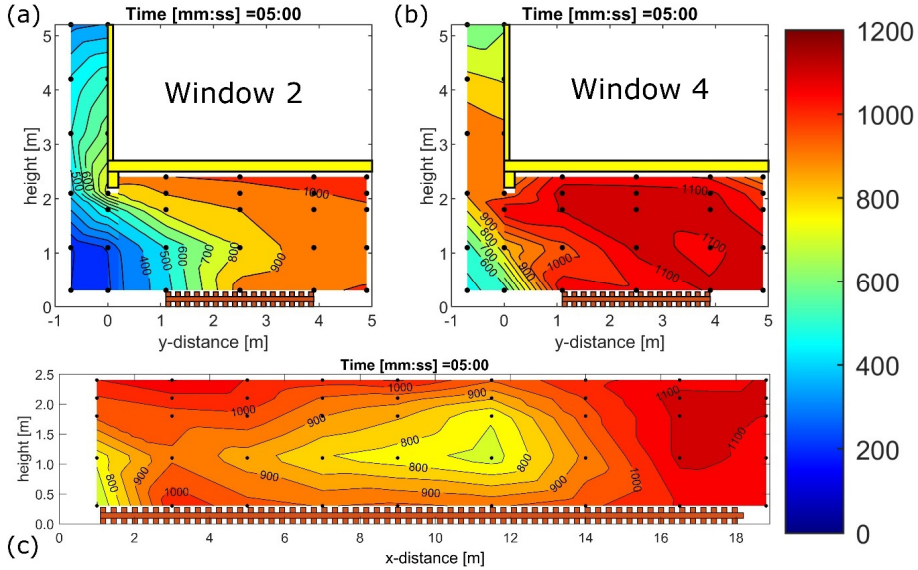

Fig. 26 The temperatures were more uniform in the cross-section through Window 4 (b) compared to the other windows, represented by Window 2 (a). The temperature distribution across the length of the compartment is given in (c).
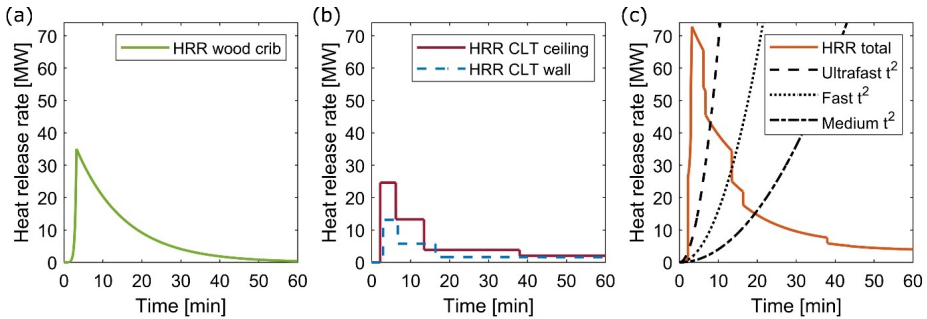
Fig. 27 Heat release rate for (a) the wood crib, (b) the CLT wall and ceiling, and (c) total (wood crib + CLT). The fire growth rate was faster than the ultrafast t^2-curve.

Non-uniform charring

Similar as in #FRIC-01, the charring rate into the wood was initially high and decreased for each subsequent 10 mm interval until the second flashover occurred. The charring rates were 2.68, 1.44, 0.38 and 0.27 mm/min for the 0–10 mm, 10–20mm, 20–30 mm and 30–40 mm, respectively.

The average charring rate over the almost three-hour duration was 0.56 mm/min for the ceiling and 0.60 mm/min for the back wall. The average final char depth was 97 mm ± 13 mm (std, n = 150) for the ceiling and 106 mm ± 7 mm (std, n = 121) for the back wall. Also here, increased charring of the ceiling was seen towards the back wall, see Fig. 28. Furthermore, the upper parts of the wall were more charred than the lower parts. The differences were approx. 30 mm in the ceiling and 10 mm on the wall. In addition, less charring was seen closer to the end walls.

Interestingly, the char depth was lowest at locations that had experienced the highest temperatures, i.e., inside Window 4, and highest in the centre of the compartment where the temperatures had been among the lowest in the most intense burning phase. Thus, temperature differences cannot be the main cause of the non-uniform char pattern. Instead, the differences are believed to be due to differences in oxygen concentration.
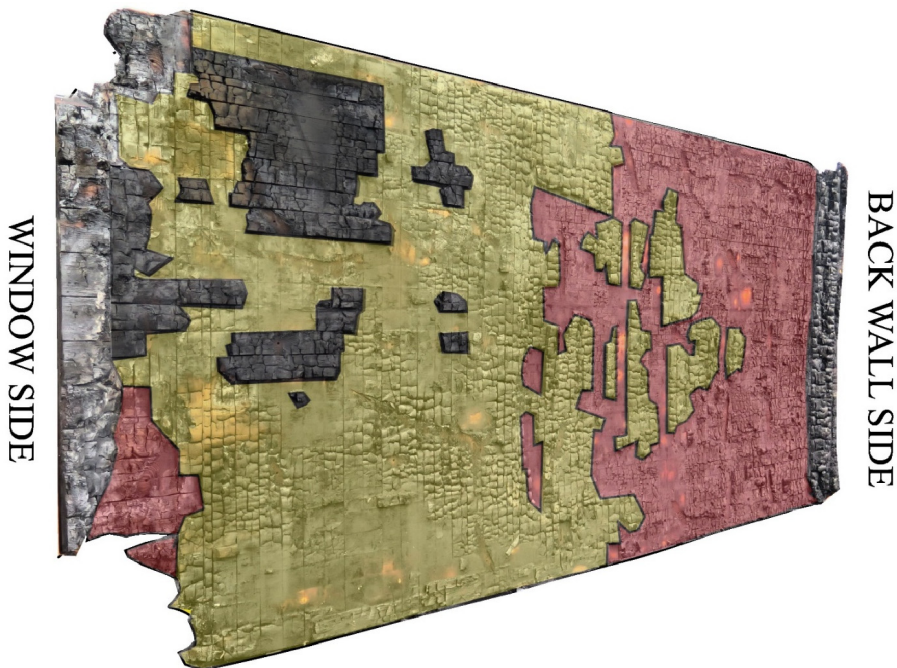
Fig. 28 Visualisation of non-uniform charring for one CLT ceiling element based on a photo. A colour filter is added to better separate the layers. Black is the 3rd layer, yellow is the 4th, and red is the 5th layer. The holes at the right and left lower corners of the window side were caused by smouldering and reignition after the end of the experiment, as this part was hard to reach with water due to safety precautions.

In the joint between the CLT wall and the bottom plank, increased charring was observed, as seen in Fig. 29. The hole was visible from 60 minutes, and is believed to be due to the lack of any sealant between the wall and the bottom plank. Hence, the hole likely formed due to a tiny gap in the joint.

Fig. 29 The fire burned through the intersection between the back wall and the bottom plank at approximately 60 min. The image is taken at a later point when the gap had become larger. The lack of a fire sealant between the bottom plank and the CLT wall enabled this and highlights that connection details are crucial to fire safety.

2.4 Paper III – Numerical simulation of fire spread in large-scale open CLT compartment

This section presents a short summary of the method and the most important results of Paper III.

2.4.1 Method

The experimental setup of #FRIC-02 was built up in FDS. In the simulation, the wood crib was resolved, i.e., the mesh size around the wood crib was similar to the wood stick thickness (5 cm). The rest of the compartment had a mesh size of 10 cm, while the outer domain had a 20 cm grid. The total domain was 31.8 m x 17.6 m x 12.0 m and consisted of 19 multigrid blocks with a total number of approx. 3.5 million cells. It took about a week (150 hours) to run a simulation time of 10 minutes on a computer with the following hardware: 2 AMD EPYC 7402 24-Core Processor with 265 GB memory.

The fire spread mechanism was simulated by an ignition temperature of the wood, both wood crib and CLT, of 300 °C and a prescribed burning rate, i.e., a heat release rate per unit area, of 260 kW/m^2.

A reference simulation was conducted with no wind added, and compared against a simulation with a constant wind of 2 m/s coming diagonally from behind the compartment, as in the real experiment, see Fig. 30.

The effect of the exposed back wall in #FRIC-02 was simulated by removing the exposed back wall and replacing it with gypsum boards, as in #FRIC-01. The results of the two different configurations were then compared.

Fig. 30 The wind was coming diagonally from behind the compartment, as seen by the direction of the smoke. The image was taken by a drone.

2.4.2 Main results

In many ways, the simulation was able to reproduce key results of #FRIC-02, including the fast fire spread rate and the non-symmetrical external flames, despite using a simple fire spread model.

In the simulation, the fully developed fire was reached at 02:47 (mm:ss), i.e., 26 seconds earlier than in #FRIC-02. Of those 26 seconds, 17 seconds could be assigned to a faster ignition of the CLT ceiling.

The fire spread mechanisms were visually similar to what was observed in #FRIC-02. After ignition of the ceiling, the flames first spread under the ceiling and the upper part of the wall. Shortly after, the fire spread across the wood crib and lower part of the wall.

The simulation with the implemented wind conditions of #FRIC-02 (Fig. 30) was able to reproduce the non-symmetrical flames to a large extent, see Fig. 31 and Fig. 32, while the simulation without any wind had more symmetrical flames. The simulation with wind also revealed that a significant underpressure was created outside Window 4 when the wind was coming diagonally from behind. This underpressure assisted in dragging smoke and flames mainly out of Window 4, similar to what was observed in #FRIC-02. Also, the simulation reproduced that the external flames covered the entire window height and effectively inhibited air inflow through that window. The uneven air supply in the simulation also here created an almost homogeneous temperature inside Window 4, while large temperature variations were seen for the other parts of the compartment.
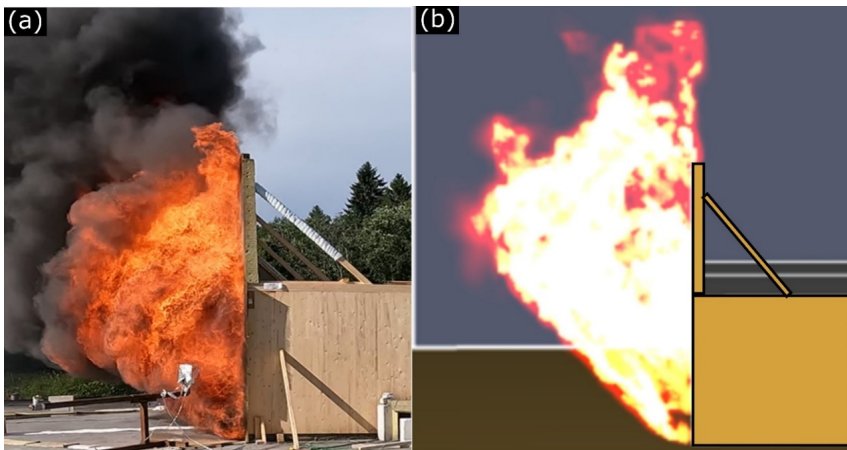

Fig. 31 The external flame covered the entire window height in both #FRIC-02 (a) and the simulation (b). The images are taken shortly after flashover.
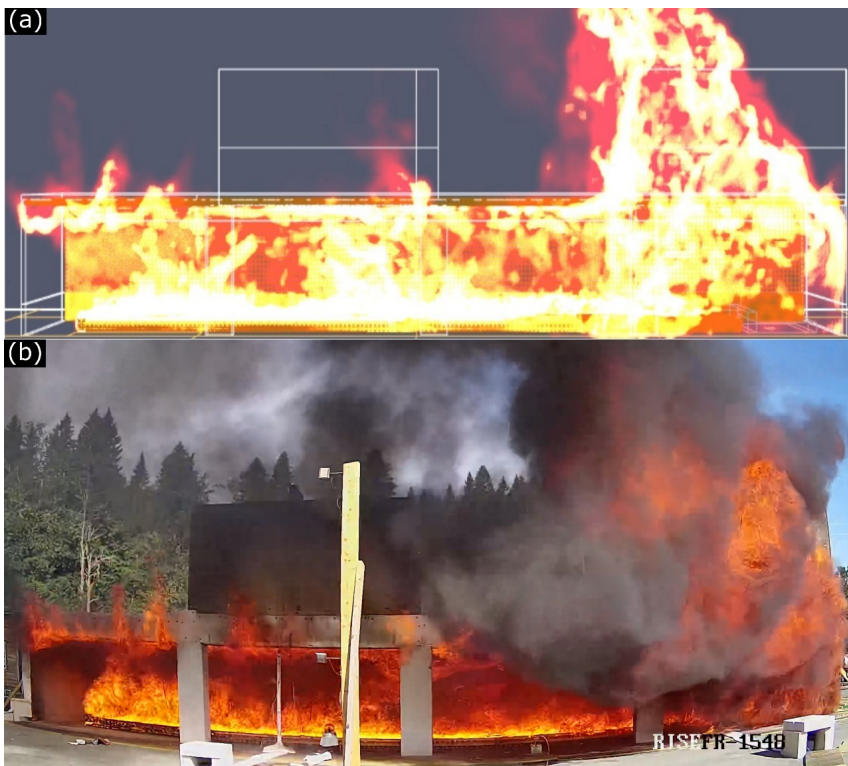
Fig. 32 The simulation (a) was able to reproduce the non-symmetrical external flames in #FRIC-02 (b).

2.5 Paper IV – Experimental study of the charring of I-joists and recession of combustible insulation in light timber frame assemblies with comparison to Eurocode 5

This section presents a short summary of the method and the most important results of Paper IV [76].

2.5.1 Method

Two I-joist types (see Fig. 33), solid wood and laminated veneer lumber (LVL), each with three different flange sizes and four combustible insulation products, have been tested in a furnace. The insulation used was cellulose fibre loose-fill, wood fibre loose-fill, wood fibre batt and a phenolic foam batt.
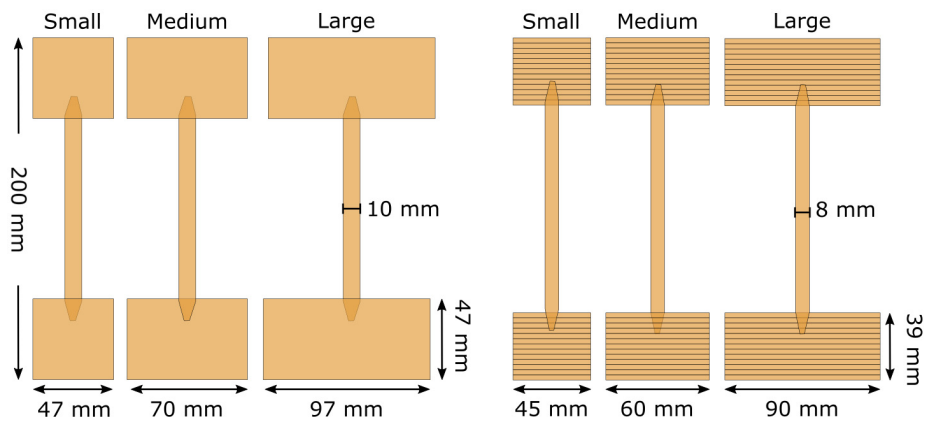
Fig. 33 Overview of the two flange types: solid wood and LVL, with three different flange sizes.

The I-joists were installed in a timber frame with two chambers. In each chamber, one type of I-joists with three different flange sizes was installed. The cavities between the I-joists and the frame were completely filled with insulation. The build-up and dimensions are shown in Fig. 34.

Five test specimens were prepared and tested in accordance with the standardised time-temperature curve. The specimens were installed with a 15 mm gypsum board type F on the exposed side. The tests were run until the gypsum board naturally fell down and for some period longer after that. The duration of the furnace testing varied from 40-75 minutes depending on how well the insulation protected the flanges.

After the end of the tests, the hot surface was rapidly cooled down to stop any further charring of the I-joists and combustible insulation.

Pieces of the I-joists were cut out, and the final char depth and cross-sectional area were measured. Based on temperature readings from the embedded TCs, the charring rates of the flanges and the recession rates of the combustible insulation were calculated.

At last, the obtained charring rates were compared with the calculated values of the design model for rectangular members in the current Eurocode 5 [54] and the model for I-joists proposed in the upcoming Eurocode 5 [58].
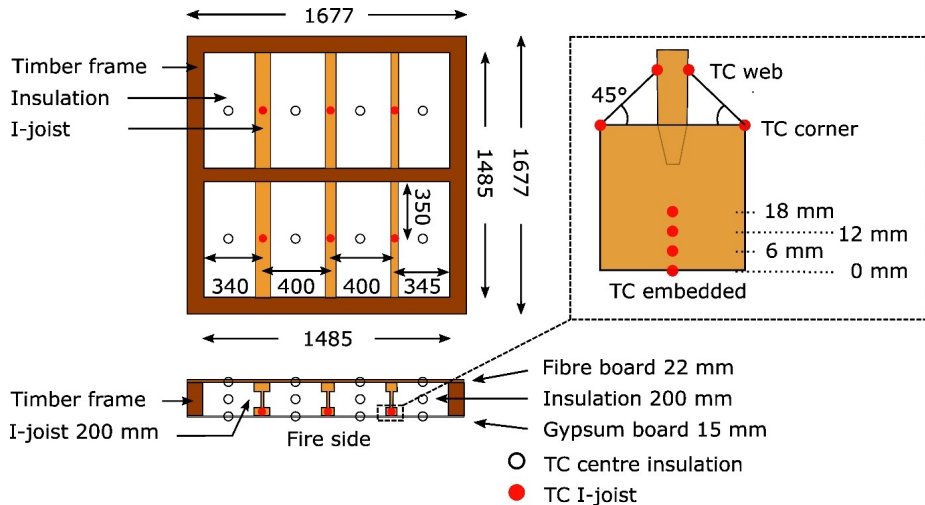
Fig. 34 Build-up of test specimen in plan and cross-section, and position of thermocouples. Dimensions in mm.

2.5.2 Main results

The remaining cross-section area of all I-joist flanges had a trapezoid-like or rounded shape, which is characteristic of lateral charring. Hence, the experiments clearly demonstrated two-dimensional charring of I-joists when protected with combustible insulation, see Fig. 35.

Moreover, the charring rates of the flanges of solid wood and laminated veneer lumber (LVL) were comparable, and the charring rate decreased with increasing flange size. Despite large differences between the different insulation products, all four insulation products had a lower recession rate than typical reported values for glass wool insulation (15-28 mm/min [77]). In addition, the cellulose insulation had a recession rate as low as 1.1 mm/min, which is lower than any value reported for combustible insulation earlier. The obtained recession rates are presented in Table 1.

Table 1 Recession rates measured next to the flange for the different insulation types.

Insulation	Recession rate ± std. deviation [mm/min]
Wood fibre batt	3.3 ± 0.7
Wood fibre loose-fill	2.3 ± 0.5
Phenolic foam batt	5.7 ± 2.3
Cellulose loose-fill	1.1 ± 0.04

49%   52%   57%   55%   58%   69%
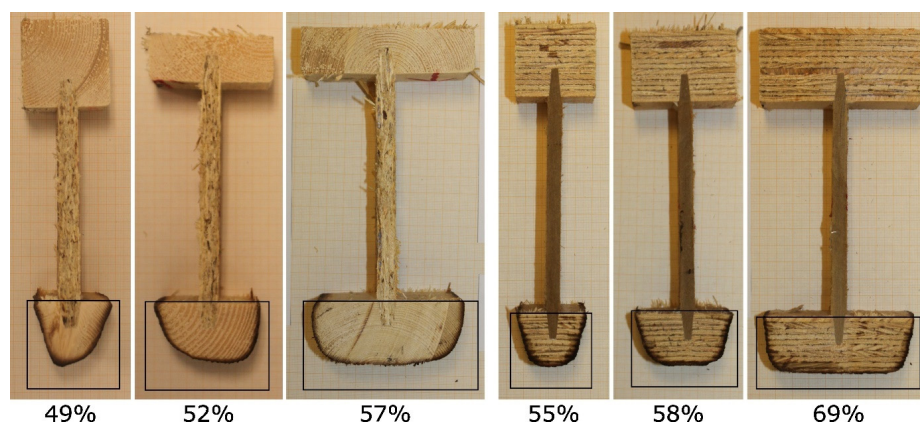
Fig. 35 Example of remaining cross-sections for I-joists with different flange sizes and types. The black rectangles show the size of the flanges before exposure to fire, while the numbers represent the remaining cross-section area. The I-joists to the left have a solid wood flange, while the ones to the right have flanges of LVL. The I-joists are from Test no. 4 and were protected with wood fibre insulation.

The low recession rates found can possibly be explained by a different test setup and negligible shrinking of the insulation compared to other tests. Further, the recession rates in this test series were mainly measured in the protected phase, while reported values are often reported for the post-protected phase.

When comparing the charring rates against the design model of rectangular cross-sections in the current version of Eurocode 5 [54], all charring rates in the protected phase were lower than the calculated ones. Compared to the new design method for I-joists in the final draft of the new Eurocode 5 [58], the calculated charring rates were closer to the measured ones, and most calculated values were on the conservative side. The comparison of the experimental and calculated charring rates is given in Table 2.

.

Table 2 Charring rates calculated based on results from the experiments during the protected phase compared to calculated charring rates based on EN 1995-1-2:2004 (current Eurocode 5) and prEN 1995-1-2:2021 (final draft of the new Eurocode 5).

Test ID[1]	Experimental	EN 1995-1-2:2004		prEN 1995-1-2:2021	
	$a1_{max}$	β_m	$\beta_m - a1_{max}$	β_m	$\beta_m - a1_{max}$
Test 1	[mm/min]	[mm/min]	[mm/min]	[mm/min]	[mm/min]
T1MaSHb	0.56	0.79	0.23	0.69	0.13
T1MaMHb	0.45	0.67	0.22	0.60	0.15
T1MaLHb	0.43	0.67	0.24	0.54	0.10
Test 2					
T2HuSClf	0.58	0.79	0.22	0.70	0.12
T2HuMClf	0.58	0.67	0.09	0.63	0.05
T2HuLClf	0.61	0.67	0.06	0.55	-0.06
T2MaSClf	0.61	0.79	0.18	0.69	0.08
T2MaMClf	0.54	0.67	0.13	0.60	0.05
T2MaLClf	0.52	0.67	0.15	0.54	0.02
Test 3					
T3HuSHlf	0.69	0.79	0.11	0.70	0.01
T3HuMHlf	0.60	0.67	0.07	0.63	0.03
T3HuLHlf	0.40	0.67	0.27	0.55	0.15
T3MaSHlf	0.76	0.79	0.03	0.69	-0.08
T3MaMHlf	0.65	0.67	0.02	0.60	-0.06
T3MaLHlf	0.54	0.67	0.13	0.54	0.00

1) The Test ID is built up as follows: T1: Test no. 1. Ma and Hu are the I-joist types, where Ma is solid and Hu is LVL. S, M, and L are the flange sizes. b is insulation batt, while lf is for loose-fill insulation.

In general, the insulation stayed well in place after gypsum board failure. This is believed to be due to the I-joist profile, which is beneficial in keeping the insulation in place. This advantage could be exploited in practical installation of insulation.

Due to the lack of repetitions of the experiments, results should be considered as indicative.

2.6 Additional results from the CLT experiments

This section adds new details to the results in Papers I and II and provides additional results not published earlier.

2.6.1 Reversed temperature gradient at back wall

In #FRIC-02, large temperature variations were measured, and several examples have been given. For instance, it was mentioned that the temperature gradient decreased with increasing height close to the wall inside Window 4. This is shown more clearly here. Fig. 11 presents temperatures at five different heights 0.1 m away from the back wall at two different locations: X = 7.0 m, which is in the centreline of Window 2, and X = 16.5 m, which is in the centreline of Window 4.

Fig. 11 shows that the temperatures at X = 7.0 m had a typical behaviour with increasing temperatures for increasing heights. For X = 16.5 m, however, there was a non-typical behaviour. Until approx. 3 minutes, the temperature gradient was normal, while it became reversed after 3 minutes, i.e., the highest temperatures were located close to the floor and the lowest temperatures close to the ceiling. This clear trend lasted until approx. 8 minutes, where the maximum temperatures shifted to 1.8 and 2.1 m height. First after 14.5 minutes, the maximum temperature was again located at the highest ceiling height. The temperature at 0.3 m height at this time was likely higher than at 1.1 m height because the TC was located much closer to the burning wood crib.

Another related observation was that the temperatures at X = 7.0 were almost uniform in the most intense burning phase. At 3-7 min, there was less than 100 °C difference between the minimum and maximum temperatures. At X=16.5 m, the difference was more than 200 °C.

The reason for this behaviour is not perfectly understood, but it is likely related to the different oxygen concentrations of those two locations. One hypothesis is that the oxygen concentration in X= 16.5 m was highest at the lower heights and was reduced with increasing heights.
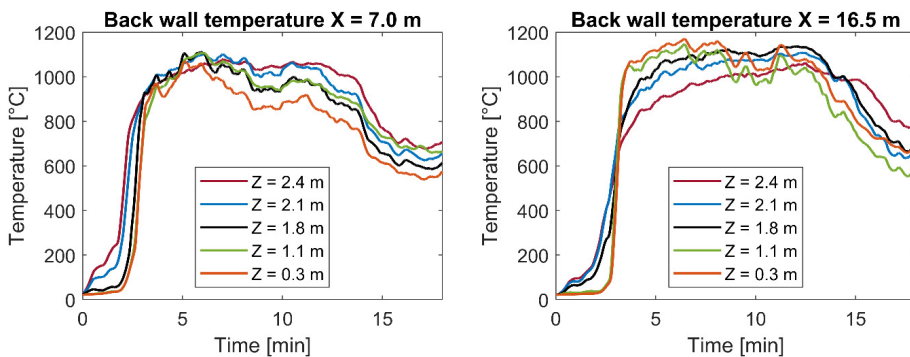

Fig. 36 Temperatures at different heights (Z) 0.1 m from the back wall in #FRIC-02. At X = 7.0 m, the temperatures increase with increasing height, while for X = 16.5 m, the temperatures decrease with increasing height between 3 and 8 minutes. The temperatures are averaged over 30 seconds.

2.6.2 Ceiling temperatures

Ceiling temperatures for different distances away from the back wall are given in Fig. 37. At X = 16.5 m, the temperatures inside the compartment (i.e., excluding Y = 0.0 m) increased with increasing distance from the back wall. The largest increase occurred from Y= 4.9 m to Y= 3.9 m. Over time, the temperature at Y = 4.9 m increased, while the other temperatures remained almost constant. At 12.5 minutes, the temperatures at Y = 3.9, 2.5 and 1.1 m dropped significantly, and from 14 minutes, the temperature at Y = 4.9 m was the highest and experienced a significant reduction from 15 minutes. This change was likely linked to the cessation of flames at the CLT, where the flames started extinguishing earlier at distances closer to the window opening and last closest to the wall.

At X = 7.0, the temperatures were more uniform, and no clear temperature gradient was present until 8 minutes. However, from this point, there was a weak temperature gradient with higher temperatures closer to the back wall. Also here, the temperatures dropped rapidly after 12.5 minutes, and it appears that the extinguishment of flames at the CLT started at the location closest to the opening and last closest to the back wall.
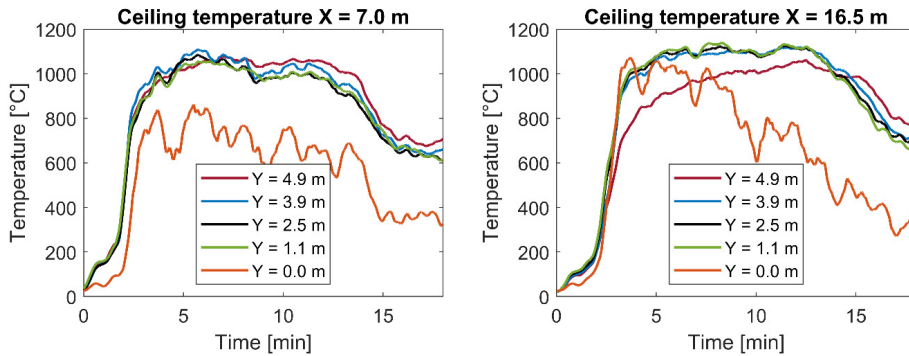

Fig. 37 Temperatures at different distances (Y) from the opening 0.1 m below the ceiling (Z=2.4 m) in #FRIC-02. Y= 0.0 is in the window opening, and Y = 4.9 m is 0.1 m from the back wall. X = 7.0 m is the centreline through Window 2, and X = 16.5 m is the centreline through Window 4. The temperatures are averaged over 30 seconds.

2.6.3 Average gas temperatures

Although temperatures have been presented in different ways in Paper II, this section gives another perspective by comparing average gas temperatures of #FRIC-02. In Fig. 38, average gas (TC) temperatures are presented for different locations along the length of the compartment (X). The presented values are the average of five TCs at height (0.32 m, 0.82 m, 1.12 m, 1.82 m, 2.02 m, 2.42 m) and averaged over 60 seconds. Due to the non-uniform spacing along the height, the averaged values are slightly shifted towards the temperatures at higher heights. Nevertheless, the average values give a good overview of how the temperatures varied at different locations in the compartment. Shortly after flashover (4 ± 0.5 min), the gas temperatures were highest at the ends of the compartment and lowest in the centre. At the right end of the compartment (X ≥ 16.5 m), the temperatures were very

uniform, and this location had the highest average temperatures in the post-flashover phase. The difference to other locations became higher with increasing time. That the average temperature started decreasing first at the left end (X = 1 m) makes sense since the crib and the CLT started burning first at this location.
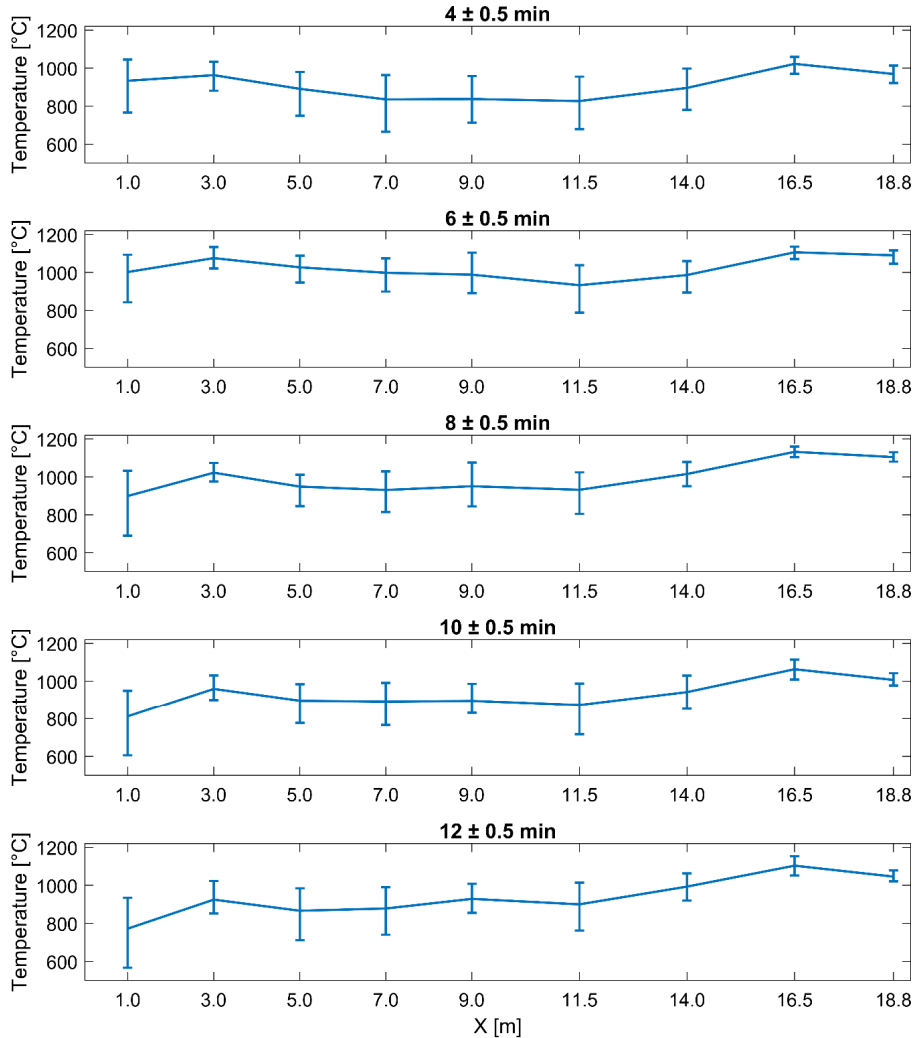
Fig. 38 Comparison of average temperatures at different X-locations through the centre of the compartment, i.e., Y = 2.5 m. The average temperature represents the average temperature for each TC tree and is averaged over 60 seconds. The error bars show the minimum and maximum temperatures in this period.

Fig. 15 shows the average temperature for each TC tree along the Y-axis at X = 7.0 m (Window 2) and X = 16.5 m (Window 4). This comparison shows large differences in the gas temperatures at these two locations of the compartment. Inside Window 2, there was a decreasing temperature gradient from the back of the room (Y = 4.9 m) towards the window opening (Y = 0.0 m). The difference between the minimum and maximum temperatures was 250 °C for the TC-tree at the back of the room and increased to approx. 750 °C for the TC-tree in the opening.
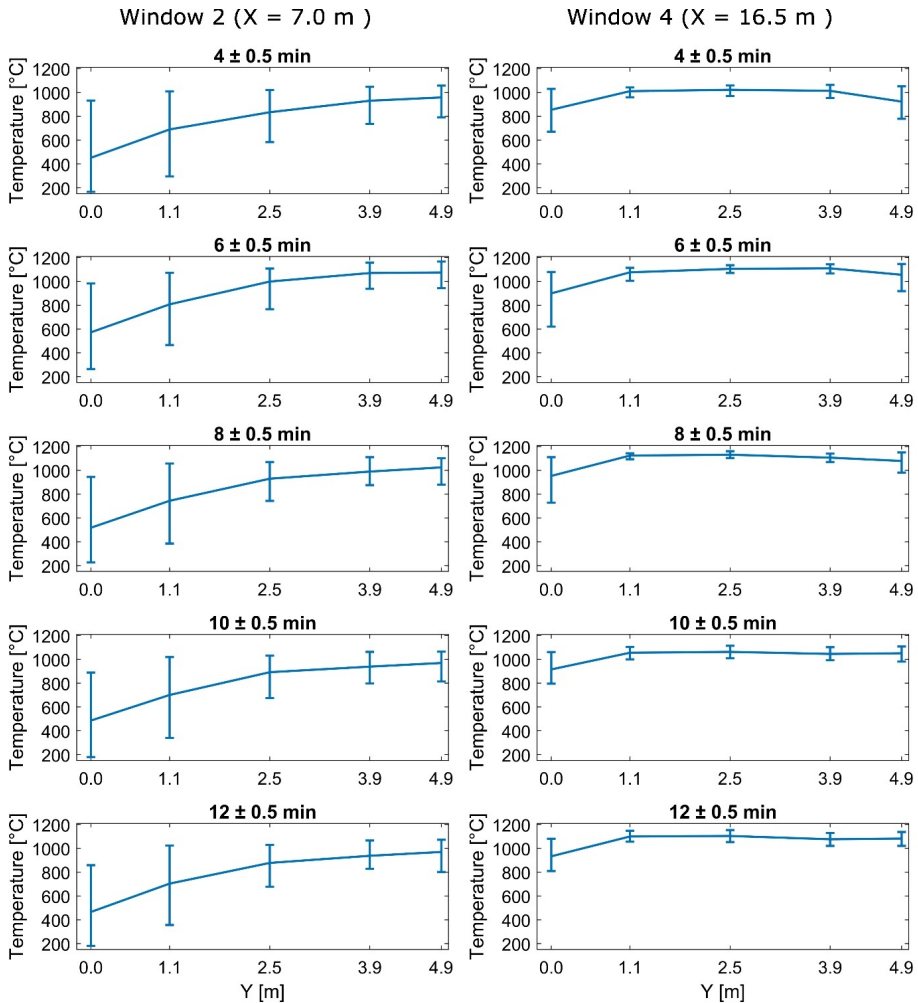

Fig. 39 Comparison of average temperatures at different Y-locations through the centreline through Windows 2 and 4. The average temperature represents the average temperature for each TC-tree and is averaged over 60 seconds. The error bars show the minimum and maximum temperatures in this period.

Inside Window 4, however, the temperatures were more homogenous. For Y = 1.1 – 3.9 m, the difference between minimum and maximum temperatures was approx. 100 °C. Lower average temperatures and larger difference between minimum and maximum values were present close to the wall (Y = 4.9 m) and in the opening (Y= 0.0 m).

The differences can be explained by the different flow fields in the compartment, where air was mainly supplied through Windows 1-3, as discussed further in Paper II.

2.6.4   Moisture migration

Clear signs of moisture migration inside the CLT elements were observed at the edge of the back wall, see Fig. 40. This is recognised by the water/foam bubbles at the surface of the edge of the back wall. In addition, layers 2 and 4 appear more wet than layers 1, 3 and 5, which makes sense based on the lamella orientation of the different layers. The moisture content was not measured, but this should be more focused on in future experiments.
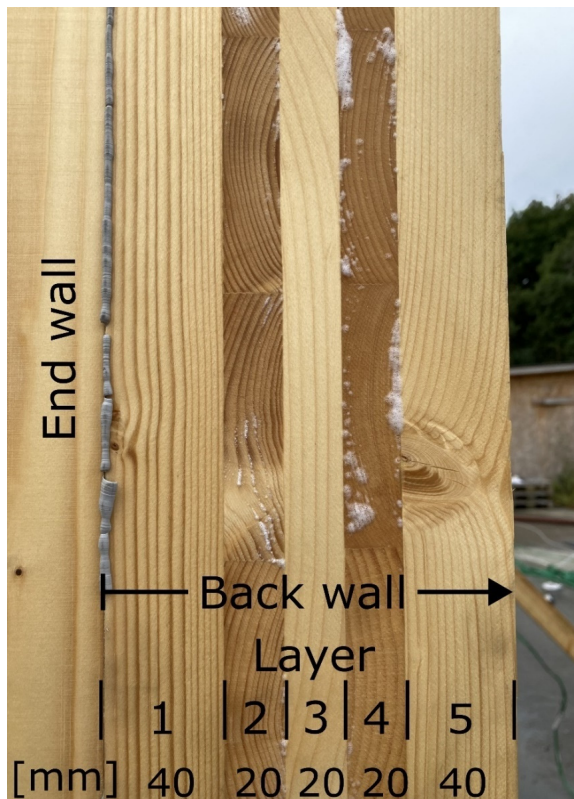
Fig. 40 Water migration towards the CLT edges of the back wall was observed after the experiment was terminated. This is recognised by the apparently wet surface of layers 2 and 4 and foam appearing out between the yearlings. The grey stuff on the left is fire sealant between the back wall and the end wall.

2.6.5 Charring of the wall in #FRIC-02

As explained in Paper II, the charring was more pronounced at the lower parts of the wall and less charred close to the end walls. This section extends the visual observations of the non-uniform charring.

Fig. 41 shows a part of the back wall and visualises that the charring was less pronounced at the upper part of the wall. This is recognised by most of the 4th layer remaining, while at lower heights, only small parts of the 4th layer are remaining. The build-up of the CLT layers is shown in Fig. 40.
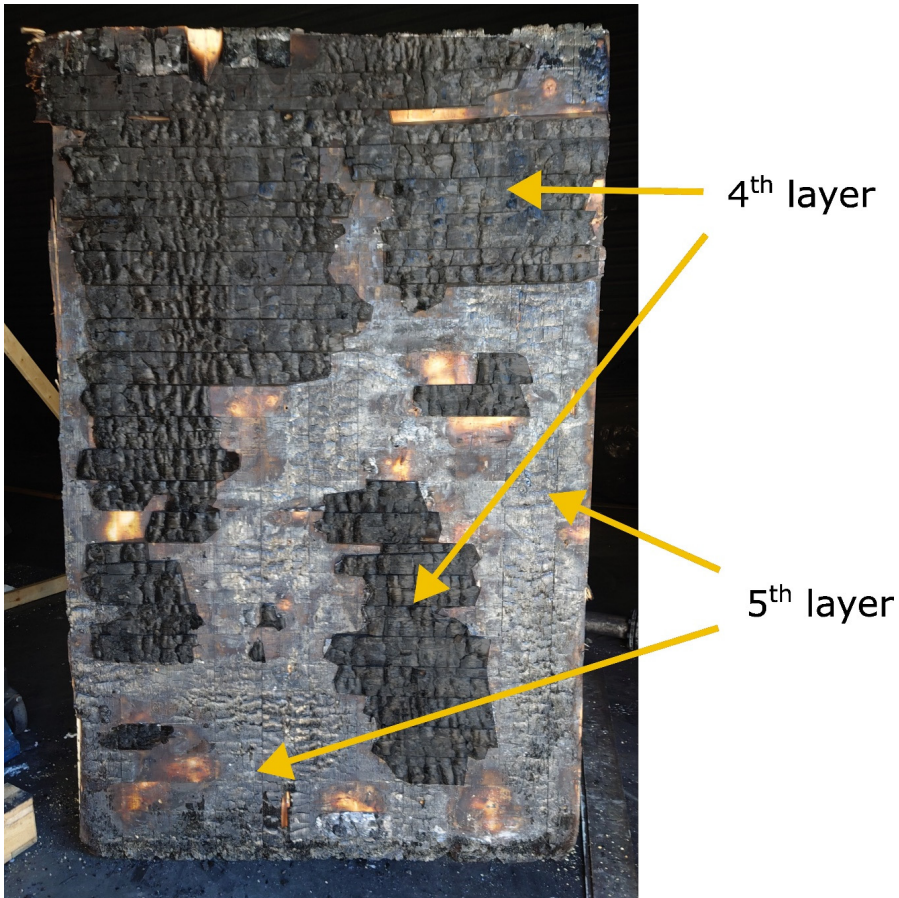
Fig. 41 Charring of a part of the back wall from #FRIC-02. The charring was less pronounced at the upper part of the back wall. This is recognised by the 4th layer almost fully remaining at the upper part, while the 4th layer is completely gone at the bottom of the wall. For information, the 1st layer was the originally exposed layer. A black colour filter is added to the 4th layer in the image to better separate it from the 5th layer. The back wall element was originally much wider but broke into pieces.

Fig. 42 shows less charring of the back wall close to the end wall. This is recognised by more of the 4th layer remaining at the leftmost part of the wall compared to the rightmost part of the image.

Fig. 42 Charring of the back wall close to the left end wall of #FRIC-02. The back wall is less charred closer to the end wall. The bright spots are fresh wood and show areas that recently have been exposed due to the fall-off of the layer above. A black colour filter has been added to the image to separate the remaining layers better.

Fig. 43 shows that the end wall was significantly charred behind the two layers of gypsum board type F [68]. Interestingly, the charring pattern here differed from the pattern on the back wall, i.e., the charring was mostly pronounced at the upper part of the wall. This is recognised by the 1st layer remaining only at the lower part. Moreover, in the middle part, the second layer is only discoloured, which means that the first layer recently has fallen off. At the upper part of the wall, the 1st layer has been fully consumed, and a clear charring of the 2nd layer can be seen.

The non-uniform charring of the back wall and the ceiling could be explained by differences in oxygen concentration and temperatures throughout the compartment. For the end walls, the influence of oxygen was only minor as gypsum boards still covered the end wall until extinguishing took place, see Fig. 44. During the extinguishing process, the gypsum boards broke into pieces, and the CLT on the end walls became exposed. Thus, most of the wall was likely not exposed to oxygen during the experiment, but the upper part of the wall may have been exposed to some oxygen after some time.

This would occur as a result of the ceiling above the top edge of the gypsum board being consumed, which provides a path for oxygen to enter behind the gypsum board.

Hence, the increased charring at the upper part of the wall is likely due to increased temperatures with increasing heights and possibly the presence of oxygen after some time.
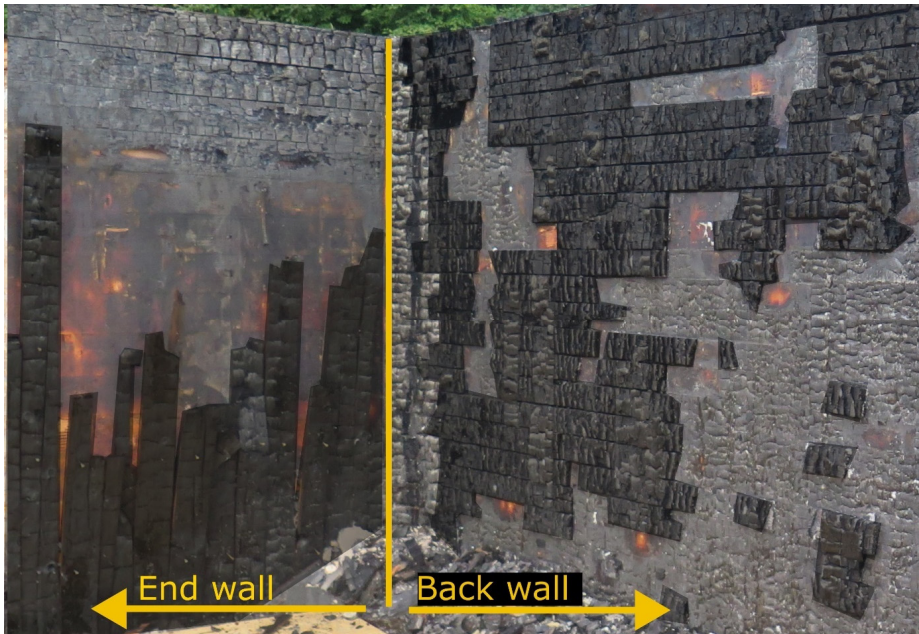
Fig. 43 Comparison of charring of the left end wall and the leftmost part of the back wall of #FRIC-02. The end wall was protected with 2 x 15 mm gypsum boards type F [68] until extinguishment. The image is taken after extinguishment and thus without gypsum boards.

Fig. 44 The gypsum boards at the end walls were intact until the extinguishment of #FRIC-02. The image also shows that the fire was far from being close to self-extinguishing when manually extinguished. Image from 175 minutes

Fig. 45 visualises some additional damages not shown in Paper II. The facade wall above Window 4 was clearly damaged by fire despite being protected with 30 mm stone wool. Buckling of the back wall can be seen in several places. Furthermore, there are signs of charred and burned areas at the bottom of the wall and at the joint between the back wall and the ceiling. This highlights that a fire could penetrate joints much faster than through the core of the elements. Thus, construction details are critical to ensure compartmentation in CLT buildings exposed to long-duration fires.

Fig. 45 Damages seen from the back side of the compartment of #FRIC-02 after the end of the experiment.

3 Additional details of the CLT experiments

This chapter extends the method description of the CLT experiments (Papers I and II) and gives insight into details relevant to others planning a large-scale CLT fire experiment. The method is also evaluated with a critical eye to improve the experimental setup in a future experiment.

3.1 Construction and test setup details

3.1.1 Time schedule of construction

An overview of how the compartment was built is given in Fig. 46. In total, it took 13 working days to prepare the compartment before the first experiment. However, before the construction started, all sensors had been labelled, the TC trees were prepared, and the facade walls were built. After the first experiment, all TCs and PTs were taken down, and gypsum boards and insulation on the ground were removed. Then, the ceiling was lifted off and replaced by a new one. All TCs were controlled, damaged ones were replaced, and the instrumentation was installed again. The scale measuring the mass loss of the small crib was rebuilt, and the small and large continuous cribs were again prepared. The reset of the experimental setup took four working days. There are both pros and cons of having such a tight time schedule. By running the experiments directly after each other within relatively few days, the costs of renting the testing area, personnel, etc., are kept at a minimum, weather conditions are more likely to be about the same, and the moisture content of the wood crib is less likely to change much. On the contrary, with a tight schedule, there is less time to make any major improvements to the experimental setup, and there is little time to go through and check that all the data and video recordings look fine.

3.1.2 Gypsum boards and protection of the back wall

To maintain the back wall undamaged through the first experiment, it was protected by two layers of 15 mm gypsum boards type F [68]. The outer layer was shifted half a board width to avoid overlapping joints. In addition, it was decided to avoid having screws too close to the edge, as this has been shown to increase the likelihood of cracking and failure of gypsum boards [78]. Hence, a screw pattern template was made to ensure an identical screw pattern for all gypsum boards, see Fig. 47. No spackling paste was added to the joints based on experience from furnace testing, showing that this has little effect on the fire performance, and to save time.

A zone model made by Daniel Brandon [79] was used to estimate the temperatures behind the gypsum boards. It was concluded that two layers should be sufficient to protect the timber without any charring. The calculations were correct, and the wall appeared undamaged when the gypsum boards were removed, see Fig. 48.

Three TCs were installed at the intersection between the gypsum board and the back wall to control the temperatures the wall was exposed to. Such measurements are recommended as

they give a live indication of whether the protection provided by the gypsum board is sufficient to properly protect the CLT.

Fig. 46 Images from the rigging of the compartment and the final experimental setup. The image at the bottom is from #FRIC-01.
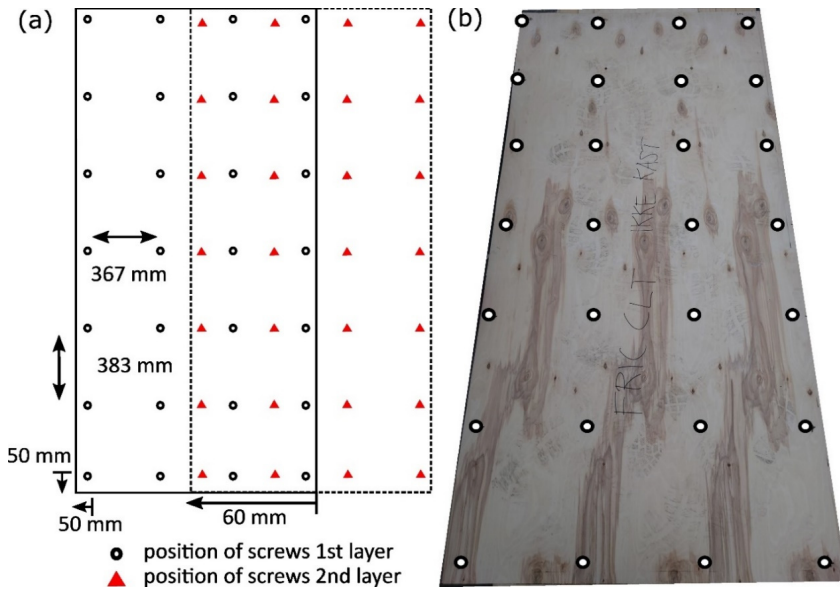
Fig. 47 a) Screw pattern for gypsum boards. Solid lines show the first layer, and dotted lines show the second layer. b) Screw pattern template. All holes have in the figure been marked with a symbol for easier visualisation.
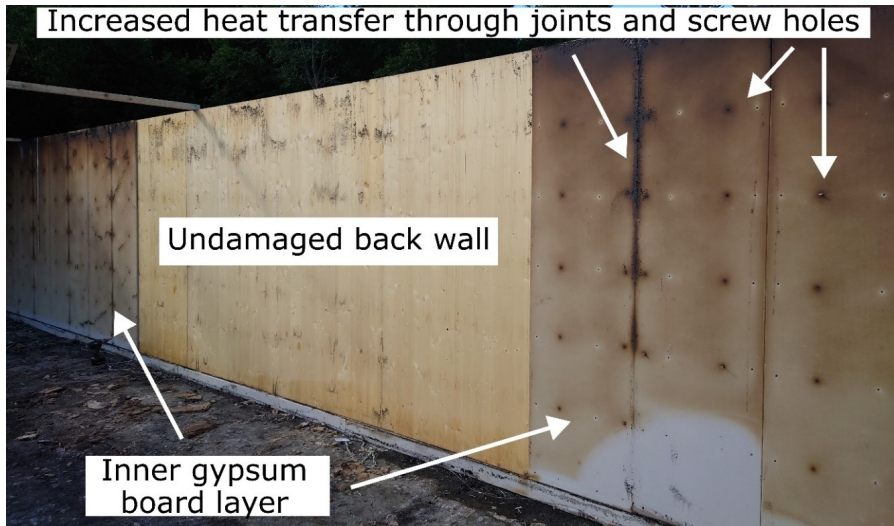
Fig. 48 The CLT back wall appeared undamaged after #FRIC-01 when the two gypsum board layers protecting it were removed. The gypsum boards shown belonged to the innermost layer. Increased heat transfer was seen at the joints between gypsum boards at the outermost layer and through the screws at which the outermost layer was fixed to the CLT.

After the removal of the gypsum boards, the walls seemed quite moist after being left with moist gypsum boards attached for two days after extinguishing. However, the wall dried up sufficiently until the second test day, and the moisture content in the CLT elements was measured to 14%. As the new CLT ceiling had a moisture content of 13%, we do not consider this increase a flaw in the experimental setup. However, for future experiments, it is recommended to remove wet gypsum boards earlier or allow a longer time for the reused CLT to dry up.

3.1.3   Protection of the glulam beam

A glulam beam was located above the window openings to support the ceiling elements and distribute the load to four columns of aerated concrete. The glulam beam was protected with two overlapping layers of ceramic fibre insulation to avoid joints leading directly to the wood, see Fig. 49. This setup protected the glulam beam well after the first experiment, and the beam was reused in the second experiment, but with new insulation. In #FRIC-01, several hot spots were detected by an infrared camera in the corner between the exposed ceiling and the protected beam before extinguishment. After extinguishment in #FRIC-02, smouldering burned a hole through the ceiling at two locations and transitioned to flaming combustion. Thus, it seems likely that the insulation facilitated ideal conditions for those hot spots to occur.

Fig. 49 The glulam beam was protected with two overlapping layers of 25 mm ceramic fibre insulation. This was sufficient to protect the beam in #FRIC-01.

3.1.4   Protection against rain

The weather in Trondheim, Norway, is quite unstable, and since the experiments were conducted outdoors, measures had to be taken to prevent the CLT elements from exposure to rain. Large tarps were used to protect the compartment during the rigging time, as seen in Fig. 50. This worked quite well, although securing them properly took longer than anticipated. The compartment was built on a testing area with a 2% tilted floor to accumulate contaminated extinguishing water. Without any countermeasures, this tilted angle would have caused any water on the backside of the compartment to flow straight through the compartment and

soaked the insulation batts. To avoid this, a sealant was added under the wall. With the back wall sealed, any water would then accumulate on the back side of the compartment, as seen in Fig. 51. Any accumulated water was quickly removed.

Fig. 50 The compartment was protected against rain with several large tarps.
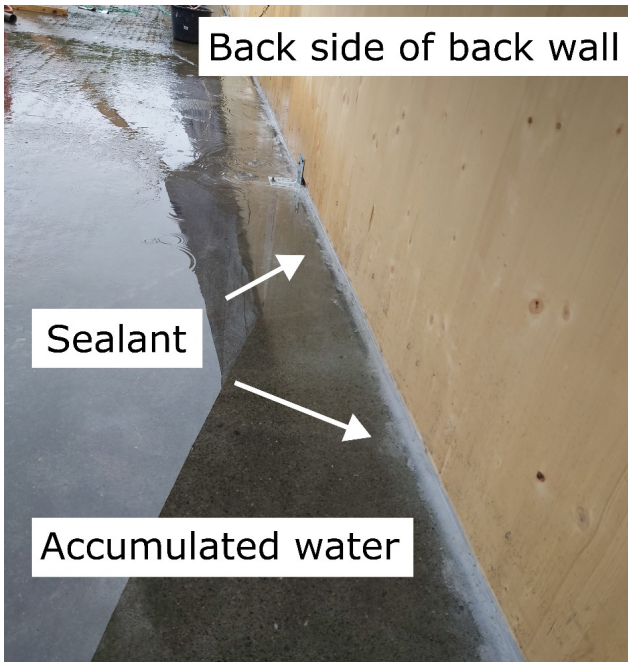
Fig. 51 Accumulated water on the back side of the compartment after a rain shower.

If the CLT back wall had been positioned directly on the ground, it would have been directly in contact with this accumulated water, and the lower part of the CLT would likely have been quite moist. This was avoided by having a bottom plank directly on the ground and the wall on top of that, see the top left image in Fig. 46.

The tilted floor also caused the ceiling height to vary slightly in the compartment, from 2.47 m at the back wall to 2.57 m at the opening. However, the wood crib was levelled so that the distance to the ceiling was uniform across the entire crib.

3.1.5   Storing and drying of the wood sticks for the crib

To lower the cost of the wood crib, the wood sticks were ordered from a local sawmill and had a high moisture content when they arrived. For three months, they were stored and dried inside. As storing 4000 m of wood sticks is quite space-consuming, the longest sticks (Fig. 52) had to be moved to an outdoor tent two weeks before the first experiment, as the area was booked for other activities. When measuring the moisture content of the wood sticks, the long sticks had a higher moisture content than the shorter ones. This difference was likely due to the different storage conditions the last weeks. Although the tent protected against rain, the temperatures were lower than indoors, especially at night, and the relative moisture content of the air was probably higher. For future experiments, storing all wood sticks in the same conditions until testing is recommended.

Fig. 52 The wood sticks for the cribs were dried indoors for several months before the experiments.

3.3 Wood crib

When using a wood crib as a fuel, it is important to consider that the geometry and the porosity factor, i.e. the ratio of the air-to-fuel mass flow rates, could have an impact on the burning behaviour [73]. The porosity factor (ϕ) is given through Eq. (2).

$$\phi = \frac{A_{CS}}{A_S} \cdot s^{0.5} b^{0.5} \tag{2}$$

where, A_{CS} is the total cross-sectional area of the vertical shafts in the crib [cm^2], A_S is the total surface area of wood exposed to air [cm^2], s is the pacing between the sticks and b is the thickness of a single wood stick [cm].

For burning of wood cribs, two regimes have been defined: 1) The porosity-controlled regime ($\phi < 0.075$ cm) and the open regime ($\phi > 0.075$ cm). In the porosity-controlled regime, the burning rate is controlled by how much air that can be drawn into the crib. In the open regime, the spacing does not have any effect on the burning rate and the shafts are considered well-ventilated. The burning is instead controlled by the thermal feedback from the compartment and the geometry of the wood crib. The porosity factor of #FRIC-01 and -02 was 0.19 cm, which is well above the threshold for the open regime. In comparison, the porosity factor of the Malveira experiment [44] was 0.25 cm, and thus quite similar.

3.4 Ignition package

The wood crib was, in both experiments, ignited with heptane. Due to local draft conditions in #FRIC-01, the heptane fire was tilted away from the wood crib (Fig. 53), and when the heptane fire burned out, the wood crib fire almost extinguished with only 5 cm of the crib burning with small flames.

Fig. 53 The heptane fire in #FRIC-01 was tilted away from the wood crib due to local draft conditions, and very little of the wood crib was burning when the heptane fire burned out.

Although it is unfortunate to change the ignition package for experiments that are meant to be compared, it was considered too risky to keep it unchanged. It was feared that slightly different wind conditions or a wood crib with a marginally higher moisture content would cause the wood crib to extinguish completely. Hence, the number of heptane trays was increased from 10 to 14, and the amount of heptane in each tray was increased from 0.5 L to 0.7 L, with a total increase of the heptane from 5.0 L to 9.8 L. In addition, the trays were located more under the crib for easier ignition of the wood sticks at the end.

Considering a heptane amount of 5.0 L in #FRIC-01, a density of 684 kg/m^3, a heat of combustion of 44.5 MJ/kg, a burning efficiency of 0.8 and a burning time of 180 seconds, the average HRR was approx. 0.7 MW. The HRR of the wood crib in this period is considered negligible.

With a burn-out time of 210 seconds in #FRIC-02, the average HRR from the combustion of heptane was approx. 1.1 MW. During the initial fire, about 0.15 m of the crib was burning. Also this fire was partly tilted towards the end wall. The maximum HRR of the wood crib fire before ignition of the ceiling was calculated to be approx. 0.3 MW, when considering a burning rate of $7.5 \cdot 10^{-3}$ kg/s per 50 mm length (similar to the maximum rate measured by the scale), a net heat of combustion of 16 MJ/kg and a combustion efficiency of 0.8. Thus, the initial fire size in #FRIC-02 was approx. 1.4 MW and about twice as large as in #FRIC-01.

A relevant question is, therefore, whether a fire size of 1.4 MW is unrealistically high for a typical CLT compartment. According to Zulmajdi et al. [80], a fire size of 1.4 MW could be caused by several ordinary items, including an armchair, a cabinet or a bed/sofa. Such items are found in most buildings, and it is therefore concluded that the ignition package was not unrealistically large.

For the direct comparison of the experiments, it was unfortunate that the ignition package was changed. Nonetheless, the different ignition methods gave some results that would not have been seen without the change. In #FRIC-01, the fire dynamics were clearly changed by the ignition of the ceiling. This change was not that clear in #FRIC-02, as the fire burned so shortly before the ceiling was ignited. Moreover, the larger ignition package in this experiment demonstrated that a fast ignition of the ceiling could occur with a fire size that is expected to occur for several ordinary items.

In a future experiment, however, it is recommended to test the ignition setup before the actual experiment. The crib must be built identical in width and height but does not have to be so long. 0.3 - 0.5 m would be sufficient for the preliminary test. With such a setup, the positioning, number of trays, and the heptane amount could be determined in an iterative process.

The setup and amount of heptane were inspired by other travelling fire experiments [23, 40, 44], where the wood cribs were ignited at one end by a line burner. A comparison of the different ignition packages is given in Table 3.

Table 3 Comparison of ignition packages for different travelling fire experiments

Experiment	Code Red #01 [23]	Code Red #02 [46]	Malveira [44]	#FRIC-01	#FRIC-02
Number of trays	12		1	10	14
Area of trays	150 mm x 250 mm		2.4 m x 0.1 m	150 mm x 220 mm	
Total fuel area	0.45 m^2		0.24 m^2	0.33 m^2	0.46 m^2
Fuel per tray	0.5 L of methanol	1.0 L of methanol	5 L kerosene 0.5 L diesel	0.5 L of heptane	0.7 L of heptane
Total fuel volume	6.0 L	12.0 L	5.5 L	5.0 L	9.8 L
Width of wood crib	6.0 m		2.4 m	2.8 m	
Wood sticks	30 mm x 30 mm		50 x 50 mm^2	50 mm x 50 mm	
Fuel area per meter of crib width	0.08 m^2/m		0.10 m^2/m	0.12 m^2/m	0.17 m^2/m
Position of trays	Below crib		In front of the crib	5 cm below the crib	15 cm below the crib

As seen from the table, the ignition package of #FRIC-01 was not smaller than the ones from the Code Red and the Malveira experiments. However, the crib dimension in Code Red was smaller and would thus ignite faster, but on the other side methanol has about half the heat of combustion as heptane. The wood crib of the Malveira experiment had approximately the same wood crib dimension and the same fuel density per crib width. Logically, the chosen ignition package should have been sufficient to ignite the crib properly. Thus, it appears that the non-optimal ignition was caused by the wind and not a too little ignition package. It seems likely that the ignition setup of #FRIC-01 would have been sufficient to ignite the wood crib properly if the trays had been positioned more under the wood crib, as in the Code Red experiments.

3.5 Determining the net heat of combustion

In #FRIC-01 and #FRIC-02, the heat release rate (HRR) was determined from Eq. (3):

$$\dot{Q} = \dot{m}\, \Delta H_C\, \chi \qquad (3)$$

Where $\dot{m}$ is the mass loss rate, ΔH_C is the net heat of combustion and χ is the combustion efficiency factor.

The net heat of combustion is the energy released from burning wood (gross heat of combustion) and subtracting the energy needed to evaporate the produced water. The net heat of combustion varies between wood species and with moisture content but is typically in the range of 17.5 ± 2.5 MJ/kg [13]. To choose 17.5 MJ/kg could give a rough estimate. However, a more accurate value can be calculated if the moisture content and the gross heat of combustion are known [81]. Below is an example showing the method for calculating the net heat of combustion for the CLT used in #FRIC-01.

The CLT was made of Norwegian spruce and had an average moisture content (dry value) of 12.8%. According to [82], Norwegian spruce has a heat of combustion of 19.96 MJ/kg and a calorific value of 18.66 MJ/kg for dry wood. Although named heat of combustion in the reference, the value of 19.96 MJ/kg is the high heating value (HHV), while 18.66 MJ/kg is the lower heating value (LHV) of dry wood. Since the wood is moist when burned, the net heat of combustion must be known, which assumes that all the water produced exists in the gas phase.

Dry wood has no free water, but it contains approx. 6% of hydrogen in which 1 kg hydrogen is converted to 9 kg H_2O when the wood is burned. The LHV is lower than the HHV as it retracts the heat of evaporation for this water, while HHV does not.

The relation between the HHV and the LHV is shown in Eq. (4):

$$LHV = HHV - \frac{mass_{H_2O}}{mass_{Wood}} \cdot H_v = [19.96 - 0.06 \cdot 9 \cdot 2.47]MJ/kg = 18.63\ MJ/kg \quad (4)$$

H_v is the heat of evaporation for water and is 2.47 MJ/kg at 15°C.

The reason why Eq. (4) gave the value 18.63 MJ/kg instead of 18.66 MJ/kg is that the wood in reference [82] likely had a slightly different content of hydrogen or that the chosen value for the heat of vaporisation did not match the test conditions perfectly.

The LVL has already accounted for the water produced by the hydrogen, but the free water must still be retracted. The amount of free water is given by the moisture content.

The CLT had a moisture content, f, of 0.128 (or 12.8%) based on the dry value, see Eq. (5):

$$f = \frac{m - m_0}{m_0} \quad (5)$$

where m is the mass of the wet wood, and m_0 is the dry wood. However, the moisture content based on the moist value, w, is needed, as given in Eq. (6):

$$w = \frac{m - m_0}{m} \quad (6)$$

The relation between f and w is given by Eq. (7):

$$w = \frac{f}{f + 1} \quad (7)$$

The moisture content, w, then becomes 0.113 or 11.3%.

The net heat of combustion can then be calculated through Eq. (8):

$$\Delta H_C = LHV \cdot (1 - w) - w \cdot H_v \quad (8)$$

For the CLT, the net heat of combustion then becomes:

$$\Delta H_C = [18.66 \cdot (1 - 0.113) - 0.113 \cdot 2.47]\ MJ/kg = 16.3\ MJ/kg$$

A similar calculation was performed for the wood crib.

3.6   Measurements and sensors

3.6.1   Scale to measure mass loss

The heat release rate (HRR) is an important measure of a fire experiment [83]. In general, there are two methods to determine the HRR of a fire:

1) **Oxygen consumption calorimetry**: In this method a large hood is needed to accumulate all smoke gases. The reduction in oxygen concentration can then be used to predict the HRR, as there is almost a constant relation between the energy released for different materials and the oxygen consumed [84].

2) **Mass loss rate:** If the mass loss rate (MLR) of the fuel is known, the HRR can be estimated by multiplying it with the heat of combustion for the given material.

Neither of the two above-mentioned methods is straightforward for large-scale testing. Concerning the first method, it is challenging to accumulate all the smoke for such a large experiment, and if the hardware is not already in place, this option is not possible. The second option could also be practically challenging, especially if the MLR for the CLT wall, ceiling and wood crib should be measured separately. This was achieved in the CLT experiments by RISE in Sweden [18], showing that it is manageable. However, through conversation with the authors, it was pointed out that preparing this setup was challenging, took much more time than anticipated and thus was very costly.

Due to no oxygen calorimetry available and a low budget, a low-cost alternative of no. 2) was chosen to determine the HRR of the wood crib, inspired by Rackauskaite et al. [40]. The method consisted of three steps: 1) Define a MLR per unit of the wood crib. 2) Integrate the MLR over the entire crib to find the total MLR. 3) Convert the MLR to HRR. Rackauskaite et al. defined the MLR per unit length as the average mass loss between the onset and cessation of flaming combustion. In contrast to Rackauskaite et al., the MLR per unit length was in these experiments based on the actual mass loss of a part of the crib positioned on a scale. The MLR per unit length was then combined with the fire spread across the wood crib, which gave a total MLR of the entire crib. This method then assumes that the entire wood crib burns with a similar burning rate as the small crib farthest away from the ignition point. This is an estimation but seems to be a valid assumption based on the good match between the area under the HRR curve and the energy content of the crib.

The scale was built up of four load cells and a steel plate. Both the load cells and the plate were protected from heat as well as possible. The load cells were protected with insulation on the sides, see Fig. 55, and on the top. The steel plate had a layer of 30 mm stone wool insulation on the top. In such a setup, it is important that the metal plate is only resting on the load cells. This is a simple task during the installation. However, a steel plate will likely deform and buckle in a fire and must be given sufficient space for such deformations. Otherwise, the steel plate might end up resting on something else than the load cells, and the scale would give a false result. The scale was positioned at the opposite end of the ignition point to ensure that the extra height of the crib did not affect the fire spread rate.
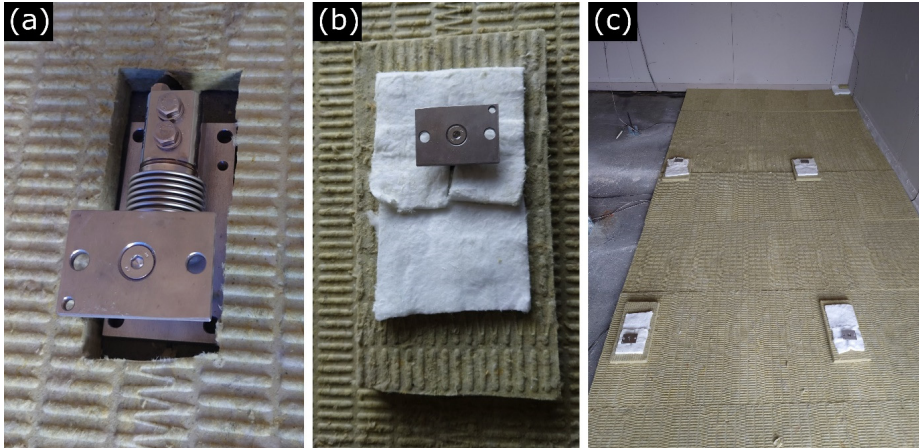
Fig. 54 Thermal protection of the load cells. (a) Load cell positioned on the floor with a stone wool batt around. (b) Load cell further protected with ceramic fibre insulation. (c) Arrangement of the four load cells before the steel plate was added. A layer of ceramic fibre insulation was also added between the top of the load cell and the metal plate (not shown here).

In #FRIC-01, the data signal from the scale was lost shortly after flashover, probably due to heat overload, but was recovered during the final decay phase of the fire. The thermal protection of the load cells and the steel plate was, therefore, enhanced before #FRIC-02. The change consisted of adding aerated concrete blocks as extra protection from the sides and having one extra layer of 30 mm stone wool insulation boards on top of the steel plate (two in total), see Fig. 55. In addition, extra layers of insulation were put between the load cells and the steel plate. Despite a more intense fire and higher temperatures in #FRIC-02, the load cells were unaffected by the heat, and the signal lasted throughout the fire and seemed to give reliable data on the mass loss.

Overall, the scale setup worked well, and the fact that the area under the heat release rate curves matched so well with the energy content of the wood crib is a good indicator that the MLR prediction was good. This method is a more complex setup than the method of Rackauskaite et al. as it requires a well-insulated scale. Nonetheless, such a setup would likely give a better match to the total MLR of the crib as the MLR per unit length is derived from an actual mass loss measurement and that the MLR per unit length changes over time.

Fig. 55 Image of the small wood crib on the scale. In #FRIC-02, aerated concrete blocks were added to the sides of the scale for better thermal protection.

3.6.2   TCs used to generate a temperature map

When conducting a large-scale experiment with hundreds of TCs, it could be a major task to get an overview of all the temperature changes inside the compartment. A good way of visualising the temperature data is to present them in a 2D temperature map. To do so, the TCs should ideally be arranged in a uniform pattern and have a sufficiently good resolution, i.e., not too large distances between them.

Thus, the arrangement of the TC trees was carefully chosen so that the temperatures could be presented as a 2D temperature plot through the XZ-axis at Y=2.5 m and through the YZ-axis through Windows 2 and 4, see Fig. 56. An example of the 2D maps is given in Fig. 57.
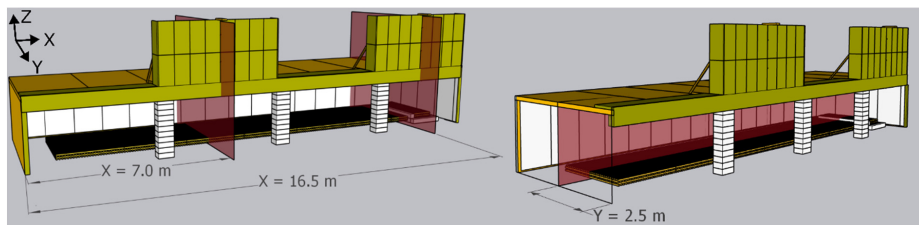

Fig. 56 The red shaded areas represent the YZ-plane through Windows 2 and 4 and the XZ-plane at Y=2.5 m.
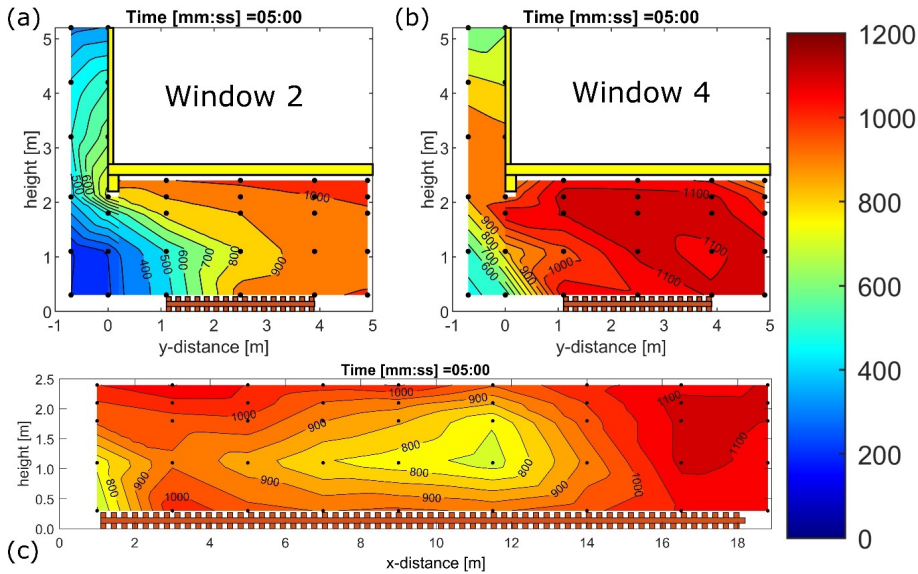
Fig. 57 Example of temperature map of YZ and XZ cross-sections for #FRIC-02. a) YZ cross-section through Window 2, b) YZ cross-section through Window 4. c) XZ cross-section.

This setup gave a good overview of the temperature distribution along the X-axis and the Y-axis. Nonetheless, the following improvements are suggested for future experiments:

- Similar distance should be used between all TCs on the same TC tree.
- Less distance should be used between TC-trees close to the ignition point.
- TC-trees should cover the entire width of the compartment, not start at 1.0 m, as in our experiments.
- To better capture the external flame, more than one TC tree should be located outside and farther from the compartment.

The MATLAB code for the XZ temperature map in PDF format is given in Appendix A.

3.6.3 Determination of gas temperatures and incident radiative heat fluxes

Standard plate thermometers (PT) [67], see Fig. 58, and 1.5 mm thermocouples type K (TC) [85] were used to measure both the temperature and the heat fluxes. TCs are intended to measure the gas temperatures, but due to the size of the wire, they also capture some radiative heat. Hence, the real gas temperature differs slightly from the measured value, but the measurements could still serve as a good indicator of the gas temperature.
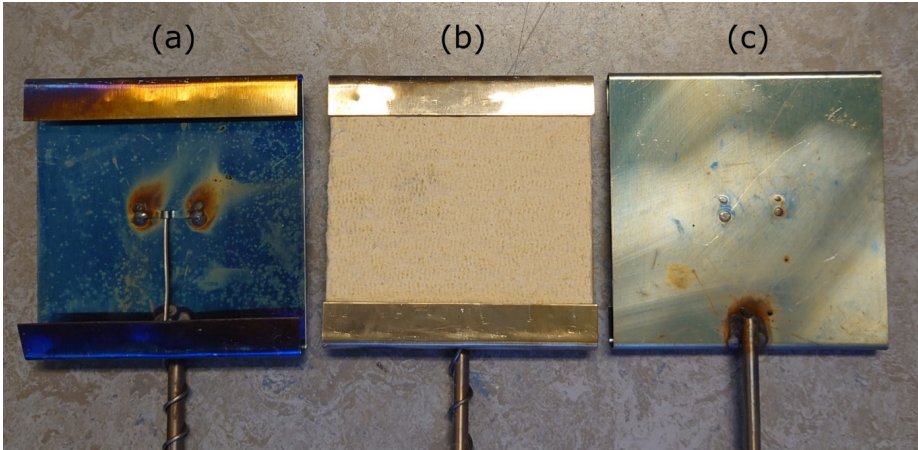
Fig. 58 The standard PT consists of a shielded TC attached to a 0.7 mm thick metal plate with a 10 mm thick insulation pad on the back. The metal plate is 100 mm x 100 mm. (a) PT from the back side without the insulation installed. (b) PT from the back side with insulation. (c) PT from the front side.

In fire testing, the PTs are a good supplement to TCs as they are more affected by the radiative heat and give a good measure of the surface temperature of a well-insulated material. PTs are also used in standardised furnace testing to control the temperature, and temperatures of a fire experiment measured with a PT could, therefore, be compared against the temperature of a furnace test. Furthermore, a PT can be used to approximate the adiabatic surface temperature and the incident radiative heat flux and is a cost-effective and robust alternative to more expensive heat flux meters.

To find the incident heat flux, a simplified 1D heat balance equation for the PTs is set up, see Eq. (9). The description below summarises the theory given in the book *Temperature Calculation in Fire Safety Engineering* by Ulf Wickström [86].

$$\varepsilon_{PT} \, \dot{q}''_{inc} - \varepsilon_{PT} \sigma T_{PT}^4 + h_{PT}\big(T_g - T_{PT}\big) + k_{PT}\big(T_g - T_{PT}\big) = C_{PT} \frac{dT_{PT}}{dt} \qquad (9)$$

where

- the first term is the radiant heat absorbed.
- the second term is the radiative emitted heat.
- the third term is heat absorbed due to convection.
- the fourth term is heat lost by conduction through the insulation.
- the fifth term is the rate of heat stored in the PT (assuming lumped heat capacity).

To find the incident radiation, $\dot{q}''_{inc}$, the equation must be rearranged, see Eq. (10):

$$\dot{q}''_{inc} = \sigma T_{PT}^4 + \frac{(h_{PT} + k_{PT})\big(T_{PT} - T_g\big) + C_{PT} \dfrac{dT_{PT}}{dt}}{\varepsilon} \qquad (10)$$

where

σ	is the Stefan Boltzmann constant: $5.67\cdot10^{-8}$	[W/m^{2}K^4]
T_{PT}	is the PT temperature	[K]
T_g	is the gas temperature	[K]
h_{PT}	is the convective heat transfer coefficient for the PT	[W/m^{2}K]
ε	is the emissivity	[-]
k_{PT}	is the thermal conduction coefficient for the PT	[W/m^{2}K]
C_{PT}	is the heat capacity of the PT	[J/m^{2}K]

The term $\frac{dT_{PT}}{dt}$ can be approximated by Eq. (11):

$$\frac{dT_{PT}}{dt} \approx \frac{\Delta T_{PT}}{\Delta t} = \frac{T_{PT}^{j+1} - T_{PT}^{j}}{t^{j+1} - t^{j}} = \frac{T_{PT}^{j+1} - T_{PT}^{j}}{\Delta t} \tag{11}$$

where j and $j+1$ represent two consecutive data recordings, and Δt is the corresponding time difference. The transient term, $C_{PT}\frac{dT_{PT}}{dt}$, can be neglected under steady-state conditions or in relatively slow processes. Typical values are: $k_{PT} = 8\ W/m^2K$, $C_{PT} = 4200\ J/m^2K$ and $h_{PT} = 10\ W/m^2K$.

In these experiments, a TC was located next to the PTs to approximate the gas temperature (Fig. 59). Ideally, the TCs should have been thinner to measure the gas temperature more accurately. Nonetheless, this error is considered to have little impact on the results as the radiative term dominates at high temperatures.
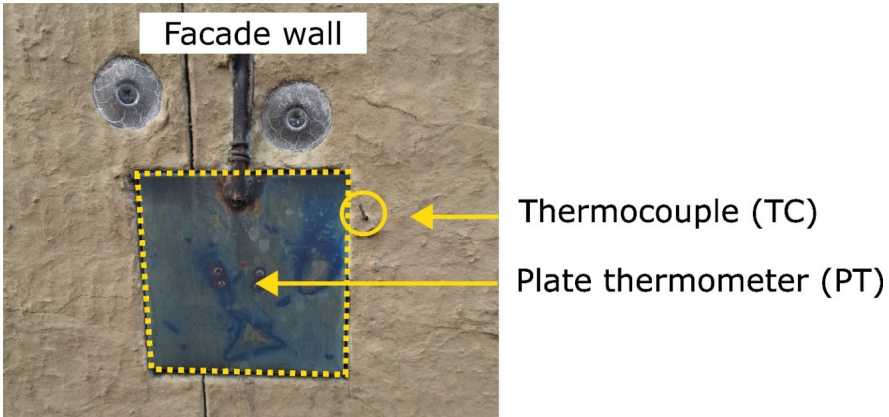

Fig. 59 PT flushed with the facade wall and the TC beside it.

3.6.4 Embedded TCs inside the CLT

Knowing how the charring front propagates through the CLT is important knowledge, as this can be used to estimate the mass loss and heat release rate. Furthermore, the temperature through the cross-section is relevant for predicting the remaining structural capacity of the CLT.

The most common way to determine the char front is to use a temperature threshold, typically 300 °C, as an indicator of charring.

In several experiments, this has been studied by inserting a TC in a drilled hole from the non-exposed side of the CLT. However, in recent years, it has become more and more apparent that this method is unreliable in several ways [87-89]:

1) The TC wire is a highly conducting material compared to the wood and would act as a thermal sink, with the result that the TC measures a too low value.

2) The measurement point of a TC is usually located a few mm inside of the tip of the wire, and it is challenging to know exactly at what depth the temperature is measured.

3) As the CLT is often quite thick, typically 100 - 175 mm, a deep hole is needed to insert the TCs from the non-exposed side. Furthermore, the diameter of the drilled hole should be as small as possible to avoid convective heat losses through the hole. A long drill bit length combined with a small diameter is hard to find, and drilling straight for such deep holes with a small drill bit size could be challenging.

Based on these arguments, it was obvious that the holes had to be drilled from the thinnest side of the CLT. This would give TCs parallel to the isotherm and cancel out all the disadvantages mentioned above. In some experiments, the installation of TCs parallel to the isotherm has been made during the manufacturing of the CLT elements. In my case, that was not possible. Since both the back wall and the ceiling consisted of several elements, it was considered the best choice to insert the TCs from the rebate joint (Fig. 60).
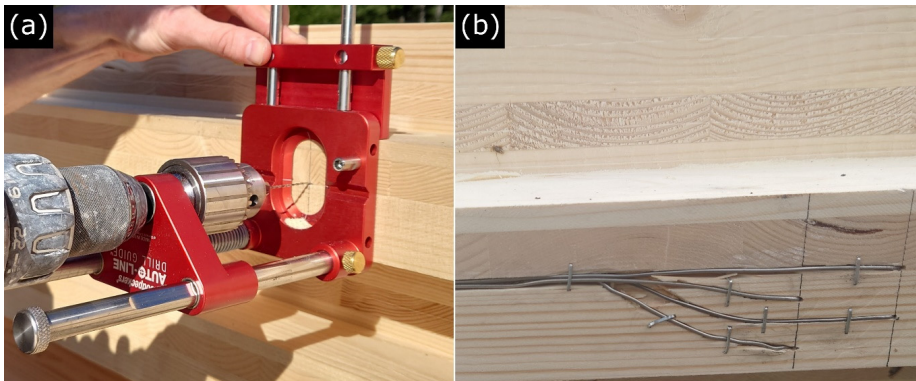

Fig. 60 (a) TCs were embedded from the rebate joint, and the use of a drill guide ensured straightly drilled holes. (b) The TC wires were hidden and protected in precut slits.

The holes were drilled straight by using a drill guide. The perpendicularity of the holes was checked visually by controlling the angle of the drill bit placed inside the holes. A drill bit size of 1.6 mm was used, while the TCs were 1.5 mm. This was just enough to insert the TCs, and there was essentially no space around the TCs. The TCs were positioned at 10, 20, 30 and 40 mm depth and at the surface (0 mm) to define the start of the exposure. The TC wires followed the isotherm for at least 50 mm and were then hidden in precut slits into the wood to protect them from mechanical damage during construction and to not cause any gaps in the joint after installation.

Overall, this setup worked out as intended. However, having more TCs embedded deeper into the CLT would have been beneficial, especially in #FRIC-02, where the charring continued past the first layer. In addition, it would have been useful to have TCs located in more positions throughout the compartment. This would have given a better foundation for determining whether the relatively large scattering of the charring rates in the first 10 mm was due to inaccurately located TCs (i.e. actual depth deviated from 10 mm) or that they actually reflected the different charring rates at different locations in the compartment.

3.6.5   Organizing the instrumentation

When conducting experiments with many sensors, in this case around 150, it is crucial to have full control over them. Thus, each single sensor was adequately labelled with a unique name, which also served to identify its exact location in the compartment. Also, to avoid a mess with all the running TC wires, they were bundled, as shown in Fig. 61.

Fig. 61 All sensors were named adequately by a unique ID and organised in bundles.

The TC-trees were attached to a steel chain and fixed to the ceiling by two 120 mm screws. In both experiments, this was sufficient to prevent the TC-trees from falling down. The TC-trees were anchored to the floor to hang straight (Fig. 62). The height was manually adjusted to the correct height after installation. However, due to the stiffness of the TC trees, the TC-trees did not hang perfectly straight. Thus, a certain displacement, up to a few cm, of the X and Y positions of the TCs could be expected. Using thinner TCs wires would likely have improved

this, but thinner wires are also more fragile and prone to break. In my opinion, the 1.5 mm TC is a preferred choice over the thinner ones due to its robustness. Another option to improve the X and Y locations would have been to install the TC-trees on a rack stand. However, this would likely have been an obstacle to the continuous wood crib. It would also have taken longer time to prepare, as this would have involved some kind of welding work. Also, due to the large dimension of the compartment, a few cm displacements of the X and Y positions are considered negligible.
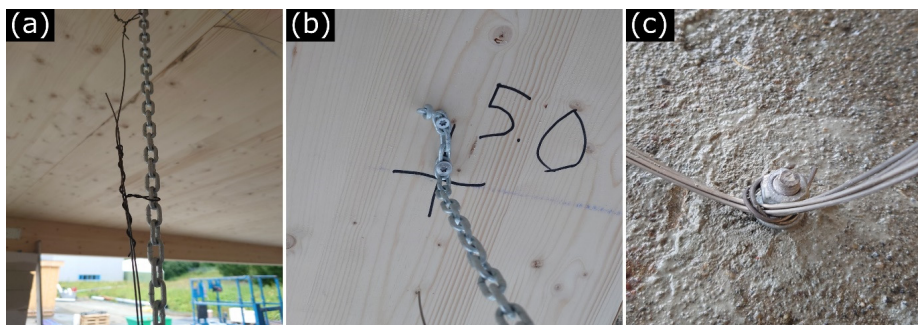
Fig. 62 (a) The TC trees were attached to a chain, (b) fixed to the ceiling by two 120 mm long screws, and (c) anchored to the concrete floor by an expansion bolt.

3.6.6 Heat flux at a distance

An external flame might cause the fire to spread to a neighbouring building. The incident heat flux at a distance would indicate whether a nearby building is at risk of being ignited. Two PTs were installed at 8.0 m distance from the centre of the compartment. The distance was chosen as this is the prescribed safe distance in the building regulations in Norway. Unfortunately, the PTs gave no readings for either of the experiments. The error was not located after the first test, and thus repeated in #FRIC-02 due to the tight time schedule between the experiments and the lack of time to look closely through all the measured data. Although there was no valid measurement of the heat flux at a distance, the distinct discolouration of the wooden board at which the PTs were mounted, clearly shows that the radiation at 8 m was significant in #FRIC-02, see Fig. 63. Also, due to the non-symmetrical external flames, this location, in front of the centre of the compartment, was not where the strongest radiation was present.
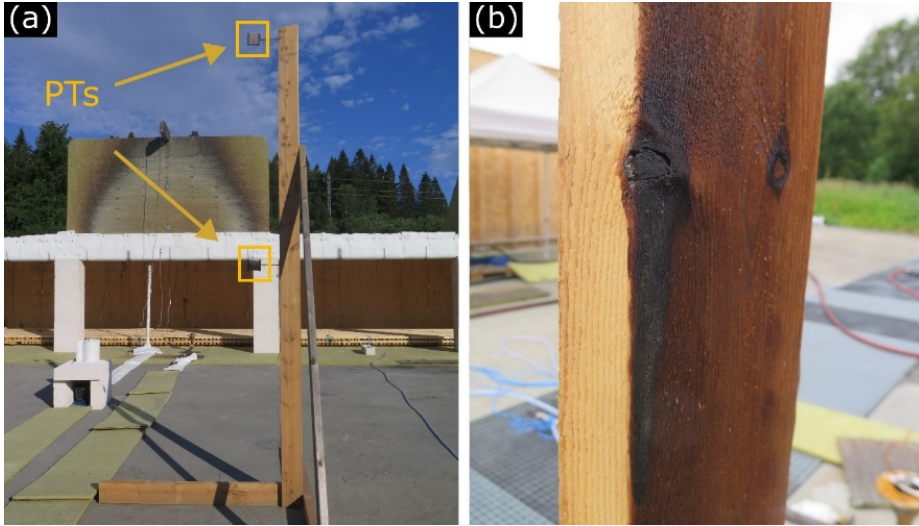
Fig. 63 (a) Plate thermometers (PTs) 8 m away from the centre of the compartment. (b) Clear signs of charring and discolouring of the wooden board at the front side.

3.6.7 Cameras

Several different camera setups were used to capture the fire, see Fig. 64. There were two different water-cooled cameras: one simple setup with a GoPro camera inside a Pyrex column filled with water and a protected garden hose used to recirculate the water. Excessive water ran out of the notch and away from the fire. All the cameras protected in this way survived the fire. A more sophisticated water-cooled setup was the 360° camera setup, where a chemical reaction bulb was turned upside down on top of the camera and filled with water, inspired by Hoehler [90]. Also this camera survived the fire. However, the video quality was not as good
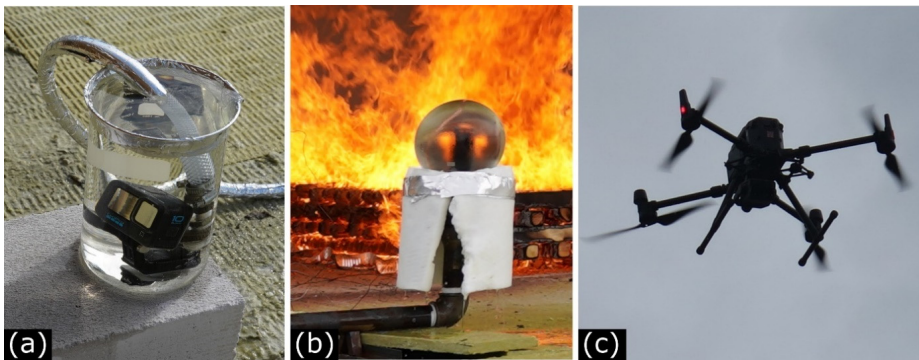
Fig. 64 Examples of cameras used. (a) A GoPro camera inside a Pyrex column with recirculating water. (b) A water-cooled 360 camera inspired by Hoehler [90]. (c) A drone.

as we had hoped. The main reason was that the water pipes had not been flushed before inserting the camera, resulting in rusty water flowing through the system and making the glass and camera lens dirty. Since this was a new setup for both me and the crew from RISE Fire Research, we had no experience with how it would behave when exposed to a fire. Hence, we did not dare to put it inside the compartment, both due to the increased likelihood of rupture of the glass, but also as we did not want a spill of water inside the compartment in case of rupture.

For the water-cooled camera setup, the following improvements are suggested:

1) Cover the backside of the glass with aluminium foil or similar to avoid reflections.

2) Find a way to charge the battery under water as this setup has a limited recording time when only powered by the battery.

3) Make sure all the involved equipment is clean. The glass should be properly cleaned beforehand, and all pipes, tubes, etc., where water will flow through should be flushed before installing the glass and the camera.

4) Keep the recirculation of water to a minimum to avoid disturbances in the water, which in turn might disturb the video quality. A large water flow would also introduce air bubbles, which may adsorb to the glass surface and reduce the image quality of the recorded videos.

In addition to the water-cooled camera setups, there were two different types of air-cooled camera setups. The front and top sides of the camera, except for the lens, were covered by aluminium tape and a layer of welding cloth. The lens was cooled down by an ordinary PC fan in the first experiment and pressurised air in the second experiment. The advantage of this setup was that a charger could easily be installed, and it is a very cheap setup. These cameras gave relatively good, close-up images but were automatically turned off after a while due to overheating. A tip for future use is to use a more powerful air-blower, perhaps a hair drier blowing cold air, to avoid the cameras to be overheated and shutting down. Another tip is to have a leash attached to the camera so that it can be pulled away in case of too severe conditions. This might not save the camera but would likely save the recordings already made.

Furthermore, a drone was used to observe potential fire spread to the top of the ceiling, to vegetation nearby and to make high-quality videos from different angles. The drone was provided by the local fire brigade and was equipped with both a regular camera and an infrared camera. As it was a more advanced drone, it was controlled by a drone pilot from the fire brigade. We got some nice-looking videos from the drone, but in hindsight, we could have used the drone more effectively to capture behaviours that are not easily observed through TCs or regular cameras. Examples of such behaviours are given in Fig. 65-Fig. 67.
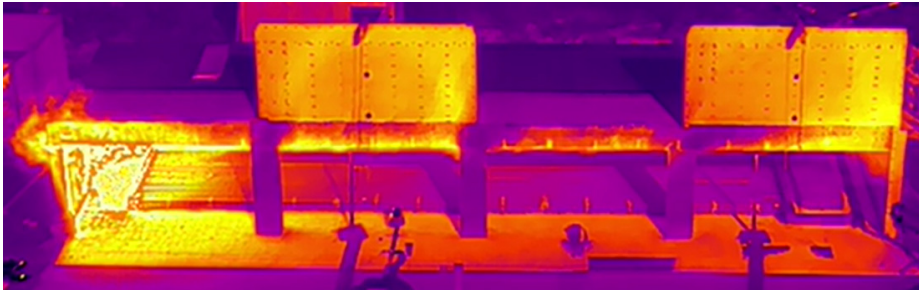
Fig. 65 Infrared image of the compartment before ignition of the ceiling in #FRIC-02. The colour differences at the wood crib gives an indication of how much of the crib that is affected by the initial fire.
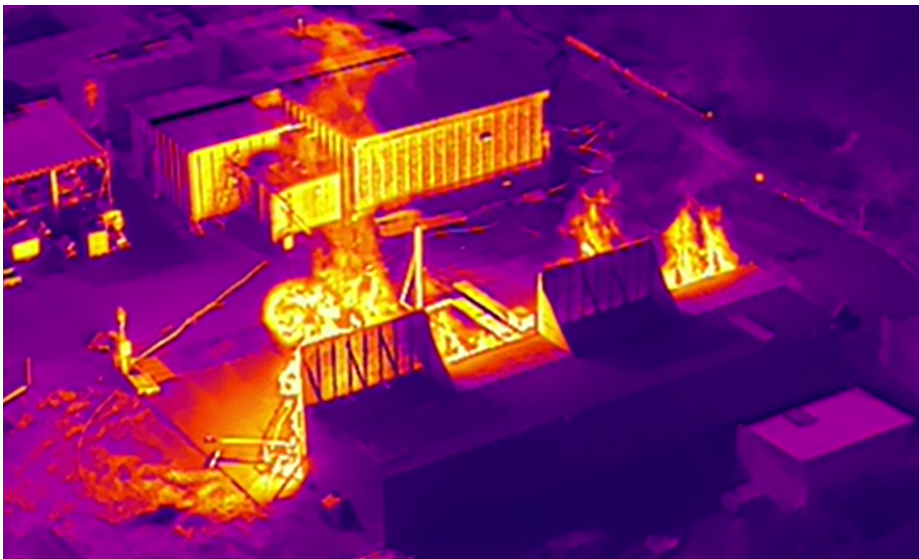
Fig. 66 Infrared image from the back side of the compartment in #FRIC-02. The back side of the facade wall above Window 4 is clearly hotter than the one above Window 2. The image also reveals that irradiation to the top surface of the ceiling was limited.
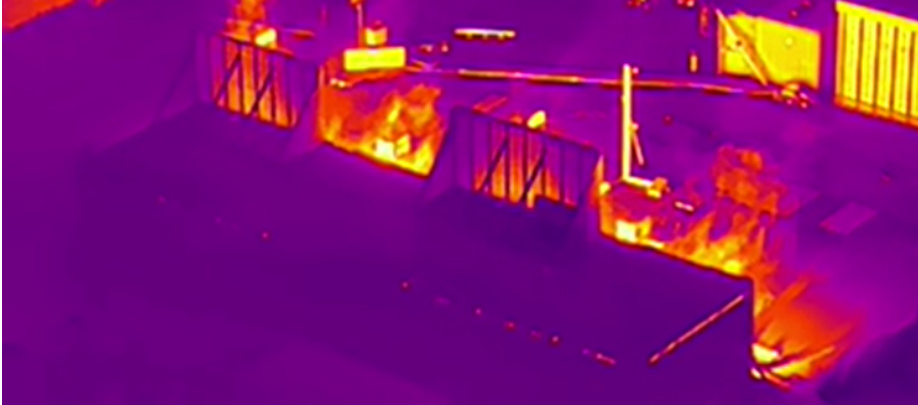
Fig. 67 The infrared camera revealed leakage points at several locations between the wall and the ceiling intersection in #FRIC-01. Here, the temperatures at the back side of the facade walls appear more even between the two facade walls.

At last, several IP cameras were located 15-20 m from the compartment at different angles. They provided very good and stable images but were not able to capture in detail what happened under the ceiling, like the fire spread and self-extinguishment of flames. These cameras were not protected in any way but survived the fire exposure.

Despite several lessons learned, most of the video materials were, in general, of good quality, and played a key role in analysing and understanding the different phenomena of the two experiments.

3.6.8 Char depth analysis

To know the final char depth of the CLT is interesting from several points of view. Firstly, it gives an exact value of how much is remaining of the original CLT thickness, which is directly linked to the remaining load-bearing capacity. Secondly, the char depth relates to the total mass burned. Thirdly, the final char depth is a good reference for validating theoretical models for predicting char depth.

The method of determining the char depths in these experiments was inspired by Schmid et al. [91], where the mass loss of CLT elements was found by drilling a uniform pattern and measure the remaining thickness after the char layer was physically removed. Although I intended to replicate the method, I quickly realised that it was not manageable. The drill pattern of Schmid et al. was 50 mm x 50 mm on a 1 m x 1 m sample. In my case, this would have given an incredibly good resolution and a very accurate measure of the mass loss. However, with such high resolution, I would have needed about 4200 measurements for each CLT panel and 33 600 measurements if all eight panels had been measured.

In #FRIC-01, I ended up measuring five of the eight panels with a grid pattern of 500 mm x 500 mm, and in total, 400 measurements. The remaining three panels were saved for load-bearing analysis. For #FRIC-02, three of eight elements of the ceiling and three pieces of the

back wall were measured, in total 300 measurements. The reason for the fewer elements from #FRIC-02 was that the elements were far more damaged and harder to bring out in one piece.

Despite reducing the number of measurements considerably, it was still a formidable task, and it took me and a master student almost two weeks to accomplish. A reason why it took so long was that the handling of such large elements is much more complicated than smaller ones.

The drilling and the measurements were mainly performed when the elements were standing, see Fig. 68, as the elements in this way could be reached from both sides.

Fig. 68 The elements were raised for easy access from both sides. The vertical stripes are signs of the physically removed char layer around the drilled holes. The element at the picture is one of the ceiling elements from #FRIC-01.

The relatively narrow measurement distances made it possible to observe clear trends. For instance, in both experiments, the charring in the ceiling was deeper close to the back wall than close to the window openings. The char depth was also less pronounced close to the end walls and the elements were more charred in the centre of the compartment. An advantage of this method is that no expensive equipment is needed, and it is quite accurate.

For future CLT experiments, it is recommended to take a systematic photo shoot of all elements. This would complement the char depth measurements and allow for the observation of trends in the char pattern across the entire lengths of the exposed surfaces.

3.6.9 Gas measurements

To have some overview of the oxygen concentration during the fire is beneficial, as it could indicate whether the fire is fuel- or ventilation controlled. In addition, knowing the oxygen concentration at different locations could give a more accurate analysis and understanding of charring behaviour and self-extinguishment, as both are directly affected by the oxygen concentration [20, 92].

Gas measurements (O_2, CO, and CO_2) were made at three locations in the compartment: two at the top of Windows 2 and 4 and one under the ceiling close to the back wall. In both experiments, the oxygen concentration close to the back wall was higher than expected, and it seems likely that a joint leakage occurred.

In hindsight, it would have been better to have more oxygen sensors to better understand the flow field of the gases.

4 Discussion of methodology

In this section, insight into the process of determining the final experimental setup of the CLT experiments is given and difficulties and trade-offs that had to be dealt with in the process are discussed. Moreover, suggestions for improvements for the I-joist experiments and the CFD-simulations are then discussed.

4.1 CLT experiments

4.1.1 Why a large-scale experiment?

Small- and medium-scale experiments are cost-effective and can be used to explore and study qualitative aspects of CLT behaviour in compartment fires. However, as Liu and Fischer [51] point out, large-scale experiments are important to verify small- and medium-scale results to assess the findings at realistic scales. Furthermore, several review papers have highlighted a general lack of data from large-scale experiments [31] and especially large-scale experiments with exposed CLT [51, 64, 65].

Conducting a successful large-scale fire experiment requires a lot of planning and logistics, and a good understanding of how different parameters are measured. Besides, such experiments are costly, and it is almost impossible to run a perfect experiment as so many factors can influence the result.

As I had six years of experimental fire testing background at RISE Fire Research and had quite a large budget for a PhD-student through the Fire Research and Innovation Centre (FRIC), I was motivated to plan and arrange a series of large-scale CLT experiments.

From this decision was made, there were many questions to be answered, like:

- How large should the compartment be? Should it have a square shape or a more oblong shape?
- How many experiments could be run with regard to costs, planning and execution time, analysis, etc.?
- What should the opening factor be?
- What should the fuel load density be, and what should the fuel package look like?
- How should the instrumentation be set up, and what measurements should be prioritised with regard to costs, preparation time, value of the results, etc.?
- How much preparation would be needed, and at what time could I latest run the experiments and still be able to do the analysis and publish the results?

4.1.2 Size

In recent years, several travelling fire experiments have been conducted with non-combustible surfaces, but just a few with exposed CLT. Hence, the size and shape were chosen to be similar to many of the already conducted travelling fire experiments, as the results then easier could be compared to previous results. The final setup was a compartment with a floor area of 95 m^2 and an oblong shape. To our knowledge, this size ranks as the third largest compartment experiment with exposed CLT, only surpassed by the Code Red experiments of 352 m^2 [23, 46] and the recent experiment by Su et al. of 204 m^2 [50].

4.1.3 Exposed surfaces

Originally, the plan was to conduct one experiment with the ceiling exposed and the other with the back wall exposed. To have the ceiling exposed was relevant as such a scenario would either confirm or nuance the very rapid fire spread observed in the Code Red experiments [23, 46]. Having only the back wall exposed was interesting, as such setup never had been studied in a travelling fire scenario. However, due to the slow fire development in #FRIC-01 before the ceiling ignited, we feared that the exposed wall would not ignite at all. Hence, the original plan was reconsidered, and it was decided having both the wall and the ceiling exposed. Another option could have been to shift the position of the wood crib next to the wall, but that again would have given a completely different test scenario as the flames of the wood crib would have been impinging on the wall from the beginning. Another argument supporting this change was that it would be a waste not to expose the ceiling when we had a new CLT ceiling available.

4.1.4 Fuel

Many travelling fires have been designed to represent open-plan offices, which often have a large floor area. Hence, for easier comparison, also here a fuel load density (FLD) representative of an office building was chosen. The FLD was approx. 353 MJ/m^2 in both experiments. This is lower than the suggested value of 420 MJ/m^2 for offices in Eurocode 1 [49]. However, as pointed out by Su et al. [50], the FLD of offices was determined decades ago when it was more common to have lots of books and papers physically available. Nowadays, most work occurs electronically, and the FLD in modern offices is probably lower than the value suggested in the Eurocode.

In fire experiments, the variable fuel load is commonly represented through the following alternatives: 1) real furniture, 2) mock-up furniture, 3) gas or pool fires, or 4) wood cribs. In these experiments, the wood crib alternative, no. 4) was chosen, based on the following arguments:

- Burning of wood cribs is well studied and described in the literature, and it is a common way of representing the variable fuel. Furthermore, this approach has been used in many travelling fire experiments. Thus, a comparison against other experiments would then be easier.
- The burning rate and fire spread across a wood crib would be much more affected by the compartment environments, like feedback from the surroundings, compared to gas burners or pool fires. This is also more in line with how real furniture would behave.
- Since the ceiling height of the CLT compartment was lower than typically found in actual offices, a continuous wood crib along the floor was beneficial over real furniture to maximise the distance between the fuel and ceiling.

4.1.5 Opening factor and ventilation conditions

In addition to the lack of large-compartment data, there has been a clear bias in choosing opening factors corresponding to ventilation-controlled fires [51, 64, 65]. Hence, to create

new knowledge, an opening factor of 0.18 $m^{1/2}$ was chosen, which is representative of a modern compartment or an office building [93], but larger than for most CLT experiments conducted.

The window configuration with openings in one wall only resembles many modern buildings. Aside from this, the configuration was chosen as windows in several walls would have made the fire more vulnerable to be affected by wind in the spread direction. The configuration also aligns with several other travelling fire experiments [39, 44, 45], which enables comparison of results.

Unlike actual buildings, the window openings had no glasses installed and were open throughout the experiment. This is a common approach in compartment fire testing but is still a decision that might affect how realistic the experiment is.

The key parameter determining whether a building fire could behave as in the experiments depends on whether the window glasses break. Ordinary window glasses are expected to break early in a fire. However, some glass types are less prone to break [94, 95]. The fire development is, therefore, highly dependent on the type of window glasses used.

With no glasses installed, these experiments are relevant to buildings with glasses that break early or very large compartments where the oxygen supply is good without any window breakage.

Furthermore, if glasses had been installed in the window openings, we would have had less control of the air supply, it would have been harder to reproduce the experiments, and it would have been more challenging to compare the results with other experiments as most experiments have been performed with open ventilation openings from the start.

4.2   CFD simulations

It is both time and cost consuming to run large-scale experiments. A more affordable alternative is to run CFD simulations. However, due to the complexity of fires, simulations should be validated against experimental data. In the simulation presented in Paper III, an FDS model was made to simulate the #FRIC-02 experiment. The fire spread mechanism was simulated by an ignition temperature of 300 °C and a prescribed burning rate, i.e., a heat release rate per unit area, of 260 kW/m^2.

This is a simple but effective way of simulating fire spread across a wood crib. However, this method also has its limitations. The main disadvantage is the constant burning rate of the wood, which does not reflect real conditions very well. In reality, the burning rate will be coupled to the thermal environment and the ventilation conditions. This was clearly seen in the CLT experiments, where the maximum burning rate of the wood crib was approx. 25% higher in #FRIC-02 than in #FRIC-01. Another aspect not included is that the burning rate of the wood crib reduces over time due to the reduction of surface area and volume and the creation of a char layer. In both #FRIC-01 and -02, the mass loss rate per unit length of the crib decayed exponentially, while in the simulation, it remained constant after ignition.

In the simulation, the wood crib was resolved, i.e., the mesh size around the wood crib was similar to the wood stick thickness (5 cm). This is an advantage as the surface area, at least initially, was identical to the crib surface area of #FRIC-02.

Such a simulation could be helpful to get an idea of how the fire develops and the intensity of external flames. However, running the fire until burn-out would take a very long time or require a very powerful computer. For a given case, a possible solution could be to use FDS to simulate the start of the fire until the fully developed fire is reached and use a zone model to predict the remaining time-temperature curve of the fire [79].

Difficulties and numerical instability occurred when trying to simulate the wind conditions from #FRIC-02. This was solved by having a sufficiently large outside domain. In addition, to stabilise the wind conditions during the fire simulation, a separate case with no fire was run until the wind was stable and then imported into the fire simulation.

4.3 I-joist experiments

The experimental setup was to a large extent adopted from similar experiments [96]. In hindsight, several improvements to the experimental setup have been discovered, and are discussed below:

1) **Thermocouples**

   The TCs attached to and embedded into the I-joists flanges were not sheathed as in the CLT experiments, but glass fibre protected TCs with a twisted junction at the end. The reason for choosing those was mainly their low cost and that such a setup had been used in similar experiments with success [96]. However, in our experiments, the temperature readings were reliable only until the wire was directly exposed to flames, i.e., until gypsum board failure. In the end, this resulted in fewer data points to calculate the charring rates and no valid data points in the post-protected phase. Instead of using glass-fibre protected TCs, it would have been better to use sheathed TCs as they function well even when exposed directly to flames. They are far more expensive, but the costs could have been kept low by reusing them in several experiments. A possible solution could, for instance, have been to extend the wires sufficiently that the test specimen could be lifted off without the need to cut the wires.

2) **Insulation types**

   Before the experiments, it was argued that there was no need to test glass and stone wool insulation as they had been tested before. However, as it turned out that those experiments had been run with a different setup (rectangular members instead of I-joists) and with a different way of measuring the recession rates, comparing the results was not straightforward. In hindsight, it would have been better to include an experiment with glass wool and stone wool for direct comparisons.

3) **Flange type**

   Instead of testing I-joists with both LVL and solid flanges, it would have been better to focus on one type only, as this would have given twice as many data points for each flange size, thus providing results with less uncertainty.

5 Discussion of results

5.1 CLT experiments

Fire spread

At the end of 2023, there have in total been six large (published)experiments, including #FRIC-01 and -02, that have focused on how exposed CLT surfaces, but predominantly an exposed ceiling, affect the fire development and fire spread rate in large compartments.

In all of them, the fire dynamics have significantly changed from the point the ceiling was ignited. In all experiments, the flames have spread rapidly below the ceiling, and created an increased radiative heat flux to the surroundings and effectively preheated the variable fuel load. The effective preheating from the flames under the ceiling, is the main driver for the fast fire spread rates that have been observed. In several of the experiments, a fire growth rate faster than the ultrafast t^2-curve has been obtained.

The clear shift in the fire dynamics after ignition of the ceiling was particularly clear in #FRIC-01, where the average fire spread rate before ignition of the ceiling was 54 mm/min and increased to 1.2 m/min after ignition of the ceiling. As the crib had only spread 1.5 m during the first half an hour, and the fire did not grow much in size after 22 minutes due to burn-out of the first part, gives a good indication of how the fire likely would have developed further if no CLT ceiling was present, or if the ceiling had been at a higher height where it had not been ignited. To some extent, the development aligns with the Malveira fire experiment [44], where the first 40% of the ceiling was non-combustible and the last 60% of the ceiling of a combustible cork layer. The fire spread slowly for about 4 h until the fire spread reached below the cork area. From this point on, the fire spread to the rest of the room within minutes. These two incidents demonstrate clearly how much impact a burning ceiling has on the overall fire dynamics.

In #FRIC-02, the average fire spread rate after ignition of the ceiling was 15 m/min across the ceiling and 12 m/min across the wood crib. In both experiments, the fire spread rate followed an exponentially increasing curve, indicating that significantly larger compartments would not necessarily take significantly more time to ignite under similar conditions.

Part of the reason why the average spread rate of #FRIC-01 was one-tenth of #FRIC-02, was due to the flashing waves, where the flames travelled back and forth three times before the fully developed fire was reached. The flashing waves demonstrated in large scale that a CLT surface is dependent on an external heat flux to sustain burning even directly after ignition. This could be relevant for fire safety design of CLT compartments with a low likelihood of ceiling-impinging flames (e.g., with a high ceiling) and a low potential for collection of combustible gases under the ceiling, e.g., compartments with ceiling beams of limited height and high ventilation openings.

Video analysis showed that the wall acted as a bridge between the ceiling and the crib, and the large differences after ignition of the ceiling between #FRIC-01 and -02 cannot be explained by the differences in the ignition method. The incident heat flux at the back wall in #FRIC-01, which was 10–40 kW/m^2 between the 1st and 2nd flashing wave, strongly suggests that a combustible wall had ignited in #FRIC-01 as well, if present.

In both experiments, the charring rate was highest for the first 10 mm and was reduced for each subsequent 10 mm into the wood. This behaviour can be explained by the initial rapid mass loss rate for combustion of wood, followed by a reduced rate when a char layer is formed. The large differences can, to some extent, also be explained by the large variations in temperature and heat fluxes during the first 40 mm of charring. Although the high charring rate for the first 10 mm did not have a significant impact on the total charring rate, it contributed to a large amount of pyrolysis gases being produced in the first few minutes after ignition, which facilitated the rapid fire spread rate and external flames.

Compared to the Code Red experiments, which also had only the ceiling exposed [23, 46], the fire spread in #FRIC-01 was slower both before (54 mm/min vs. 660 mm/min) and after the ignition of the ceiling (1.2 m/min vs. 9 m/min). The slower fire spread across the crib could, to some extent, be explained by the differences of the wood crib. In the Code Red experiments, the crib was made of thinner sticks, 30 mm x 30 mm instead of 50 mm x 50 mm, which ignite faster due to the increased surface-to-volume ratio. In addition, the Code Red experiments had thin strips of cardboard in the first meter of the crib, enhancing the fire development initially. Another factor that might have influenced the fire spread rate is the moisture content of the wood sticks, which was slightly higher in these experiments compared to Code Red, 14.5% vs. 13.5%. In addition, it is worth mentioning that the top layer of the wood crib had a moisture content of 16% ±0.6%, and since the fire spread happened along the top layer first, this could have played an additional role.

In #FRIC-02, the fire spread rate after ignition of the ceiling (11.7 m) was even faster than the Code Red experiments (9 m/min) despite having a wood crib with thicker wood sticks, being less prone to ignite. This demonstrates that the contribution of an exposed wall could compensate for a variable fuel design, which is not favourable for a fast fire spread. Ultimately, this indicates that a fire could develop fast also in a room with a high ceiling height if several surfaces in addition to the ceiling are exposed. An example of such a development is the school gym fire in Oslo, which developed to a fully developed fire despite a very low fuel load density (see Section 5.3).

Moreover, the results of #FRIC-02 should be an eye-opener to fire safety engineers that combining a combustible wall and ceiling in large, ventilated spaces could cause a very rapid developing fire from the point the CLT is ignited.

Heat release rate and temperatures

In both experiments, the contribution of the CLT had a significant effect on the total heat release rate (HRR). However, in #FRIC-02 it was estimated a 32 MW (78%) higher maximum total HRR than in #FRIC-01. Besides the 13 MW increase due to the exposed back wall, the HRR of the CLT ceiling increased by 3.5 MW (21%) and the wood crib increased by 15 MW (75%) despite having the exact same wood crib arrangement. Of these 15 MW, 5 MW was due to the higher HRR per unit length caused by higher temperatures and more considerable heat fluxes towards the wood crib. The remaining 10 MW was due to the faster fire spread across the wood crib, which caused a larger part of the crib to burn simultaneously at a higher HRR per unit length.

The increased HRR of the CLT ceiling was due to 21% and 28% faster charring rates in #FRIC-02 than in #FRIC-01 for 0-10 mm and 10-20 mm into the CLT.

The large difference in the HRR can explain the large differences in the temperatures. In the most intense period of #FRIC-02, the temperatures in the whole compartment were 1010–1172 °C, while they were 785–1038 °C in #FRIC-01.

External flames

During the most intense burning, external flames emerged from all window openings. In #FRIC-01, the flaming was symmetrical with approximately equally sized flames out of all openings. In #FRIC-02, the external flaming was more pronounced and strongly non-symmetrical. Flames were much larger out of one window, and the flames filled almost the entire window opening for a short period of time. The differences in the severity of the external flames are demonstrated through the differences in the calculated heat fluxes at the facade. The incident heat flux at 2.8 m above the window soffit was above 50 kW/m^2 for approx. 10 seconds in #FRIC-01 and above this value for approx. 5.5 minutes in #FRIC-02. Such a high exposure to the façade has the potential to spread a fire to the compartment above and effectively ignite a combustible façade if present.

From previous CLT experiments, it is well known that external flames tend to increase with the presence of exposed combustible surfaces [97-99]. However, the external flames of #FRIC-02 still gave new insight into this topic. Firstly, it was shown that large external flames can occur also for compartments with large ventilation openings. Secondly, it was shown that external flames could be strongly non-symmetrical. Both the size and the non-symmetrical shape of the flames were reproduced in an FDS simulation. Thus, it can be concluded that this behaviour was affected by ordinary wind velocities coming diagonally from behind the compartment. The wind velocity was 2 m/s on average, with gust velocities of 5 m/s during the most intense external flaming, so quite ordinary wind conditions.

According to the FDS simulation (Paper III), 47% of the combustible gases were burnt outside. This strengthens the suggestion in #FRIC-02 that the maximum external flame could have been 46 MW or larger.

Another factor that probably also played a role here, but that was not given so much attention in Paper II, was the immensely fast fire spread the last meters of the compartment, in which the fire spread across the second half of the wall and wood crib (i.e. ~9.5 m) in approx. 10 seconds. It is also known from cone calorimeter testing that the mass loss rate of wood is especially high directly after ignition [100]. When combining this information, it is logical that directly after flashover, a very large amount of pyrolysis gases was produced, and there was neither space for all of these gases inside the compartment nor sufficient oxygen to burn all the combustibles gases inside. Hence, it makes sense that the external flame was particularly large outside Window 4 directly after flashover.

Flame extinction of CLT and decay phase

In both experiments, self-extinguishment of the CLT surfaces (i.e., cessation of flaming combustion) occurred within 15 minutes after flashover. During the self-extinguishment, the temperatures decreased by several hundred degrees and initiated the decay phase of the fire. Summarised, from ignition of the CLT, these fires developed fast with high maximum temperatures but had a relatively short post-flashover phase. In #FRIC-01, self-extinguishment occurred at surface (PT) temperature of 695–705 °C, corresponding to a heat flux of 49–52 kW/m^2. This was well in line with previous findings at bench-scale [21], suggesting a critical heat flux of 43.6 ± 4.7 kW/m^2. In #FRIC-02, however, self-extinguishment occurred at a temperature of 805–845 °C and a heat flux of 70–84 kW/m^2. This is much higher than previously reported values and could have been caused by the low oxygen concentration in the compartment or due to the presence of a thicker char layer.

The decay phase that followed was almost linear in both experiments, with an average temperature decay rate of 7.1 °C/min in #FRIC-01 and 5.7 °C/min in this experiment. The 20% slower decay rate in #FRIC-02 can be explained by the re-radiation between the wall and the ceiling and more heat stored in the CLT wall than in the gypsum boards.

Delamination and final char depth

#FRIC-01 revealed that delamination of CLT could occur before the char front has reached the glue line when using an ordinary PUR adhesive. This ultimately means that the effective thickness of the exposed CLT layer before delamination happens is less than the actual thickness. This also means that two preheated surfaces of fresh wood become exposed. The reason why several lamellas were loose, and some were hanging down, can be explained by two factors. Firstly, only part of the lamella length was detached due to the non-uniform char depth along the lamellae length. Secondly, a lamella not entirely charred through will have some remaining strength that prevents it from falling down or breaking into pieces.

It was also demonstrated that delamination could occur without causing a reignition if the gas temperature is low enough. Such information could be utilised in improving zone models [79] and predicting whether delamination and reignition would occur.

In #FRIC-02, it was shown that with certain different test conditions, this kind of delamination, which created two oppositely exposed surfaces with an air gap between, provided optimal conditions for reignition and the transition to a second flashover. Another interesting detail of the second flashover was when the charred CLT in the ceiling and the back wall started burning again. This transition led to temperatures up to 1050 °C, just 100 °C lower than in the first flashover despite the lack of the wood crib. After the most intense burning phase which lasted a few minutes, the fire varied in intensity but had never a temperature lower than 550 °C below the ceiling and 500 °C by the wall until the fire was manually extinguished at 175 minutes.

During the second flashover, several delaminated lamellae pieces fell down. The largest pieces observed were about 100 cm x the lamella width. However, most pieces were smaller

than this. That delamination is recognised by entire lamellae lengths falling off is, therefore, not necessarily true.

That the fire was still ongoing after almost three hours could be explained by the thin (20 mm) intermediate layers in combination with an adhesive known to cause delamination. With such thin layers, fresh wood was added to the fire with relatively short time intervals and contributed to maintaining a high compartment temperature.

The reason why the delamination led to a second flashover in #FRIC-02 and not in #FRIC-01 was most likely the difference in gas temperature at the time of delamination. In #FRIC-01, the gas temperature under the ceiling was approx. 220 °C at the time of delamination, and 430–445 °C in #FRIC-02.

In both experiments, but in particular in #FRIC-02, the charring was strongly non-uniform with increased charring of the ceiling closer to the back wall and increased charring of the upper parts of the wall. The differences were approx. 30 mm in the ceiling and 10 mm on the wall. Despite massive delamination of the CLT, the average charring rate for the entire test duration was not particularly high: 0.56 mm/min for the ceiling and 0.60 mm/min for the back wall. Also, the average char depth of the wall was higher than that of the ceiling, which is in line with findings in previous experiments, summarised by Mitchell et al. [101].

Ventilation-controlled or fuel-controlled

This experiment had a larger opening factor than the majority of CLT experiments performed, and based on the traditional distinction for compartment fires, it would be considered a fuel-controlled fire (Regime-II).

Despite the well-ventilated compartment, both #FRIC-01 and #FRIC-02 experienced external flames in the most intense burning phase. This behaviour, in combination with the low oxygen concentrations measured, especially in #FRIC-02, highlights that the fire in the most intense burning phases had characteristics more like a ventilation-controlled fire.

Summarised, the fire appeared neither as a true fuel-controlled fire nor a ventilation-controlled fire, as it had elements of both. In several ways, this appearance matched the new proposed regime, *Regime-II-CLT*, proposed by Gorska et al. [102, 103]. They concluded that the burning of exposed CLT would induce additional momentum-driven flows, higher outflow velocities and less time for sufficient mixing, which would lead to more extensive external flames. Similar observations were made by Pope et al. [104].

Temperature distribution

In both experiments, large temperature variations were seen throughout the compartment. In the experiments by Gorska et al., the highest temperatures were measured in the middle height of the compartment due to inefficient mixing between combustible gases and oxygen under the ceiling. However, those results are opposite to what was observed in #FRIC-01 and -02, where the lowest temperatures were measured in the middle height of the compartment. This

can be explained by the relatively large distance between the wood crib and the ceiling and the large window openings.

In #FRIC-02, the temperatures were also strongly affected by the wind, in which less air was supplied through Window 4 compared to the other windows. This resulted in almost uniform temperatures inside Window 4. Inside the other windows, larger temperature gradients were measured.

Smouldering and reignition after termination of the experiment

#FRIC-02 was extinguished just before a test duration of three hours. This was done for two reasons: 1) to avoid a collapse of the compartment, which would have complicated the extinguishing process, and 2) to have some of the CLT remaining for post-measurements.

Another round of extinguishing was carried out approx. two hours after termination of the experiment. Then, the compartment was left unattended. After 7-8 hours after extinguishment, the compartment was burning again in at least two locations on top of the compartment above the opening. Exactly when reignition happened is unknown, as the compartment was not continuously observed after extinguishment.

It is believed that reignition happened when the smouldering process had charred completely through the ceiling as this would provide oxygen to the process [105]. From char depth measurements close to the burned-through section, it is assumed that there was about 70 mm remaining of the CLT after extinguishment. Smouldering in this area was likely maintained due to insufficient extinguishing in the inner corner between the ceiling and the insulated glulam beam, as this location was hard to reach from the outside of the compartment. Extinguishing was performed from the outside as it was not considered safe to be inside the compartment. Another factor that might have influenced this process is the protection of the glulam beam by insulation. The insulation has likely helped maintain the temperature in this area, limited the access to oxygen, and may also have protected the charred wood from being directly cooled by water.

In an actual building fire, some areas could be hard to reach by water due to confinement, concealed spaces or that some areas are not considered safe to enter, and extinguishment must be done at a distance. Thus, it seems likely that ongoing smouldering, as observed in #FRIC-02 and in the Code Red experiments [24], is a potential risk that needs to be considered in actual fires.

Limitations and validity of the results

The experiments were conducted without any automatic extinguishing system, and no measures were made to extinguish the fire before three and four hours after the start of the experiments. This setup was chosen as the aim of the experiment was to study fire spread and fire dynamics without influence from an extinguishing system or a fire brigade. Also, a well-ventilated compartment with a high opening factor was chosen, as there was a lack of

experimental data on this type of configuration. Thus, the results from these experiments are relevant for a compartment which fulfils the following conditions:

- A room, compartment or enclosure with large surface areas of combustible materials, including offices, living rooms, lobbies, etc., in a CLT building, but also balconies with wooden ceilings, wooden car parks and sports halls with exposed combustible surfaces.
- No automatic extinguishing system installed or where the installed system fails to activate.
- A well-ventilated room, either through window glasses that break early, a sufficiently large room volume where the oxygen supply is good even without any broken windows, or simply where the compartment already is well-ventilated, for instance, a semi-open car park, a balcony etc.

Moreover, none of the experiments were loaded. A similar but loaded compartment would likely not have caused any difference in #FRIC-01 but would likely have led to a collapse of the ceiling in #FRIC-02 some time after the second flashover. Nevertheless, the main results of #FRIC-02 would not have been changed.

5.2 CFD simulations

The CFD simulations using FDS were able to reproduce the fast fire spread and the non-symmetrical flames of #FRIC-02. It also gave more insight into the effect of wind, and that wind coming diagonally from behind would create an underpressure in front of the compartment where the wind is passing by. This underpressure would affect the air supply through the windows, which consequently affects the oxygen concentration and the temperature distribution inside the compartment. These results show that a CFD simulation could be useful to further explore mechanisms of fire development in a specific fire experiment, and thus supplement the understanding obtained from measurements and video analysis.

Moreover, the simulations also revealed a few key limitations of the methodology used. The total MLR in the simulation was 5.6 kg/s shortly after flashover, which is the same value as estimated in #FRIC-02. However, this good match was achieved with an underestimation of the MLR of the CLT by 37% and an overestimation of the wood crib MLR of 41%. Thus, the discrepancies effectively cancelled each other out. This is a clear weakness of the model, and it seems like the good match in the total MLR was more by chance than due to a very accurate simulation of the wood crib and the CLT.

Moreover, the effect of replacing the exposed back wall with an encapsulated back wall was also studied. The results indicated that the fire would develop almost as fast as with the back wall exposed, which does not align with the observations of #FRIC-01. It is noted that the ignition package in the simulation was larger than in #FRIC-01, but it still seems unrealistic. A hypothesis was suggested, which explained the results due to the too high MLR of the wood crib and too low MLR of the back wall. The consequence of such an imbalance of the MLR contribution is that removing the exposed wall constitutes a too little change in the overall setup, and we, therefore, end up with almost the same result.

The hypothesis was tested out by running another simulation with updated values for the heat release rate per unit area (HRRPUA) for the wood crib and the CLT, which better matched the estimated MLR values from the experiment. These changes led to a slower fire spread rate, but still much faster than expected based on the results from #FRIC-01. This underlines that fire is a complex phenomenon, and the choice of the simple fire spread model seems unable to accurately predict the fire spread for a random CLT compartment setup.

The model could possibly have been more accurate with more optimised values for the HRRPUA and the ignition temperature. This could be an option if one should reproduce results as close as possible to a known outcome. However, this is trickier if there is no data to compare against. Thus, a better solution in the long term is to develop further the single-scheme, or possibly the parallel scheme, advanced pyrolysis model where the burning rate is coupled to the temperature and the oxygen concentration [106], and thus also directly to the surroundings. With such a setup, the MLR and HRR of a wood crib or CLT elements would change with the number and orientation of CLT surfaces.

5.3 Discussion of a real incident – fast fire spread in school gym

This section gives insight into the fire development of an actual fire in a large room with large surfaces of exposed wood and large windows along one wall. Overall, a fire and geometry somewhat related to the #FRIC-01 and -02 experiments.

On the 24th of April 2023, a massive fire occurred in a school gym at Lambertseter School in Oslo, Norway, see Fig. 69. The information presented here has not been published elsewhere and provides new information and an extended understanding compared to what is already presented in media [107, 108]. The content is based on a conversation 14th of September 2023 with the investigation leader at Oslo Fire Brigade, who was responsible for the investigation of the fire. The investigation report is currently confidential and not available.

Fig. 69 Massive fire at Lambertseter school gym. Here, all windows have been broken. The image was taken approx. 16 minutes after ignition. Photo: Glenn Berggren, used with permission.

The gym had combustible materials in form of wood panels in the ceiling, end walls, and part of the long walls, as seen in Fig. 70. Windows were located along one entire long wall, see Fig. 71.

The gym was not in use when the fire started, and there was no extra fuel on the floor except for the wooden floor. The floor area of the room was approx. 15 m x 28 m = 420 m^2, and the ceiling height was approx. 6 m.

The fire started in a waste basket similar to the one highlighted in Fig. 70. Approx. 7 minutes after the ignition of the waste basket, the fire had spread to the ribbon cladding where the basket was hanging and to an equipment room behind, and the first flames impinged on the ceiling of the gym.

At approx. 7.5 minutes, a window was blown open by the pressure build-up in the room, and about one minute later, an exit door was blown open by the pressure. Shortly after, an external flame, almost like a jet fire, burned fiercely out of the door opening [108]. In discussion forums, it has been speculated that this jet fire must have been due to storage of gas cylinders.

However, this was not case, instead the jet fire occurred as a result of the imbalance between combustible gases and oxygen inside the room and the pressure build-up that had been created.

The fire was detected after 3.5 minutes after ignition by smoke sensors located in the ceiling of the gym. The activation of the sensors triggered a direct call to the fire brigade. The first fire truck arrived at 11 minutes and started to extinguish the fire at 13 minutes. Within this time, more and more of the windows were broken.

After 14 minutes, flames emerged out of all window openings.

At 15 minutes, the smoke gases ignited, leading to a flashover inside the gym. The fire was at its most intense at 16.5 minutes.

Fig. 70 Image of Lambertseter school gym before the fire. The fire started in a waste basket similar to the one highlighted. The location was in another entrance corridor more to the left of the image perspective. The image is edited with permission by SG AS [109].

Fig. 71 The window wall of the school gym before the fire. The door to the left was blown open by the pressure. Photo: Google Maps/Google Street View.

This fire is a real example showcasing that a fire can develop fast in a large compartment with a high ceiling height despite little fuel on the floor. Although the details of the fire spread inside the room are not perfectly clear, it is still evident that the combustible lining was the main contributor to the fire spread as there simply were very few other combustible items in the room. This incident serves as a real-life reminder that combustible surfaces should not be neglected when considering fire safety of large compartments.

Besides the fast fire spread, the external flames emerging from the windows had a high velocity, extended several meters from the facade, and covered the entire opening height for a short period [108]. In fact, quite similar development as observed in #FRIC-02.

Most travelling fire experiments, and fire experiments in general, have had no windows installed, just openings. Many are sceptical about the realism of this kind of test setup, which assumes that windows would break early in a fire. From the available information on the school gym fire, it seems like the closed windows affected the fire development in several ways. A smoke layer was formed, trapping combustible gases inside the room and caused a significant pressure build-up. Moreover, the jet-like fire emerging from the door opening shortly after it was blown open indicates that the compartment was strongly under-ventilated at this point.

How large the pressure was is unknown, but as the pressure could blow open both a window and an exit door, it must have been significant. This illustrates that the pressure build-up may be just as critical as temperature exposure for compromising the integrity of windows and doors in the early stages of a fire. The opening of the door and window seemed to trigger a change in the fire dynamics, and with more and more windows being broken, the fire could grow larger and larger until all combustibles were burning.

The compartment characteristics with no fuel load on the floor except the floor itself, a high ceiling height, closed windows, and large combustible surfaces are relevant for many room types, including lobbies, entrance halls, reception areas, etc.

The fire also demonstrated that several key aspects typically associated with CLT, like a fast fire spread rate and extensive external flaming, could be just as relevant for a room with a non-combustible structure (steel or concrete) but with an exposed wooden cladding.

5.4   CLT – a material in the future?

CLT has become so popular and widespread that its use is far beyond the current knowledge on how exposed CLT affects the fire dynamics and fire spread. In countries where CLT is trending, there are typically performance-based building regulations. This means that a certain flexibility is allowed. For instance, having surfaces of exposed wood would be accepted, given that the building could provide a safety level similar to or better than a reference building. In addition, for lower building heights, a prescriptive set of rules is commonly available.

We know that many CLT buildings have large surfaces of exposed CLT. From #FRIC-01, #FRIC-02 and similar experiments, it is demonstrated that a fire might develop very fast in large rooms with exposed CLT after ignition of the CLT. In many buildings, an automatic extinguishing system is the main barrier to mitigating the effect of exposed wood. Although just a few large-scale CLT experiments with an automatic extinguishing system have been conducted [48, 98, 110, 111], the large statistical data of sprinkler effectiveness on a variety of different fires [112] strongly suggests that a properly designed and maintained automatic extinguishing system would extinguish or control a fire also in a CLT building, and thus preventing the rapid fire spread as seen in #FRIC-01 and -02.

However, far from all CLT buildings have an automatic extinguishing system installed. Thus, it seems likely that many buildings worldwide have a CLT configuration that could cause a rapidly developing fire. A rapidly developing fire is more prone to cause large damage to property. Firstly, because the fire has grown larger before the fire brigade arrives at the fire scene, and secondly, a large fire in itself is harder to extinguish. A rapidly growing fire is also a bigger threat to personal safety as the available egress time is reduced.

Hence, it seems like the performance-based design or prescriptive rules related to exposed wood have had a blind spot in ensuring that fire safety is guaranteed at an acceptable level for all buildings.

Historically, building regulations have often been changed after large fire catastrophes. The fire in the Grenfell Tower is an example of a fire tragedy which resulted in stricter building regulations [113]. When regulations are changed in the wake of such catastrophes, they may end up being unnecessarily strict, thus possibly excluding an entire segment of materials or products from the market. This is also a risk for CLT in case of a devastating fire.

Given that a catastrophic fire occurs in a CLT building, this could end up restricting exposed wood in all buildings above a certain height and area, either through regulations, public dissatisfaction, or difficulties in getting such buildings insured. This would be a major setback for the CLT industry and the path towards a more sustainable building industry.

To avoid that such a devastating fire occurs, it is critical that we have sufficient knowledge of how the fire risks change when we introduce large surfaces of exposed wood into our buildings. Additionally, the known hazards must be effectively communicated to all parties involved in the process of building with CLT [114]. Furthermore, if an automatic sprinkler system should be the main barrier against fire, it is critical that the system is properly set up and regularly maintained and controlled. In the large-scale CLT compartment experiment by Hox [110], the sprinkler system was not able to extinguish or control the fire in a corridor

when the sprinkler system (two nozzles) was disconnected in the adjacent room where the fire started.

Despite new knowledge has been gained through several large-scale experiments lately, including #FRIC-01 and -02, there are still several knowledge gaps to fill. To move forward, it is crucial that more people, including building owners, architects, engineers, the CLT industry and other relevant building stakeholders become more proactive and take ownership of this problem.

The CLT industry tends to be sceptical of conducting certain fire experiments, as they might showcase results that are considered unfortunate for the industry. However, it must be highlighted that it is much better to experience 'unfortunate' results in a controlled fire experiment than in a real building fire.

To round off this section, I would like to cite Danny Hopkin's LinkedIn comment [115] about a magazine article [116] that only addressed the positive results from a CLT test series:

"What [the industry/timber lobby] fail to appreciate is that [communicating only the positive results] is unhelpful to their end-game too. Something can only be 'sustainable' if you have addressed the hazards and don't flirt with a future ban."

5.5 I-joist experiments

The I-joists experiments have gained experimental data on how I-joists protected with combustible insulation behave in a standardised furnace test. The charring rates from the exposed side in the protected phase were mostly on the conservative side when compared against the current model for rectangular cross-sections and the proposed new model for I-joists.

However, when combining I-joists and combustible insulation, only considering the char depth from the exposed side can give a false impression of the remaining cross-section. For one specimen, this was clearly demonstrated. There was a good linear fit for the data points in the protected phase, and the measured charring rates were conservative. With this information, 20 mm of the flange was expected to remain at gypsum board fall-off. However, the flange was fully charred after just 2 minutes in the post-protected phase, which does not make sense. An increase in the charring rate must have been present already in the protected phase, and very little of the flange was likely remaining at gypsum board fall-off. Hence, it seems unlikely that the charring rate was constant in the entire protected phase. By comparing the lateral charring of the other flanges of the same experiment, it was evident that the lateral charring in this flange was significant, which makes sense based on the result. This example demonstrates that more complex models are needed to determine the remaining cross-section of I-joists when combined with combustible insulation.

Lateral charring is particularly important when considering I-joists, as the structural capacity is strongly dependent on the exposed flange and the web. A rectangular member would be charred similarly under similar conditions, but lateral charring would not influence a rectangular member in the same way, as it has the same cross-section profile along its whole length. The challenge with lateral charring is especially high for I-joists with small flange widths.

The results showed that all tested insulation types had a lower recession rate than the generic value of glass wool insulation. If these values can be confirmed in other experiments, this means that glass wool insulation can be replaced by a biobased insulation, thus providing a more sustainable alternative.

In one experiment, the effect of insulation fall-down on the charring was demonstrated, as the insulation on one side of the flange fell down but remained in place on the other side. The different exposure led to a much more pronounced charring of the side where the insulation had fallen down. Essentially, insulation fall-down causes the flange to be exposed to flames from three sides (exposed, lateral and top), which effectively reduces the remaining cross-section. In addition, the web will be directly exposed to flames. Both of these events will significantly reduce the remaining load-bearing capacity of the I-joist. Hence, avoiding the insulation of falling down is beneficial for the load-bearing capacity.

Insulation is, in general, prone to fall down when the gypsum boards fall down. However, in these experiments the insulation generally stayed well in place after gypsum board failure. This was likely due to the profile of the I-joists and the oversizing of the insulation batts, which assisted in keeping the insulation in place. This could be exploited in the fire safety

strategy of I-joist. However, clear instructions details are needed if this should be implemented in actual installations.

Through this test series, it has been revealed that the way the protection level of combustible insulation is determined may not be representative of combustible insulation used in combination with I-joists. In the suggested setup to define the protection level, shrinking of the insulation will play a major role when determining the recession rate. However, in this setup, shrinking did not seem to play a large role. This is believed to be due to the characteristic I-joist profile and the oversizing of the insulation batts, which could contribute to keeping the insulation in place after gypsum board fall-off.

Limitations

None of the experiments were loaded. This might have influenced the time until gypsum board failure but is not expected to have affected the overall results. Furthermore, it is known that combustible insulation may influence the fire dynamics in a compartment fire as they contribute to additional pyrolysis gases. This effect is not studied or assessed here.

6   Conclusion

In this thesis, fire experiments of CLT and I-joists have been conducted to gain new knowledge and a better understanding of how these products behave in a fire.

CLT experiments

The CLT experiments, #FRIC-01 (exposed ceiling) and #FRIC-02 (exposed ceiling and wall), aimed to better understand and gain knowledge on how two different configurations of CLT affect the fire dynamics in a large compartment, including fire spread and travelling fire behaviour, self-extinction of flaming combustion, external flames, charring behaviour and delamination of CLT, and the decay phase. The following points are considered the most important findings:

Fire spread and travelling fire behaviour

- The CLT ceiling in #FRIC-01 ignited first at 32.5 min. At this point, the fire had only spread 1.5 m along the crib, and the first part of the crib had started burning out. The late ignition could be explained by an initial slow fire development, flames not impinging on the ceiling and the limited conditions for a thick smoke layer to build up due to the large ventilation openings.

- The fire dynamics and fire spread rate changed significantly following the ignition of the CLT ceiling, in which flames rapidly travelled beneath the ceiling and created a strong radiative heat flux to the wall and the floor. After ignition of the ceiling in #FRIC-02, the fire spread continuously across the room until the fully developed fire was reached. In #FRIC-01, however, the flames instead travelled back and forth several times before the fully developed fire was achieved 13 minutes later. Despite this oscillating behaviour of the flames, which have been named *flashing waves*, the wood crib fire grew larger during each wave, and its development was thus accelerated by the waves. This was recognised by the distinct shift in the fire spread rate, which increased from an average value of 54 mm/min before the ceiling ignition to 1.2 m/min after ignition.

- The rate of fire development of #FRIC-01 was in strong contrast to previous experiments and may be relevant for compartment designs with a low likelihood of ceiling-impinging flames (e.g., with a high ceiling) and a low potential for collection of combustible gases under the ceiling, e.g., compartments with ceiling beams of limited height.

- In #FRIC-02, the fire spread across the room in just 91 seconds after ignition of the ceiling. This corresponds to an average fire spread rate of 12 m/min across the wood crib and 15 m/min across the ceiling. To my best knowledge, this is the fastest fire spread rate registered in a travelling fire with only wood as fuel.

- In both experiments, the fire spread rate increased exponentially, which indicates that significantly larger compartments would not necessarily take significantly more time to ignite under similar conditions.

Charring rate

- The average final char depth of the CLT ceiling was 26 mm ± 4 mm standard deviation (n = 250) in #FRIC-01 with an average charring rate of 1.1 mm/min. The charring was least pronounced at the ignition end of the compartment (24 mm) and the most pronounced from the centre and towards the other end (29 mm). Also, a few mm increased charring was observed close to the back wall.

- In #FRIC-02, the average final char depth was 97 mm ± 13 mm (std, n = 150) for the ceiling and 106 mm ± 7 mm (std, n = 121) for the back wall. Also here, increased charring of the ceiling was seen towards the back wall. Furthermore, the upper parts of the wall were more charred than the lower parts. The differences were approx. 30 mm in the ceiling and 10 mm on the wall. Despite delamination, the average charring rate was quite low, with 0.56 mm/min for the ceiling and 0.60 mm/min for the back wall.

- The charring rate was initially high but was reduced significantly for each subsequent 10 mm into the CLT. The charring rates for 0–10, 10–20 and 20–30 mm into the wood were 2.23, 1.13 and 0.35 mm/min, respectively in #FRIC-01, and 2.68, 1.43 and 0.38 mm/min, respectively in #FRIC-02. The initially high charring rates did not affect the total average charring rate much but contributed to a large amount of pyrolysis gases being produced in the first few minutes after ignition, which facilitated the rapid fire spread rate and external flames.

External flames

- In both experiments, external flames emerged from all window openings during the most intense burning phase. However, due to the larger HRR in #FRIC-02, the external flames were larger and were present for a longer time. The incident heat flux at 2.8 m above the window soffit was above 50 kW/m^2 for approx. 10 seconds in #FRIC-01 and above this value for approx. 5.5 minutes in #FRIC-02. Furthermore, in #FRIC-02, most of the flames emerged out from one window opening. The flames were particularly large directly after flashover, covered almost the entire window opening and reached more than 3 m above the window soffit. It is estimated that the external flames directly after flashover had a HRR of 66 ± 20 MW for a short period.

- The large and non-symmetrical flames can be explained by the wind coming diagonally from behind, creating an underpressure outside one window in particular, which dragged smoke and flames out of that window. This effect also reduced the inflow of air through that window, which caused more homogeneous temperatures in this part compared to the rest of the compartment.

- Another contributing factor to the large external flames was the very rapid fire development which created a large amount of pyrolysis gases in a short time.

- A CFD simulation of the experiment reproduced the large and non-uniform flames to a great extent and confirmed the influence of wind. This result demonstrated that large external flames can occur even in well-ventilated compartments with exposed CLT under quite ordinary wind conditions.

Maximum temperatures and heat release rates

- The temperatures were during the most intense period 1010–1172 °C in the whole compartment, while in #FRIC-01, they were 785–1038 °C. The more extreme temperatures were caused by a 32 MW (78%) higher maximum total HRR in #FRIC-02 than in #FRIC-01. Besides the 13 MW increase due to the exposed back wall, the HRR of the CLT ceiling increased by 3.5 MW (21%) and the wood crib increased by 15 MW (75%) despite having the exact same wood crib arrangement. Of these 15 MW, 5 MW was due to the higher HRR per unit length caused by higher temperatures and more considerable heat fluxes towards the wood crib. The remaining 10 MW was due to faster fire spread across the wood crib, which caused a larger part of the crib to burn simultaneously at a higher HRR per unit length.

Self-extinguishment of CLT and the decay phase

- Self-extinguishment of CLT (i.e., cessation of flaming combustion) occurred in both experiments within 15 minutes after flashover. In #FRIC-01, this happened at temperatures of 695 – 705 °C measured by a plate thermometer, corresponding to an incident heat flux of 49 – 52 W/m^2. In #FRIC-02, this happened at 805 – 845 °C and 70 – 84 kW/m^2, which are higher than previously reported. The higher values are believed to be due to the low oxygen concentration in the compartment and possibly due to the presence of a thicker char layer than in #FRIC-01.

- The process of self-extinguishment behaved in a similar manner as the fire spread, in which it started from the ignition side and continued across the compartment in almost the same time as the fire spread the same distance, i.e., 11 minutes in #FRIC-01 and 3 minutes in #FRIC-02. The following decay phase was nearly linear in both experiments, with an average temperature reduction of 7.1 °C/min in #FRIC-01 and 5.7 °C/min in #FRIC-02. The slower decay phase in #FRIC-02 can be explained by the increased heat feedback between wall and ceiling and more heat stored in the CLT wall than in the gypsum boards.

Delamination and second flashover

- In #FRIC-01, it was observed that several lamellas were loose, and some were hanging down due to delamination. The layer behind was mostly discoloured and not charred, proving that delamination happened before the exposed lamellae had been charred fully through.

- The reason why the loose and partly hanging lamellas did not fall down, can be explained by two factors. Firstly, only part of the lamella length was detached due to the non-uniform char depth along the lamellae length. Secondly, a lamella not entirely charred through will have some remaining strength that prevents it from falling down or breaking into pieces.

- When delamination happens before the exposed layer has charred through, the effective thickness of the layer becomes less than the actual thickness. Furthermore, this kind of delamination exposes two preheated surfaces of fresh wood with a small air gap in between.

- No reignition occurred, but a few hot spots were detected by an infrared camera. This result aligns with a few other experiments by showing that delamination of CLT does not always lead to a second flashover. Also worth highlighting is that self-extinguishment of the CLT in this experiment was achieved despite using an adhesive that lacks a demonstrated resistance against glue-line integrity failure.

- In #FRIC-02, delamination caused several small fires to spontaneously occur in both the wall and the ceiling approx. 50 minutes after the flames of the CLT had extinguished. Within 10 minutes, the flames developed until a fully developed fire with temperatures up to 1050 °C, i.e., almost as high as after the first flashover. After the most intense burning phase which lasted a few minutes, the fire varied in intensity but had never a temperature lower than 550 °C below the ceiling and 500 °C by the wall until the fire was manually extinguished at 175 minutes.

- The reason why a second flashover occurred in #FRIC-02 and not in #FRIC-01 can be explained by the different gas temperatures next to the CLT at the point when delamination happened, approx. 220 °C for #FRIC-01 and 430 – 445 °C in #FRIC-02.

- Several hot spots were detected in #FRIC-01 behind the delaminated lamellas and in the corner between the ceiling and the insulated glulam beam. No reignition happened after extinguishment.

- In #FRIC-02, the CLT reignited in at least two locations on top of the compartment above the glulam beam 7–8 h after the end of the experiment. This was likely due to insufficient extinguishing in the corner between the ceiling and the insulated glulam beam which allowed smouldering to continue in this area.

CFD-simulation

- The simulations were able to reproduce the fast fire spread of #FRIC-02 and gave increased insight into the effect of wind on the fire dynamics.

- A CFD simulation can be useful to further explore mechanisms of fire development in a specific fire experiment, and thus supplement the understanding obtained from measurements and video analysis.

Findings from a real incident – Lambertseter school gym fire

The findings of the CLT experiments have been supplemented by findings from an actual fire in a school gym, which had a somewhat related geometry and large surfaces of exposed wood. The floor area was approx. 420 m², the ceiling height was approx. 6 m, and windows were present along one wall. The key findings are given below:

- A fire that initially started in a waste basket in an empty school gym developed into a fully developed fire before the fire brigade was able to start extinguishing, despite that the activation of the smoke sensors triggered a direct call to the fire brigade.

- The main driver for the fast fire spread was the combustible lining of the floor, ceiling and parts of the wall as there simply were very few other combustible items in the room.

- The fire also demonstrated that several key aspects typically associated with CLT, like a fast fire spread rate and extensive external flaming, could be just as relevant for a room with a non-combustible structure (steel or concrete), but with an exposed wooden cladding.

- The windows and doors were initially closed, but the pressure build-up due to the increased temperature was sufficient to blow open an exit-door and a window. The supply of fresh air from this point triggered a change in the fire dynamics and led to a flashover approx. 7 minutes later. This illustrates that the pressure build-up may be just as critical as temperature exposure for compromising the integrity of windows and doors in the early stages of a fire.

- Besides the fast fire spread, the external flames emerging from the windows had a high velocity, extended several meters from the facade, and covered the entire opening height for a short period. In fact, quite similar development as observed in #FRIC-02.

- This fire is a real example showcasing that a fire can develop fast in a large compartment with a high ceiling height despite little fuel on the floor. The compartment characteristics with no fuel load on the floor except the floor itself, a high ceiling height, closed windows, and large combustible surfaces are relevant for many room types, including lobbies, entrance halls, reception areas, etc.

I-joists

Through five furnace tests, the aim was to gain experimental data on charring rates of I-joists and recession rates for different types of combustible insulation.

- The charring rates increased with increasing flange size and the charring rates of solid wood and laminated veneer lumber were comparable.

- The charring rates for the flanges were 0.40–0.76 mm/min for the protected phase. These rates were, in general, conservative compared to the current and upcoming design model of Eurocode 5.

- Lateral charring was significant also in the protected phase, and should not be neglected as the load-bearing capacity of the I-joists is strongly dependent on the remaining cross-section of the flange.

- The insulation stayed in general well in place due to oversizing of the insulation batts and the I-joist profile, which assisted in keeping the insulation from falling-down.

- All the tested types of bio-based combustible insulation had recession rates lower than glass wool: 3.3 ± 0.7 mm/min for the wood fibre batt, 2.3 ± 0.5 mm/min for the wood fibre loose-fill, and 1.1 ± 0.04 mm/min for the cellulose loose-fill.

- Due to the lack of repetitions of the experiments, results should be considered as indicative.

7   Future work

CLT

Although these experiments have contributed with new information about how exposed surfaces affect the fire dynamics of a large, ventilated compartment, future research is still needed on the following topics:

- How the effect of an exposed ceiling changes with increased ceiling height.
- How an exposed wall would influence the fire dynamics.
- Whether adding an exposed wall could even out the effect of having a high ceiling height.
- How wind could impact the fire dynamics and external flames.
- At which gas temperatures would delamination lead to reignition.
- What parameters that facilitate continued smouldering of CLT and glulam beams after burn-out of the variable fuel load.
- How modern glass types behave in fires and how their behaviour affects the fire development in large open compartments with exposed CLT.

I-joists

Further research is needed on the following topics:

- Advanced analysis of the lateral charring.
- More insulation products to be tested as they clearly have large differences.
- More studies focusing on the fall-down time and shrinkage of the insulation as these parameters directly affect the calculated recession rates.
- Assess whether the current setup for defining protection levels of new insulation is relevant for insulation used in combination with I-joists.

References

[1]   IEA, "2022 Global status report for buildings and construction: Towards a zero-emission, efficient and resilient buildings and construction sector.," United Nations Environment Programme (2022). Nairobi, Kenya, 2022 2022. https://www.unep.org/resources/publication/2022-global-status-report-buildings-and-construction

[2]   IPCC, "Climate Change 2023: Synthesis Report. Contribution of Working GroupsI, II and III to the Sixth Assessment Report of the Intergovernmental Panel on Climate Change [Core Writing Team, H. Lee and J. Romero (eds.)]," IPCC, Geneva Switzerland, 2023.

[3]   G. Meng, "Wood and Engineered Wood Products: Stress and Deformation," in *Engineered Wood Products for Construction*, G. Meng Ed. Rijeka: IntechOpen, 2021, p. Ch. 1.

[4]   ARUP. "HAUT, Amsterdam - Designing and engineering the Netherlands' tallest timber-hybrid residential building." Accessed: 16.10.2023. https://www.arup.com/projects/haut

[5]   Dezeen. "Ascent skyscraper in Milwaukee becomes world's tallest timber building." Accessed: 16.10.2023. https://www.dezeen.com/2022/08/03/ascent-tower-milwaukee-worlds-tallest-timber-building/

[6]   Moelven. "Mjøstårnet." Accessed: 16.10.2023. https://www.moelven.com/mjostarnet/

[7]   *International Building Code (ICC IBC-2021)*, ANSI, 2021.

[8]   V. Kotradyova, E. Vavrinsky, B. Kalinakova, D. Petro, K. Jansakova, M. Boles, and H. Svobodova, "Wood and Its Impact on Humans and Environment Quality in Health Care Facilities," *International Journal of Environmental Research and Public Health,* vol. 16, no. 18, 3496, 2019. [Online]. Available: https://www.mdpi.com/1660-4601/16/18/3496.

[9]   A. Ojala, J. Kostensalo, J. Viik, H. Matilainen, I. Wik, L. Virtanen, and R. Muilu-Mäkelä, "Psychological and physiological effects of a wooden office room on human well-being: Results from a randomized controlled trial," *Journal of Environmental Psychology,* vol. 89, 102059, 2023/08/01/ 2023, doi: https://doi.org/10.1016/j.jenvp.2023.102059.

[10]   M. Li, S. Zhang, Y. Gong, Z. Tian, and H. Ren, "Gluing techniques on bond performance and mechanical properties of cross-laminated timber (CLT) made from Larix kaempferi," *Polymers,* vol. 13, no. 5, 733, 2021, doi: https://doi.org/10.3390/polym13050733.

[11]   F. Wiesner, D. Thomson, and L. Bisby, "The effect of adhesive type and ply number on the compressive strength retention of CLT at elevated temperatures," *Construction and Building Materials,* vol. 266, 121156, 2021/01/10/ 2021, doi: https://doi.org/10.1016/j.conbuildmat.2020.121156.

[12]   H.-E. Blomgren, S. Pei, Z. Jin, J. Powers, J. D. Dolan, J. W. v. d. Lindt, A. R. Barbosa, and D. Huang, "Full-Scale Shake Table Testing of Cross-Laminated Timber Rocking Shear Walls with Replaceable Components," *Journal of Structural Engineering,* vol. 145, no. 10, 04019115, 2019, doi: https://doi.org/10.1061/(ASCE)ST.1943-541X.0002388.

[13]   A. I. Bartlett, R. M. Hadden, and L. A. Bisby, "A Review of Factors Affecting the Burning Behaviour of Wood for Application to Tall Timber Construction," *Fire Technology,* vol. 55, no. 1, pp. 1-49, 2019/01/01 2019, doi: https://doi.org/10.1007/s10694-018-0787-y.

[14]   K. L. Friquin, "Material properties and external factors influencing the charring rate of solid wood and glue-laminated timber," *Fire and Materials,* vol. 35, no. 5, pp. 303-327, 2011, doi: https://doi.org/10.1002/fam.1055.

[15]   R. Emberley, C. Gorska, A. Bolanos, A. Lucherini, A. Solarte, D. Soriguer, M. G. Gonzalez, K. Humphreys, J. P. Hidalgo, C. Maluk, A. Law, and J. L. Torero, "Description of small and large-scale cross laminated timber fire tests," *Fire Safety Journal,* vol. 91, pp. 327-335, 2017, doi: https://doi.org/10.1016/j.firesaf.2017.03.024.

[16]   R. M. Hadden, A. I. Bartlett, J. P. Hidalgo, S. Santamaria, F. Wiesner, L. A. Bisby, S. Deeny, and B. Lane, "Effects of exposed cross laminated timber on compartment fire dynamics," *Fire Safety Journal,* vol. 91, pp. 480-489, 2017, doi: https://doi.org/10.1016/j.firesaf.2017.03.074.

[17] J. Su, P.-S. Lafrance, M. S. Hoehler, and M. F. Bundy, "Fire Safety Challenges of Tall Wood Buildings–Phase 2: Task 3-Cross Laminated Timber Compartment Fire Tests. Report no. FPRF-2018-01-REV," NFPA (National Fire Protection Association), Quincy, Massachusetts, USA, 2018. Accessed: March 28, 2023. https://tsapps.nist.gov/publication/get_pdf.cfm?pub_id=925297

[18] D. Brandon, J. Sjöström, A. Temple, E. Hallberg, and F. Kahl, "RISE report - Final Project Report - Fire Safe implementation of visible mass timber in tall buildings - compartment fire testing (2021:40)," RISE Fire Research, 2021. http://urn.kb.se/resolve?urn=urn:nbn:se:ri:diva-58153

[19] D. Hopkin, W. Węgrzyński, M. Spearpoint, I. Fu, H. Krenn, T. Sleik, C. Gorska, and G. Stapf, "Large-scale enclosure fire experiments adopting CLT slabs with different types of polyurethane adhesives: genesis and preliminary findings," *Fire,* vol. 5, no. 2, 2022, doi: https://doi.org/10.3390/fire5020039.

[20] J. Cuevas, J. L. Torero, and C. Maluk, "Flame extinction and burning behaviour of timber under varied oxygen concentrations," *Fire Safety Journal,* vol. 120, 103087, 2021, doi: https://doi.org/10.1016/j.firesaf.2020.103087.

[21] R. Emberley, T. Do, J. Yim, and J. L. Torero, "Critical heat flux and mass loss rate for extinction of flaming combustion of timber," *Fire Safety Journal,* vol. 91, pp. 252-258, 2017, doi: https://doi.org/10.1016/j.firesaf.2017.03.008.

[22] X. Li, X. Zhang, G. Hadjisophocleous, and C. McGregor, "Experimental study of combustible and non-combustible construction in a natural fire," *Fire Technology,* vol. 51, no. 6, pp. 1447-1474, 2015, doi: https://doi.org/10.1007/s10694-014-0407-4.

[23] P. Kotsovinos, E. Rackauskaite, E. Christensen, A. Glew, E. O'Loughlin, H. Mitchell, R. Amin, F. Robert, M. Heidari, D. Barber, G. Rein, and J. Schulz, "Fire dynamics inside a large and open-plan compartment with exposed timber ceiling and columns: CodeRed #01," *Fire and Materials,* vol. 47, no. 4, pp. 542-568, 2023, doi: https://doi.org/10.1002/fam.3049.

[24] H. Mitchell, R. Amin, M. Heidari, P. Kotsovinos, and G. Rein, "Structural hazards of smouldering fires in timber buildings," *Fire Safety Journal,* vol. 140, 103861, 2023/10/01/ 2023, doi: https://doi.org/10.1016/j.firesaf.2023.103861.

[25] F. Wiesner, A. Bartlett, S. Mohaine, F. Robert, R. McNamee, J.-C. Mindeguia, and L. Bisby, "Structural Capacity of One-Way Spanning Large-Scale Cross-Laminated Timber Slabs in Standard and Natural Fires," *Fire Technology,* vol. 57, no. 1, pp. 291-311, 2021/01/01 2021, doi: https://doi.org/10.1007/s10694-020-01003-y.

[26] T. Gernay, J. Zehfuß, S. Brunkhorst, F. Robert, P. Bamonte, R. McNamee, S. Mohaine, and J.-M. Franssen, "Experimental investigation of structural failure during the cooling phase of a fire: Timber columns," *Fire and Materials,* vol. 47, no. 4, pp. 445-460, 2023, doi: https://doi.org/10.1002/fam.3110.

[27] R. Crielaard, J.-W. van de Kuilen, K. Terwel, G. Ravenshorst, and P. Steenbakkers, "Self-extinguishment of cross-laminated timber," *Fire Safety Journal,* vol. 105, pp. 244-260, 2019/04/01/ 2019, doi: https://doi.org/10.1016/j.firesaf.2019.01.008.

[28] D. Brandon and C. Dagenais, "Fire Safety Challenges of Tall Wood Buildings – Phase 2: Task 5 - Experimental Study of Delamination of Cross-Laminated Timber (CLT) in Fire," FPRF-2018-05, 2018.

[29] *ANSI/APA PRG 320-2018 Standard for Performance-Rated Cross-Laminated Timber*, ANSI, USA, 2018.

[30] A. Frangi, M. Fontana, and A. Mischler, "Shear behaviour of bond lines in glued laminated timber beams at high temperatures," *Wood Science and Technology,* vol. 38, no. 2, pp. 119-126, 2004/05/01 2004, doi: https://doi.org/10.1007/s00226-004-0223-y.

[31] J. Sjöström, D. Brandon, A. Temple, E. Hallberg, and F. Kahl, "RISE report - Exposure from mass timber compartment fires to facades (2021:39)," RISE Fire Research, 2021.

112

[32]   L. A. Bisby, A. Bartlett, R. McNamee, J. Zehfuss, J.-M. Franssen, F. Robert, C. Tessier, and S. Mohaine, "Epernon Fire Tests Programme - Synthesis Report," 2020.

[33]   R. McNamee, J. Zehfuss, A. I. Bartlett, M. Heidari, F. Robert, and L. A. Bisby, "Enclosure fire dynamics with a cross-laminated timber ceiling," *Fire and Materials,* vol. 45, no. 7, pp. 847-857, 2020, doi: https://doi.org/10.1002/fam.2904.

[34]   J. Sjöström, D. Brandon, A. Temple, J. Anderson, and R. McNamee, "External fire plumes from mass timber compartment fires—Comparison to test methods for regulatory compliance of façades," *Fire and Materials,* vol. 47, no. 4, pp. 433-444, 2023, doi: https://doi.org/10.1002/fam.3129.

[35]   T. Engel and N. Werther, "Impact of Mass Timber Compartment Fires on Façade Fire Exposure," *Fire Technology,* vol. 59, pp. 517-588, 2023, doi: https://doi.org/10.1007/s10694-022-01346-8.

[36]   J. Stern-Gottfried and G. Rein, "Travelling fires for structural design–Part I: Literature review," *Fire Safety Journal,* vol. 54, pp. 74-85, 2012/11/01/ 2012, doi: https://doi.org/10.1016/j.firesaf.2012.06.003.

[37]   V. Gupta, J. P. Hidalgo, D. Lange, A. Cowlard, C. Abecassis-Empis, and J. L. Torero, "A Review and Analysis of the Thermal Exposure in Large Compartment Fire Experiments," *International Journal of High-Rise Buildings,* vol. 10, no. 4, pp. 345-364, 2021, doi: https://doi.org/10.21022/IJHRB.2021.10.4.345.

[38]   A. Nadjai, A. Naveed, M. Charlier, O. Vassart, S. Welsh, A. Glorieux, and J. Sjostrom, "Large scale fire test: The development of a travelling fire in open ventilation conditions and its influence on the surrounding steel structure," *Fire Safety Journal,* vol. 130, 103575, 2022/06/01/ 2022, doi: https://doi.org/10.1016/j.firesaf.2022.103575.

[39]   J. P. Hidalgo, A. Cowlard, C. Abecassis-Empis, C. Maluk, A. H. Majdalani, S. Kahrmann, R. Hilditch, M. Krajcovic, and J. L. Torero, "An experimental study of full-scale open floor plan enclosure fires," *Fire Safety Journal,* vol. 89, pp. 22-40, 2017, doi: https://doi.org/10.1016/j.firesaf.2017.02.002.

[40]   E. Rackauskaite, M. Bonner, F. Restuccia, N. Fernandez Anez, E. G. Christensen, N. Roenner, W. Wegrzynski, P. Turkowski, P. Tofilo, M. Heidari, P. Kotsovinos, I. Vermesi, F. Richter, Y. Hu, C. Jeanneret, R. Wadhwani, and G. Rein, "Fire experiment inside a very large and open-plan compartment: x-ONE," *Fire Technology,* vol. 58, pp. 905-939, 2022, doi: https://doi.org/10.1007/s10694-021-01162-6.

[41]   M. Heidari, E. Rackauskaite, M. Bonner, E. Christensen, S. Morat, H. Mitchell, P. Kotsovinos, P. Turkowski, W. Wegrzynski, P. Tofilo, and G. Rein, "Fire experiments inside a very large and open-plan compartment: x-TWO," presented at the Proceedings of the 11th International Conference on Structures in Fire (SiF2020), The University of Queensland, Brisbane, Australia, 2020.

[42]   D. Rush, X. Dai, and D. Lange, "Tisova Fire Test – Fire behaviours and lessons learnt," *Fire Safety Journal,* vol. 121, 103261, 2021/05/01/ 2021, doi: https://doi.org/10.1016/j.firesaf.2020.103261.

[43]   V. Gupta, A. F. Osorio, J. L. Torero, and J. P. Hidalgo, "Mechanisms of flame spread and burnout in large enclosure fires," *Proceedings of the Combustion Institute,* vol. 38, no. 3, pp. 4525-4533, 2021, doi: https://doi.org/10.1016/j.proci.2020.07.074.

[44]   J. P. Hidalgo, T. Goode, V. Gupta, A. Cowlard, C. Abecassis-Empis, J. Maclean, A. I. Bartlett, C. Maluk, J. M. Montalvá, A. F. Osorio, and J. L. Torero, "The Malveira fire test: Full-scale demonstration of fire modes in open-plan compartments," *Fire Safety Journal,* vol. 108, 102827, 2019, doi: https://doi.org/10.1016/j.firesaf.2019.102827.

[45]   S. Nothard, D. Lange, J. P. Hidalgo, V. Gupta, M. S. McLaggan, F. Wiesner, and J. L. Torero, "Factors influencing the fire dynamics in open-plan compartments with an exposed timber ceiling," *Fire Safety Journal,* vol. 129, 103564, 2022/05/01/ 2022, doi: https://doi.org/10.1016/j.firesaf.2022.103564.

[46]   P. Kotsovinos, E. G. Christensen, E. Rackauskaite, A. Glew, E. O'Loughlin, H. Mitchell, R. Amin, F. Robert, M. Heidari, D. Barber, G. Rein, and J. Schulz, "Impact of ventilation on the fire dynamics of an open-plan compartment with exposed timber ceiling and columns: CodeRed #02," *Fire and Materials,* vol. 47, no. 4, pp. 569-596, 2023, doi: https://doi.org/10.1002/fam.3082.

[47]   P. Kotsovinos, E. G. Christensen, A. Glew, E. O'Loughlin, H. Mitchell, R. Amin, F. Robert, M. Heidari, D. Barber, G. Rein, and J. Schulz, "Impact of partial encapsulation on the fire dynamics of an open-plan compartment with exposed timber ceiling and columns: CodeRed #04," *Fire and Materials,* vol. 47, no. 4, pp. 597-626, 2023, doi: https://doi.org/10.1002/fam.3112.

[48]   P. Kotsovinos, E. G. Christensen, J. Gale, H. Mitchell, R. Amin, F. Robert, M. Heidar, D. Barber, G. Rein, and J. Schulz. (2022) The Effectiveness of a Water Mist System in an Open-plan Compartment with an Exposed Timber Ceiling: CodeRed #03. *FPEeXtra*.

[49]   *EN 1991 1-2 (2002) Eurocode 1: Actions on structures - Part 1-2: General actions - Actions on structures exposed to fire*, CEN, Brussels, Belgium, 2002.

[50]   J. Su, E. Gibbs, M. Weinfurter, P.-S. Lafrance, K. Gratton, A. Frade, and P. Leroux, "Large-scale fire tests of a mass timber building structure for MTDFTP," National Research Council of Canada, 2023. https://doi.org/10.4224/40003036

[51]   J. Liu and E. C. Fischer, "Review of large-scale CLT compartment fire tests," *Construction and Building Materials,* vol. 318, 126099, 2022, doi: https://doi.org/10.1016/j.conbuildmat.2021.126099.

[52]   N. Barker. (2023) Mass timber "definitely not the right way to go" says Benjamin Kromoser. *Dezeen*. https://www.dezeen.com/2023/03/23/benjamin-kromoser-timber-revolution-interview/

[53]   V. Kodur, J. Stein, R. Fike, and M. Tabbador, "Comparative fire performance of traditional lumber and engineered wood joists," *Journal of Structural Fire Engineering,* vol. 8, no. 1, pp. 2-13, 2017, doi: https://doi.org/10.1108/JSFE-01-2017-0003.

[54]   *EN 1995-1-2 (Eurocode 5): Design of timber structures - Part 1-2: General - Structural fire design*, CEN, Brussels, Belgium, 2004.

[55]   K. N. Mäger, M. Tiso, and A. Just, "Fire Design Model for Timber Frame Assemblies with Rectangular and I-Shaped Members. International Scientific Conference on Wood & Fire Safety," in *International Scientific Conference on Wood & Fire Safety*, 2020, pp. 268-274, doi: https://doi.org/10.1007/978-3-030-41235-7_40

[56]   K. N. Mäger and A. Just, "52-16-1 Preliminary Design Model for Wooden I-joists in Fire," presented at the International Network on Timber Engineering Research (INTER) Meeting 52., 2019.

[57]   J. König, "Fire exposed simply supported wooden I-joists in floor assemblies. SP Report 2006:44.," 2006.

[58]   *Final draft of prEN 1995-1-2. Eurocode 5: Design of timber structures - Part 1-2: General-Structural fire design*, CEN, 2021.

[59]   H. E. Nelson, "Engineering View of the Fire of May 4, 1988 in the First Interstate Bank Building, Los Angeles, California (NIST IR 89-4061)," 1989.

[60]   B. R. Kirby, D. E. Wainman, L. N. Tomlinson, T. R. Kay, and B. N. Peacock, "Natural fires in large scale compartments," *International Journal on Engineering Performance-Bases Fire Codes,* vol. 1, no. 2, pp. 43-58, 1999.

[61]   R. G. Gann, A. Hamins, K. McGrattan, H. E. Nelson, T. J. Ohlemiller, K. R. Prasad, and W. M. Pitts, "Reconstruction of the fires and thermal environment in World Trade Center buildings 1, 2, and 7," *Fire Technology,* vol. 49, pp. 679-707, 2013.

[62]   J. Gales, "Travelling fires and the St. Lawrence Burns project," *Fire Technology,* vol. 50, pp. 1535-1543, 2014, doi: https://doi.org/10.1007/s10694-013-0372-3.

[63]   J. G. Quintiere, *Principles of fire behavior, 2nd edition*. CRC Press, 2016.

114

[64] E. Rackauskaite, P. Kotsovinos, and D. Barber, "Letter to the Editor: Design Fires for Open-Plan Buildings with Exposed Mass-Timber Ceiling," *Fire Technology,* vol. 57, no. 2, pp. 487-495, 2021/03/01 2021, doi: https://doi.org/10.1007/s10694-020-01047-0.

[65] G. Ronquillo, D. Hopkin, and M. Spearpoint, "Review of large-scale fire tests on cross-laminated timber," *Journal of Fire Sciences,* vol. 39, no. 5, pp. 327-369, 2021, doi: https://doi.org/10.1177/07349041211034460.

[66] K. McGrattan, R. McDermott, M. Vanella, E. Mueller, S. Hostikka, and J. Floyd, "Fire Dynamics Simulator User's Guide, Sixth Edition," National Institute of Standards and Technology, 2023.

[67] *EN 1363-1:2020. Fire resistance tests - Part 1: General Requirements*, CEN, Brussels, Belgium, 2020.

[68] *EN 520:2004+A1:2009. Gypsum plasterboards - Definitions, requirements and test methods*, CEN, Brussels, Belgium, 2004.

[69] A. S. Bøe. *Supplementary data to large-scale fire experiment with exposed cross-laminated timber in ceiling - #FRIC-01*, DataverseNO, 2022-08-19/, doi: https://doi.org/10.18710/ZIYHH3.

[70] A. S. Bøe. *Supplementary data to large-scale fire experiment with exposed cross-laminated timber in ceiling and wall - #FRIC-02*, DataverseNO, doi: https://doi.org/10.18710/DMJDSD.

[71] A. S. Bøe. *Supplementary data to fire experiments with I-joists and combustible insulation*, DataverseNO, doi: https://doi.org/10.18710/2O7QSP.

[72] A. S. Bøe, K. L. Friquin, D. Brandon, A. Steen-Hansen, and I. S. Ertesvåg, "Fire spread in a large compartment with exposed cross-laminated timber and open ventilation conditions: #FRIC-01 - exposed ceiling," *Fire Safety Journal,* no. 103869, 2023, doi: https://doi.org/10.1016/j.firesaf.2023.103869.

[73] V. Gupta, J. L. Torero, and J. P. Hidalgo, "Burning dynamics and in-depth flame spread of wood cribs in large compartment fires," *Combustion and Flame,* vol. 228, pp. 42-56, 2021, doi: https://doi.org/10.1016/j.combustflame.2021.01.031.

[74] A. S. Bøe, K. L. Friquin, D. Brandon, A. Steen-Hansen, and I. S. Ertesvåg, "Fire spread in a large compartment with exposed cross-laminated timber and open ventilation conditions: #FRIC-02 - Exposed wall and ceiling," *Fire Safety Journal,* vol. 141, no. 103986, 2023/12/01/ 2023, doi: https://doi.org/10.1016/j.firesaf.2023.103986.

[75] M. Bonner, W. Węgrzyński, and G. Rein, "Visual fire power: An algorithm for measuring heat release rate of visible flames in camera footage, with applications in facade fire experiments," *Fire Technology,* vol. 59, pp. 191-215, 2023, doi: https://doi.org/10.1007/s10694-022-01341-z.

[76] A. S. Bøe, K. N. Mäger, K. L. Friquin, and A. Just, "Experimental Study of the Charring of I-Joists and Recession of Combustible Insulation in Light Timber Frame Assemblies with Comparison to Eurocode 5," *Fire Technology,* vol. 59, no. 6, pp. 3283-3325, 2023/11/01 2023, doi: https://doi.org/10.1007/s10694-023-01464-x

[77] A. Just, "Post protection behaviour of wooden wall and floor structures completely filled with glasswool," in *6th International conference on Structures in Fire*, 2010.

[78] A. Just and D. Brandon, "Optimizing the fire protection of massive timber structures (RISE report: 2019-109)," Smart Housing Småland, 2019. http://diva-portal.org/smash/get/diva2:1656386/FULLTEXT01.pdf

[79] D. Brandon, A. Temple, and J. Sjöström, "RISE report - Predictive method for fires in CLT and glulam structures – A priori modelling versus real scale compartment fire tests & an improved method (2021:63)," RISE Fire Research, 2021.

[80] I. U. Zulmajdi, M. Z. Mohd Tohir, T. C. S. Yaw, M. Y. Harun, and M. S. Md Said, "Statistical Distribution of Heat Release Rate Data for Single Household Items," *Fire Technology,* 2023/10/03 2023, doi: https://doi.org/10.1007/s10694-023-01493-6.

[81] S. R. Turns, *An Introduction to Combustion - Concepts and Applications, 3rd edition*. McGraw-Hill, 2012.

[82]   M. Aniszewska and A. Gendek, "Comparison of heat of combustion and calorific value of the cones and wood of selected forest trees species," *Forest Research Papers,* vol. 75, no. 3, pp. 231-236, 2014. [Online]. Available: https://depot.ceon.pl/handle/123456789/5332.

[83]   V. Babrauskas and R. D. Peacock, "Heat release rate: The single most important variable in fire hazard," *Fire Safety Journal,* vol. 18, no. 3, pp. 255-272, 1992/01/01/ 1992, doi: https://doi.org/10.1016/0379-7112(92)90019-9.

[84]   D. Drysdale, *An introduction to fire dynamics (3rd edition).* John Wiley & sons, 2011.

[85]   *IEC 60584-1:2013 Thermocouples - Part 1: EMF specifications and tolerances*, IEC, Brussels, Belgium, 2013.

[86]   U. Wickström, *Temperature Calculation In Fire Safety Engineering.* Springer, 2016.

[87]   I. Pope, J. P. Hidalgo, R. M. Hadden, and J. L. Torero, "A simplified correction method for thermocouple disturbance errors in solids," *International Journal of Thermal Sciences,* vol. 172, 107324, 2022/02/01/ 2022, doi: https://doi.org/10.1016/j.ijthermalsci.2021.107324.

[88]   R. Fahrni, J. Schmid, M. Klippel, and A. Frangi, "CORRECT TEMPERATURE MEASUREMENTS IN FIRE EXPOSED WOOD," presented at the World Conference on Timber Engineering (WCTE), Seoul, South Korea, 2018.

[89]   J. V. Beck, "Thermocouple Temperature Disturbances in Low Conductivity Materials," *Journal of Heat Transfer,* vol. 84, no. 2, pp. 124-131, 1962, doi: https://doi.org/10.1115/1.3684310.

[90]   M. S. Hoehler, "On the development of a transparent enclosure for 360° video cameras to observe severe fires in situ," *Fire Safety Journal,* vol. 120, 103024, 2021, doi: https://doi.org/10.1016/j.firesaf.2020.103024.

[91]   J. Schmid, M. Klippel, M. Viertel, R. Presl, R. Fahrni, A. Totaro, and A. Frangi, "Charring of timber - Determination of the residual virgin cross-section and charring rates," presented at the World Conference on Timber Engineering 2020, Santiago, Chile, 2020.

[92]   F. Richter, F. X. Jervis, X. Huang, and G. Rein, "Effect of oxygen on the burning rate of wood," *Combustion and Flame,* vol. 234, 111591, 2021, doi: https://doi.org/10.1016/j.combustflame.2021.111591.

[93]   D. Brandon, J. Sjöström, E. Hallberg, A. Temple, and F. Kahl, "RISE report - Summary report - Fire Safe implementation of visible mass timber in tall buildings - compartment fire testing (2020:94)," 2020.

[94]   Y. Wang, "The breakage behavior of different types of glazing in a fire," in *The Proceedings of 11th Asia-Oceania Symposium on Fire Science and Technology 11th*, 2020: Springer, pp. 549-560.

[95]   V. Babrauskas, "Glass breakage in fires," *Fire Science and Technology Inc,* 2011.

[96]   M. Tiso and A. Just, "Fire protection provided by insulation materials—a new design approach for timber frame assemblies," *Structural Engineering International,* vol. 27, no. 2, pp. 231-237, 2017, doi: https://doi.org/10.2749/101686617X14881932435899.

[97]   T. Hakkarainen, "Post-Flashover Fires in Light and Heavy Timber Construction Compartments," *Post-Flashover Fires in Light and Heavy Timber Construction Compartments,* vol. 20, no. 2, 2002, doi: https://journals.sagepub.com/doi/abs/10.1177/0734904102020002074.

[98]   A. Frangi and M. Fontana, "Fire Performance of Timber Structures under Natural Fire Conditions," *Fire Safety Science,* vol. 8, pp. 279-290, 2005, doi: https://doi.org/10.3801/IAFSS.FSS.8-279.

[99]   A. Bartlett and A. Law, "Influence of excess fuel from timber lined compartments," *Construction and Building Materials,* vol. 235, no. 117355, 2020, doi: https://doi.org/10.1016/j.conbuildmat.2019.117355.

[100]   E. Sanned, R. A. Mensah, M. Försth, and O. Das, "The curious case of the second/end peak in the heat release rate of wood: A cone calorimeter investigation," *Fire and Materials,* vol. 47, no. 4, pp. 498-513, 2023, doi: https://doi.org/10.1002/fam.3122.

116

[101]   H. Mitchell, P. Kotsovinos, F. Richter, D. Thomson, D. Barber, and G. Rein, "Review of fire experiments in mass timber compartments: Current understanding, limitations, and research gaps," *Fire and Materials,* vol. 47, no. 4, pp. 415-432, 2023, doi: https://doi.org/10.1002/fam.3121.

[102]   C. Gorska, J. P. Hidalgo, and J. L. Torero, "Fire dynamics in mass timber compartments," *Fire Safety Journal,* vol. 120, 103098, 2021, doi: https://doi.org/10.1016/j.firesaf.2020.103098.

[103]   C. Gorska, "PhD thesis - Fire dynamics in multi scale timber compartments," PhD, The University of Queensland, Australia, 2019.

[104]   I. Pope, V. Gupta, H. Xu, F. Wiesner, D. Lange, J. L. Torero, and J. P. Hidalgo, "Fully-developed compartment fire dynamics in large-scale mass timber compartments," *Fire Safety Journal,* 104022, 2023/10/06/ 2023, doi: https://doi.org/10.1016/j.firesaf.2023.104022.

[105]   M. A. Santoso, E. G. Christensen, J. Yang, and G. Rein, "Review of the Transition From Smouldering to Flaming Combustion in Wildfires," (in English), *Frontiers in Mechanical Engineering,* Review vol. 5, 2019-September-18 2019, doi: https://doi.org/10.3389/fmech.2019.00049.

[106]   A. Rinta-Paavola and S. Hostikka, "A model for the pyrolysis of two Nordic structural timbers," *Fire and Materials,* vol. 46, no. 1, pp. 55-68, 2022, doi: https://doi.org/10.1002/fam.2947.

[107]   Newsbeeezer. "Heavy fire in Lambertseter High School." Accessed: 09.01.2023. https://newsbeezer.com/norwayeng/heavy-fire-in-lambertseter-high-school/

[108]   VG. "Kraftig brann på Lambertseter videregående skole." Accessed: 18.09.23. https://www.vg.no/nyheter/innenriks/i/8J7EJr/brenner-kraftig-paa-lambertseter-vgs

[109]   SG-AS. "Lambertseter videregående skole." SG. Accessed: 18.09.23. https://www.sg-as.com/nb/referanser/lambertseter-videregaende-skole

[110]   K. Hox, "Branntest av massivtre. SP report: A15101," 2015. https://risefr.no/media/publikasjoner/upload/2015/spfr-a15101-branntest-av-massivtre.pdf

[111]   Y. J. Ko and N. Elsagan, "Investigation of the performance of fire suppression systems in protection of mass timber residential buildings," *Indoor and Built Environment,* vol. 32, no. 1, pp. 230-241, 2023, doi: 10.1177/1420326x221138415.

[112]   M. Ahrens, "US experience with sprinklers," NFPA, 2021. https://www.nfpa.org//-/media/Files/News-and-Research/Fire-statistics-and-reports/Suppression/ossprinklers.pdf

[113]   F. Rankl, "Building regulations and safety," House of Commons Library, CBP 8482, 2023.

[114]   D. Barber and R. Gerard, "Summary of the fire protection foundation report-fire safety challenges of tall wood buildings," *Fire Science Reviews,* vol. 4, no. 5 (2015), 2015, doi: https://doi.org/10.1186/s40038-015-0009-3.

[115]   D. Hopkin. "What they fail to appreciate is that it's unhelpful to their end-game too. Something can only be 'sustainable' if you have addressed the hazards and don't flirt with a future ban." LinkedIn. https://www.linkedin.com/posts/dannyjhopkin_masstimber-activity-7102917912482443265-ELtn?utm_source=share&utm_medium=member_desktop

[116]   ReNewCanada. (2023) CWC report reinforces safety of mass timber demonstration fire tests results. *ReNew Canada*. https://www.renewcanada.net/cwc-report-reinforces-safety-of-mass-timber-demonstration-fire-tests-results/

Part II – Research Output

Paper I

Fire spread in a large compartment with exposed cross-laminated
timber and open ventilation conditions: #FRIC-01 – Exposed ceiling

Andreas Sæter Bøe,

Kathinka Leikanger Friquin, Daniel Brandon,

Anne Steen-Hansen, Ivar S. Ertesvåg

Fire spread in a large compartment with exposed cross-laminated timber and open ventilation conditions: #FRIC-01 – Exposed ceiling

Andreas Sæter Bøe [a,*], Kathinka Leikanger Friquin [a,b], Daniel Brandon [c], Anne Steen-Hansen [a,d], Ivar S. Ertesvåg [e]

[a] *Department of Civil and Environmental Engineering, Faculty of Engineering, NTNU - Norwegian University of Science and Technology, Trondheim, Norway*
[b] *Department of Architecture, Materials and Structures, SINTEF Community, Trondheim, Norway*
[c] *RISE Fire Research, Lund, Sweden*
[d] *RISE Fire Research AS, Trondheim, Norway*
[e] *Department of Energy and Process Engineering, Faculty of Engineering, NTNU - Norwegian University of Science and Technology, Norway*

ARTICLE INFO

ABSTRACT

Exposing cross-laminated timber (CLT) structures in buildings is increasingly popular in modern buildings. However, large timber surfaces, window facades, and different geometries can change the fire dynamics in a compartment. The effect of those parameters, therefore, needs to be studied. Two large-scale CLT compartment fire experiments (95 m^2) have consequently been performed. The experiments were designed to represent a modern office building with an open-plan space and large window openings. In this experiment, #FRIC-01, the ceiling was exposed. The wood crib fire developed slowly and travelled approximately 1.5 m before the ceiling ignited at 32.5 min. Thereafter the fire spread rapidly across the ceiling and wood crib before it shortly after retracted. Three such cycles of rapid spread followed by a retraction occurred within 13 min, whereby the wood crib fire grew larger for each cycle. After the flames extended through the compartment for the fourth time, the fire remained fully developed. After a short period of intense burning, the CLT self-extinguished while the wood crib fire was still burning. The compartment withstood full burnout, and no reignition occurred despite some delamination and using an adhesive that lacks a demonstrated resistance against glue-line integrity failure.

1. Introduction

The use of engineered wood products, e.g., glue-laminated and cross-laminated timber (CLT), has increased massively in recent years. The increased popularity is caused by the many advantages of building with wood, like prefabrication, low carbon footprint, easy handling and mounting, and its aesthetic look. In addition, the implementation of performance-based building regulations and prescriptive regulations with solutions for mid-rise timber buildings have opened the possibility of designing taller timber buildings.

Alongside the development of innovative wood products, there is a potential of introducing new fire risks that previously have not been present. Examples are faster fire spread, larger external flames, and longer fire duration. Over the last decades, several small, medium and large-scale CLT compartment experiments have been performed. These experiments have highlighted several essential features of compartment fires with exposed CLT. One characteristic of these experiments is the

increased heat release rate compared to experiments without exposed CLT. This is caused by wood being a combustible material and adds a significant amount of pyrolysis gases to the fire. Also, since most CLT compartment experiments have been ventilation-controlled, a large ratio of the combustible gases has burnt outside the compartment as external flames [1]. This phenomenon has long been known [2,3] and later confirmed by several authors through large-scale experiments [4–7].

However, a recent study [8] has shown that the increase of the external flame with exposed CLT is less for compartments with medium and large openings than previously observed in compartments with small openings. In another study [9], the exposed CLT played a minor role to the size of the external flame when the variable fuel load density was high. Despite increasing the amount of exposed CLT, the external flame size was about unchanged, and only slightly higher temperatures at the facade were measured. This was explained by the high variable fuel load density (1085 MJ/m^2), as the percentage increase of

---

* Corresponding author.
 E-mail address: andreas.s.boe@ntnu.no (A.S. Bøe).

combustible gases from a CLT surface then becomes lower than for a similar compartment with a lower variable fuel load density.

Furthermore, the number of exposed surfaces and their orientation relative to each other affect the fire dynamics and duration [4,10,11]. Another reason for the prolonged fire duration is gypsum board fall-off and delamination of CLT (also known as glue-line integrity failure or premature char fall-off). Both result in fresh wood being exposed to the fire [4,12].

The char layer that forms during combustion of wood gives some protection to the fresh wood behind. To sustain burning, an external heat flux above a critical level must be applied to the surface, otherwise, the burning will stop [13–16]. It is important to note that smouldering may continue for several hours after visible flames are extinguished [17, 18]. Smouldering can weaken the structural capacity of timber members [19,20] and transition back to flaming combustion, which eventually might develop into a fully developed fire.

Self-extinction has been observed for compartments with one [12, 21] or two [10,22] exposed surfaces. However, the possibility of self-extinction should not be directly connected to the number of exposed surfaces, as it also depends on several other factors, such as the lamella thickness [14,23], the opening factor [24], and the duration of the fire determined by the variable fuel load density.

Although many CLT experiments have been conducted, most have been in relatively small compartments, with openings corresponding to typical ventilation-controlled fires. According to Ref. [25], 70% of all CLT compartment fire experiments had a floor area less than 25 m^2, 86% less than 50 m^2, and 86% had openings corresponding to a ventilation-controlled fire.

With the increased popularity among architects and engineers, CLT is now also found in public and office buildings. These often have large windows to allow for natural light and have open-plan spaces, which is considerably different with regard to opening factor and compartment size compared to most CLT compartment experiments [18,26], but also to compartment fires in general [27].

Overall, due to the size and geometry, buildings with large open-plan areas are often more likely to experience travelling fires. A travelling fire moves in space with a defined leading and trailing edge [28]. Several fire experiments have been conducted to study this phenomenon, like the Edinburgh travelling fire experiments [29], the TRAFIR experiments [30], the X-ONE [31] and X-TWO [32], and the Tisova fire experiment [33]. Fire spread rates in travelling fire experiments in compartments with non-combustible linings have varied significantly. The slowest fires took several hours to travel across the compartment, with flame spread rates of 1–60 mm/min [30,33]. The fastest spread was observed across a 29 m long wood crib in 12 min, with an average spread rate of 2.4 m/min [31].

Travelling fire experiments have predominantly been conducted in compartments with non-combustible surfaces, and the effects of wooden surfaces have barely been studied. Nevertheless, a few recent publications have provided important knowledge to this topic.

A CLT ceiling was found to influence the fire spread rate in a small-scale experiment [34], where the fire spread rapidly across the ceiling once ignition of the ceiling occurred. In the Malveira travelling fire experiment [35], 60% of the ceiling consisted of a combustible cork layer. The fire spread slowly for about 4 h until the fire spread reached below the cork area. From this point on, the fire spread vigorously across the cork ceiling, and the fire front on the wood crib on the floor accelerated quickly. The contribution of the cork was comparable to a wooden ceiling. In the experiments CodeRed #01 [17] and CodeRed #02 [36], the presence of a CLT ceiling caused the fire to spread across the room in 5 and 8 min, respectively. These are the largest compartment fire experiments with exposed CLT performed to date, with a floor area of 352 m^2. The flames impinged at the CLT ceiling shortly after ignition of the wood crib on the floor and caused ignition of the ceiling within 3 min in CodeRed #01 and 5 min in CodeRed #02. The flames spread quickly across the ceiling and reached the end of the

compartment approximately 2.5–3 min later, corresponding to an average spread rate of approximately 9 m/min. In CodeRed #01, the leading edge of the ceiling flames reached the end of the compartment 20 s before the leading edge of the wood crib, which demonstrates that the radiation to the floor was intense. The impact of the CLT ceiling was clearly demonstrated, as the results could be directly compared to the identical experiments without exposed CLT, X-ONE [31] and X-TWO [32]. In these experiments, the fire spread across the room in 12 and 22 min, respectively. In addition to the increased fire spread rate, the heat release rate was doubled, and external flames were visually larger.

The few travelling fire experiments with a combustible ceiling have revealed that the current understanding of fire dynamics and fire spread in large open-plan compartments with exposed CLT is limited. The flame spread rates in the experiments with a combustible ceiling significantly exceeded the flame spread rates found in compartment experiments without exposed combustible surfaces ($\leq$1 m/min) [37–41]. Such fast fire spread rates might impact available evacuation time, and the fire size can be significant before the fire brigade arrives [42].

These findings suggest that it is essential to expand the knowledge on how exposed CLT affects the fire spread and fire safety in large open-plan spaces with CLT [25,43,44]. This includes a better understanding of the feedback mechanisms between the combustible surfaces and the variable fuel load and how this interaction changes the fire dynamics, fire spread, fire duration and external flames. Due to the low number of large open-plan compartment experiments with exposed CLT, many aspects are not yet studied at full scale. The experiments performed to date have:

- comprised compartments with relatively small openings, which allowed significant collection of the smoke layer under the ceiling before ignition,
- involved impingement of the initial fire on the ceiling, which might in practice not occur for compartments with high ceilings and smaller ignited items,
- not involved exposed wall surfaces.

To increase the knowledge of fire development and fire dynamics in well-ventilated, large open-plan compartments with exposed CLT, and address the points listed above, two large-scale experiments have been conducted. The aim was to study the fire development and spread, heat release rate, temperature distribution inside the compartment, charring rate for the CLT, and external flames, for different configurations of exposed CLT surfaces. The first experiment, #FRIC-01, had exposed CLT in the ceiling, while in the second experiment, #FRIC-02, the ceiling and one wall were exposed. The first experiment is described and analysed in this article.

2. Methods

2.1. Methodology

The experiment was designed to study how exposed CLT, large ventilation openings and a large open-plan area affect the fire development and spread in a compartment. The fire development, flame heights and flame spread are studied through visual observations, measured temperatures in the compartment and heat flux towards surfaces, and calculations of the heat release rates for the variable fuel and CLT.

2.2. Experimental setup

2.2.1. Compartment

The compartment in the experiment was built of CLT elements in three walls and the ceiling, while the fourth wall was almost entirely open with four large openings. The CLT elements in the roof rested on the three CLT walls. They were supported on the fourth wall by a 140

mm × 315 mm glulam beam resting into a pre-cut hole in the CLT end walls and supported by three aerated concrete columns. The inner geometry of the compartment was 18.80 m × 5.00 m × 2.52 m (L x W x H). Deviations up to ±0.05 m were present for the ceiling height caused by a slightly tilted floor, with the highest level by the window wall. The deviations are not included in the drawings. A sketch of the experimental setup is shown in Fig. 1, and pictures of the compartment are given in Figs. 2 and 3.

The beam and the three columns in the window wall created four openings of 4.25 m width and 2.20 m height, with a total opening area of 37.4 m². This corresponds to an opening factor (OF) of 0.18 m$^{1/2}$ calculated by OF = $A_V H_V^{1/2}/A_T$, where A_V and H_V represent the area and height of the openings, while A_T is defined as the total area of the enclosure surfaces, including the opening areas [45].

The roof consisted of eight CLT elements overlapping with a lap joint, while the back wall was built of four elements. The roof elements were 5.14 m long and 2.45 m wide, while the back wall elements were 2.45 m tall and 4.82 m wide. The CLT elements in the back wall and ceiling were 140 mm thick and made of 5 layers (40-20-20-20-40 mm), while the end walls were built of 80 mm thick CLT with three layers (30-20-30 mm). The CLT elements were produced in accordance with EAD 130005-00-0304 [46]. The wood in the elements was Norwegian spruce, and the glue between the layers was a regular polyurethane adhesive named Loctite 2 HB-S. The density of the CLT elements was approximately 484 kg/m³ (based on measurement of one element), with moisture content (dry value) of 12.8% ± 0.3% (standard deviation, n = 48) measured with a moisture meter. The exposed CLT area was 95% (89.3 m²) of the floor area since the glulam beam and some insulation covered approx. 0.25 m of the ceiling width, see Fig. 3 and further details below.

Two façade walls were positioned above Windows 2 and 4 to provide a more realistic behaviour of the external flame. The façade walls were 2.45 m high and 5.00 m wide. They were built up by a wooden frame covered by a 12 mm thick oriented strand board and 30 mm thick stone wool insulation on the exposed side, see Figs. 1 and 2.

The compartment was built on a concrete floor, which was protected by 30 mm thick stone wool insulation to prevent concrete spalling during the experiments. The walls were protected by two layers of 15 mm thick fire-rated gypsum boards Type F [47]. The outer gypsum board layer was shifted with a half board width to the innermost layer to avoid continuous joints leading directly into the wood. Both layers were fastened by 41 mm long gypsum board screws. The screws were positioned 50–70 mm from the board edge and with 350–400 mm distance between screws. A screw pattern template was used to ensure a similar screw pattern for all gypsum boards.

The glulam beam and edges of the CLT at the front wall were protected with two layers of 25 mm thick ceramic fibre insulation. The outer layer was shifted half a width to avoid overlapping joints. The outer layer covered 100 mm of the exposed CLT ceiling along the glulam beam.

The experiment was performed outdoors. On the day of the experiment, the weather was cloudy, with negligible wind and no precipitation. The temperature at the start of the experiment was 15 °C and
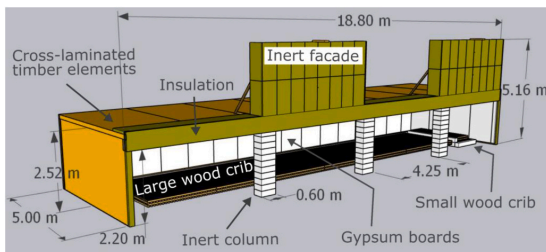

Fig. 2. The compartment with the burning wood crib fire before the ceiling was ignited. The small crib is at the right end of the compartment. The fire shows at which end the wood crib was ignited.
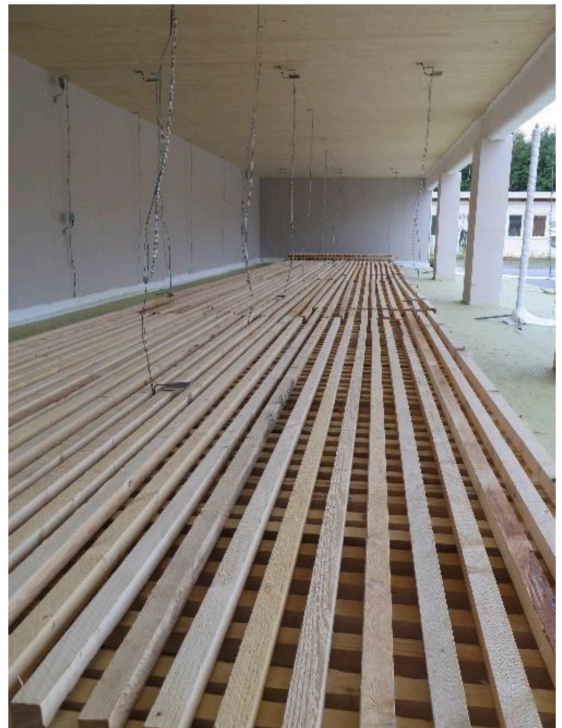

Fig. 3. View from inside the compartment, showing the large wood crib, the exposed CLT ceiling and the protected walls. The glulam beam (above window openings) is covered with ceramic fibre insulation, creating a reservoir height of 0.36 m.

gradually increased to 20 °C during the experiment.

2.2.2. Wood crib

The variable fuel load in the compartment was represented by a long continuous wood crib, 15.5 m × 2.8 m x 0.2 m, and a smaller wood crib, 1.0 m × 2.8 m x 0.2 m. The small crib was placed on a scale 0.2 m higher than the large crib. The large and the small cribs are hereafter referred to as one unit, "the wood crib". The wood crib contained wood sticks with a cross-section of 50 mm × 50 mm, stacked horizontally on top of each other in four layers, where the sticks in each layer were perpendicular to the previous layer. The sticks laid perpendicular to the crib length were 2.8 m, while the parallel ones were 4.3 m long. The moisture content was measured by drying samples of the sticks in an oven, according to ISO 12570 [48]. The average moisture content was 14.5%, with 13% ±

Fig. 1. Sketch of the compartment.

0.8% (standard deviation, n = 20) and 16% ± 0.6% (standard deviation, n = 20) for the short and long sticks, respectively. The difference in moisture content between the long and short sticks was likely caused by different storage conditions during the two last weeks before the experiment. The wood used was Norwegian spruce, with an average density of 486 kg/m^3 ± 40 kg/m^3 (standard deviation, n = 25). The distance between the sticks was 50 mm, which gave a crib porosity factor of 0.19 cm. The porosity factor is related to the ratio of the mass flow rate of air to fuel inside vertical shafts of a crib, expressed through dimensions of the crib [49]. 0.19 cm corresponds to the open regime, where the crib burning is not controlled by the porosity (spacing between the sticks) but rather by the thermal feedback from the compartment and the geometry of the wood crib [49]. The total mass of the crib was 2065 kg, determined by weighing all sticks. This corresponds to a fuel load density of 353 MJ/m^2 (per floor area) when using a heat of combustion of 16.0 MJ/kg (see Section 2.4.2 for derivation).

2.2.3. Ignition

Ten aluminium metal trays with dimensions 150 mm × 220 mm × 50 mm (L × W × H) were positioned at 70 mm distance to each other directly below the edge of the wood crib at the left end of the compartment to get a uniform fire across the width of the crib. The first stick of the bottom wood crib layer was removed to make room for the trays to be positioned with 1/3 of the tray directly below the crib. Each tray was filled with 0.5 L of heptane, with a total amount of 5.0 L.

2.3. Instrumentation and measurements

Temperature and incident radiant heat flux at different locations inside the compartment were measured with 120 thermocouples (TC) of type K 1.5 mm [50] and 24 plate thermometers (PT) [51]. TCs are commonly used to measure gas temperatures, although they are slightly affected by radiative heat transfer. The PTs measure surface temperatures of materials with good insulation properties and may be used to calculate the adiabatic surface temperature and the incident radiative heat flux towards the surface [52] (see Section 2.4.1).

Positioning of the TCs was chosen to measure temperature distributions in X, Y and Z-direction at strategic locations. The zero-point for X, Y and Z was defined on the floor at the inner side of the left end wall in the window opening. The thermocouples were arranged in TC-trees, where the TCs were attached to a steel chain (Ø4 mm) hanging from the ceiling. Due to the varying ceiling height of ±0.05 m, the TCs were aligned with reference to the ceiling. For easier reading throughout the article, the TC height from the floor is presented as if the ceiling height was constant at 2.52 m. A detailed overview of the positions of all sensors is given in Figs. 4–6.

TCs and PTs were mounted on the façade above Windows 2 and 4 to estimate the incident radiant heat flux from the external flame, see
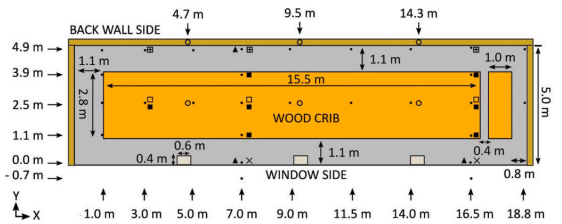

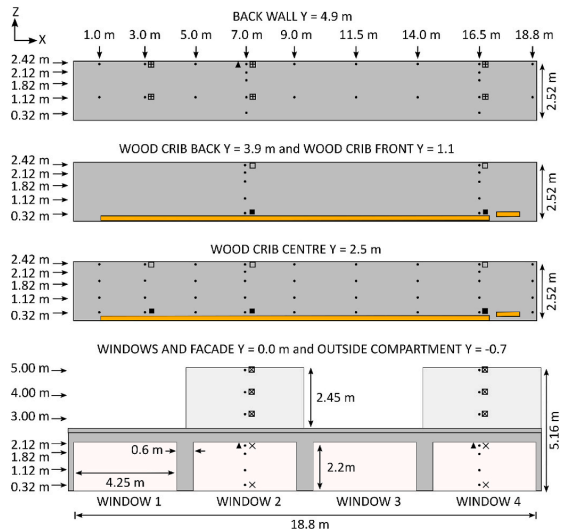**Fig. 5.** Instrumentation in the XY-plane (plan view). For symbols, see Fig. 4.

Fig. 6. Instrumentation in XZ-plane. For Y = −0.7 m, only TCs are present, no gas sensors or bidirectional probes. For symbols, see Fig. 4.

Section 2.4.1. The PTs were flush with the insulation surface, while the TCs were located next to the PTs 20 mm in front of the façade. The TCs and PTs were positioned 0.8 m, 1.8 m, and 2.8 m above the top of the window opening. A TC-tree was located 0.7 m in front of the façade walls to measure the flame temperatures. The distance of 0.7 m was chosen based on this being the centre of the flame according to the Law-model [53], where the depth of the external flame is equal to 1/3 of the window height. Two PTs were located 8.0 m in front of the compartment. However, due to an unknown error, these gave no signals during
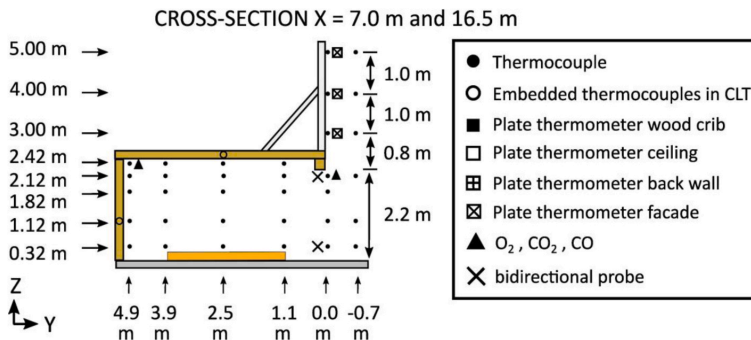

Fig. 4. Instrumentation in the YZ-plane (cross-section) at X = 7.0 m and 16.5 m. For X = 16.5, only gas measurements in the window opening.

the experiment.

The experiment was recorded by eight video cameras, including three IP cameras at a 15–20 m distance, an air-cooled GoPro camera, a water-cooled 360° camera inspired by Hoehler [54], two water-cooled GoPro cameras in Pyrex columns with circulating water, and a drone. Video recordings were used to evaluate fire spread and flame heights.

Gases were sampled from the compartment at three different locations, see Figs. 4–6. The gas was cooled and dried before the oxygen (O_2), carbon monoxide (CO) and carbon dioxide (CO_2) concentrations were measured by a gas analyser. The measurement ranges for the different gas sensors were 0–21% for O_2, 0–10% for CO_2 and 0–5000 ppm for CO. Four bidirectional probes [55] were used to measure the gas velocity in and out of Windows 2 and 4, as shown in Figs. 4–6.

To monitor the temperature development in the CLT, 1.5 mm sheathed TCs type K were embedded into some elements at 0, 10, 20, 30 and 40 mm depth from the element surface at locations: X = 4.7, 9.5 and 14.3 m. The TCs embedded in the back wall were installed at 1.12 m height, and the TCs embedded in the ceiling were installed at the centre line of the room, Y = 2.5 m. The TCs were installed in 1.6 mm holes drilled 40 mm into the elements from the rebate joint parallel to the isotherm, as this was considered the most reliable method for measuring the temperature [56–58]. The holes were drilled with a drill guide to get perpendicular holes and in a zig-zag pattern to increase the vertical distance between overlaying holes, see Fig. 7. The TC wires were embedded into the wood through pre-cut slits to protect the wire from mechanical damage during construction, and to not cause an air gap in the joint after installation. The embedded TCs of the back wall were used to measure the temperature behind the gypsum boards and inside the CLT. Due to a logger error, data were only available from the embedded TCs at X = 14.3 m.

The temperatures of the embedded TCs were also used to calculate the charring rates at different depths into the CLT. The charring rates were calculated from the time difference of two embedded TCs to reach 300 °C. The 300 °C isotherm is considered the location of the charring front [59].

After the experiment, the char depth was measured on five of the eight CLT elements in the ceiling with a method inspired by Ref. [60]. A 500 mm × 500 mm grid pattern was drawn on the unexposed side of the CLT, and perpendicular holes were drilled in each cross-point. The char layer was then physically removed by a steel brush around each drilled hole, and the remaining thickness of the CLT was measured by a digital calliper. The total thickness of the CLT had increased by 2 mm due to increased moisture content caused by the manual suppression of the fire with water. This increase was corrected for in the calculation of the char depth, as the increase, in general, could be assigned to the four intact layers.
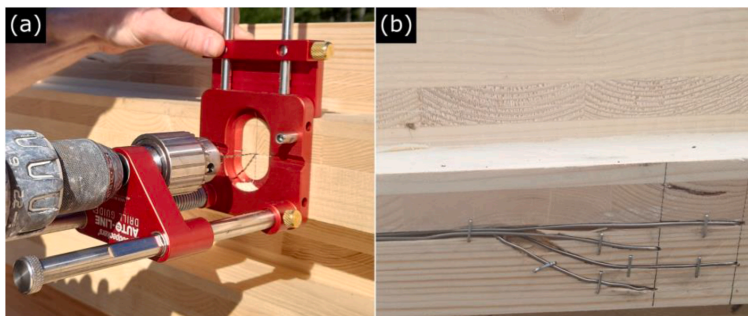
2.4. Data analysis methods

2.4.1. Method to determine incident heat flux

Measurements from the PTs and TCs were used to determine the incident radiation heat flux [W/m^2] through equation: $\dot{q}''_{inc} = \sigma T^4_{PT} + (1/\varepsilon)[(h+K)(T_{PT}-T_g)+C(T^{j+1}_{PT}-T^j_{PT})/\Delta t]$ [52], where ε is the emissivity of the PT (0.9), σ is the Stefan-Boltzman constant (5.67 ·10^{-8} W/(m^2 K^4)), T_{PT} is the temperature of the PT, T_g is the gas temperature, h is the convective heat transfer coefficient (10 W/m^{2}K), K is the thermal conduction coefficient (8 W/(m^{2}K)), and C is the heat capacity of the PT (4200 J/(m^{2}K)). j and $j+1$ represent two consecutive data recordings, and Δt is the corresponding time difference. Here, Δt was 1 s. The gas temperature was approximated using the 1.5 mm TC close to the PT. It is noted that this measurement is influenced by radiation. However, the error of this approximation has a negligible influence on the upper range of incident radiant heat fluxes measured.

2.4.2. Heat release rate of the wood crib and CLT

The method to estimate the heat release rate (HRR) for the wood crib was inspired by the method used in X-ONE [31]. It was also used in the CodeRed experiments [17] and consists of three steps: 1) Determine the mass loss rate (MLR) per unit length of the wood crib. 2) Integrate over wood crib length to find the total MLR. 3) Convert MLR to HRR.

In contrast to the method of [31], the MLR per unit length in this experiment was based on a real MLR measurement from the small wood crib (1.0 m × 2.8 m) positioned on a scale at the right end of the compartment, see Fig. 1. This is considered an improvement as the MLR changes with time and is not a constant value through the duration of the fire. The HRR was approximated by $\dot{Q} = \dot{m}\,\Delta H_C\,\chi$, where the mass loss rate ($\dot{m}$) is multiplied by the net heat of combustion (ΔH_C) and a combustion efficiency factor (χ). The combustion efficiency factor was set to 0.8, and the net heat of combustion was set to 16.0 MJ/kg. The latter is considered as the lower heating value for moist wood, derived from the calorific value of 18.66 MJ/kg for dry wood [61] and a moisture content (dry value) of 14.5% [48]. The product of the combustion efficiency factor and the net heat of combustion is the effective heat of combustion.

The integration of MLR over the wood crib length was made by dividing the wood crib into 50 mm long elements and adding the MLR per unit length to all elements based on the start of burning for each element. The start of burning for each element was based on the fire spread across the wood crib found through video analysis. A curve of the total MLR was then found by summarising the MLR for all the 50 mm wood crib elements for each time unit (1 s). The primary assumption for this model is that the crib per unit length burns in the same way from ignition as the small wood crib on the scale.

The MLR for the CLT ceiling was determined from the average charring rate for each 10 mm into the wood, the density (484 kg/m^3)

Fig. 7. (a) A drill guide was used to drill perpendicular holes into the CLT from the rebate joint. (b) The TCs embedded in the CLT were installed parallel to the isotherm in a zig-zag pattern.

and surface area (89.4 m²) of the exposed CLT. The HRR was calculated with a combustion efficiency of 0.8 and a net heat of combustion of 16.3 MJ/kg. The higher heat of combustion is due to the lower moisture content of the CLT compared to the wood crib sticks.

2.4.3. Gas velocity measurements through bidirectional probes

Gas velocities were measured by bidirectional probes, as described in ISO 9705-1 Appendix D [55]. The velocities are here calculated similarly as by Ref. [4], originating from Ref. [62].

3. Results

3.1. Fire development

The wood crib was ignited, as described in Section 2.2.3. The heptane flames had a height of 1.0–1.5 m in the beginning and tilted towards the left end wall, away from the wood crib. This behaviour of the flames is believed to be due to local draft conditions. The heptane fire caused the formation of a thick black smoke layer below the ceiling across the entire compartment, and a slight discolouring was observed in the CLT ceiling closest to the left end wall. However, the ceiling did not ignite. The fire gradually decreased in size from around 2.5 min after ignition of the heptane, and the smoke layer was diluted. At 3.5 min, the heptane fire burned out, and the wood crib fire almost died out, with only 5 cm high flames over the first 5 cm length of the crib. During the next 30 min, the fire spread slowly and grew in size to cover about 1.5 m length of the crib, covering an area of approx. 3 m² and the crib fire base area stabilised at this size after 22 min, see Fig. 8. The base area of the fire was here defined as the length of the burning crib (i.e., the position of leading-trailing edge) multiplied by the width of the crib. The base area stabilised at approx. 3 m² because the fuel in the first part of the crib was burning out. The flame height during this period varied from 0.5 to 2.2 m, and flames were not impinging the ceiling, see Figs. 2 and 8.

At 32.5 min, the ceiling ignited above the wood crib fire. Thereafter, the fire took approx. 13 min to spread across the whole crib and cause a stable burning fire. Within these 13 min, the fire was travelling back and forth in four distinct cycles or waves, see Fig. 9. As we do not know of such behaviour being reported earlier, we have in this article chosen to name them *flashing waves*. The waves were characterised by a rapid flash fire below the ceiling, followed by a spread along the top layer of the wood crib, triggered by the intense radiation from the flames beneath the ceiling. Each wave caused external flaming out of the window openings. After a short, intense fire with a duration of 30–60 s, the flames underneath the ceiling were gradually reduced, and the radiation-dependent fire on the top layer of the wood crib was reduced or even extinguished in some areas. The flames underneath the ceiling spread almost to the end of the compartment for each wave. After the 1st and 2nd waves, the ceiling fire retracted entirely to full extinguishment (see Figs. 10 and 11). After each retraction, the wood crib fire had grown in both length and intensity compared to before the wave. The leading

edge of the wood crib fire reached the end of the compartment in the 3rd wave (see Fig. 12). Despite the whole compartment burning, the fire pulled back again after a short period. Eventually, in the 4th wave, after 45:30 (mm:ss), all combustible surfaces in the compartment had ignited without any retraction. This stable burning of the whole compartment was defined as flashover.

After flashover, the fire burned intensely for about a minute and then gradually decreased in intensity. From 49 min on, the fire was clearly most intense at the right end, with small external flames emerging only from Window 4. The self-extinguishment of flames in the CLT ceiling started around 50 min from the left end (ignition end) of the compartment and continued towards the other end over the next 11 min, see Fig. 13. The wood crib fire was burning with continuous flames along the crib until 61 min. From 61 to 95 min, the wood crib fire was burning more and more discontinuously (i.e., with larger and larger areas of the crib without flames), starting from the left end of the compartment and moving rightwards. There were no visible flames from the wood crib after 95 min. The compartment was observed for a total of 4 h. At this point, very little of the wood crib was left, and some lamellas of the CLT were hanging down from the ceiling in the centre of the compartment. Hot spots were present around the delaminated areas. Manual fire suppression with water was then conducted, and no reignition was observed after the extinguishment.

After the compartment had cooled down, it was visually inspected, see Fig. 14. A few cracks at the surface of the gypsum boards were seen, but all of them remained in place. The inner gypsum board layer was undamaged except for some discolouring under the joints of the outer layer. The protected CLT back wall was undamaged.

A summary of the fire development is given in Table 1, while detailed information about temperatures, charring rates, mass loss rates, heat release rate, and external flames is found in the following sections.

3.2. Compartment temperatures

Temperatures below the ceiling, at the back wall and on top of the wood crib measured by PTs are shown in Figs. 15–17 and give an overview of the development of the fire. The first peak at 3 min originated from the heptane fire. After the extinguishment of the heptane fire, the temperatures slowly increased below the ceiling and at the upper part of the back wall due to the development of the wood crib fire. The maximum ceiling temperature reached a plateau between 22 and 33 min, which corresponds well with the almost constant fire base area for this period, see Fig. 8.

After 32.5 min, the ceiling spontaneously ignited. Temperatures in the entire ceiling increased rapidly but to a higher level near the ignition point and lower at longer distances. Increased temperatures were also measured at the wall, most pronounced at the upper part of the wall. In the figures, the retraction of the 1st flashing wave is recognised by a slight decrease in almost all temperatures except for the wood crib at X = 3.0 m, where the temperature continued to increase. In other words,
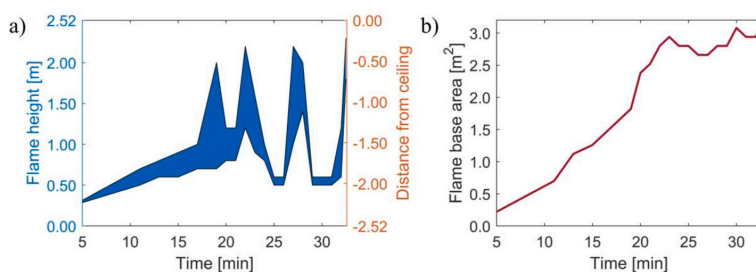

Fig. 8. (a) Flame height of wood crib fire. The shaded area represents the minimum and maximum height of the flame along the width of the crib. (b) Base area of wood crib fire before ignition of the ceiling.
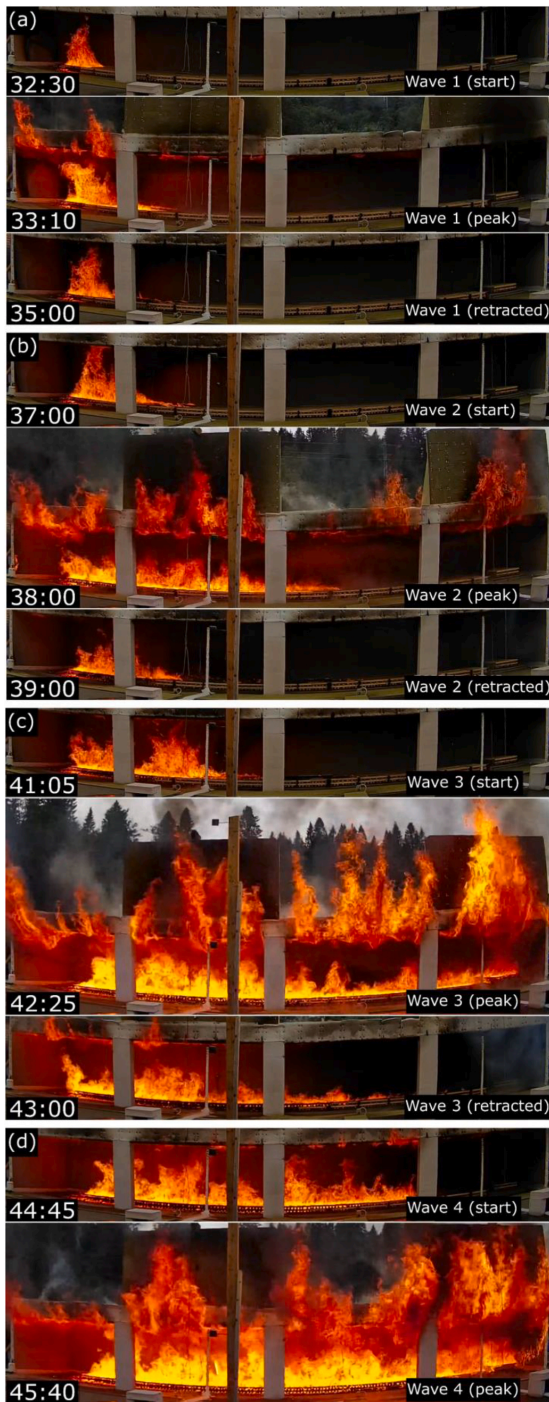
Fig. 9. (a), (b), (c) and (d) represent the 1st, 2nd, 3rd and 4th flashing waves, respectively. Time is given as (mm:ss) after ignition.

the wood crib fire during the 1st flashing wave spread beyond this point and did not retract. The wood crib temperatures farther away increased slightly and remained at this temperature until the next flashing wave. The 2nd flashing wave, see Fig. 9(b), started at 37 min and followed the same behaviour as the 1st wave. There were considerable temperature variations in the compartment during this period, with part of the compartment fully burning and the other part having temperatures close to ambient temperatures. After 42 min, the minimum compartment temperature also increased significantly, and the fire was at this point affecting the temperature in the entire compartment. This corresponds with the 3rd flashing wave, which led to the entire compartment burning, see Fig. 12. Although the fire retracted also after the 3rd wave, the wood crib fire grew substantially and covered more than half of the crib, and the temperatures of the non-burning parts remained high. The 4th wave occurred shortly after the end of the 3rd and led to a stable burning fire in the entire compartment. The highest temperatures were reached at 45–46 min, with the peak temperature of 1040 °C measured on top of the wood crib in the centre of the compartment.

The decay phase was initiated by a sudden drop in temperatures and continued with the extinction of flames in the ceiling. The extinction of flames started from the left side at approximately 50 min and continued to the right side. The last flames were gone at 61 min. During the extinction of the CLT, the oxygen concentration was 16–17% measured 100 mm below the top of Windows 2 and 4 (Fig. 25). The temperatures below the ceiling were 695–705 °C, corresponding to an incident heat flux of 49–52 kW/m². During the extinguishment of CLT, the average compartment temperature dropped from 910 °C to 650 °C.

The decay phase then continued almost linearly over the next 90 min, with an average temperature decay rate below the ceiling of 7.1 ± 0.5 °C/min. During the decay phase, there was little temperature difference along the Y-axis of the ceiling, i.e., between the window and back wall (Fig. 15). For the wood crib (Fig. 17), this difference was more pronounced, with the highest temperatures in the centre of the crib. The difference between the minimum and maximum compartment temperatures during most of the post-flashover and decay phase was between 200 and 400 °C.

During the 1st flashing wave, the thin paper of the gypsum boards ignited on the left end wall and the nearest part of the back wall, see Fig. 18. The maximum PT temperatures at the back wall close to the wood crib fire (X = 3.0 m) were 476 and 670 °C at 1.1 m and 2.4 m height, respectively. The corresponding maximum heat flux at 2.4 m height was 78 kW/m² and stabilised at 40 kW/m² until the next wave. At 1.1 m height, the maximum heat flux was 15 kW/m² before it reduced to approx. 10 kW/m² and slowly increased to 20 kW/m² before the second wave.

To better visualise the temperature variations in the compartment, temperature maps for the XZ and YZ cross-sections were made from the TC measurements through linear interpolation. In the XZ cross-section, see Fig. 19, strong temperature gradients were observed both in the X and Z direction. At locations where only the ceiling has ignited and not the wood crib, the temperature increased noticeably from the floor to the ceiling. However, for locations where both the crib and the ceiling had ignited, the lowest temperature was in the middle height of the room (Z ~ 1.0–1.8 m). The difference was as much as 300 °C between the coldest and the hottest regions. The highest temperatures were measured in the centre of the compartment with regard to X-axis, with temperatures above 1000 °C both below the ceiling (Z = 2.4 m) and above the crib (Z = 0.3 m). Such high temperatures occurred first at flashover and lasted only a few minutes. In the YZ-cross-section, see Fig. 20, there was a strong temperature gradient along the Y-axis. The temperatures were higher in the cross-section through Window 2 than Window 4 until the flames in the wood crib and CLT were extinguished.

The maximum temperature on the surface of the CLT behind the two layers of gypsum boards on the back wall was 106 °C. The maximum temperature at the glue line at 40 mm depth was 67 °C. The maximum temperatures for different depths into the wood were measured at
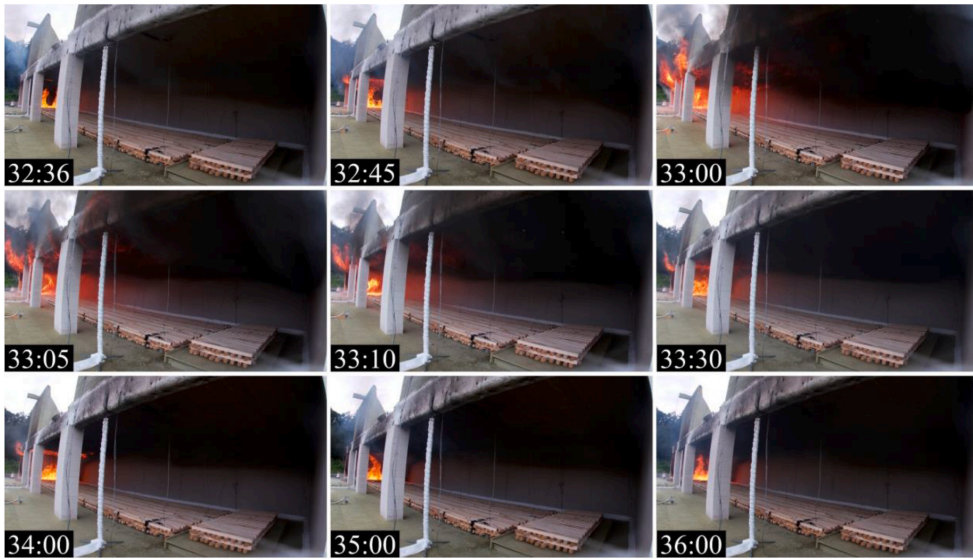
Fig. 10. Development of the 1st flashing wave. The ceiling ignites at 32:36, and within 30 seconds, flames reach almost to the end of the compartment. Flames retract after a short period. Time is given as (mm:ss) after ignition.
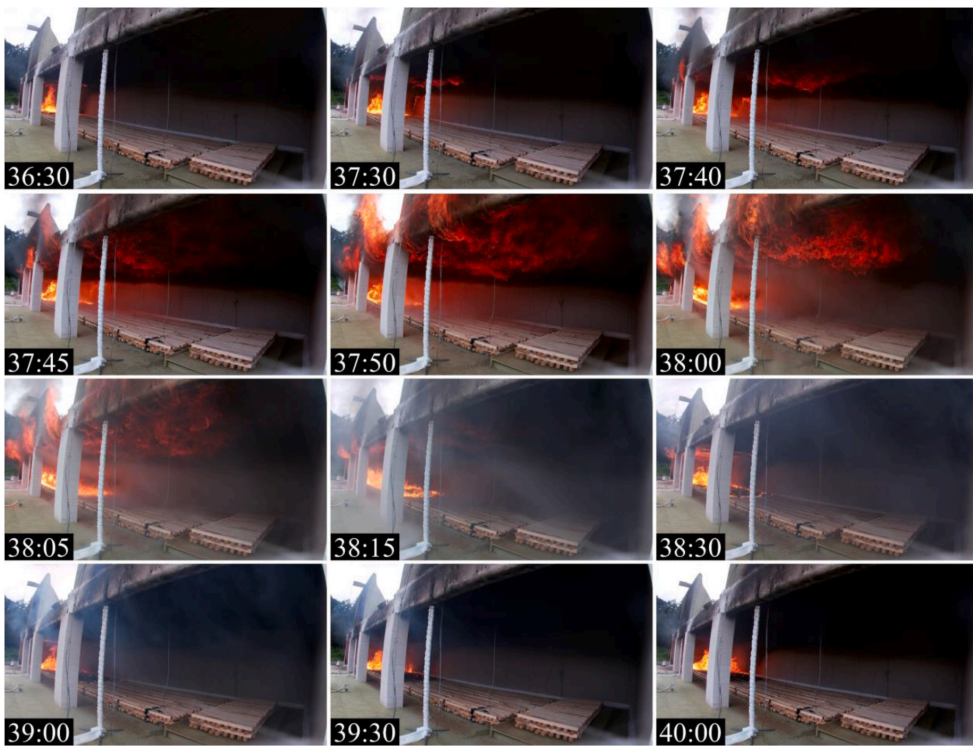

Fig. 11. Development of the 2nd flashing wave. At ~36:30, the ceiling reignites, and the flames spread below the ceiling by burning the combustible gases of the smoke layer. After a short, intense burning, the flames in the ceiling and top of the wood crib retract. Time is given as (mm:ss) after ignition.
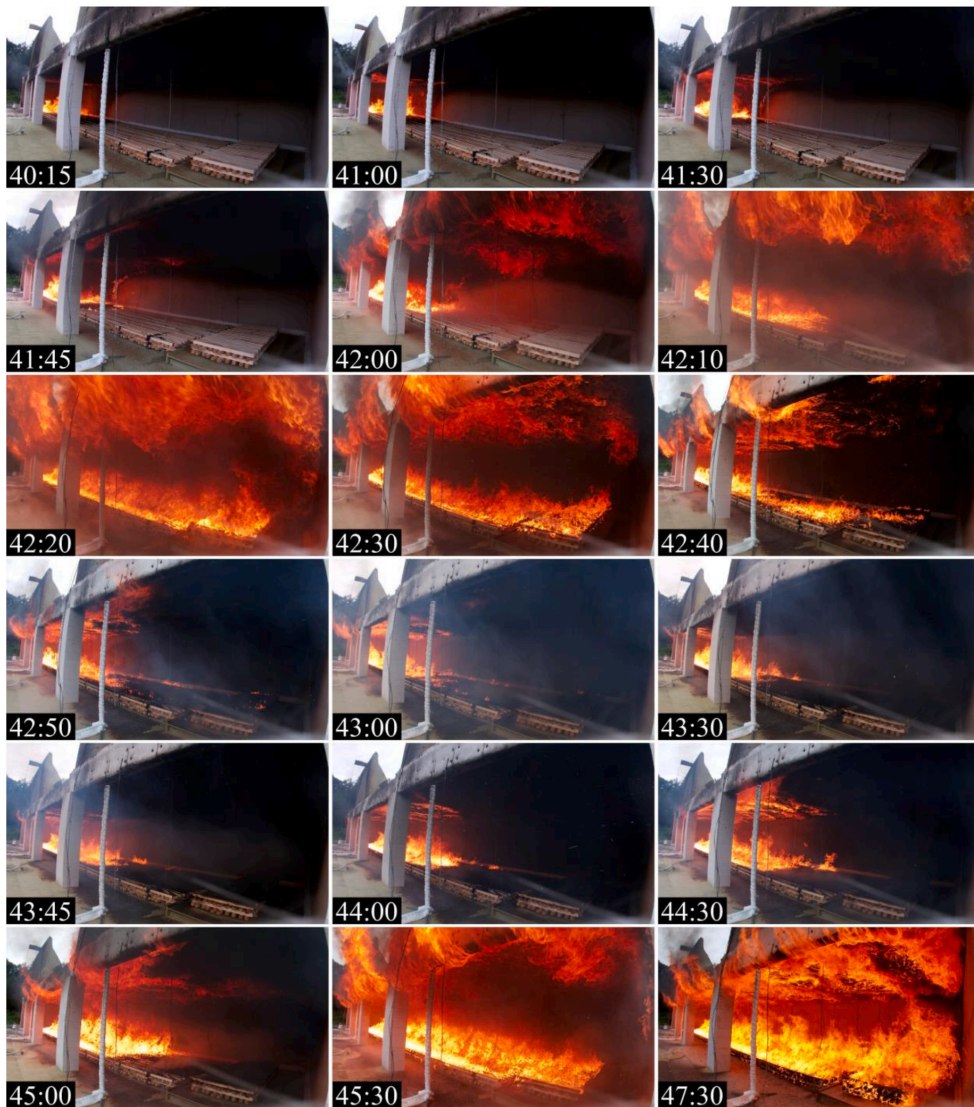
Fig. 12. Development of the 3rd and 4th flashing wave. Initiation of the 3rd wave occurs with reignition of the ceiling at ~40:15. Within 2 minutes, the flames have spread to cover the entire ceiling and crib. After a few seconds of the entire compartment burning, the flames below the ceiling and on top of the crib retract. The 4th wave occurs shortly after the retraction of the 3rd and leads to a stable flashover. Time is given as (mm:ss) after ignition.

125–140 min, i.e., more than 75 min after the most intense phase of the fire. After 300 min, the temperatures in the fire-exposed layer (0–40 mm) were almost uniform, at approx. 55 °C. These measurements were only from one position on the wall, i.e., X = 14.3 m and Z = 1.12 m.

3.3. External flames

External flames were present during the flashing waves and for a period of a few minutes after flashover. The largest flames exceeded the façade wall (i.e., flame height approx. 3 m above the window soffit) but were most of the time lower than the height of the façade wall. During the most intense external flaming immediately after flashover, the flames were approximately uniform for Windows 2, 3 and 4, while

flames out of Window 1 were clearly smaller, see Fig. 9 (d). The external flames did in general not cover the entire window opening, see Fig. 9 (b–c).

The measured temperatures on the facades above Windows 2 and 4 are shown in Fig. 21. The temperature profiles above the windows were similar for the two windows but shifted slightly in time in relation to each other. This is because high temperatures were reached above Window 2 earlier than Window 4 as the fire was developing in this part of the compartment first. The temperature development above Window 4 had a more prolonged decay phase, as the crib at this end of the compartment burned out at last. Above both windows, four distinct short-lived peaks were observed, which correspond to external flames during the flashing waves.

Fig. 13. Cessation of flaming combustion in the ceiling occurred while the wood crib was still burning. Photo from 62 min.

Fig. 14. Compartment after burn-out of the wood crib. No gypsum boards had fallen down, and the wood crib was completely consumed.

The incident heat fluxes towards the façade above Windows 2 and 4 were calculated based on the PT and TC measurements, see Section 2.4.1, and are given in Fig. 22. The incident heat flux to the façade was highest during the flashing waves. For Window 2, the heat flux was at its highest during the 3rd and 4th wave, with a short-lived intensity of 20, 55 and 70 kW/m^2 at 2.8 m, 1.8 m, and 0.8 m above the window soffit, respectively. The large difference between 2.8 m and 1.8 m gives an indication of the height of the external flame.

For Window 4, the highest heat fluxes occurred during the 3rd flashing wave with a short-lived intensity of 60, 85 and 90 kW/m^2 at 2.8 m, 1.8 m, and 0.8 m.

After flashover, the heat fluxes were higher outside Window 2 until 50 min. From this point on, the heat fluxes were slightly higher above Window 4.

The size of the external flame was related to the gas flow velocity through the compartment windows. Gas flow velocities were calculated from the bidirectional probes, see Section 2.4.2, and are shown in Fig. 23. Characteristics of the experiment can be observed in the velocity profile for the gas flow through the windows. The first peak seen directly after the ignition of heptane was caused by smoke filling the upper part of the compartment and exiting out of Window 4. When the heptane fire was extinguished, the smoke layer vanished, and the gas velocity out from Window 4 was reduced to zero. In general, the flow out from

Table 1
Summary of the fire development.

| Time [min]	Observation	Figure
0–3.5	Heptane trays are burning.	
3.5–32.5	Wood crib fire increases slowly in size, both with regard to flame height and area.	Figs. 2 and 8
32.5–33.5	**1st flashing wave.** The ceiling ignites without the wood crib flames impinging the ceiling. Fire spreads rapidly across the ceiling and partly across the wood crib.	Figs. 9 (a), Fig. 10
36.5–39	**2nd flashing wave.** Fire spreads again across the ceiling and the wood crib. External flaming out of all windows.	Figs. 9 (b), Fig. 11
41.5–42.5	**3rd flashing wave.** Fire spreads until the whole compartment is burning, with external flaming out of all windows. The ceiling fire retracts to approx. 9 m, and wood crib fire to approx. 11 m.	Figs. 9 (c), Fig. 12
45–45.5	**4th flashing wave.** Fire spreads to the end of the compartment for both the crib and the ceiling and causes a flashover without any retraction. Intense compartment fire with large external flames out of all windows.	Figs. 9 (d), Fig. 12
46–50	Fire intensity slightly reduced.	
50–61	**Self-extinction of CLT.** Intensity is reduced, and external flames are clearly smaller. Flames in the ceiling extinguish from left to right. Wood crib fire becomes more and more reduced, but there is still a continuous wood crib fire.	Fig. 13
61–95	Wood crib fire burn discontinuously, starting from the left end and moving right.	Fig. 13
95–240	Decaying temperatures, no visible flames, and no re-ignition.	Fig. 14
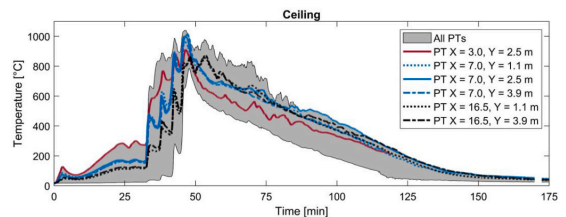
Fig. 15. Temperatures 100 mm below the ceiling measured by PTs facing downwards. The grey area covers all measurements by PTs in the compartment. X and Y represent the position of the PTs.
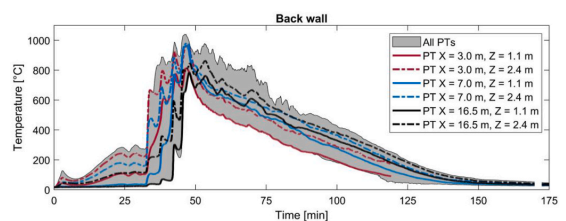

Fig. 16. Temperatures 100 mm in front of the back wall measured by PTs facing away from the wall. The grey area covers all measurements by PTs in the compartment. X and Z represent the position of the PTs.

Window 4 was higher than for Window 2. The flow out from Window 2 peaked at 10 m/s at 47 min before it dropped significantly and then again at 49 min. This corresponds with the observations of no external flaming out of this window. The velocity through Window 4 increased to a maximum of 12 m/s at 52 min and thereafter gradually reduced. The flow into the compartment slowly increased through Window 2 from ignition, while the flow through Window 4 was zero until flashover. An
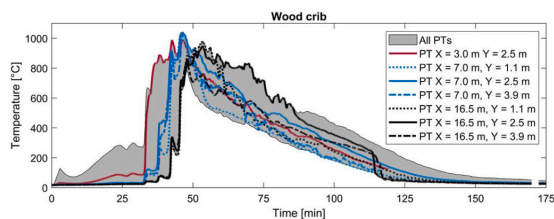
Fig. 17. Temperatures on top of the wood crib measured by PTs facing upwards. The grey area covers all measurements by PTs in the compartment. X and Y represent the position of the PTs.

Fig. 18. During the first flashing wave, the heat exposure to the walls was sufficient to ignite the paper of the gypsum boards on the walls close by.

increase in inflow velocities occurred through both windows at flashover but with the highest velocity through Window 2.

3.4. Fire spread across ceiling and wood crib

The fire spread across the ceiling and the wood crib is shown in Fig. 24, where the spread was slow until the ignition of the ceiling. Thereafter, the spread was dominated by the four flashing waves. The waves were always initiated by a spread across the ceiling first, shortly followed by a spread across the wood crib. The flames under the ceiling travelled almost to the end in the first two waves and reached the end in the final two waves. The leading edge of the flame spread remained at its maximum position just a few seconds before the flames retracted, starting in the ceiling. The ceiling fire retracted completely after the two first waves, while the wood crib fire grew larger after each wave. An exponentially increasing curve gave a good fit to the fire spread across the wood crib when the flashing waves were filtered out. The derivative of the fitted curve was then used to estimate the fire spread rate across the wood crib. Before the ceiling was ignited at 33 min, the fire spread rate in the crib increased from 0 to 3 mm/s, with an average rate (harmonic mean) of 0.9 mm/s (54 mm/min). After this point, the spread rate increased from 3 mm/s to 60 mm/s over the next 13 min, with an average spread rate of 20 mm/s (1.2 m/min). The fitted curve was also used to estimate the wood-crib total mass loss rate and HRR (see Section 3.5). No fitted curve was made to the fire spread across the ceiling due to the immense effect of the flashing waves. However, as seen in Figs. 10–12, the flames below the ceiling travelled across the compartment in 60 ± 30 s during the flashing waves.

3.5. Gas measurements

The concentration of oxygen (O_2), carbon monoxide (CO) and carbon dioxide (CO_2) were measured at three different locations as described in Section 2.3. The results are shown in Fig. 25. The O_2 concentration was about unchanged until the ceiling ignited. Thereafter, O_2 decreased in a pulsating way corresponding to the flashing waves. The lowest O_2 measured was approx. 9% and 12.5% at flashover in Windows 2 and 4, respectively. After this point, the O_2 increased steadily. The increase was

faster in Window 2 compared to Window 4, which corresponds with the earlier extinguishing of the CLT in this section. The lowest O_2 at the back wall was slightly below 19%. However, the measurement at the back wall was higher than expected and may have been caused by a leakage in the tube collecting the gas.

The CO_2 concentration increased with approximately the same percentage as the oxygen decreased. The concentration of CO increased significantly after the ignition of the ceiling, and the highest levels were measured during the flashing waves. Between 37 and 51 min, the CO levels increased above the measuring range of the sensors, 5000 ppm, and are therefore unknown. After 53 and 60 min, the CO levels increased in Windows 2 and 4. This is related to the extinction of flames in the CLT and indicates that smouldering is still ongoing, producing CO.

3.6. Charring of CLT ceiling

After the experiment, the final char depth was measured through the method explained in Section 2.3. The results are shown in Fig. 26, with a dark green marking for the areas with the smallest char depths and dark red for the most considerable char depths. The arithmetic average of the char depth was 26 mm with a standard deviation of 4 mm, corresponding to an approximate mass loss of 1125 kg. The char depth was strongly non-uniform, with the most severe charring from the centre of the ceiling towards the right side of the compartment, and less charring at the left side of the ceiling, although this part had the longest fire duration. The char depth was also larger near the back wall than near the window wall. This was observed along the whole length of the compartment.

In the centre of the compartment where the final char depth was largest, see Fig. 26, some delamination of the 1st layer had occurred. This is shown in Fig. 27(a), where several lamellas were partly loose and hanging from the ceiling and clearly detached from the layer behind. We refer to this behaviour as delamination, although the lamellas apparently had not detached along their entire length. Delamination occurred, although the char depth had not reached the first glue line in the CLT. This was caused by the temperature in the glue line exceeding the operational temperature of the glue and adhesion between the glue and the timber was therefore lost. Shortly before the experiment was terminated and extinguished, it was examined with an infrared camera. Some hot spots were detected behind the loose lamellas and next to the glulam beam, indicating that charring was still ongoing.

The temperatures at the glue-line interface were at maximum 194, 180 and 164 °C at location X = 4.7, 9.5 and 14.3 m and were reached after 120 min, more than an hour after the maximum compartment temperatures. These temperatures corresponded well with the observation that the visible lamellas of the 2nd layer were mainly discoloured and not charred (Fig. 27(a)).

Fig. 27(b) shows charring at one of the locations where the charring rate of the CLT was measured. The char depth was between 20 and 30 mm at this location. No signs of a corner effect at the CLT joints were observed, although the TCs were installed from the rebate joint.

Charring rates of the CLT are given in Table 2 and calculated from the embedded TCs at 0, 10, 20, 30 and 40 mm depths into the CLT and the final average char depth measured after the experiment, see Section 2.3.

Charring was defined to start when the CLT burned continuously, i. e., the short burning periods during the flashing waves were neglected.

3.7. Mass loss rate and heat release rate

The wood-crib mass loss and mass loss rate during the fire experiment were determined as described in Section 2.4.2. Due to overheating of the scale during part of the experiment, data were lost from 50 to 75 min. A decaying exponential curve was fitted to the existing data.

The MLR per unit length (50 mm) was found by derivation of the mass loss curve of the small crib and divided by 20 to convert the numbers from 1 m length to the unit length. The results are shown in
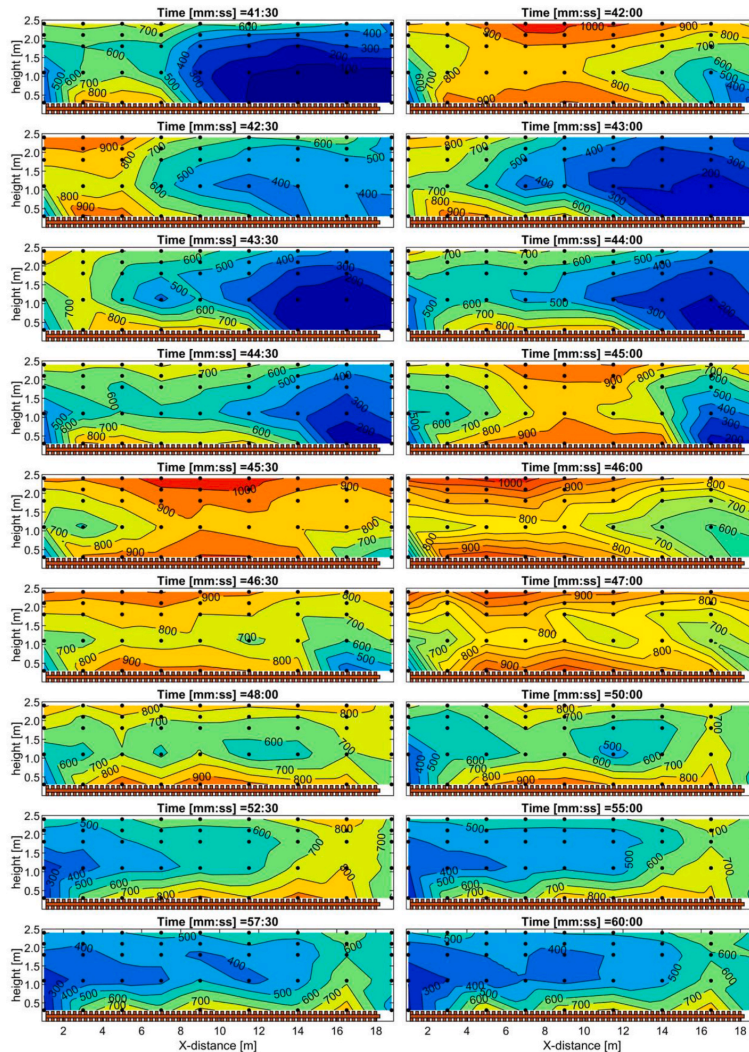
Fig. 19. Temperature maps of the cross-section through the XZ-plane at Y = 2.5 m. The black dots represent the positions of the TCs. The maps show the progression of the 3rd flashing wave (41:30–42:30), 4th flashing wave (45:00–45:30) leading to flashover (45:30) and the start of the decay phase with the extinguishing of the CLT (50:00–60:00).

Fig. 28.

The total MLR, for large and small crib combined, was obtained by combining the fire spread across the wood crib (Fig. 24) and the MLR per unit length shown in Fig. 28. An illustration of this method is given in Fig. 29. The estimated maximum MLR for the crib was 1.53 kg/s, which is converted to 4.14 g/(s m^2), in terms of the surface area of the wood sticks. The MLR of the crib was enhanced by the thermal feedback from the compartment, and a lower value would, therefore, be expected for a similar crib fire in open air.

The estimated MLR of the CLT was found based on the charring rates in Table 2, see Section 2.4.2. The MLR was at its maximum 1.61 kg/s, corresponding to 18 g/(s m^2).

The HRR is shown in Fig. 30. The HRR of the crib is at maximum 20 MW. The curve has a sharp peak, with a steeper increase than decrease. The HRR of the CLT has a stepwise pattern as it was based on the

charring rates. The step values are 21.0, 10.5 and 3.5 MW. The total HRR has a peak value of 41 MW, which equals a HRR per unit floor area of 436 kW/m^2. From the ignition of the ceiling, the HRR development has a growth rate between the fast and ultrafast t^2-curve [45].

The area under each HRR curve gives the energy released for the wood crib, the CLT and in total. Since a combustion efficiency of 0.8 was used, the area should ideally correspond to 80% of the energy content of the initial wood crib mass (2065 kg) and the mass of the burned CLT (1125 kg), which equals 33.0 GJ and 18.3 GJ for the CLT. The area below the HRR curve for the wood crib was 82% of the energy content of the initial wood crib, while the area below the HRR curve for the CLT was equal to 97% of the energy content of the mass of burned CLT.
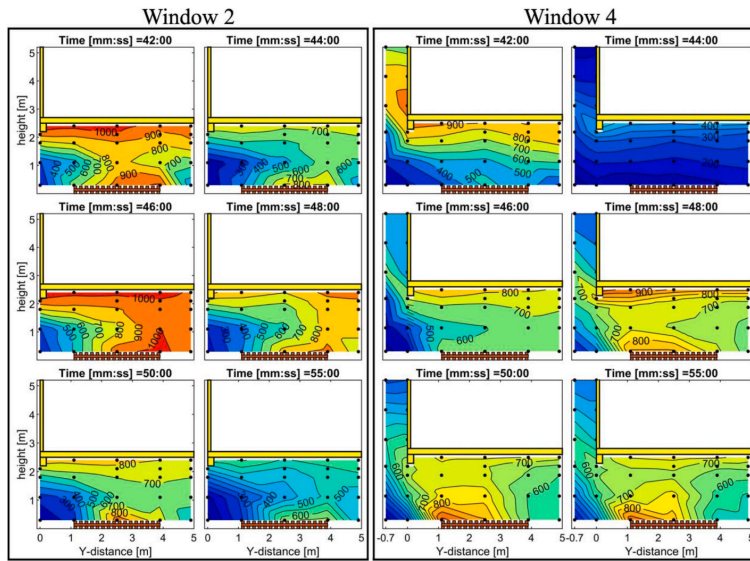
Fig. 20. Temperature maps of the cross-sections through the centre of Window 2 (X = 7.0 m) and Window 4 (X = 16.5 m) during part of the 3rd flashing wave (42:00), flashover (46:00) and the start of decay phase (50:00–55:00). The black dots represent the positions of the TCs. Temperatures for the outside area are missing for Window 2 due to a logger failure.
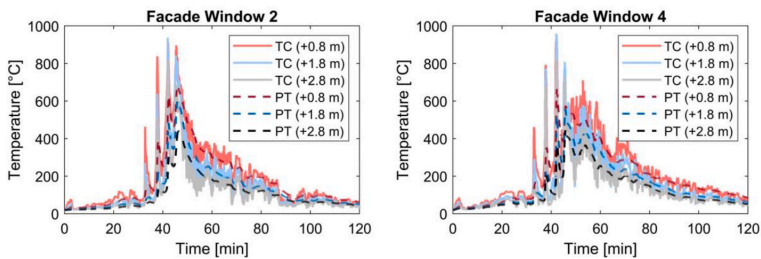

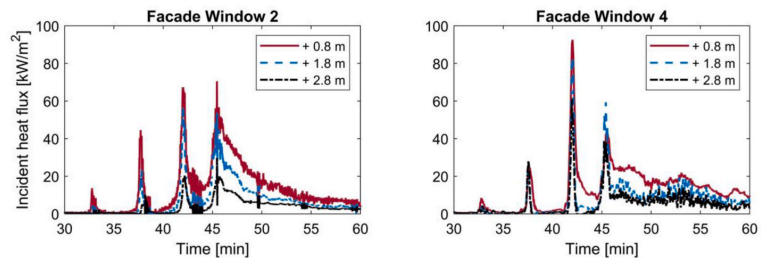**Fig. 21.** Temperature measurements at the façade above Window 2 and Window 4. + 0.8, 1.8, 2.8 m are the heights above the window soffit.

Fig. 22. Incident heat fluxes above Windows 2 and 4 calculated from PT and TC measurements at the façade above Window 2 and Window 4. + 0.8, 1.8, 2.8 m are the heights above the window soffit.

4. Discussion

4.1. Fire spread

The fire spread can be divided into two phases, before and after the ignition of the ceiling. In the beginning, the fire spread was slow for several reasons; the flames reached 0.5–2.2 m above the floor but were not impinging the ceiling, and surfaces with non-impinging flames require a higher heat flux to ignite than surfaces with an impinging flame [63]. In addition, due to open windows and only a 0.36 m deep reservoir created by the glulam beam, a thick smoke layer was not able to form. Hence, the radiation towards the ceiling was not sufficient to ignite the CLT. The slow fire spread before the ignition of the ceiling is a good indicator of how the fire would have continued to spread if the CLT
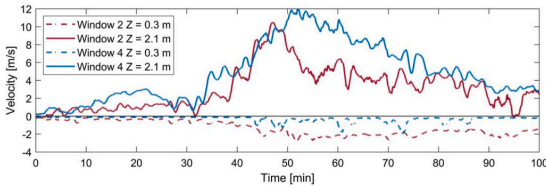
Fig. 23. Gas flow velocities in and out of Windows 2 and 4. The values are averaged over 30 s. Positive values represent outward flow, and negative values inward flow.
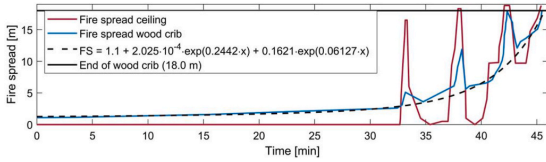

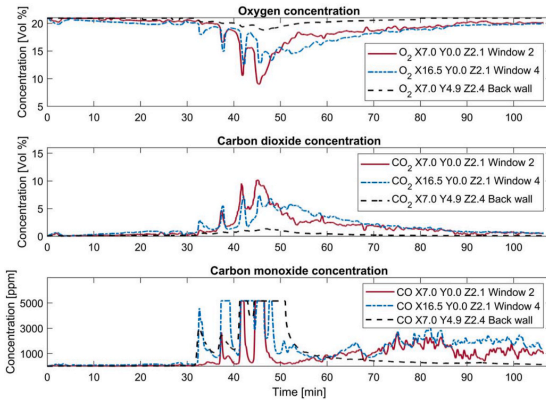**Fig. 24.** Fire spread across the wood crib and the CLT ceiling.

Fig. 25. Oxygen (O_2), carbon monoxide (CO) and carbon dioxide (CO_2) concentration.

ceiling had been protected or not present. This is in line with other travelling fire experiments with a similar wood crib, geometry and ventilation conditions [30,35]. Fire behaviour in such conditions could be explained by the theoretical model called "Weak-plume localised

fire" [64].

The ceiling was ignited at around 33 min by a combination of hot smoke and radiation from the flames. The late ignition of the ceiling compared to the CodeRed experiments [17,36] is an important observation which is relevant for the fire safety design of CLT compartments with a low likelihood of ceiling-impinging flames (e.g. with a high ceiling) and a low potential for collection of combustible gases under the ceiling, e.g. compartments with ceiling beams of limited height and high ventilation openings.

From the ignition of the ceiling, the fire dynamics changed completely, and the fire spread was significantly faster. A characteristic behaviour in this experiment was the flashing waves, in which the flames travelled back and forth several times. Although the fire retracted after each wave, the wood crib fire grew larger. The temperatures in the compartment increased as well after the retraction of each wave, including locations far away from the wood crib fire, despite the compartment being well-ventilated. Thus, the combustible materials in the wood crib and ceiling farther away from the ignition source were preheated and, therefore, more prone to ignite at a later point. This can explain the shorter and shorter durations between the flashing waves.

The temperature profiles adapted well to the visual impression of the flames during both the flashing waves and flashover. For instance, the lowest temperatures were present at a height of 1.0–1.8 m above the floor in the most intense burning phase, which can be explained by the absence of flames at this height. It was burning both in the ceiling and above the wood crib, but none of these flames reached the middle height of the room.

The fire spread rate corresponded well with an exponentially increasing curve. Thus, the maximum and the average fire spread rates would likely have been higher if the compartment had been longer. Flashing waves have not been reported from any other research on travelling fires, but a localised flash without the retraction is called a "Zonal Intense Burning" [64].

The flame spread direction in both the ceiling and across the wood crib was directly influenced by the glulam beam. Although the glulam beam only reached 0.36 m below the ceiling, it created an effective barrier for the smoke to exit out of the closest window. Hence, the smoke was instead effectively guided towards the other end of the compartment, where it exited out of Window 4 as the smoke layer filled up the volume entrained by the glulam beam. This explains the higher outward flow velocities through Window 4 compared to Window 2 before ceiling ignition. When the ceiling ignited, it had already been preheated for a while. This contributed to a fast flame spread across the ceiling. With the burning ceiling, and the intense radiation onto the wood crib, the wood crib fire also started to spread. As the wood crib was already burning, the spread could be considered a piloted ignition. The slower fire spread across the wood crib compared to the ceiling can be explained by the crib being less preheated before the spread took place. Several of the characteristics of this experiment, including the rapid flame spread

BACK WALL

	0.2	0.7	1.2	1.7	2.2	5.0	5.5	6.0	6.5	7.0	9.8	10.3	10.8	11.3	11.8	14.5	15.0	15.5	16.0	16.5	16.8	17.3	17.8	18.3	18.8	AVG
4.8	21	27	24	22	24	31	27	24	22	24	30	32	33	33	32	33	32	33	30	29	29	26	25	25	27	28
4.3	22	25	22	19	28	22	25	22	19	27	30	30	32	36	27	25	28	27	30	28	30	29	23	22	27	26
3.8	23	23	24	25	29	23	23	24	25	29	27	33	32	28	26	25	32	29	30	33	29	27	24	23	25	27
3.3	27	24	25	22	29	27	24	25	22	29	27	33	27	32	27	25	32	34	32	31	29	28	22	23	25	27
2.8	26	29	22	22	26	26	29	22	22	26	30	30	30	28	26	38	35	36	29	32	30	30	24	24	28	28
2.3	30	26	26	20	27	30	26	26	20	27	28	28	30	32	28	29	30	28	28	31	27	28	25	23	23	27
1.8	25	27	24	22	23	25	27	24	22	23	21	30	32	31	30	27	29	28	28	31	26	27	25	25	21	26
1.3	22	23	20	22	25	22	23	20	22	25	22	24	28	32	26	26	30	33	29	26	24	24	21	22	23	24
0.8	24	24	20	22	21	24	24	20	22	21	19	25	27	27	20	23	31	25	26	25	23	22	21	23	24	23
0.3	20	21	22	24	22	20	21	22	24	22	28	26	26	32	24	40	27	30	31	25	22	26	24	26	24	25
AVG	24	25	23	22	25	25	25	23	22	25	26	29	30	31	27	29	31	30	29	29	27	27	24	23	24	

WINDOW WALL

IGNITION SIDE

Fig. 26. Final char depth [mm] presented as a 2D plan view of the CLT ceiling. The bold numbers at the left side and top represent the X and Y locations [m] given in Fig. 5.
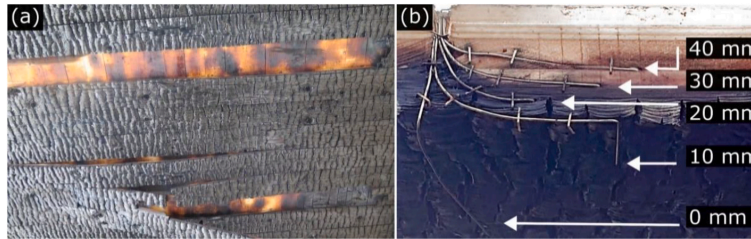
Fig. 27. (a) Examples of delamination of the CLT ceiling. (b) Example of charring close to the TCs embedded in the CLT. The 0 mm TC was attached to the surface of the CLT and was used to define the onset of charring at this point.

Table 2
Onset of charring at different depths, and charring rates of CLT ceiling.

Location	Time to reach 300 °C [min]					Charring rate [mm/min]				
	0 mm	10 mm	20 mm	26[a] mm	30 mm	0–10 mm	10–20 mm	20-26[a] mm	20–30 mm	0-26[a] mm
X 4.7 m	37.6	43.1	52.3	–	81.2	1.81	1.36	0.35	0.35	1.02
X 9.5 m	41.5	45.2	59.8	–	–	2.69	1.09	–	–	1.13
X 14.3 m	45.2	49.7	66.8	–	–	2.21	0.93	–	–	1.26
Average	41.4	46.0	59.6	77.0[b]	–	2.23	1.13	0.35	–	1.13

[a] 26 mm is the average final char depth of the CLT ceiling.
[b] 77 min is the time to reach 26 mm based on the charring rate between 20 and 30 mm at X 4.7 m and the average time to reach 20 mm char depth.
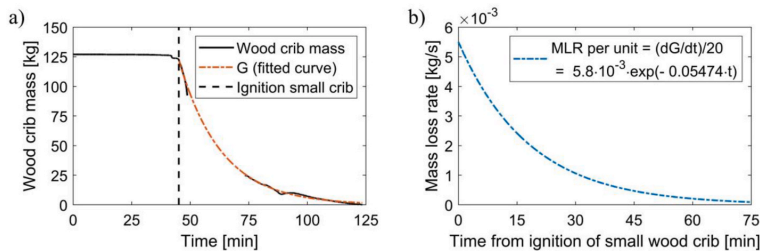
Fig. 28. (a) Mass change of the small wood crib (1.0 m × 2.8). (b) Mass loss rate per unit length (50 mm) of the small wood crib.

underneath the ceiling and the increased fire spread rate of the wood crib after ignition of the ceiling, were also observed by Nothard et al. [34]. The geometry, opening factor and moveable fuel of the experiment are comparable, except that their experiment was smaller in scale.

The fire spread rate after ceiling ignition was on average 1.2 m/min (20 mm/s) across the wood crib, which is considerably slower than the spread rate across the crib in the CodeRed experiments, with an average spread rate after ignition of the ceiling of 9.6 m/min (160 mm/s) in CodeRed #01 and 9.0 m/min (150 mm/s) in CodeRed #02. However, the wood crib in those experiments was made of 30 mm × 30 mm wood sticks and 5 mm thick wood fibreboard strips. Despite a larger distance between the wood crib and the ceiling (~2.7 m), the flames were impinging the ceiling. Hence, the setup was designed for a faster combustion and had an average spread rate of 0.6 m/min (11 mm/s) even before the ceiling was ignited. These differences highlight that the type of fuel and whether the flames are impinging the ceiling greatly impact the fire spread rate.

4.2. Flashing waves

A characteristic flame behaviour in this experiment was the flashing waves. Fires have been observed to travel back and forth in large compartments earlier [38], although at a completely different rate and caused by the lack of oxygen. Hence, the behaviour observed in this experiment has not been reported earlier, to our knowledge. The

mechanisms behind this phenomenon can be explained by the general extinction theory for flames [65] and are related to the self-extinction of flaming combustion of CLT [66–68] and the feedback reaction between the wood crib and the exposed ceiling.

All the flashing waves started with ignition of the CLT ceiling above the existing wood crib fire. Since the ceiling had been preheated before ignition, the initially small flames from the ceiling grew rapidly to cover a larger area. The burning CLT was then able to ignite the combustible gases of the smoke layer, which had filled the entire reservoir created by the glulam beam. From Figs. 10–12, it is apparent that the main driving force for the flame spread below the ceiling was burning of combustible gases in the smoke layer. The combustible gases were likely produced by heating of the CLT, as emission of combustible gases are known to occur from CLT, or wood in general, before it ignites. Some combustible gases were also likely due to inefficient burning of the wood crib and the CLT.

The flames beneath the ceiling caused a high heat flux towards the wood crib, which enlarged the existing wood crib fire and caused the fire to spread along the top layer of the wood crib.

The retraction of the flames started at the far end of the compartment. Here, the flames beneath the ceiling had predominantly been supplied by combustible gases produced at the other end of the compartment. A few seconds after ignition of the CLT, the pyrolysis gases produced before ignition had been combusted, and only combustion of pyrolysis gases produced continuously was ongoing. This transition caused a natural reduction in flame size.
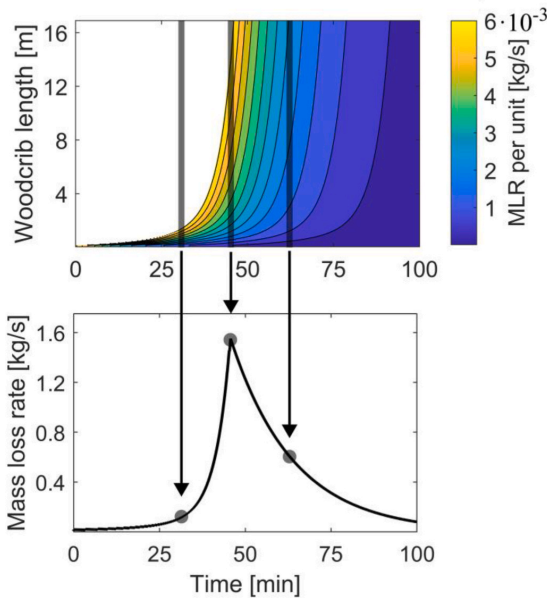
Fig. 29. Illustration of how the mass loss rate for the whole wood crib was determined. At the top, the MLR per unit length is represented by contour lines as a function of time and wood crib length. The curve is a combination between Figs. 24 and 28. By summation over the MLR per unit length for all wood crib units at one time point (illustrated by grey lines), the MLR for the given time point is generated (grey dots).

Moreover, the external heat flux to the ceiling decreased with increasing distance from the initial wood crib fire, caused by two mechanisms: Firstly, close to the initial wood crib fire, the radiation to the ceiling was high due to the well-established wood crib fire. However, with increasing distance from the initial wood crib fire, mainly the top layer of the crib was burning, and the radiation to the ceiling was strongly reduced. Secondly, farther away from the initial wood crib fire, a larger fraction of the heat produced was used to heat the air and surrounding materials, as these had been preheated less than materials and air closer to the initial wood crib fire.

Summarised, the extinction and retraction of the flames at the leading edge were due to too low supply of new combustible gases to sustain burning after the combustible gases of the smoke layer had been consumed. The low supply of combustible gases can be explained by the

low temperatures of the compartment and the CLT. At X = 16.5 m, the PT temperatures below the ceiling were at maximum 270 °C, 436 °C and 645 °C during the 1st, 2nd, and 3rd flashing waves, respectively.

Extinction of flames might also occur if the oxygen concentration is reduced below a critical level depending on temperature [65]. The minimum oxygen concentrations at X = 16.5 m were 18.0%, 14.9% and 12.5% during the 1st, 2nd, and 3rd flashing waves, respectively. These values are higher than the critical oxygen concentration for sustained burning [65], and the contribution from the oxygen concentration seems to play a minor role here.

Usually, a wood crib fire is able to sustain burning on its own without any external heat flux [49]. However, since mainly the top layer of the crib was burning, the combustion was highly dependent on the external heat flux. With the retraction of the flames below the ceiling, the incident heat flux towards the wood crib was reduced to a level which no longer could sustain combustion, and the wood crib fire retracted as well.

Despite the retraction of the flames, the temperature maintained at a higher level than before the flashing waves, as seen in Figs. 15–17. This higher temperature preheated the material, which led to shorter and shorter times between the flashing waves, and the flashing wave increased in intensity and duration for each new wave, see Figs. 10–12.

4.3. Self-extinguishment of flames in CLT

Self-extinguishment of CLT when the variable fuel has burned out is an important factor for safe implementation of CLT in buildings [66]. This has been observed in several CLT experiments [17,18,36] and was also observed in this experiment.

After flashover, the whole ceiling burned for only a few minutes before extinction started from the left side after around 50 min and was completely extinguished after 61 min. Extinction of the flames in the CLT after flashover was recognised by a significant drop in the average compartment temperature after 50 min, followed by an almost linear decay curve. The relatively long extinguishing time aligned with the time the fire travelled across most of the wood crib. This indicates that the heat flux to the ceiling from the wood crib reached a critical level to sustain the flaming combustion of the CLT. The CLT was extinguished at a PT temperature of 695–705 °C and heat fluxes of 49–52 kW/m². This is slightly higher than the suggested critical heat flux of 43.6 ± 4.7 kW/m² for the same wood type in small-scale experiments [13]. Nevertheless, the fact that extinguishment of the flames occurred at similar temperatures and heat flux levels indicates that the extinguishment of CLT can be predicted based on the temperature in a compartment fire.

The PT temperatures related to extinction were higher than extinction temperatures when considering the XZ temperature map (Fig. 19). However, this can be explained by using TCs instead of PTs, as PTs are generally more exposed to radiation from the surroundings than TCs.
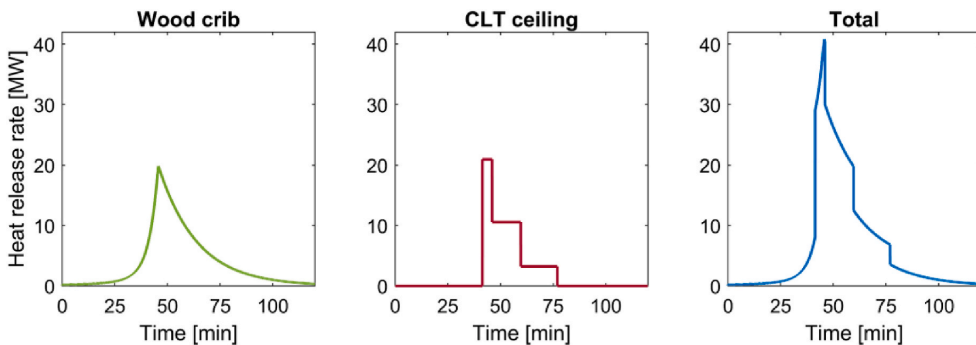

Fig. 30. Estimated heat release rates of the wood crib and the CLT ceiling.

4.4. Charring rate and heat release rate

The charring rate of the CLT varied significantly from the first 10 mm to the subsequent 10 mm intervals. The charring rate for the first 10 mm was 2.23 mm/min (Table 2), which is higher than values often reported for average charring rates of CLT [44,69]. The average charring rate over the entire CLT char depth of approx. 1 mm/min (Table 2), on the other hand, is in line with the average charring rates reported earlier [44,69].

Mitchell et al. [44] reported that high charring rates are related to large openings, which can be explained by increased charring with high oxygen concentrations [70]. However, the high charring rates for the first 10 mm followed by reduced charring rates are here instead believed to be caused by a combination of the natural mass loss rate variation found in wood and the significant variations in temperature and heat fluxes during the experiment, which are known to influence the charring rate [70]. The natural mass loss variations in the wood are clearly shown by looking at a typical mass loss rate curve for wood in a cone calorimeter experiment, where there is an initial peak in the mass loss rate directly after ignition, followed by a reduced but stable mass loss rate [71]. This behaviour is due to the formation of a char layer that works as an insulation layer to the uncharred wood.

As the charring rate is related to the HRR, the high initial charring rate also led to a high initial HRR peak. Although this high HRR only lasted a few minutes, the contribution from the CLT to the HRR during this period was significant. It will be a driving force for increased fire spread and large external flames and should not be neglected.

The stepwise pattern of HRR for CLT, see Fig. 30, is obviously not accurate. However, it gives a good representation of the actual curve, although a shorter distance between the embedded TCs would have given an even more realistic curve. Nevertheless, we consider this presentation of the HRR to be a better approach than presenting the HRR as a constant value between the start and end of charring. As an example, in the CodeRed-experiments, the contribution from the CLT was reported to be similar to the wood crib based on a constant HRR contribution from the CLT [17]. With the strongly varying HRR measured in this experiment, it is safe to assume that the HRR of the CodeRed-experiments also changed through the fire. Hence, the peak HRR for the CLT in the CodeRed-experiments was likely higher than for the wood crib in the most intense phase of the fire.

The MLR of the wood crib was based on the measured mass loss of the small wood crib. As the small crib was elevated 0.2 m higher than the large crib, it was positioned at the end of the compartment to not influence the fire spread across the wood crib. In addition, it was easier to protect signal wires from heat when positioned at the end than if it had been in the centre.

The wood crib burning before ignition of the ceiling likely burned with a lower maximum MLR than assumed from the calculations, as the re-radiation from the surfaces to the crib was minimal before ignition of the ceiling. However, the part of the crib burning before the ceiling ignited was relatively small compared to the whole crib, and we have neglected this difference in calculation of the total MLR for the whole crib. From the point the ceiling was ignited, the burning wood crib received considerable feedback from the ceiling above, somewhat similar to the small crib at the end.

The energy released from the wood crib (i.e., the area under the HRR curve) was 82% of the energy content of the initial mass of the crib. This is a good match with the assumed combustion efficiency of 0.8 and confirms that the measuring method for the mass loss rate and the method to determine the HRR based on this was suitable. The energy released from the CLT (i.e., the area under the HRR-curve) was 97% of the energy of the mass loss, and therefore 17% points higher than what it should have been when using a combustion efficiency of 0.8. The deviation can be explained by some uncertainties in both the method to estimate the total mass loss and the method to determine the HRR from the charring rate. Such a deviation is therefore considered to be

acceptable.

The maximum HRR of the CLT was approximately the same as the peak HRR of the wood crib, although lower in general. This is shown by comparing the total energy released from the wood crib and the CLT. 61% of the total energy released originated from the wood crib, and 39% from the CLT.

Besides the own HRR contribution from the CLT, it also increased the HRR of the wood crib. This is clearly shown by comparing the wood crib fire spread rate before and after the ignition of the ceiling. Without the contribution from the CLT, the wood crib fire would have developed much slower, which is indicated by Fig. 8. Here, the flame base area was almost constant between 20 and 33 min before ignition of the ceiling as the leading and trailing edge of the fire travelled at approximately the same rate.

4.5. Char depth and delamination

The char depth was strongly non-uniform across the ceiling, see Fig. 26. The reason for the uneven charring is believed to be caused by temperature and oxygen differences throughout the compartment. The largest char depth along the X-axis was located where the highest temperatures were measured, see Figs. 15 and 19. The lower char dept at the left end of the compartment, where the fire had been present for the longest time, is likely due to the fire in the first 30 min being relatively small with low temperatures below the ceiling. Also, the duration of the post-flashover phase was the shortest at this end. The differences in Y-direction are believed to be due to a higher oxygen concentration under the ceiling in the back of the room compared to the window side. However, this cannot be proven, as the oxygen measurement in the back of the room probably was affected by a leakage.

The arithmetic average of the char depth of the entire CLT ceiling was 26 mm. This is 14 mm from the glue line, and pronounced delamination was unexpected. However, some delamination occurred in the centre of the compartment, see Fig. 27(a), where the char depth was thicker, see Fig. 26. Visual examinations after the experiment showed that even for the areas with delamination, the charring had not reached the glue-line. Hence, delamination must have occurred due to the adhesive losing its bonding properties at lower temperatures than the charring temperature. Precisely at which temperatures delamination occurred cannot be determined. However, the maximum temperature at 40 mm depth was 164–194 °C, around 120 min. It is, therefore, likely that the delamination also occurred around that time. An argument supporting this is the discolouring of the second layer (Fig. 27a), which is known to occur around 200 °C [63,67]. This is close to the measured temperatures at the glue line. In addition, the temperature below the ceiling at 120 min was approx. 220 °C and declining. This low temperature can explain why the charring did not continue into the second layer and caused a reignition.

The main reason for the limited delamination was the combination of a relatively short post-flashover phase and the thick outer layer of 40 mm. A CLT element with a thinner outer layer (e.g., 30 mm) would likely have delaminated on the entire ceiling area in a similar way.

Nevertheless, this result aligns with a few other experiments [4,21] by showing that delamination of CLT does not always lead to a second flashover. Also worth highlighting is that self-extinguishment of the CLT in this experiment was achieved despite using an adhesive that lacks a demonstrated resistance against glue-line integrity failure.

The char depth is often linked to the duration of the fire or the fuel load density. However, it is essential to note that the heat release rate and the temperature in the compartment also play a role here. This is shown by comparing this experiment to the CodeRed-experiments, where the fuel load density was 50% compared to this experiment (186 vs 353 MJ/m^2). Despite a lower fuel load density and shorter fire duration in the CodeRed experiments, the CLT burnt for about the same time (12 vs 15 min), and the char depths were about the same (25 vs 26 mm). This comparison shows that total char depth cannot be

determined based on the fuel load density alone. A similar conclusion was made in the Epernon experiments [19].

4.6. External flames

External flames were present during the flashing waves and for a short period after flashover. The external flames were clearly lower from Window 1 than from the other windows, see Fig. 9 (d). This can be explained by the crib being almost completely burnt out in this section of the compartment at flashover. The most intense burning phase and the presence of external flames were short. This is shown through temperatures and heat fluxes in Figs. 21 and 22. Generally, the incident heat flux is lower than the highest values measured in comparable CLT compartment experiments [4,5,9]. This is as expected since most other experiments have been ventilation-controlled, in contrast to the large ventilation openings here, allowing for a larger fraction of the combustible gases to be burnt inside the compartment. In addition, with the large openings, the excess pyrolysis gases were burnt over a larger area, with correspondingly shorter flame height, compared to if the openings had been slimmer [8].

4.7. Ventilation conditions

This experiment had a larger opening factor than the majority of performed CLT experiments, and it would be considered a fuel-controlled fire (Regime-II) based on the traditional distinction for compartment fires [63]. An observation throughout the experiment was the lack of visible smoke during large periods of the fire. This indicates a clean and complete combustion and corresponds well with the relatively high oxygen concentration measured out of Windows 2 and 4. The lack of smoke is also a visual proof of the compartment fire being fuel-controlled during most of the experiment. However, an observation that contradicts the fire to be fuel-controlled was the large external flames at the peak of the 3rd flashing wave and flashover. Their presence shows that a large fraction of the combustible gases produced were burnt on the outside. Such behaviour would typically be considered for ventilation-controlled fires as a sign of too little oxygen to burn the gases inside the compartment. However, as the outflowing gas had an oxygen concentration of minimum 9.5–12%, the non-burned combustible gases were likely a result of insufficient mixing of oxygen and combustible gases.

Summarised, the fire appeared neither as a true fuel-controlled fire nor a ventilation-controlled fire, as it had elements of both. In several ways, this appearance matches the new proposed regime [72], *Regime-II-CLT*. A characteristic of this regime is the higher outflow velocities and less time for sufficient mixing, in which both would lead to a larger external flame. This adapts well to the observations in this experiment. Another characteristic of Regime-II-CLT is that the highest temperatures should be present in the centre height of the room due to insufficient mixing below the ceiling, but this does not match the temperature profile observed in this experiment.

5. Conclusion

A large-scale compartment (95 m^2) fire experiment with an exposed CLT ceiling has been performed. The setup was designed to fill a gap in the current knowledge about fire spread and fire dynamics in large, well-ventilated open-plan compartments with a CLT ceiling. This experiment is among the largest CLT experiments conducted to date and gives a unique perspective on fire dynamics related to an open-plan compartment with an exposed CLT ceiling and large window openings.

- Ignition of the ceiling occurred first at 32.5 min, which could be explained by flames not reaching the ceiling and limited conditions for a thick smoke layer to build up.

- From the point when the ceiling was ignited, the fire dynamics changed completely, and the flames spread quickly across the ceiling and wood crib. Instead of developing into a full flashover directly, the fire travelled back and forth in four distinct flashing waves within 13 min, whereby the wood crib fire grew larger for each wave. Such flashing waves are a new observation for travelling fires.
- The average fire spread rate before the ignition of the ceiling was 54 mm/min (0.9 mm/s), while the rate was 1.2 m/min (20 mm/s) after the ignition of the ceiling. This strengthens previous findings that a CLT ceiling greatly influences the fire spread rate and fire dynamics from the point the ceiling is ignited.
- After a short post-flashover phase, the intensity of the fire was rapidly reduced, and the CLT ceiling self-extinguished over a period of approx. 10 min while the wood crib fire was still burning.
- The charring was most pronounced in the centre of the ceiling and towards the back of the room.
- Some delamination was observed, although the average char depth did not reach the glue line. No reignition or fire growth was observed within 4 h. It is highlighted that this was achieved despite using an adhesive that lacks a demonstrated resistance against glue-line integrity failure.
- External flames were present during the flashing waves and for a short period after flashover. The incident heat flux at the façade was lower than the highest values measured in other comparable CLT compartment experiments.
- The experiment presented here differs significantly from those previously published by having a larger opening factor, the flames did not impinge the ceiling, and there was less potential for combustible gases to accumulate under the ceiling. The rate of fire development was in strong contrast to that of previous experiments and may be relevant for compartment designs with a low likelihood of ceiling-impinging flames (e.g., with a high ceiling) and a low potential for collection of combustible gases under the ceiling, e.g., compartments with ceiling beams of limited height.

Queensland, and Johan Sjöström at RISE for valuable discussions in the planning phase of the experiments.

Appendix A. Supplementary data

Supplementary data to this article can be found online at https://doi.org/10.1016/j.firesaf.2023.103869.

References

[1] A. Bartlett, A. Law, Influence of excess fuel from timber lined compartments, Construct. Build. Mater. 235 (2020), 117355, https://doi.org/10.1016/j.conbuildmat.2019.117355.

[2] A. Frangi, M. Fontana, Fire performance of timber structures under natural fire conditions, Fire Saf. Sci. 8 (2005) 279–290, https://doi.org/10.3801/IAFSS.FSS.8-279.

[3] T. Hakkarainen, Post-flashover fires in light and heavy timber construction compartments, Post-Flashover Fires Light Heavy Timber Constr. Compart. 20 (2) (2002). https://journals.sagepub.com/doi/abs/10.1177/0734904102020002074.

[4] J. Su, P.-S. Lafrance, M.S. Hoehler, M.F. Bundy, Fire Safety Challenges of Tall Wood Buildings–phase 2: Task 3-Cross Laminated Timber Compartment Fire Tests. Report No. FPRF-2018-01-REV, NFPA (National Fire Protection Association), Quincy, Massachusetts, USA, 2018. Accessed: March 28, 2023. [Online]. Available: https://tsapps.nist.gov/publication/get_pdf.cfm?pub_id=925297.

[5] J. Sjöström, D. Brandon, A. Temple, E. Hallberg, F. Kahl, RISE Report - Exposure from Mass Timber Compartment Fires to Facades (2021:39), RISE Fire Research, 2021.

[6] L.A. Bisby, A. Bartlett, R. McNamee, J. Zehfuss, J.-M. Franssen, F. Robert, C. Tessier, S. Mohaine, Epernon Fire Tests Programme – Synthesis Report, 2020.

[7] R. McNamee, J. Zehfuss, A.I. Bartlett, M. Heidari, F. Robert, L.A. Bisby, Enclosure fire dynamics with a cross-laminated timber ceiling, Fire Mater. 45 (7) (2020) 847–857, https://doi.org/10.1002/fam.2904.

[8] J. Sjöström, D. Brandon, A. Temple, J. Anderson, R. McNamee, External fire plumes from mass timber compartment fires—comparison to test methods for regulatory compliance of façades, Fire Mater. (2023), https://doi.org/10.1002/fam.3129 n/a, no. n/a.

[9] T. Engel, N. Werther, Impact of mass timber compartment fires on façade fire exposure, Fire Technol. 59 (2023) 517–588, https://doi.org/10.1007/s10694-022-01346-8.

[10] R.M. Hadden, A.I. Bartlett, J.P. Hidalgo, S. Santamaria, F. Wiesner, L.A. Bisby, S. Deeny, B. Lane, Effects of exposed cross laminated timber on compartment fire dynamics, Fire Saf. J. 91 (2017) 480–489, https://doi.org/10.1016/j.firesaf.2017.03.074.

[11] X. Li, X. Zhang, G. Hadjisophocleous, C. McGregor, Experimental study of combustible and non-combustible construction in a natural fire, Fire Technol. 51 (6) (2015) 1447–1474, https://doi.org/10.1007/s10694-014-0407-4.

[12] A.R. Medina Hevia, Fire Resistance of Partially Protected Cross-Laminated Timber Rooms, Master thesis, Carleton University, Ottawa, Ontario, 2014.

[13] R. Emberley, T. Do, J. Yim, J.L. Torero, Critical heat flux and mass loss rate for extinction of flaming combustion of timber, Fire Saf. J. 91 (2017) 252–258, https://doi.org/10.1016/j.firesaf.2017.03.008, 2017/07/01.

[14] R. Crielaard, J.-W. van de Kuilen, K. Terwel, G. Ravenshorst, P. Steenbakkers, Self-extinguishment of cross-laminated timber, Fire Saf. J. 105 (2019) 244–260, https://doi.org/10.1016/j.firesaf.2019.01.008, 2019/04/01.

[15] T. Ohlemiller, Smoldering Combustion. SFPE Handbook of Fire Protection Engineering, Society of Fire Protection Engineers, 2002.

[16] J. Cuevas, J.L. Torero, C. Maluk, Flame extinction and burning behaviour of timber under varied oxygen concentrations, Fire Saf. J. 120 (2021), 103087, https://doi.org/10.1016/j.firesaf.2020.103087, 2021/03/01.

[17] P. Kotsovinos, E. Rackauskaite, E. Christensen, A. Glew, E. O'Loughlin, H. Mitchell, R. Amin, F. Robert, M. Heidari, D. Barber, G. Rein, J. Schulz, Fire dynamics inside a large and open-plan compartment with exposed timber ceiling and columns: CodeRed #01, Fire Mater. (2022), https://doi.org/10.1002/fam.3049 vol. n/a, no. n/a.

[18] D. Brandon, J. Sjöström, A. Temple, E. Hallberg, F. Kahl, RISE Report - Final Project Report - Fire Safe Implementation of Visible Mass Timber in Tall Buildings - Compartment Fire Testing (2021:40), RISE Fire Research, 2021 [Online]. Available: http://urn.kb.se/resolve?urn=urn:nbn:se:ri:diva-58153.

[19] F. Wiesner, A. Bartlett, S. Mohaine, F. Robert, R. McNamee, J.-C. Mindeguia, L. Bisby, Structural capacity of one-way spanning large-scale cross-laminated timber slabs in standard and natural fires, Fire Technol. 57 (1) (2021) 291–311, https://doi.org/10.1007/s10694-020-01003-y, 2021/01/01.

[20] T. Gernay, J. Zehfuß, S. Brunkhorst, F. Robert, P. Bamonte, R. McNamee, S. Mohaine, J.-M. Franssen, Experimental investigation of structural failure during the cooling phase of a fire: timber columns, Fire Mater. 47 (4) (2023) 445–460, https://doi.org/10.1002/fam.3110.

[21] D. Hopkin, W. Węgrzyński, M. Spearpoint, I. Fu, H. Krenn, T. Sleik, C. Gorska, G. Stapf, Large-scale enclosure fire experiments adopting CLT slabs with different types of polyurethane adhesives: genesis and preliminary findings, Fire 5 (2) (2022), https://doi.org/10.3390/fire5020039.

[22] R. Emberley, C.G. Putynska, A. Bolanos, A. Lucherini, A. Solarte, D. Soriguer, M. G. Gonzalez, K. Humphreys, J.P. Hidalgo, C. Maluk, A. Law, J.L. Torero,

[23] Description of small and large-scale cross laminated timber fire tests, Fire Saf. J. 91 (2017) 327–335, https://doi.org/10.1016/j.firesaf.2017.03.024, 2017/07/01.

[23] C. Gorska, PhD Thesis - Fire Dynamics in Multi Scale Timber Compartments, PhD, The University of Queensland, Australia, 2019.

[24] M. Hoehler, J. Su, P.-S. Lafrance, M. Bundy, A. Kimball, D. Brandon, B. Östman, Fire safety challenges of tall wood buildings : large-scale cross-laminated timber compartment fire tests, in: Presented at the SiF 2018 - the 10th International Conference on Structures in Fire, 2018. Belfast, UK, 2018. [Online]. Available: http://urn.kb.se/resolve?urn=urn:nbn:se:lnu-diva-77612.

[25] J. Liu, E.C. Fischer, Review of large-scale CLT compartment fire tests, Constr. Build. Mater. 318 (2022), 126099, https://doi.org/10.1016/j.conbuildmat.2021.126099.

[26] G. Ronquillo, D. Hopkin, M. Spearpoint, Review of large-scale fire tests on cross-laminated timber, J. Fire Sci. 39 (5) (2021) 327–369, https://doi.org/10.1177/07349041211034460.

[27] J.L. Torero, A.H. Majdalani, C. Abecassis-Empis, A. Cowlard, Revisiting the compartment fire, Fire Saf. Sci. 11 (2014) 28–45.

[28] V. Gupta, J.P. Hidalgo, D. Lange, A. Cowlard, C. Abecassis-Empis, J.L. Torero, A review and analysis of the thermal exposure in large compartment fire experiments, Int. J. High-Rise Build.g 10 (4) (2021) 345–364, https://doi.org/10.21022/IJHRB.2021.10.4.345.

[29] J.P. Hidalgo, A. Cowlard, C. Abecassis-Empis, C. Maluk, A.H. Majdalani, S. Kahrmann, R. Hilditch, M. Krajcovic, J.L. Torero, An experimental study of full-scale open floor plan enclosure fires, Fire Saf. J. 89 (2017) 22–40, https://doi.org/10.1016/j.firesaf.2017.02.002.

[30] A. Nadjai, A. Naveed, M. Charlier, O. Vassart, S. Welsh, A. Glorieux, J. Sjostrom, Large scale fire test: the development of a travelling fire in open ventilation conditions and its influence on the surrounding steel structure, Fire Saf. J. 130 (2022), 103575, https://doi.org/10.1016/j.firesaf.2022.103575, 2022/06/01.

[31] E. Rackauskaite, M. Bonner, F. Restuccia, N. Fernandez Anez, E.G. Christensen, N. Roenner, W. Wegrzynski, P. Turkowski, P. Tofilo, M. Heidari, P. Kotsovinos, I. Vermesi, F. Richter, Y. Hu, C. Jeanneret, R. Wadhwani, G. Rein, Fire experiment inside a very large and open-plan compartment: x-ONE, Fire Technol. 58 (2022) 905–939, https://doi.org/10.1007/s10694-021-01162-6.

[32] M. Heidari, E. Rackauskaite, M. Bonner, E. Christensen, S. Morat, H. Mitchell, P. Kotsovinos, P. Turkowski, W. Wegrzynski, P. Tofilo, G. Rein, Fire experiments inside a very large and open-plan compartment: x-TWO, in: Presented at the Proceedings of the 11th International Conference on Structures in Fire (SiF2020), The University of Queensland, Brisbane, Australia, 2020.

[33] D. Rush, X. Dai, D. Lange, Tisova fire test – fire behaviours and lessons learnt, Fire Saf. J. 121 (2021), 103261, https://doi.org/10.1016/j.firesaf.2020.103261, 2021/05/01.

[34] S. Nothard, D. Lange, J.P. Hidalgo, V. Gupta, M.S. McLaggan, F. Wiesner, J. L. Torero, Factors influencing the fire dynamics in open-plan compartments with an exposed timber ceiling, Fire Saf. J. 129 (2022), 103564, https://doi.org/10.1016/j.firesaf.2022.103564, 2022/05/01.

[35] J.P. Hidalgo, T. Goode, V. Gupta, A. Cowlard, C. Abecassis-Empis, J. Maclean, A. I. Bartlett, C. Maluk, J.M. Montalvá, A.F. Osorio, J.L. Torero, The Malveira fire test: full-scale demonstration of fire modes in open-plan compartments, Fire Saf. J. 108 (2019), https://doi.org/10.1016/j.firesaf.2019.102827.

[36] P. Kotsovinos, E.G. Christensen, E. Rackauskaite, A. Glew, E. O'Loughlin, H. Mitchell, R. Amin, F. Robert, M. Heidari, D. Barber, G. Rein, J. Schulz, Impact of ventilation on the fire dynamics of an open-plan compartment with exposed timber ceiling and columns: CodeRed #02, Fire Mater. (2022), https://doi.org/10.1002/fam.3082.

[37] H.E. Nelson, Engineering View of the Fire of May 4, 1988 in the First Interstate Bank Building, 1989. Los Angeles, California (NIST IR 89-4061).

[38] B.R. Kirby, D.E. Wainman, L.N. Tomlinson, T.R. Kay, B.N. Peacock, Natural fires in large scale compartments, Int. J. Eng. Perf.-Bases Fire Codes 1 (2) (1999) 43–58.

[39] R.G. Gann, A. Hamins, K. McGrattan, H.E. Nelson, T.J. Ohlemiller, K.R. Prasad, W. M. Pitts, Reconstruction of the fires and thermal environment in World Trade Center buildings 1, 2, and 7, Fire Technol. 49 (2013) 679–707.

[40] J. Gales, Travelling fires and the st. Lawrence burns project, Fire Technol. 50 (2014) 1535–1543, https://doi.org/10.1007/s10694-013-0372-3.

[41] J.G. Quintiere, Principles of Fire Behavior, second ed., CRC Press, 2016.

[42] NFPA 1710, Standard for the Organization and Deployment of Fire Suppression Operations, Emergency Medical Operations, and Special Operations to the Public by Career Fire Departments, 2020. Quincy, MA.

[43] E. Rackauskaite, P. Kotsovinos, D. Barber, Letter to the editor: design fires for open-plan buildings with exposed mass-timber ceiling, Fire Technol. 57 (2) (2021) 487–495, https://doi.org/10.1007/s10694-020-01047-0, 2021/03/01.

[44] H. Mitchell, P. Kotsovinos, F. Richter, D. Thomson, D. Barber, G. Rein, Review of fire experiments in mass timber compartments: current understanding, limitations, and research gaps, Fire Mater. (2022), https://doi.org/10.1002/fam.3121 vol. n/a, no. n/a.

[45] EN 1991 1-2 (2002), Eurocode 1: Actions on Structures – Part 1-2: General Actions - Actions on Structures Exposed to Fire, CEN, Brussels, Belgium, 2002.

[46] EAD 130005-00-0304, Solid Wood Slab Element to Be Used as a Structural Element in Buildings, EOTA, Brussels, Belgium, 2015.

[47] EN 520:2004+A1:2009, Gypsum Plasterboards - Definitions, Requirements and Test Methods, CEN, Brussels, Belgium, 2004.

[48] ISO 12570:2000, Hygrothermal Performance of Building Materials and Products-Determination of Moisture Content by Drying at Elevated Temperature, ISO, Brussels, Belgium, 2000, 2000.

[49] V. Gupta, J.L. Torero, J.P. Hidalgo, Burning dynamics and in-depth flame spread of wood cribs in large compartment fires, Combust. Flame 228 (2021) 42–56, https://doi.org/10.1016/j.combustflame.2021.01.031.

[50] IEC 60584-1:2013, Thermocouples - Part 1: EMF Specifications and Tolerances, IEC, Brussels, Belgium, 2013.

[51] EN 1363-1:2020, Fire Resistance Tests - Part 1: General Requirements, CEN, Brussels, Belgium, 2020.

[52] U. Wickström, Temperature Calculation in Fire Safety Engineering, Springer, 2016.

[53] EN 1991-1-2 (2002), CEN, Brussels, Belgium, 2002.

[54] M.S. Hoehler, On the development of a transparent enclosure for 360° video cameras to observe severe fires in situ, Fire Saf. J. 120 (2021/03/01/2021), 103024, https://doi.org/10.1016/j.firesaf.2020.103024.

[55] ISO 9705-1, Reaction to Fire Tests - Room Corner Test for Wall and Ceiling Lining Products - Part 1: Test Method for a Small Room Configuration, ISO, Switzerland, 2016.

[56] I. Pope, J.P. Hidalgo, R.M. Hadden, J.L. Torero, A simplified correction method for thermocouple disturbance errors in solids, Int. J. Therm. Sci. 172 (2022), 107324, https://doi.org/10.1016/j.ijthermalsci.2021.107324, 2022/02/01.

[57] R. Fahrni, J. Schmid, M. Klippel, A. Frangi, Correct temperature measurements in fire exposed wood, in: Presented at the World Conference on Timber Engineering (WCTE), Seoul, South Korea, 2018.

[58] J.V. Beck, Thermocouple temperature disturbances in low conductivity materials, J. Heat Tran. 84 (2) (1962) 124–131, https://doi.org/10.1115/1.3684310.

[59] EN 1995-1-2 (Eurocode 5), Design of Timber Structures – Part 1-2: General - Structural Fire Design, CEN, Brussels, Belgium, 2004.

[60] J. Schmid, M. Klippel, M. Viertel, R. Presl, R. Fahrni, A. Totaro, A. Frangi, Charring of timber - determination of the residual virgin cross-section and charring rates, in: Presented at the World Conference on Timber Engineering 2020, Santiago, Chile, 2020.

[61] M. Aniszewska, A. Gendek, Comparison of heat of combustion and calorific value of the cones and wood of selected forest trees species, For. Res. Pap. 75 (3) (2014) 231–236 [Online]. Available: https://depot.ceon.pl/handle/123456789/5332.

[62] B.J. McCaffrey, G. Heskestad, A robust bidirectional low-velocity probe for flame and fire application, Combust. Flame 26 (1976) 125–127, https://doi.org/10.1016/0010-2180(76)90062-6, 1976/02/01.

[63] D. Drysdale, An Introduction to Fire Dynamics, third ed., John Wiley & sons, 2011.

[64] Z. Nan, A.A. Khan, L. Jiang, S. Chen, A. Usmani, Application of travelling behaviour models for thermal responses in large compartment fires, Fire Saf. J. 134 (2022), 103702, https://doi.org/10.1016/j.firesaf.2022.103702, 2022/12/01.

[65] J.G. Quintiere, A.S. Rangwala, A theory for flame extinction based on flame temperature, Fire Mater. 28 (5) (2004) 387–402, https://doi.org/10.1002/fam.835.

[66] H. Xu, I. Pope, V. Gupta, J. Cadena, J. Carrascal, D. Lange, M.S. McLaggan, J. Mendez, A. Osorio, A. Solarte, D. Soriguer, J.L. Torero, F. Wiesner, A. Zaben, J.P. Hidalgo, Large-scale compartment fires to develop a self-extinction design framework for mass timber—Part 1: literature review and methodology, Fire Saf. J. 128 (2022), 103523, https://doi.org/10.1016/j.firesaf.2022.103523, 2022/03/01.

[67] A.I. Bartlett, R.M. Hadden, L.A. Bisby, A review of factors affecting the burning behaviour of wood for application to tall timber construction, Fire Technol. 55 (1) (2019) 1–49, https://doi.org/10.1007/s10694-018-0787-y, 2019/01/01.

[68] A. Law, R. Hadden, We need to talk about timber: fire safety design in tall buildings, Struct. Eng. (3) (2020).

[69] D. Brandon, B. Östman, Fire Safety Challenges of Tall Wood Buildings – Phase 2: Task 1 - Literature Review, NFPA, 2016.

[70] F. Richter, F.X. Jervis, X. Huang, G. Rein, Effect of oxygen on the burning rate of wood, Combust. Flame 234 (2021) 111591, https://doi.org/10.1016/j.combustflame.2021.111591, 2021/12/01.

[71] D.C.O. Marney, L.J. Russell, R. Mann, Fire performance of wood (Pinus radiata) treated with fire retardants and a wood preservative, Fire Mater. 32 (6) (2008) 357–370, https://doi.org/10.1002/fam.973, 2008/10/01.

[72] C. Gorska, J.P. Hidalgo, J.L. Torero, Fire dynamics in mass timber compartments, Fire Saf. J. 120 (2021), https://doi.org/10.1016/j.firesaf.2020.103098.

Paper II

Fire spread in a large compartment with exposed cross-laminated timber and open ventilation conditions: #FRIC-02 – Exposed wall and ceiling

Andreas Sæter Bøe,

Kathinka Leikanger Friquin, Daniel Brandon,

Anne Steen-Hansen, Ivar S. Ertesvåg

Fire spread in a large compartment with exposed cross-laminated timber and open ventilation conditions: #FRIC-02 - Exposed wall and ceiling

Andreas Sæter Bøe [a,d,*], Kathinka Leikanger Friquin [b], Daniel Brandon [c], Anne Steen-Hansen [a,d], Ivar S. Ertesvåg [e]

[a] *Department of Civil and Environmental Engineering, Faculty of Engineering, NTNU – Norwegian University of Science and Technology, Trondheim, Norway*
[b] *Department of Architecture, Materials and Structures, SINTEF Community, Trondheim, Norway*
[c] *RISE Fire Research, Lund, Sweden*
[d] *RISE Fire Research AS, Trondheim, Norway*
[e] *Department of Energy and Process Engineering, Faculty of Engineering, NTNU – Norwegian University of Science and Technology, Trondheim, Norway*

ARTICLE INFO

ABSTRACT

Cross-laminated timber (CLT) is becoming increasingly popular due to its many advantages. However, it has been shown that exposed CLT can have a significant effect on fire dynamics and spread rates. Further studies are therefore needed to better understand the impact of CLT to fire safety. Two large-scale CLT compartment fire experiments (95 m^2) representing a modern office building have been performed, #FRIC-01 and #FRIC-02. This paper presents the second experiment, #FRIC-02, with exposed CLT on the back wall and the ceiling. The fire developed fast and spread across the room in less than 3.5 min from ignition of the wood crib on the floor and in 1.5 min after the ignition of the ceiling. Large external flames were observed, despite the compartment being well-ventilated. The 5-layer CLT, which comprised a 40 mm thick exposed outer layer and was face-bonded using a common European polyurethane adhesive, exhibited glue-line integrity failure and led to a second flashover after a significant period of decay. Subsequent layers of 20 mm also delaminated before the fire was manually extinguished after 3 h. Compared to #FRIC-01, the fire spread rate was faster, and temperatures, charring rates, heat release rates and external flames were higher.

1. Introduction

In recent years, cross-laminated timber (CLT) has become the preferred choice of many architects, entrepreneurs and building owners due to its aesthetic look and ability to sequester carbon dioxide. Besides all the positive sides of CLT, it is well-known that exposed timber can impact fire dynamics and the growth rate of potential fires [1–3].

There is a strong architectural drive to leave the timber structure visible, which can sometimes, dependent on the regulations, be implemented without risk-mitigating measures such as limitations of exposed wood, sprinklers, surface coatings/impregnations, and limitations of compartment dimensions. Where such measures are not taken or cannot sufficiently be relied upon, sufficient insight into the impact on fire development can be important. The effect of an exposed CLT ceiling has been shown to increase the fire spread rate, which in large floor plan compartments can lead to fire growth rates [4,5] that are typically not accounted for in European design standards [6].

In the Code Red experiments [4,5], the fire spread across a 352 m^2 compartment and developed into a full flashover in 5 and 8 min. This was significantly faster than in similar experiments without a CLT ceiling [7,8]. In #FRIC-01 [9], however, ignition of the CLT ceiling took longer. Parameters that likely led to this difference are the lower flame height of the wood crib fire relative to the ceiling height, the larger opening factor and the higher window head, allowing less smoke to accumulate under the ceiling. After the ignition of the ceiling at 32.5 min, the fire spread back and forth across the room through four flashing waves, in which the wood crib fire grew larger after each wave. The fully developed fire was reached 13 min after the ignition of the ceiling. This can still be considered fast, as several similar fire experiments without exposed CLT have used hours to travel the same distance [10,11]. Despite the floor area of Code Red being almost four times larger than #FRIC-01 (352 m^2 vs. 95 m^2), there were several similarities in the experimental setups, like the oblong geometry (34.3 m × 10.3 m × 3.0 m vs. 18.8 m × 5.0 m × 2.5 m), the large continuous wood crib and the

exposed CLT ceiling. As the fire development in #FRIC-01 significantly differed from that in the Code Red experiments, it increased insight into the strong dependence on the fire scenario, compartment design and the complexity of the fire dynamics. There is, however, a complete lack of data on large-scale fire experiments of large floor plan compartments with a combination of exposed wall and ceiling surfaces. Several compartment fire experiments (7 m² [12], 17.5 m² [13], 42 m² [14] and 48 m² [15]) have compared how different combinations of exposed surfaces affect the fire dynamics. However, all of these are of dimensions that are not representative of large floor plan compartments, and none of these experiments has studied how the fire spread rate changes with different combinations of exposed surfaces. Thus, there is a knowledge gap on how an exposed wall, in addition to a ceiling, would affect the fire spread rate in a large compartment.

Another possible consequence of having exposed CLT is the prolonged fire duration, which might occur due to delamination (also known as glue-line integrity failure or premature char fall-off) or gypsum board fall-off. In both cases, fresh preheated wood becomes exposed to the fire, and the phenomenon is often recognised by a rapid increase in the temperature and heat release rate. This effect has been observed in several experiments [14,16].

Avoiding delamination has been considered beneficial for achieving self-extinction of compartment fires, and lately, there has been an increased focus on developing adhesives that do not exhibit delamination [4,15,17].

With a regular polyurethane adhesive, several parameters affect whether delamination occurs, like the outer layer thickness of the CLT, the duration of the fire, the burning time of the CLT, and whether the CLT continue smouldering after the extinguishment of flames. It should be noted that there are examples of fires with delamination that have not caused a second flashover [9,14,18]. There are also experiments where self-extinction has been achieved without using a heat-resistant adhesive [9,12,16,18,19].

Delamination and self-extinction of CLT have been extensively studied at bench scale [19–21], and there are also a few experiments from small to large-scale [12–15,18] which have studied these related phenomenon. It has been found that the number of exposed CLT surfaces and their orientation to each other impact whether self-extinction or delamination occur due to feedback mechanisms between the exposed CLT. However, due to the few really large-scale experiments, there are still knowledge gaps on how feedback mechanisms affect self-extinction and delamination in large compartments with different orientations of exposed CLT.

As many modern wooden buildings have one or several surfaces with exposed wood, it is essential to better understand the feedback mechanisms between exposed CLT surfaces and the variable fuel load and how this interaction changes the fire spread and fire dynamics in the compartment. Hence, two large-scale experiments have been conducted in a well-ventilated, large, open-spaced compartment with exposed CLT. The experiments aimed to study how fire dynamics and fire spread rates change with two different configurations of exposed CLT. In #FRIC-01 [9], the ceiling was exposed, while in #FRIC-02, a long wall and the ceiling were exposed. The results of #FRIC-02 are presented and discussed in this paper.

2. Methods

2.1. Methodology

The effects of exposed cross-laminated timber surfaces on fire development and spread in large, open-plan compartments with open ventilation conditions are studied through a large-scale experiment. The methodology of #FRIC-02 is identical to that of #FRIC-01. Several methods have been used to describe the fire and measure the effects of the timber; analysis of video recordings, measurements of the temperatures in the compartment, heat flux towards surfaces, and calculations

of the heat release rates for the variable fuel and CLT.

2.2. Experimental setup

The experimental setup was almost identical to #FRIC-01. Hence, the information given here summarises the method and provides key information and relevant changes compared to #FRIC. For more details on the experimental setup and analysis methods, readers are referred to the article describing #FRIC-01 [9].

2.2.1. Compartment

The compartment's inner dimension was 18.8 m × 5.0 m × 2.52 m (L × W × H), and CLT elements were used in all walls and the ceiling. In contrast to #FRIC-01, this experiment (#FRIC-02) had both the ceiling (89.3 m²) and the back wall (47.1 m²) exposed. Images of the compartment are shown in Fig. 1.

The CLT of the back wall and ceiling had a thickness of 140 mm and consisted of 5 layers. The outer layers were 40 mm thick with a board width of 140 mm, whereas the three intermediate layers were 20 mm thick and had a board width of 90 mm. The CLT panels were made of Norwegian spruce and glued with Loctite Purbond HB S, a regular polyurethane (PUR) adhesive. The density of the CLT elements was approx. 484 kg/m³ (based on measurement of one element with 13% moisture content).

The compartment had four large window openings on the front wall, with a total opening area of 17.0 m × 2.2 m = 37.4 m². This corresponds to an opening factor of 0.18 m¹ᐟ². Windows 1–4 are enumerated from the left. Thermally inert facade walls with dimensions 2.45 m high and 5.0 m wide were positioned above Windows 2 and 4.

In case of heavy rain showers during the construction period, standing water would accumulate next to the back wall outside the compartment. To avoid significant water absorption into the CLT back wall under such circumstances, a 130 mm × 50 mm wooden plank was laid directly on the ground as a sacrificial layer, and the wall elements were positioned on top of that. A fire sealant was added to the wall-wall connections, the wall-ceiling connections, and between the ground and the bottom plank. By mistake, there was no sealant between the wall elements and the bottom plank. This likely led to tiny gaps of ~1–2 mm at some locations along the bottom of the wall.

#FRIC-02 was conducted one week after #FRIC-01. The walls were undamaged after being used in #FRIC-01 and therefore reused, while a new CLT ceiling was provided. The wall had been partly dried during the fire in #FRIC-01 but regained its moisture content after having been left with the wet gypsum boards for two days after the experiment. The moisture content of the exposed wall was measured to 14.1% ± 0.5% (standard deviation, n = 36) the day before the experiment took place. In comparison, the moisture content of the new CLT ceiling was 13.1% ± 1.1% (standard deviation, n = 36). The moisture content (dry value) was measured by a calibrated moisture meter.

The end walls were covered by two layers of 15 mm fire-rated gypsum boards type F [22]. The glulam beam was reused as it was undamaged from #FRIC-01, but the ceramic fibre insulation protecting it was replaced. The concrete floor was covered with new insulation boards of stone wool.

2.2.2. Wood cribs

The variable fuel was represented by two wood cribs, one long continuous wood crib (15.5 m × 2.8 m × 0.2 m) and a smaller wood crib (1.0 m × 2.8 m × 0.2 m) positioned on a scale (Fig. 1). The load cells of the scale were protected from heat by stone wool insulation (2 × 30 mm) on top and aerated concrete blocks on the sides.

The two cribs were built similarly to #FRIC-01 with 50 mm × 50 mm wood sticks in four alternating layers. The wood used was Norwegian spruce, with an average density of 486 kg/m³ ± 40 kg/m³ (standard deviation, n = 25) and a total mass of 2075 kg for both cribs. The average moisture content was 14.5%, with 12.8% ± 1.2% (standard

Fig. 1. Experimental setup from the outside and inside of the compartment. The small wood crib on the scale is on the right side of the left image.

deviation, n = 20) and 16.2% ± 1.3% (standard deviation, n = 20) for the short and long sticks, respectively. The fuel load density was 353 MJ/m^2 per floor area.

2.2.3. Ignition

Also in this experiment, the fire was ignited by heptane. 14 metal trays (150 × 220 × 50 mm) were positioned on the floor next to the wood crib on the left end. The trays were filled with 0.7 L of heptane in each and positioned 70 mm from each other. The two first bottom sticks of the crib were removed and put on top of the crib, so there were four stick layers at the beginning of the crib as well. 150 mm of the trays were positioned under the wood crib. This setup deviates slightly from the setup in #FRIC-01, and the reason for the change will be elaborated in Section 4.5.

2.2.4. Weather conditions

The wind conditions were measured by a local weather station positioned 15 m northeast of the compartment. The wind direction was diagonally from behind the right-end corner, with a wind velocity of 2 m/s and a gust velocity of 5–8 m/s, see Table 1. The gust velocity represents short-lived (<20 s) increases in the wind velocity. The wind and gust angles are given as where the wind is originating, with North as 0°. The orientation of the compartment is shown in Fig. 2.

2.3. Instrumentation and measurements

Most of the instrumentation, including thermocouples (TCs), plate thermometers (PTs), bidirectional probes, and gas sensors, were reused from #FRIC-01. Damaged TCs were replaced by new ones. The instrumentation setup is shown in Fig. 3-Fig. 5 and consists of 120 thermocouples (TCs) of type K 1.5 mm diameter, 24 standard plate thermometers (PTs), four bidirectional probes, and three gas sensors. The PTs were facing inwards into the compartment. The positions of the TCs, PTs etc., are described by the X, Y, and Z-directions, where X is the

Table 1
Wind condition from the ignition of wood crib.

Time [min]	Wind angle [°]	Wind velocity [m/s]	Gust angle [°]	Gust velocity [m/s]
0	55	2	104	5
5	29	2	125	5
10	3	3	323	8
15	42	2	14	4
20	62	2	79	5
25	4	2	308	8
30	69	2	83	6

longitudinal direction starting from the left side of the compartment, Y is the transverse horizontal direction, and Z is the vertical direction. The zero-point for X, Y, and Z is located on the floor inside the left end wall in the window opening.

TCs were also embedded into the CLT wall and ceiling at 0, 10, 20, 30 and 40 mm depths parallel to the isotherm. They were installed at three locations, X = 4.7, 9.5 and 14.3 m (Fig. 4). The TCs embedded in the back wall were installed at 1.1 m height, and the TCs embedded in the ceiling were installed along the centreline of the ceiling, Y = 2.5 m. The embedded TCs were used to determine the char depth of the CLT and charring rate throughout the experiment. For this, the 300 °C isotherm was considered the location of the charring front [23]. After the experiment, the final char depth was measured on some of the CLT elements in the wall and the ceiling.

The incident heat flux was determined using a method described by Wickström [24]. The gas velocities were measured by bidirectional probes, as explained by Ref. [14], originating from Ref. [25]. Oxygen (O$_2$), carbon monoxide (CO) and carbon dioxide (CO$_2$) concentrations were measured by a gas analyser at three different locations, shown in Figs. 3–5.

The method to estimate the heat release rate (HRR) from the wood crib was inspired by Rackauskaite et al. [7] and consisted of three steps: 1) determine the mass loss rate (MLR) per unit length of the wood crib, 2) integrate over wood crib length, 3) convert MLR to HRR.

In contrast to the method of Rackauskaite et al. [7], the MLR per unit length (here: 50 mm) in this experiment was based on a real mass loss rate measurement from the 1.0 m × 2.8 m wood crib positioned on a scale at the right end of the compartment, i.e., opposite of the ignition side (Fig. 1). The HRR was approximated through $\dot{Q} = \dot{m}\,\Delta H_C \chi$, where the MLR ($\dot{m}$) is multiplied by the net heat of combustion (lower heating value) (ΔH_C) and a combustion efficiency factor (χ). A combustion efficiency of 0.8 and a net heat of combustion of 16.0 MJ/kg were used.

The MLR for the ceiling and wall were determined based on the calculated charring rates of the CLT. The mass loss rate was then estimated based on the average charring rate for each 10 mm into the wood, the density and the surface area of the CLT. The net heat of combustion values for the wood crib and CLT were derived from the net calorific value of 18.66 MJ/kg for dry wood [26] and a moisture content (dry value) [27] of 14.5% for the wood crib, 13.1% for the ceiling, and 14.1% for the wall. The resulting net heat of combustion was 16.0 MJ/kg for the wall and the wood crib and 16.2 MJ/kg for the ceiling.

The HRR of the external flame out of Window 4 was estimated utilising a linear relation between flame volume and HRR of 1.505 ± 0.183 MW/m^3 [28]. The volume of the flame was estimated by measuring the outline of the external flame from the side and the average flame width
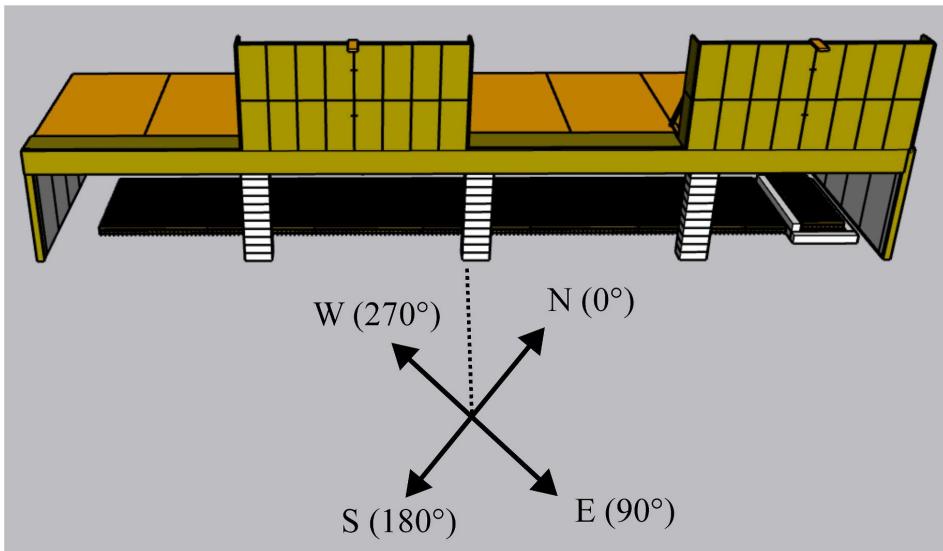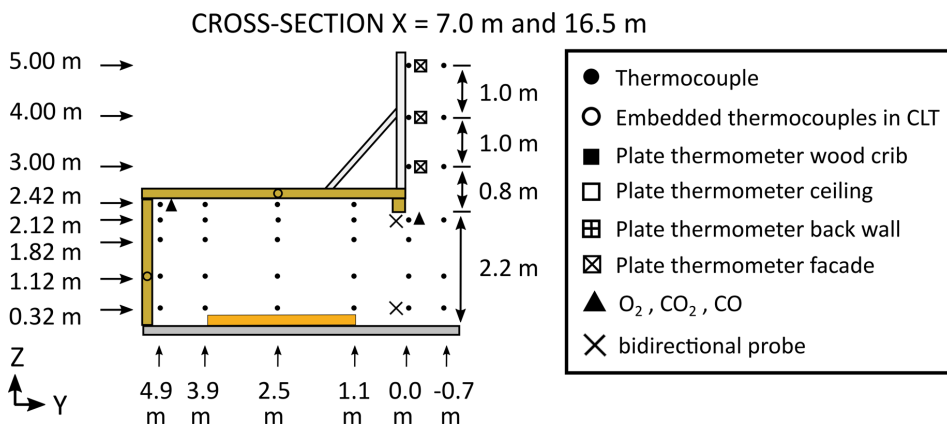
Fig. 2. Orientation of the compartment.

Fig. 3. Instrumentation in the YZ-plane (cross-section) at X = 7.0 m and 16.5 m. For X = 16.5 m, only gas measurements in the window opening. Figure from #FRIC-01.

from the front through a photo editing program. The dimensions were found by comparing them to a known reference in the images.

3. Results

3.1. Fire development

The wood crib was ignited from the left end, as described in Section 2.2.3. For the first one and a half minutes, the flames tilted towards the leftmost end wall with a flame height of 1–2 m. Ignition of the ceiling occurred at 01:42 (mm:ss) (Fig. 6). At the time of CLT ceiling ignition, 0.15 m of the length of the crib was burning together with the heptane. At 02:10, a smoke layer was covering the entire ceiling, and the flames underneath the ceiling had grown to cover approx. 4 m of the ceiling length. At 02:20, the wood crib fire was about the same size as before the

ceiling ignited, while the ceiling fire now covered approx. One-third (~6 m) of the ceiling area. The unignited wood crib was, at this point, strongly preheated by the burning ceiling, which is seen by the cloud of evaporated moisture in Fig. 6.

The first observation of the wall burning was at 02:00. At 02.30, a few meters of the upper third of the wall was burning at the left side of the compartment. From this point on, the fire spread rapidly, see Fig. 7. At 03:05, the fire had spread to about half the wood crib and three-fourths of the ceiling. At 03:10, large external flames emerged out of Window 4, and the entire length of the wood crib ignited at 03:13. This time is here defined as flashover as it was the first occurrence of all materials simultaneously burning. After the flashover, external flames appeared from all window openings, with the largest flames out of Window 4, farthest away from the ignition point.

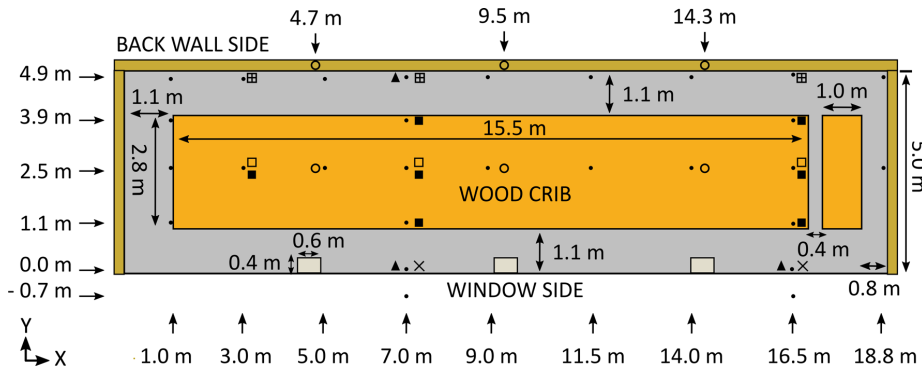After the flashover, the fire burned intensely with large external

Fig. 4. Instrumentation in the XY-plane (plan view). For symbols, see Fig. 3. Figure from #FRIC-01.
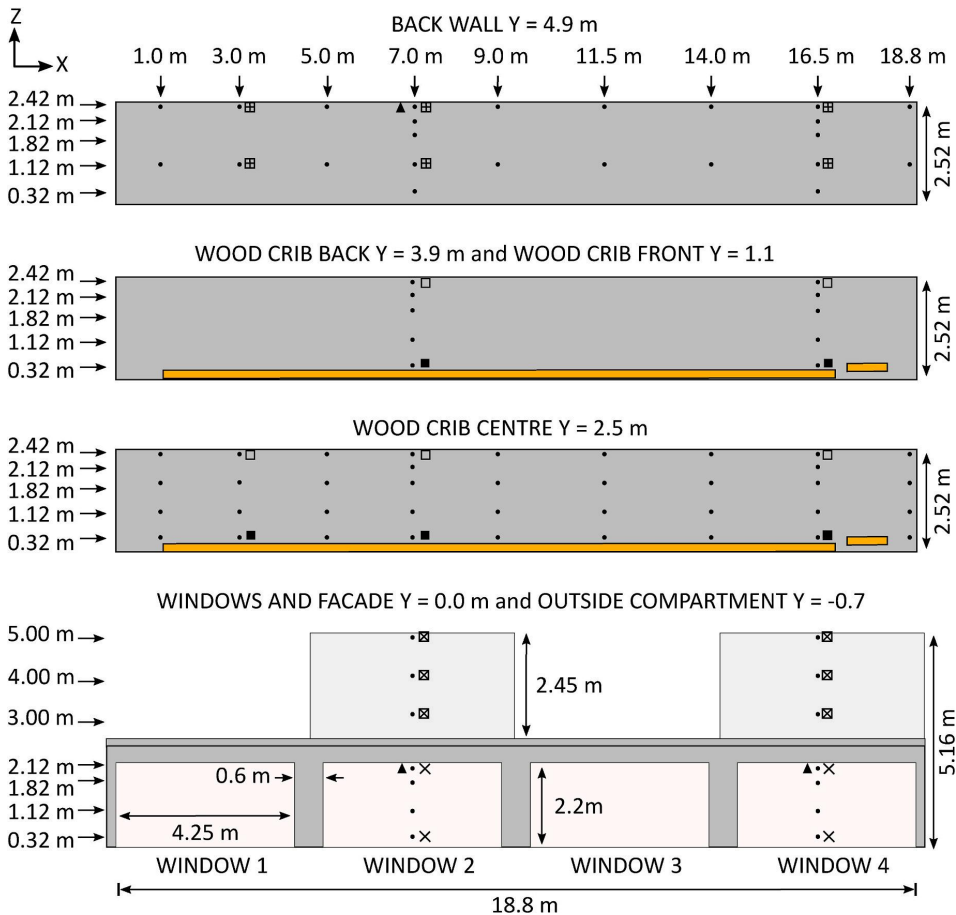

Fig. 5. Instrumentation in XZ-plane. For Y = −0.7 m, only TCs are used, not gas sensors or bidirectional probes. For symbols, see Fig. 3. Figure from #FRIC-01.

flames for about 8 min. The flames at the CLT wall and ceiling gradually extinguished from the left end of the compartment (ignition side) from about 13 min, see Fig. 8. At 16 min, all flames in the wall and ceiling were extinguished, while the wood crib was still burning. From 24 min, the crib burnt with discontinuous flames, and the last flames disappeared after 50 min.

Fig. 6. Flame spread below the ceiling after ignition of CLT seen from the left side of the compartment. Time (mm:ss).

At 66 min, small flames were observed at two different positions on the CLT of the back wall. At this point, there was barely anything left of the wood crib. Over the next 4 min, several flames appeared both in the ceiling and the wall, see Figs. 9 and 10(a). At 74 min, the multiple small flames had grown to cover the entire height of the wall for approximately two-thirds of the length and half of the ceiling width, see Fig. 11. At 76 min, almost the entire compartment was burning, and external flames appeared from the window openings. In this period, many small (10–50 cm) and some larger (50–100 cm) pieces of delaminated boards fell down and caused a large heap of glowing embers on the floor, see Fig. 10(b). The intensity of the fire varied over the next 100 min and had an increasing trend right before it was manually extinguished after 175 min. A summary of the fire development is given in Table 2.

3.2. Compartment temperatures

Compartment temperatures based on PT measurements are shown in Fig. 12-Fig. 14. Compartment temperature maps based on the TC measurements in the XZ-plane are given in Fig. 15, and in the YZ-plane in Fig. 16-Fig. 17 for Windows 2 and 4. All PT temperatures had increased to 700–1000 °C after 4 min. The peak temperatures were reached at 7 min, with temperatures between 1010 and 1172 °C for all PT locations. The hottest areas were close to the end walls. The lowest temperatures were measured in the centre of the compartment at the middle height, X = 9 m, Z = 1.0–1.5 m, as seen in Fig. 15. From 3 to 8 min, there was a reversed temperature gradient at the back of the room, with a lower temperature at 2.4 m height than at 1.1 m height, as seen in Fig. 13. Large temperature differences were also seen in the cross-section through Window 2, see Fig. 16, where a defined temperature gradient was present from the lower height of the window to the back of the room. Through Window 4 (Fig. 17), this gradient was less pronounced, and the temperatures were almost uniform in the cross-section. During the most intense burning phase, i.e., 4–8 min, the temperature difference from the back wall to Window 2 at 1.1 m height was approximately

700–800 °C. The difference for the cross-section through Window 4 was only 200–300 °C.

At 12–18 min, the temperature dropped from 1135 to 810 °C for the maximum PT measurements and from 924 to 575 °C for the minimum PT measurements. The decay rate of the compartment temperatures in this period was 52 ± 10 °C/min on average. The extinguishment of flames at the CLT wall and ceiling started from the left end and was extinguished completely between 14 and 16 min, see Fig. 8. Visible flames extinguished at temperatures (PTs) between 805 and 845 °C and an incident heat flux of 70–84 kW/m^2.

From 18 min, a temperature increase was measured by all PTs in the ceiling and some of the PTs on the back wall and the wood crib, see Figs. 12–14. This increase lasted for about 5–8 min, and the peak values were reached at 22 min. This increase is also seen in Figs. 15–17. Except for this short-lived increase, the temperatures in the whole compartment decayed after the extinguishment of flames at the CLT. The temperatures next to the ceiling and the wall decreased almost linearly, with an average rate of 5.7 ± 0.1 °C/min over the next 50 min. The ceiling temperatures in the decay phase were uniform, with just minor differences along the Y-axis. In contrast, significant differences were seen for the wood crib temperatures, with lower temperatures at the window side.

Before the initiation of the second flashover, the temperatures in the compartment had cooled down for about an hour. The temperatures measured by PTs below the ceiling and on the back wall were 386–490 °C. The temperatures at the first glue line, i.e., 40 mm depth, at 70 min in the ceiling and the wall were 173–221 °C.

We define the onset of the second flashover as occurring at 76 min, although the right part of the wall was not included until after 78 min. In the transition to the second flashover, the wall and ceiling temperatures increased rapidly and peaked at approximately 1050 °C, almost as high as during the first flashover. The temperature distribution was less uniform, with a more apparent difference between the PTs of the wall, ceiling, and wood crib. After the second flashover, the temperature

Fig. 7. (a)–(g) Fire spread across the compartment. Time (hh:mm:ss).

varied considerably but remained above 550 °C below the ceiling and 500 °C by the wall. The fire reached its minimum phase at approx. 128 min with all PT temperatures below 585 °C, corresponding to an incident heat flux of 19–28 kW/m². At this point, small flames covered a large part of the wall, see Fig. 9 (k). Visually, the fire intensity was at its minimum at 120 min, where only a few minor flames were present, see Fig. 9 (j). After this period, the temperatures and the fire intensity increased slowly until the fire was put out at 175 min. At this point, the temperatures were at their highest since 106 min.

3.3. External flames and facade temperatures

External flames were emerging from all window openings after flashover, but the size of the flames was non-uniform, with by far the largest flames appearing from Window 4, see Fig. 7 (g). The development of the external flames emerging from Window 4 is shown in Fig. 18. The flames were largest between 3 and 7 min and then gradually decreased to no flame. This is also shown in Fig. 19, where the height, volume and an estimated HRR are given.

Although short-lived, the maximum external flames from Window 4 were 6–8 m high from the ground, extending several meters above the facade wall, see Fig. 18. At maximum (Fig. 20), the flames were impinging on the facade to the top of the facade walls and then tilted away from the compartment with a ~45° angle. The depth of the external flame was approximately 3 m at the ceiling height but extended at maximum nearly 6 m from the facade at a higher point. The largest external flames had a volume of 45 ± 10 m³, see Fig. 19 (b). Utilising the linear relation between external flame volume and HRR [28], the maximum HRR of the external flame was estimated to be 66 ± 20 MW.

Another characteristic of the flame from Window 4 was that it filled almost the entire window height for a part of the window in the most intense burning phase. Hence, the neutral plane was here almost at floor level. This can be observed several times in Fig. 18 and shown over time in Fig. 19.

The temperatures measured at the facade are shown in Fig. 21. The highest temperatures were measured above Window 4 between 3 and 9 min with peak PT temperatures around 1020 °C, 865 °C and 720 °C at 0.8, 1.8 and 2.8 m above the window soffit. The exposure to the facade was also significant during the second flashover but lower than during the first flashover.

The incident heat fluxes were calculated based on the PT and TC measurements, as described in Section 2.3 and given in Fig. 22. The heat flux above Window 4 was at its maximum between 3 and 9 min, with heat flux levels fluctuating between 125 and 175 kW/m². The maximum 30-s moving average was 156, 96 and 67 kW/m² for heights 0.8, 1.8 and 2.8 m above the window soffit of Window 4, respectively. At +0.8 m height, the maximum 30-s averaged value occurred at 6 min, while the maximum value for +1.8 and + 2.8 m occurred at 3.5 and 4 min, respectively. This confirms that the largest flames lasting 30 s were present shortly after flashover, although short-lived large flames were present also later. In comparison, the values above Window 2 were significantly lower, with a 30-s average of 64, 34 and 12 kW/m².

The velocities inwards at Z = 0.3 m and outwards at Z = 2.1 m through Windows 2 and 4 were found through measurements with bidirectional probes, as described in Section 2.3. Velocities for the most intense external flaming are given in Fig. 23. The synchronisation of the time might deviate slightly from the other graphs, as the TC for synchronisation was defective, and there was a short delay between the time at which the gas was sampled until it was measured by the sensor.

The 30 s maximum average velocities outwards from the compartment at Z = 2.1 m were approximately 8 m/s through Window 2 and 14 m/s through Window 4. The duration of the outward flow was shorter for Window 2 compared to Window 4. In the figure, the average inward velocities at Z = 0.3 m were approximately the same for Windows 2 and 4, with a velocity between 2 and 4 m/s, but with stronger fluctuations in Window 4. However, the bidirectional probe at 0.3 m height in Window 4 was not set up to measure reversed flows, i.e., outward flows, as this was not expected. Hence, the average inward flow in Window 4 is likely closer to zero than presented in the figure. Several of the bidirectional probes gave unreliable data after 8 min and were therefore not included in the analysis. The unreliableness is believed to have been caused by a hole in the connections due to heat exposure.

3.4. Fire spread across CLT and wood crib

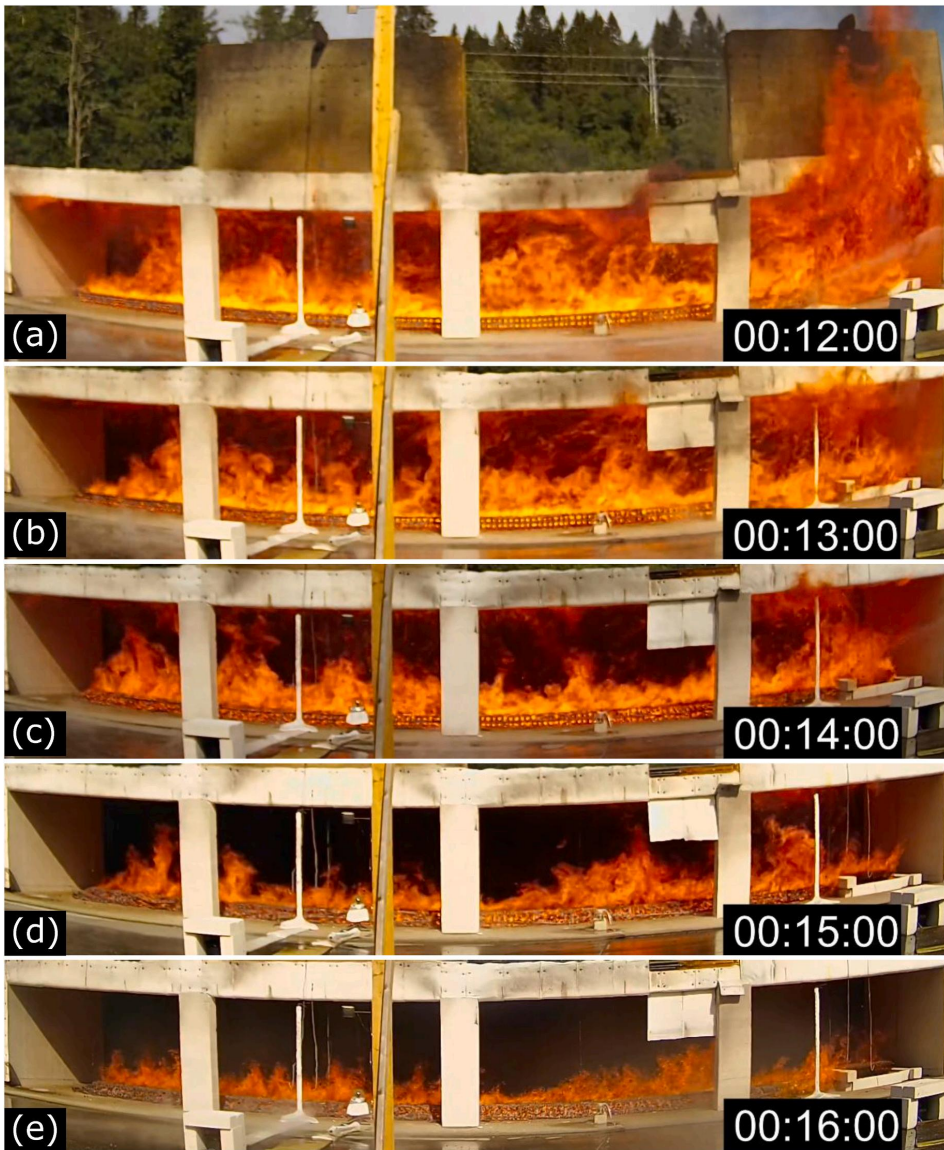The fire spread across the wood crib and ceiling was found through

Fig. 8. (a)-(e) Development of self-extinguishment of CLT while wood crib was still burning. Time (hh:mm:ss).

video analysis, and an exponential curve matched well with the spread across the wood crib, Fig. 24. The fire spread rate was then found through the derivation of the exponential curve. The (harmonic) average fire spread rate across the wood crib from ignition was approx. 5.5 m/min (90 mm/s) and 11.7 m/min (195 mm/s) from the ignition of the ceiling. The average spread rate across the ceiling was approx. 15 m/min (250 mm/s). As shown in Fig. 24, the spread rate was increasing almost exponentially. This is visualised by comparing the fire development in Fig. 7 (e)–(g), where it took 3 min for the wood crib fire to cover half of the wood crib and just 10 s to travel across the second half of the crib.

Fire spread based on the TC temperatures is shown in Fig. 25, where

a threshold of 600 °C is used to indicate flames. The flames spread first across the ceiling and the upper part of the wall, followed by ignition of the wood crib and the lower part of the wall at about the same time. At X = 7.0, the flames spread clearly from the top of the wall and downwards. This is also shown visually in Fig. 25. However, at X = 16.5, the entire height of the wall ignited within a few seconds. Compared to the visual observations of the fire spread, the 600 °C indicator gives a few seconds delay. Based on the temperature indicator, the average flame spread rate from X = 3.0–18.8 m ranged from 13 to 23 m/min.

Fig. 9. (a)–(l) Development of the second flashover. (j) Fire intensity at its minimum. (k) Fire intensity at minimum compartment temperature. Time (hh: mm:ss).

3.5. Gas measurements

Oxygen (O_2), carbon dioxide (CO_2), and carbon monoxide (CO) concentrations were measured at three different locations, as described in Section 2.3, and the results are given in Fig. 27. The O_2 concentration measured in Window 2 was not recorded due to a fault. The O_2 concentration shown is, therefore, calculated backwards from the CO and CO_2 concentrations. For short periods, both the CO and CO_2 reached the limits of the sensor, and the actual O_2 concentration will therefore be lower than what is shown in the figure. Measurements for Windows 2 and 4 are missing from 60 to 80 min and after 150 min.

The O_2 concentration measured at the window openings decreased rapidly after flashover and stabilised at 10% and 5% between 5 and 9 min for Windows 2 and 4, respectively. For a short period from 11 to 13 min, the O_2 concentration was 0% through Window 4. From 15 min, the O_2 concentration increased steadily until the second flashover occurred. During the second flashover, the O_2 was, in the most intense burning phase, reduced to 0% but was between 7 and 16% most of the time. In the back of the room, O_2 was at its lowest of 18.4% just after flashover. This level is higher than expected, possibly caused by a small leakage in the tube collecting the gas. Measurements from this location should therefore be considered with caution. The CO concentration was higher than 5000 ppm in all three locations from 4 to 16 min. From this point, the CO concentration was reduced quickly and is related to the extinguishment of flames at the CLT wall and ceiling. From 25 min, the CO concentration increased steadily in Window 2. The CO-sensor in Window 4 stopped working after 15 min.

3.6. Charring of CLT

Charring rates for the CLT are given in Table 3 and Table 4 and were measured as described in Section 2.3. For the first 40 mm, the charring followed a clear trend with a high charring rate for the first 10 mm, followed by a decreasing rate for each extra 10 mm into the wood.

The final char depths were measured at different locations and are shown in Figs. 28 and 29. The arithmetic average of the final char depth across the CLT back wall was 97 mm with a standard deviation of 13 mm and 104 mm with a 7 mm standard deviation for the CLT ceiling. Charring in the ceiling was noticeably non-uniform, with less charring at the right end of the compartment in both the wall and the ceiling. The char depth was also deeper at the bottom compared to the top of the wall. In the ceiling, the charring was evidently more pronounced close to the wall compared to the window side. The difference was more than 30 mm in several places. An example is given in Fig. 30, where the charring in some areas of the ceiling close to the window side has only reached the 3rd layer (<80 mm), while close to the wall, the charring has in most places reached the 5th layer (>100 mm). In the figure, two areas are entirely burnt through close to the window side. The main reason for this was insufficient extinguishing in the inner corner between the glulam beam and the ceiling at the end of the experiment. This area was hard to reach by water when standing on the outside. Extinguishing was not performed from the inside of the compartment due to safety concerns. Due to this insufficient extinguishing, smouldering was still occurring for several hours, and the CLT reignited in at least two locations on top of the compartment above the glulam beam. The reignition was discovered 7–8 h after the end of the experiment, but it is unknown exactly when the reignition happened. A heavy rain shower and additional manual extinguishing stopped further combustion after 8 h. The ongoing smouldering next to the glulam beam is the reason for the outliers at Y = 0.3 m in Fig. 29. Complete charring (140 mm) was also seen at the bottom of the wall several places from 60 min, see Fig. 31.

3.7. Delamination and second flashover

Both in #FRIC-01 and here, delamination was defined to occur when a part of the outer layer detaches from the second layer due to the
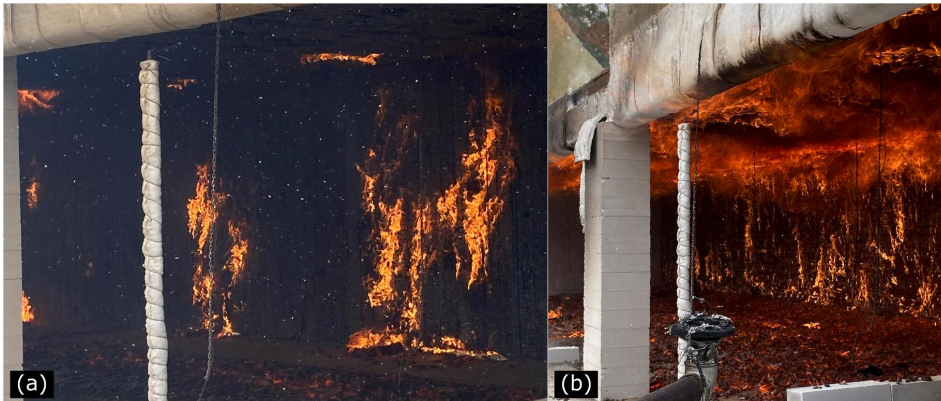
Fig. 10. (a) The first flames leading to the second flashover appeared at the lower part of the back wall and in the innermost part of the ceiling. (b) Ceiling and wall burning, and glowing embers on the floor from falling pieces. Photos were taken at 70 min (a) and 93 min (b).

Fig. 11. In the transition to the second flashover, the full height of the back wall was burning before half of the ceiling width had been included in the fire. Photo from 74 min.

Table 2
Summary of fire development.

Time (min)	Observation	Figure
0	Heptane trays were ignited.	
1.75–3.25	The fire spread first across the ceiling and the top of the wall and finally across the wood crib and lower part of the wall.	Fig. 7
3.25–11	After the flashover, external flaming was highly inhomogeneous as most external combustion occurred out of Window 4.	Fig. 7
11–13	A clear reduction in external flaming, and the burning of the CLT wall on the left end was less intense.	Fig. 8
13–16	Extinction of the CLT wall and ceiling, starting from the left end, while the wood crib was still burning continuously.	
24–40	The wood crib burnt discontinuously.	
40–50	Tiny flames were present at a few locations but eventually died out.	
66–76	Development of flames on the back wall and the ceiling, leading to a second flashover.	Figs. 9–11
76–175	A continuous fire with varying degrees of intensity.	
175	Manual extinguishment of the fire.	

adhesive losing its integrity. Uncharred, preheated wood in the second layer was then exposed.

The small flames that appeared from 66 to 70 min (Fig. 10) rapidly grew in size, and at 74 min, most of the wall and half of the ceiling were burning, see Fig. 11. A distinct change in the burning behaviour occurred between 74 and 76 min, see Fig. 9. At 74 min, the flames were mainly originating from the burning of the fresh wood of the second layer. However, at 76 min, the intensity of the flames had increased significantly, and from the images, it is evident that also the first layer was burning again. The incident heat flux towards the wall increased in this period from approx. 40 kW/m^2 to 104 kW/m^2. At this point, external flames emerged from all window openings. At 78 min, the right end of the compartment was also included in the fire.

The most intense fire lasted just a few minutes (76–81 min). After this, the fire intensity varied a lot, as seen in Fig. 9. An intermediate minimum was reached around 90 min before the fire reached a new peak at 104–106 min. At 120 min, the fire reached its minimum with only minor flames present. However, again the fire grew in intensity and at 175 min, just before it was manually extinguished, it was at its most intense since 106 min (see Figs. 9 and 12) and showed no signs of being close to self-extinction.

The varying fire intensity and temperatures were related to the delamination of the second, third and fourth lamella, which all were 20 mm thick. The estimated times for the char front to reach the different layers and cause delamination is given in Table 5. The values were calculated from the average charring rate of 0.52 mm/min for the ceiling (Table 3) and 0.67 mm/min for the wall (Table 4). Fig. 31 shows the gas temperature next to the back wall, and distinct temperature peaks are present at almost identical intervals after the second flashover. The occurrence of these peaks matches well with the estimated times for the char front progress in Table 5.

3.8. Mass loss rate and heat release rate

3.8.1. Mass loss rate

The mass loss rate of the wood crib was determined as described in Section 2.3. An exponentially decaying function was fitted to the measured mass loss of the crib on the scale and then derived to get the MLR, see Fig. 33. Compared to the real MLR averaged over 30 s, the estimated MLR based on the fitted curve gave a good match.

The MLR per unit (50 mm) length was then found by dividing the MLR from the small crib by 20. The MLR per unit length was combined with the fire spread across the wood crib, see Fig. 24, to obtain the total MLR and HRR for the wood crib. This process is explained in more detail
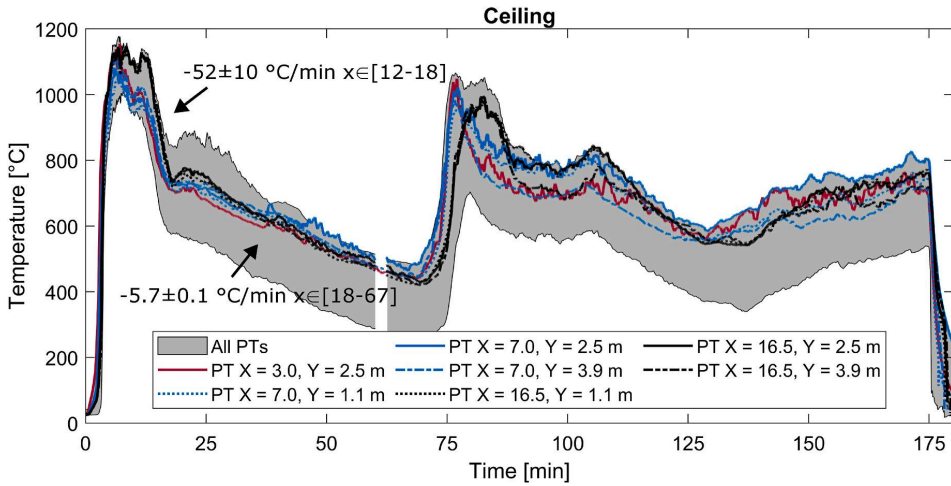
Fig. 12. Temperatures 100 mm below the ceiling measured by PTs facing downwards. The grey area covers all measurements by PTs in the compartment. X and Y represent the position of the PTs.
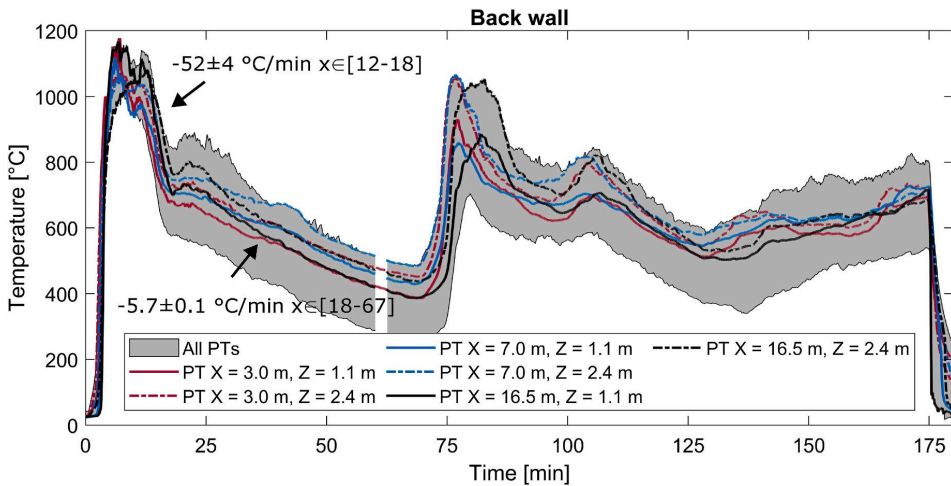

Fig. 13. Temperatures 100 mm in front of the back wall measured by PTs facing away from the wall. The grey area covers all measurements by PTs in the compartment. X and Z represent the position of the PTs.

in #FRIC-01 [9]. The estimated maximum MLR of the wood crib based on this method was 2.69 kg/s, corresponding to a burning rate of 7.28 g/(s m^2), where m^2 is the surface area of the wood sticks. The theoretical maximum mass loss and burning rate were estimated to be 2.81 kg/s and 7.60 g/(s m^2), which assumes that the entire crib starts to burn simultaneously and at a similar rate as the crib on the scale.

The mass loss rate of the CLT was based on the charring rates of the CLT, see Tables 3 and 4. The estimated maximum mass loss rate was 1.03 kg/s and 1.90 kg/s for the wall and ceiling, respectively. This corresponds to a burning rate of 0.022 kg/m^{2}s and 0.021 kg/m^{2}s.

3.8.2. Heat release rate

The HRR for the wood crib, the CLT and these combined are shown in Fig. 34, where the maximum HRR was estimated to be 73 MW. The HRR of the CLT was obtained from the charring rate of 10 mm intervals, and

the curve, therefore, has a stepwise development. The average HRR after the second flashover was 3.5 MW for the back wall and 5.5 MW for the ceiling. The development of the HRR curve was considerably faster than the ultrafast t^2 curve [6], with a fire growth rate constant, t$_\alpha$, of 27 s vs. 75 s. During the most intense burning phase (i.e., max HRR), the contribution from the wood crib was 35 MW (48%), 13 MW (18%) from the CLT wall, and 24.5 MW (34%) from the CLT ceiling.

With a combustion efficiency of 0.8, the area below the HRR curves should ideally equal 80% of the energy content of the initial wood crib mass (2075 kg), the burned mass of the CLT wall (2409 kg) and CLT ceiling (4188 kg). The area below the HRR for the wood crib was equal to 81% of the energy content of the initial wood crib mass, while the areas below the HRR curve for the CLT ceiling and wall were equal to 78% and 73% of the energy content of the mass of the burned CLT, respectively.
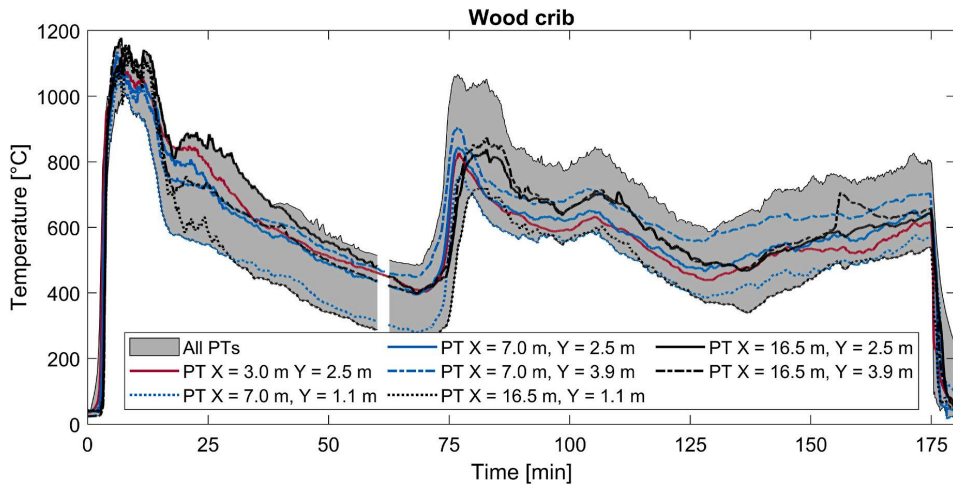
Fig. 14. Temperatures on top of the wood crib measured by PTs facing upwards. The grey area covers all measurements by PTs in the compartment. X and Y represent the position of the PTs.

4. Discussion

To our knowledge, this is the first large open-plan fire experiment combining an exposed CLT ceiling and wall. The contribution from the wall is clearly shown by comparing against the results of #FRIC-01 [9], which had a similar experimental setup, but with only the ceiling exposed.

The most important results from this experiment are the fast fire spread, the large and strongly non-uniform external flames, the second flashover after the long decay phase, and the non-uniform char depth. These results are discussed in more detail in the following sub-sections.

4.1. Fire spread

The fire developed very fast, and the wood crib fire spread across the room in 3 min and 13 s from ignition (5.5 m/min) and in 91 s from ignition of the ceiling (11.7 m/min). The fire under the ceiling reached the end of the compartment a few seconds earlier, with an average rate of 15 m/min from the ignition of the ceiling. The development of the fire spread rate was exponential, as seen in Fig. 24, indicating that the average spread rate could have been even faster in a longer compartment. The development of the total HRR was faster than the ultrafast t^2-curve and is considerably faster than the medium and fast fire growth rates suggested for different occupancies in Eurocode 1 [6]. This fire spread rate across the room was significantly faster than reported for most compartments with non-combustible surfaces, with a maximum rate of 1–2 m/min [7,8,29–31], as described in #FRIC-01 [9]. Compared to compartments with exposed CLT, the fire spread rate is even faster than the fastest spread rate in the Code Red experiments, in which the fire spread rate was 9.6 m/min across the wood crib and 12 m/min across the CLT ceiling from ignition of the ceiling [4]. A direct comparison to the spread rates of #FRIC-01 was not made here due to the pulsating behaviour of the fire spread across the ceiling and the crib. Still, there is no doubt that a CLT orientation with a ceiling and a wall facilitates a faster spread rate compared to just having the ceiling exposed.

Before the flashover, there was a clear movement of smoke and fire toward the far end of the compartment. This behaviour was due to the 0.36 m deep insulated glulam beam, which effectively guided the smoke towards the far end of the compartment. Thus, the position of beams

under a ceiling will effectively contribute to what direction smoke, and later a fire, will spread. In addition, the height of the beam will affect the thickness of the smoke layer, and thereby the temperatures in, and radiation, from the smoke layer.

Fig. 6 gives a unique insight into the mechanisms of the fast fire spread. Shortly after ignition of the ceiling, a thick smoke layer formed below the ceiling. This smoke layer contained a large fraction of combustible gases (recognised by the black colour) and is a key factor for the flame spread below the ceiling, as discussed in #FRIC-01 [9]. The radiation from the burning ceiling preheated the CLT wall and the wood crib, which is seen by the cloud of evaporated moisture at 02:20 in Fig. 6. Shortly after, the wood crib fire started to spread rapidly.

At 02:20, it is noticeable how far the flames had spread under the ceiling, while the size of the wood crib was about unchanged since the ignition of the ceiling. This highlights that the contribution from the CLT (wall and ceiling) was the dominating factor for the fast fire spread, and not what type of moveable fuel that was present. In an actual building, the fire growth rate could be limited by the oxygen supply, which is ultimately controlled by whether the window glasses break or not. A large compartment volume, either by a large floor area or a high ceiling height, would compensate for the lack of window breakage for a certain time.

4.2. Charring rate and char depth

The charring rate was highest for the first 10 mm and was reduced for each subsequent 10 mm into the wood. The stepwise charring pattern was also seen in #FRIC-01 and can likely be explained by the initial rapid mass loss rate for combustion of wood, followed by a reduced rate when a char layer is formed [19,32]. The charring rates were also likely affected by the large variations in temperature and heat fluxes during the charring of the first 40 mm. The high charring rate for the first 10 mm did not influence the total charring rate much, but it had an impact on the fire spread rate and external flames as it contributed to a large amount of pyrolysis gases being produced the first minutes after ignition. Pyrolysis gases burnt inside the compartment contribute to higher temperatures and is a driving force for the fast fire spread. Unburned gases exiting the compartment burn as an external flame, which may spread the fire to the facade, a compartment above, or an opposite building.
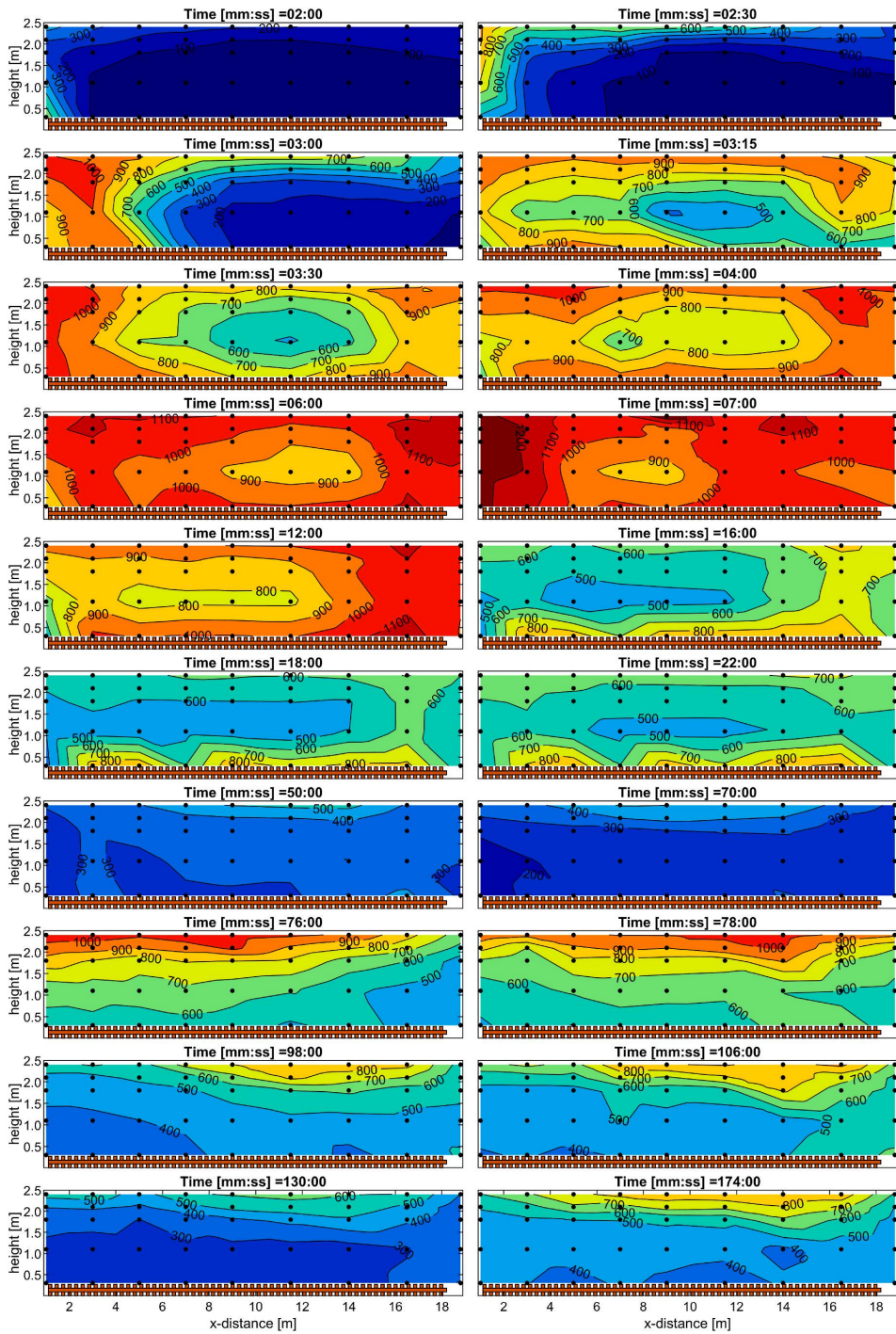
Fig. 15. Temperature map of XZ cross-section through the centre of the compartment (Y = 2.5 m).
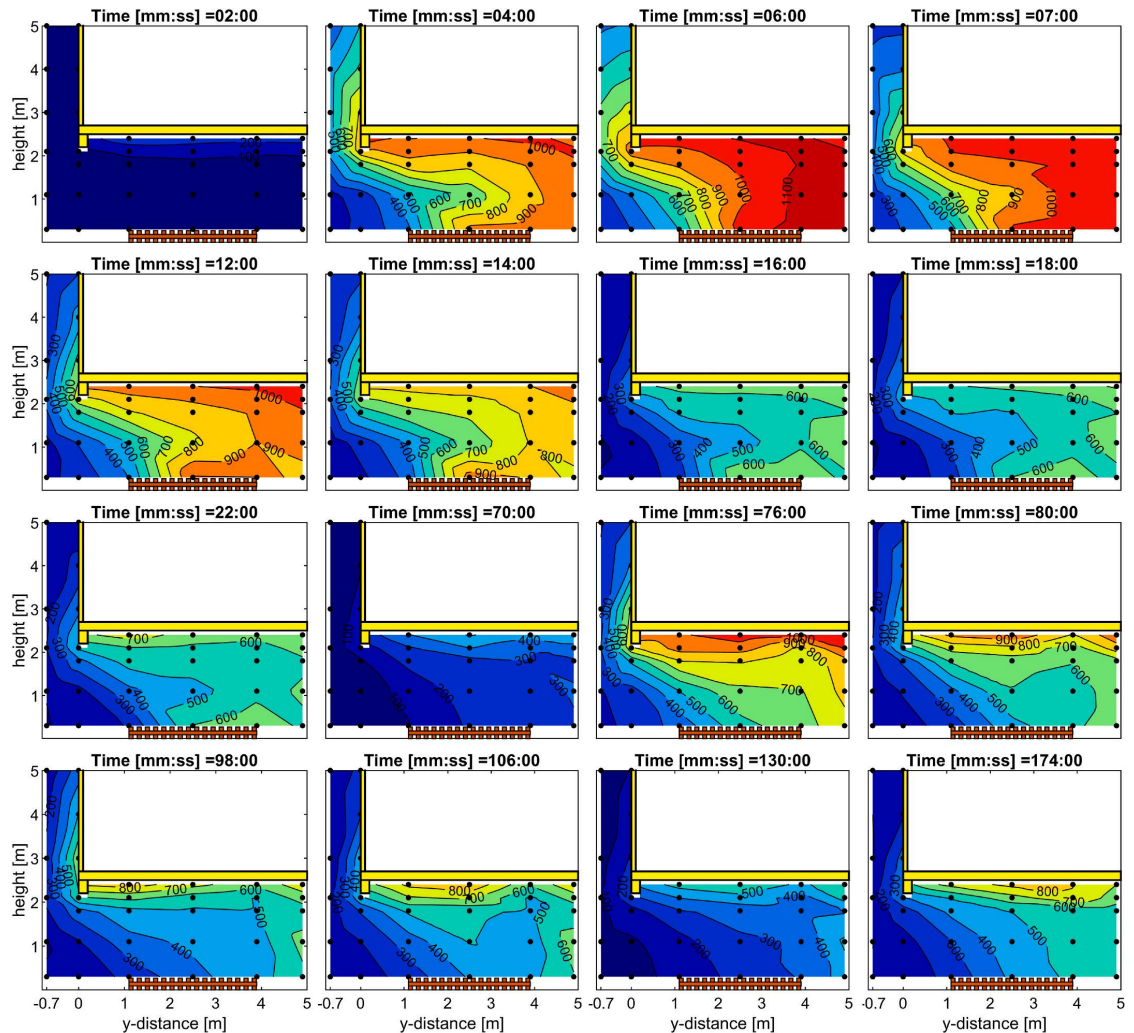
Fig. 16. Temperature map of YZ cross-section through the centre of Window 2 (X = 7.0 m).

The final char depth measured after the experiment was strongly non-uniform, with more charring on the bottom of the wall than the top and more pronounced for the part of the ceiling closest to the back wall. This is similar to #FRIC-01 but more distinct here. In addition, the charring of the wall was deeper than in the ceiling, 104 mm vs 97 mm. This corresponds with previous experiments, summarised by Mitchell et al. [3], where there is a clear trend of faster charring rates of the wall compared to the ceiling.

Furthermore, the development of the flames in the transition to the second flashover matches well with the char depth pattern shown in Figs. 28–30. This is apparent in Figs. 10(a) and Fig. 11, where the first flames leading to the second flashover appeared at the lower height of the wall and the innermost part of the ceiling. It was also clear that the wall had been more charred than the ceiling at this point, as most of the wall was burning, while just part of the ceiling had visible flames on the surface. In addition, the right end of the back wall and ceiling ignited last, as seen in Fig. 9 (e). Consequently, it appears that the non-uniform

charring pattern, in general, had developed already before the onset of the second flashover.

The uneven charring is mainly believed to be due to the different oxygen concentrations [33] throughout the compartment. It is believed that the supply of oxygen entered the compartment at a low height through the window and was transported to the back of the wall, upwards along the wall and exiting out of the compartment below the ceiling. Along such a path, the oxygen concentration would be more and more diluted, with the lowest concentration when exiting the compartment below the window soffit. Given that this path of the oxygen is correct, it can explain the large differences in char depth between the wall and ceiling and of the ceiling and wall separately. In addition, the reduced charring at the right end of the compartment can also be explained by the low oxygen concentrations in the most intense burning phase of the fire. Increased charring could also have been caused by a higher heat flux or temperature [33]. The reversed temperature gradient close to the wall in the most intense burning phase of the fire could have
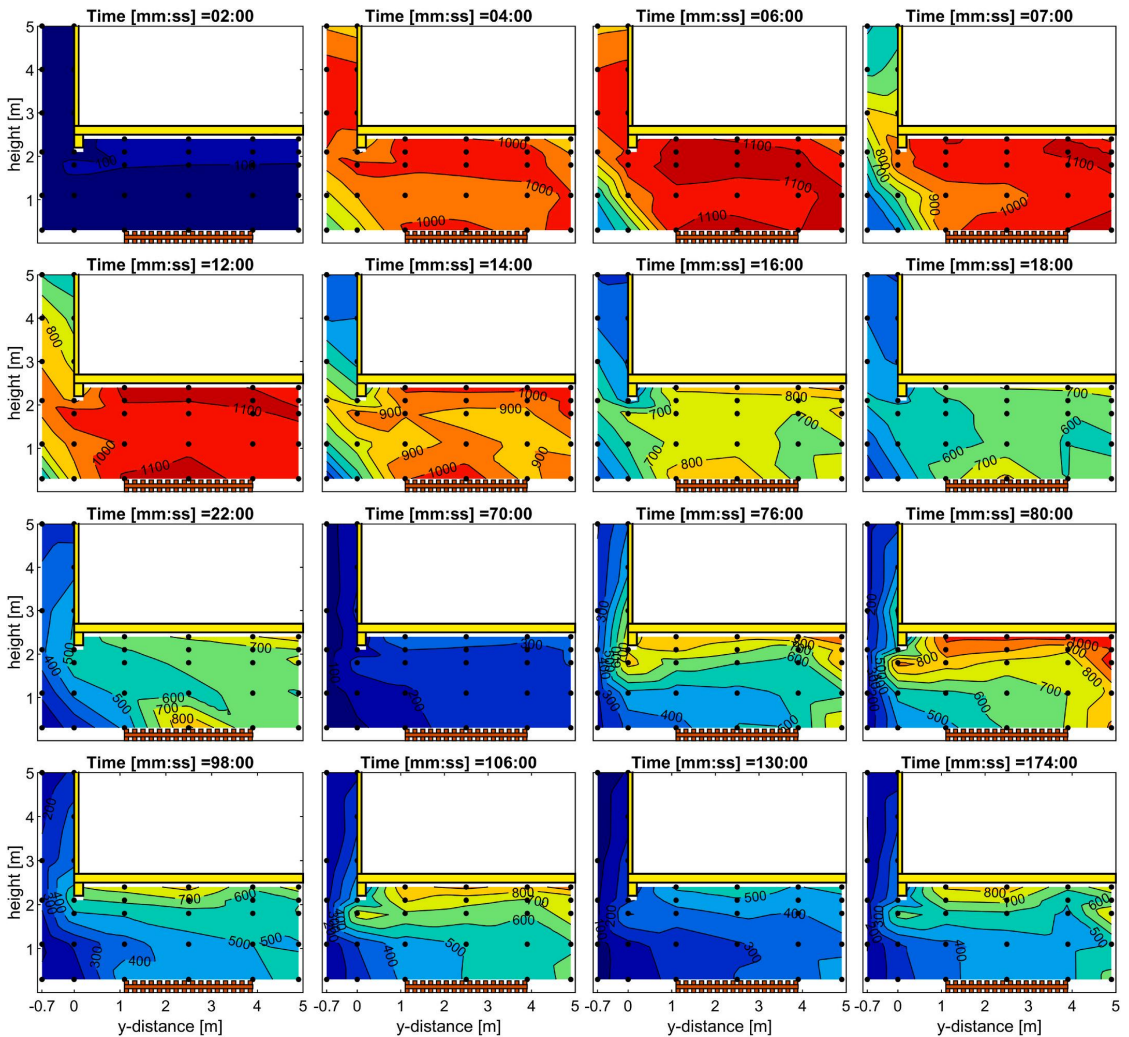
Fig. 17. Temperature map of YZ cross-section through the centre of Window 4 (X = 16.5 m).

played a role in the increased charring of the lower part of the wall. In the ceiling, however, the temperatures were the highest at the right end of the compartment, where the charring was less pronounced. This shows that temperature differences alone cannot explain the large variations in char depth.

Fig. 31 shows the burn-through below the wall and is a great example that connection details are crucial to fire safety in CLT buildings. This was caused by the lack of sealant between the wall and the bottom plank, resulting in tiny gaps for the fire to spread through. This emphasises the need for fire-rated seals between CLT elements to avoid fire spread through small gaps. Another example from this experiment was the inadequate extinguishing of the inner corner area between the ceiling and the glulam beam, which allowed smouldering combustion to continue. Ultimately, this ongoing smouldering process burned through the ceiling and caused a re-ignition which was discovered 7–8 h after termination of the experiment. A similar example of continued smouldering of CLT and a thorough discussion about this topic is given by

Mitchell et al. [34].

4.3. Self-extinguishment of flames at the CLT and second flashover

Self-extinction of flames at the CLT wall and ceiling occurred at temperatures between 805 and 845 °C (measured by PTs) and an incident heat flux of 70–84 kW/m². These values are higher than typical values for self-extinction of CLT (43.6 ± 4.7 kW/m²) [20] and higher than in #FRIC-01 (49–52 kW/m²). The higher values can possibly be explained by the lower oxygen concentration, as a lower oxygen level requires a higher critical heat flux to sustain burning [35]. At 13 min, shortly before extinguishment of the CLT, the O_2 concentration was 13% in the outflow gas through Window 2 and 0% for Window 4, measured 0.1 m below the window soffit. Another effect that may have influenced the result is the thickness of the char layer at the point of self-extinction. Although this was not measured directly, it can be assumed that the char layer was thicker than in #FRIC-01. This is based on a faster charring

Fig. 18. Side view of external flame emerging from Window 4. Time (mm:ss) after ignition. The given times might deviate slightly (±1 s) from the exact times as the start of ignition was not recorded.
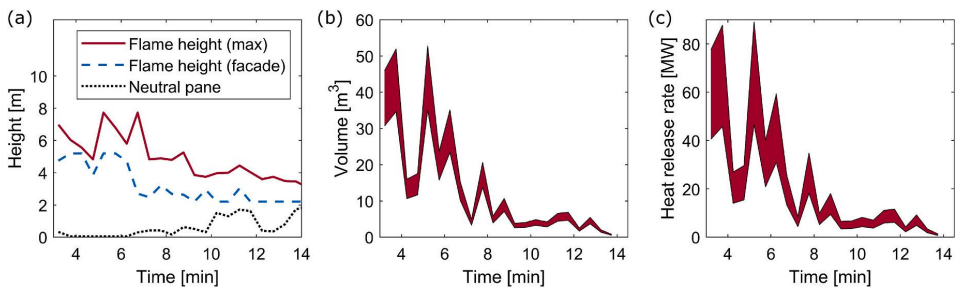

Fig. 19. Height (a), volume (b) and heat release rate (c) of the external flame from Window 4. The shaded area in (b) and (c) represent the uncertainty of the estimation.
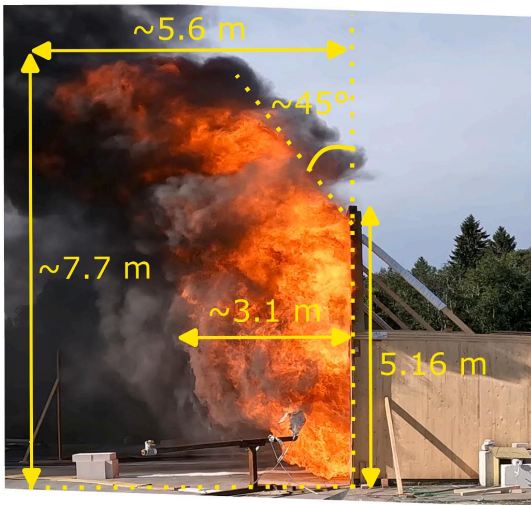
Fig. 20. Maximum external flame from Window 4. The flame height and depths are estimated based on the known facade height. Note: This flame does not represent the overall flame size but shows the absolute maximum size that occurred.

rate in #FRIC-02 but an almost identical duration of flaming combustion of the CLT compared to #FRIC-01. With a thicker insulating char layer, a higher external heat flux is needed to sustain combustion.

Shortly after the extinguishment of flames at the CLT, an apparent temperature increase was observed (Figs. 12–14). This increase was likely due to a change in the wind conditions, where the wind at this point turned to a direction coming more from the front side and to a greater extent affected the burning inside the compartment. This is shown by comparing the wind measurement at 15 and 20 min (Table 1).

Although shown earlier [14,16], this experiment is another example that a second flashover might occur after a long decay phase in compartments where no heat-resistant adhesive is implemented. Before the first flames leading to the second flashover appeared, the flaming combustion of the CLT had been out for approx. 50 min, the wood crib was completely burned out, and temperatures in the compartment had been decaying for about an hour. However, from 66 min, multiple small flames developed within 10 min to a full blaze, with peak temperatures

almost reaching the same level as in the first flashover. It was observed that several flames appeared close to the growing air gaps at the bottom of the wall, see Fig. 31. The air gaps might have speeded up the charring rate around these points. Still, since flames appeared at many different locations in the ceiling and the wall approximately at the same time, it is concluded that the air gap did not significantly affect the transition to the second flashover.

An indication of the ongoing smouldering before the second flashover was the increase in CO concentration from 25 min. A similar observation was made in #FRIC-01 [9], where the CO concentration dropped significantly at the extinction of flames but then gradually increased.

In #FRIC-01 [9], delamination (or glue line integrity failure) happened, although the char front had not reached the glue line. This was concluded based on a few lamellas hanging down and several clearly detached from the layer behind but still in place. The layer behind was mostly discoloured but not charred, which proves that the first layer, in general, had not been charred through. The reason why the lamellas were loose and hanging down, but had not fallen down, can be explained by a) only part of the lamella length was detached due to the non-uniform char depth along the lamellae length, and b) a lamella not entirely charred through will have some remaining strength that prevents it from falling down or breaking into pieces.

It is believed that the delamination process in this experiment occurred similarly as in #FRIC-01. This is supported by observations where flames emerged from behind the outer lamellas, indicating an air gap between the two outer layers. In addition, the first pieces of wood falling off were seen at 70 min, when multiple flames already had appeared. However, after the second flashover, pieces of wood were falling almost continuously during the most intense burning phase.

With the delamination occurring before the exposed lamellae was charred through, two preheated surfaces with fresh timber were exposed with a small air gap in between. The two preheated surfaces were shielded from any external radiation but were heated by the gas temperature next to the CLT and the thermal wave propagating through the first CLT layer. The gas temperature was well above 400 °C at several locations when the first flames occurred before the second flashover. From the many simultaneously occurring fires around this time, it is evident that the described conditions were ideal for a fire to emerge in the gap between the two layers.

After the second flashover, the intensity and temperatures of the fire varied strongly, as seen in Figs. 9 and 12–14. The varying intensity and the compartment still burning after 175 min can be explained by three coinciding factors. 1) The burning of wood follows a natural variation in burning intensity. 2) The intermediate CLT elements were thin, only 20
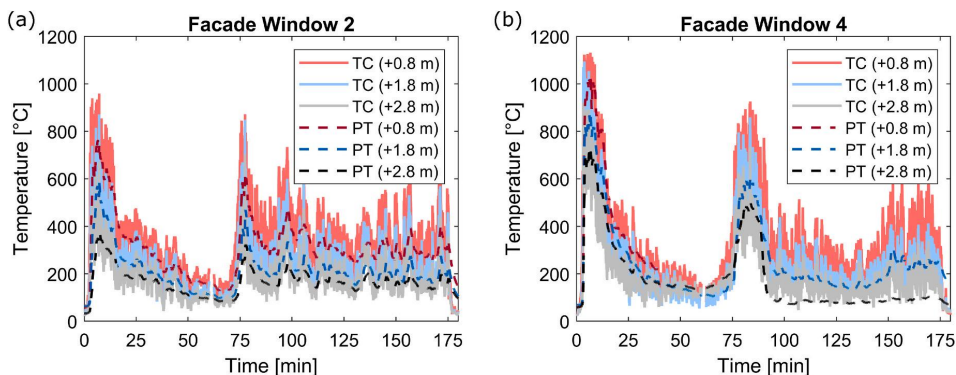

Fig. 21. Temperature measurements at the facade above Window 2 (a) and Window 4 (b). +0.8, 1.8, and 2.8 m are heights above the window soffit. The TCs are not corrected for any radiation exposure and might deviate slightly from the real gas temperature.
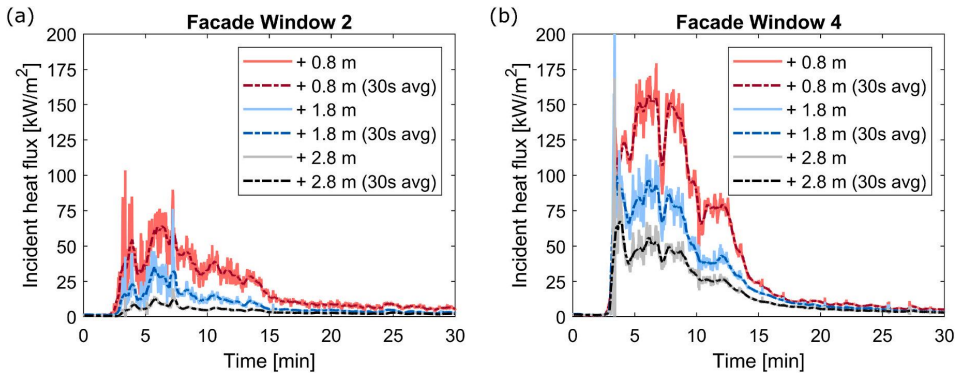
Fig. 22. Incident heat flux at the facade above Window 2 (a) and Window 4 (b). +0.8, 1.8, 2.8 m are heights above the window soffit.
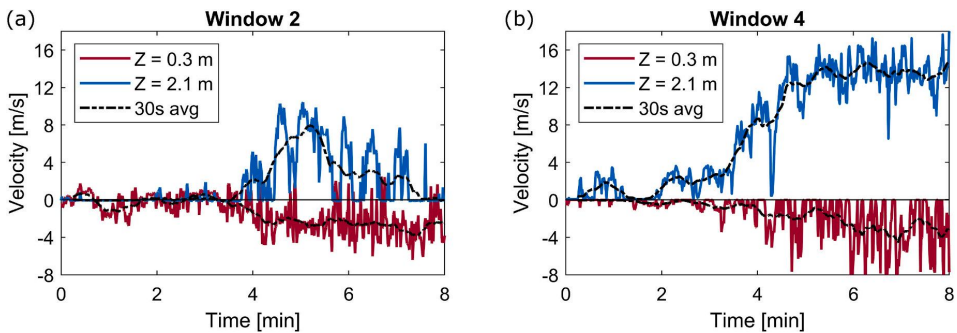

Fig. 23. Gas flow velocities inwards and outwards through Window 2 (a) and Window 4 (b). Positive values represent outward flow, and negative values inward flow.
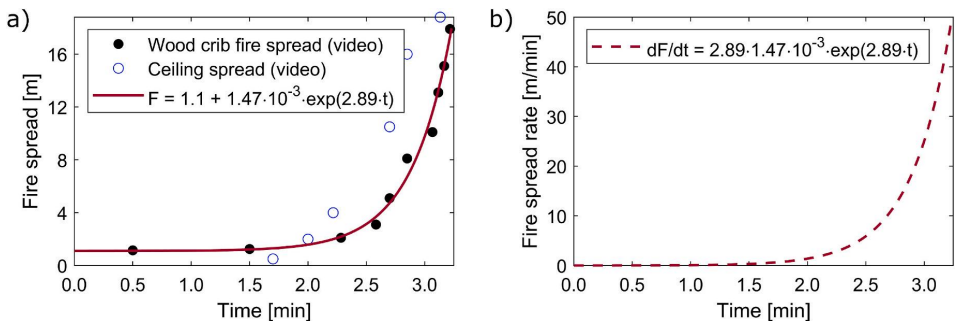

Fig. 24. (a) Fire spread across the wood crib and the ceiling. (b) Fire spread rate across the wood crib.

mm thick. 3) The adhesive of the CLT did not have sufficient resistance against glue-line integrity failure.

Firstly, part of the variation in intensity can be explained by the typical burning behaviour of wood when subjected to an external heat flux. At ignition, the wood burns with flaming combustion with a typical high charring rate. Over time a thicker and thicker char layer forms, and to sustain flaming combustion, the incident heat flux must overcome a critical value. At 120 min, the fire had its least intense period with only minor flames. The few flames present at this point appeared to be emerging from the layer behind and not from burning of the outermost

CLT layer. This corresponds well with the measured incident heat fluxes of 31 kW/m² for the back wall and 36 kW/m² for the ceiling, in which both are below the critical heat flux for self-extinguishment of flames at a CLT surface [20]. The lowest incident heat fluxes were present at 128 min, although considerably more flames were present at this point than at 120 min, see Fig. 9. This again strengthens the hypothesis that the flames were coming from the fresh timber exposed due to delamination. Since the intermediate layers were only 20 mm thick, and we assume that delamination happened before the char front had reached through, the effective thickness before delamination occurred was, therefore, less

Ceiling

Y [m]	1.0	3.0	5.0	7.0	9.0	11.5	14.0	16.5	18.8
3.9				141				188	
2.5	126	134	144	145	146	153	159	167	195
1.1				140				165	

Wood crib

Y [m]	1.0	3.0	5.0	7.0	9.0	11.5	14.0	16.5	18.8
3.9				183				197	
2.5		155	170	186	191	195	195	197	200
1.1				–				200	

Back wall

Z [m]	1.0	3.0	5.0	7.0	9.0	11.5	14.0	16.5	18.8
2.4	131	130	130	140	147	158	166	193	205
2.1				153				191	
1.8				173				194	
1.1	160	158	166	188	190	193	195	196	200
0.3				189				199	

X [m]

Fig. 25. Fire spread indicated by a TC temperature of 600 °C. The fire spread firstly across the ceiling and top of the wall, followed by lower parts of wall and the wood crib. Numbers are given in seconds after the start of the experiment. X, Y and Z represent the positions, as seen in Figs. 3 and 5.

than 20 mm.

Due to the uneven char depth (see Fig. 30) at the start of the second flashover (explained in Section 4.2), the time of delamination occurred over a range of times. This can be seen through the varying temperatures locally in the compartment, see Fig. 32. The peaks are shifted in time, corresponding to the later involvement of the left end of the wall to the fire. From the figure, it appears that the delamination cycle was approx. 30 min. The short time between the delaminations and the subsequent addition of fresh wood to the fire contributed to keep the compartment temperatures high. As an example, the PT temperature remained above 550 °C below the ceiling and 500 °C by the wall after the second flashover. In comparison, the temperatures next to the wall and ceiling after the first flashover were at the minimum 386 and 420 °C, respectively.

From the minimum temperatures at 128 min, the fire grew in intensity. When the fire was extinguished, at 175 min, it was at its most intense phase since 106 min. At this point, the incident heat fluxes to the wall and ceiling were 53 and 60 kW/m^2 and had a rising trend. If the fire had not been put out at this time, it seems likely that the fire intensity could have increased even more, possibly to a full third flashover.

Since the wall had been used in #FRIC-01, it is relevant to consider whether this affected the delamination process. The maximum temperature measured at the glue line in #FRIC-01 was 68 °C. Any official documentation on whether this temperature is sufficient to change the adhesive properties has not been received. However, small fires appeared randomly in both the wall and the ceiling almost

simultaneously just before the second flashover. This parallel behaviour strongly indicates that the CLT wall behaved similarly to the CLT ceiling, which had not been used in #FRIC-01.

4.4. External flames

The external flaming in this experiment showed some characteristic behaviour. Firstly, the external flaming was highly non-symmetrical, with most of the external combustion taking place outside Window 4. The size of the external flame out of this window varied significantly during the most intense period. For longer periods, the flame reached above the facade walls, i.e., >3 m above the window soffit. And for short periods, the flame reached 5–6 m above the window soffit and would likely have reached even higher with a taller facade wall.

Based on the video analysis of the flame and the elevated incident heat fluxes measured on the facade walls, it is reasonable to claim that such large external flames as observed in this experiment pose a significant fire risk to ignite the storey above, but also likely two storeys above, in an actual building. In addition, such large flames are a threat to cause fire spread to an opposite building due to the large flame surface area and the large flame extension from the facade.

The non-symmetrical external flames were likely affected by the wind conditions. The direction of the wind was diagonally from behind the right end, see Table 1 and Fig. 2. Such conditions would create an underpressure on the front side of the compartment. It is suspected that the underpressure caused smoke and flames to be dragged mainly out of
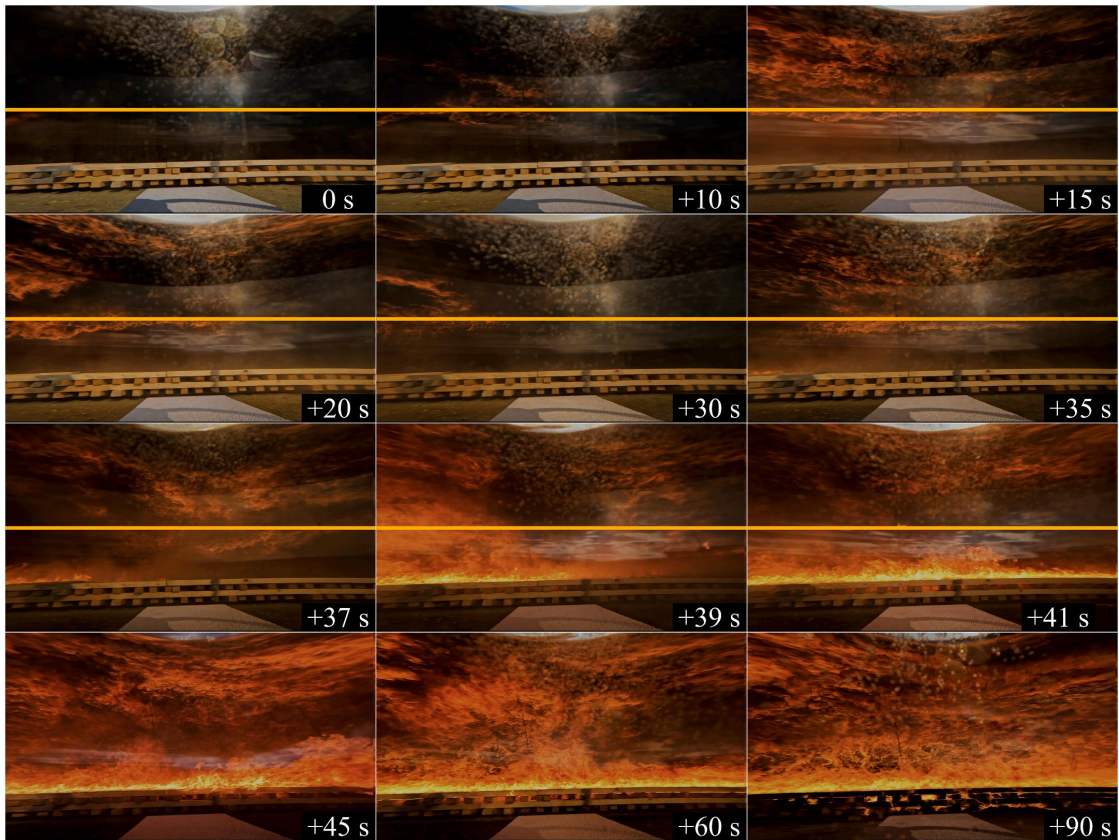
Fig. 26. The images show the fire spread sequence in the compartment. The fire spreads first across the ceiling and the upper part of the wall and then down the wall. The top layer of the wood crib ignites at about the same time flames on the wall reach the wood crib level. The yellow line shows the top of the wall. The given time represents the number of seconds after the flame first occurs below the ceiling in this video frame. The camera was located at floor level in the centre of Window 3 inside a water-filled Pyrex column. (For interpretation of the references to colour in this figure legend, the reader is referred to the Web version of this article.)

Window 4, as the other windows were more shielded from this effect by the compartment itself. It is also likely that the largest external flames occurred due to wind gusts, which amplified this effect. From the side view of the external flame, see Fig. 18, it is evident that the flame covered the entire height at part of the window closest to the edge and that the inward flow of air was reduced through Window 4 compared to the other windows. In addition, the intense fire at this point needed a large supply of air, and since less air was supplied through Window 4, the other windows had to compensate for that loss by supplying even more air. The reduced supply of air through Window 4 caused very high and uniform temperatures in the right end of the compartment and lower temperatures in the centre of the compartment where most air was supplied (Figs. 15 and 16). The non-uniform supply of air through the windows also led to very low levels of oxygen in the right end of the compartment and indicates that part of the compartment was strongly under-ventilated during the most intense fire, despite the large window openings. It is likely that this non-symmetrical behaviour of the external flame could only occur under specific wind conditions. However, it can be stated that fire safety engineering methods to determine external fire plume heights, such as the Law-model in the Eurocodes [6], do not consider such an extent of non-uniformity along the facade openings and do not include the contribution of combustible gases from the CLT to the total HRR.

The estimated HRR for the maximum external flames from Window 4 was 66 ± 20 MW, which does not align with a total HRR of 73 MW, see Fig. 34, as this would mean that two-thirds or more of the combustible gases were burnt outside. It is acknowledged that the estimation of the external flame involved significant uncertainties, both through the determination of the flame volume and by the conversion from volume to HRR. In addition, the method to determine the heat release of external combustion was developed based on smaller flames. Still, the estimated HRR of the external flame indicates that the total HRR is estimated too low, at least for some period. A factor that significantly influences the HRR is the combustion efficiency. This was set to 0.8, but given the high temperatures in the compartment and the strong re-radiation between the crib, the wall and the ceiling, it is not unlikely that the combustion efficiency could be higher than 0.8. Given that the combustion efficiency is correct, the HRR from the wood crib is considered to be quite accurate. However, the HRR from the CLT wall and ceiling is based on only three measurements each, where the average value of those is used to estimate the HRR from the CLT. Since there was quite a large difference between the minimum (1.90 mm/min) and maximum (3.28 mm/min) charring rate, it is not unlikely that the calculated average value is lower than the actual average value. Assuming a combustion efficiency of 0.9 instead of 0.8 and an average charring rate of 3 mm/min instead of 2.64 and 2.71 mm/min, the estimated total HRR ends up being 92.5 MW, almost 20
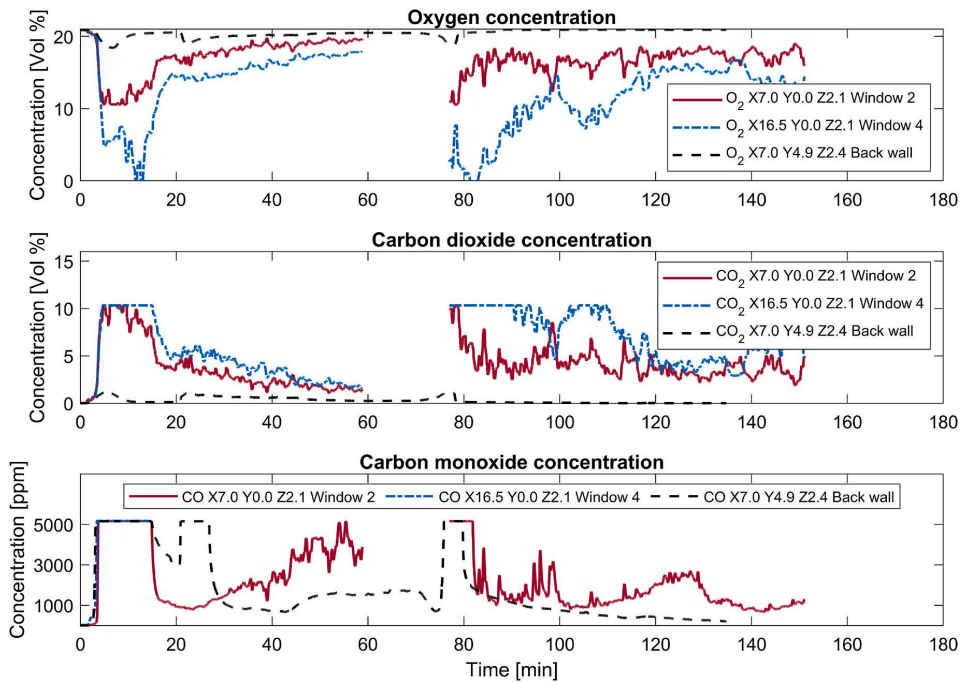
Fig. 27. O_2, CO_2 and CO concentrations of the compartment.

Table 3
Charring rates CLT ceiling.

	Time to 300 °C [min]						Charring rate [mm/min]					
	0 mm	10 mm	20 mm	30 mm	40 mm	97[a] mm	0–10 mm	10–20 mm	20–30 mm	30–40 mm	40-97[a] mm	0-97[a] mm
X4.7	2.0	5.6	13.6	38.3	81.3	175	2.74	1.25	0.40	0.23	0.61	0.56
X9.5	2.3	5.3	10.9	36.6	79.6	175	3.28	1.80	0.39	0.23	0.50	0.56
X14.3	2.5	7.7	16.0	39.2	89.9	175	1.90	1.21	0.43	0.20	0.44	0.56
Avg	2.2	6.2	13.5	38.0	83.6	175	2.64	1.42	0.41	0.22	0.52	0.56

[a] 97 mm is the average final char depth in the ceiling.

Table 4
Charring rates CLT back wall.

	Time to 300 °C [min]						Charring rate [mm/min]					
	0 mm	10 mm	20 mm	30 mm	40 mm	104[a] mm	0–10 mm	10–20 mm	20–30 mm	30–40 mm	40-104[a] mm	0-104[a] mm
X4.7	2.6	7.2	22.4	–	79.3	175	2.17	0.66	0.35	0.35	0.67	0.60
X9.5	2.9	6.5	13.1	–	–	175	2.82	1.50	–	–	–	0.60
X14.3	3.3	6.5	13.6	43.9	77.4	175	3.14	1.41	0.33	0.30	0.66	0.61
Avg	2.9	6.7	13.4	43.9	78.4	175	2.71	1.46[b]	0.34	0.32	0.67	0.60

[a] 104 mm is the average final char depth in the back wall. b) The value of 0.66 mm/min is not included in the average, as it appears to be an outlier.

MW higher than the original estimation. This underlines that with minor adjustments in the parameters affecting the HRR, it does not seem unlikely that the lower HRR estimation (46 MW) of the external flame might be correct. Determination of the HRR in large-scale experiments is challenging, and a certain uncertainty must be expected.

It is well known that the size of external flames tends to increase with exposed CLT [14]. However, this problem has mainly been attributed to compartments with small window openings, which typically result in ventilation-controlled fires [36]. This experiment is an example that large external flames might also occur when having large ventilation openings. However, to know how severe the external flames were in this experiment, it is relevant to compare them against other CLT experiments that experienced large external flames. In Fig. 35, the PT measurements of the facade above Window 4 are compared to Test 2 of the CLT experiments of Sjöström et al. [37]. The experiment had an area of 48 m^2, an opening factor of 0.062 m$^{1/2}$, a fuel load density of 560 MJ/m^2, and both the ceiling and two walls exposed. The PTs were, as in this experiment, installed flush with the facade (see Fig. 36).

As the locations of the PTs were not at the same height above the openings, a detailed comparison is not possible. Nevertheless, the
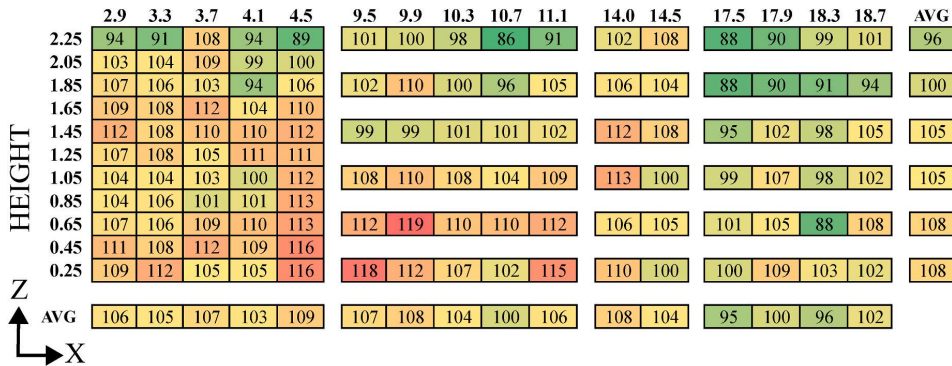
HEIGHT Z	2.9	3.3	3.7	4.1	4.5		9.5	9.9	10.3	10.7	11.1		14.0	14.5		17.5	17.9	18.3	18.7		AVG
2.25	94	91	108	94	89		101	100	98	86	91		102	108		88	90	99	101		96
2.05	103	104	109	99	100																
1.85	107	106	103	94	106		102	110	100	96	105		106	104		88	90	91	94		100
1.65	109	108	112	104	110																
1.45	112	108	110	110	112		99	99	101	101	102		112	108		95	102	98	105		105
1.25	107	108	105	111	111																
1.05	104	104	103	100	112		108	110	108	104	109		113	100		99	107	98	102		105
0.85	104	106	101	101	113																
0.65	107	106	109	110	113		112	119	110	110	112		106	105		101	105	88	108		108
0.45	111	108	112	109	116																
0.25	109	112	105	105	116		118	112	107	102	115		110	100		100	109	103	102		108
AVG	106	105	107	103	109		107	108	104	100	106		108	104		95	100	96	102		

Fig. 28. Final char depth [mm] measurements of CLT wall elements. X and Z represent compartment coordinates. Dark green marks the lowest char depths, and dark red marks the largest. (For interpretation of the references to colour in this figure legend, the reader is referred to the Web version of this article.)

BACK WALL

IGNITION SIDE Y	2.7	3.2	3.7	4.2	4.7		9.7	10.2	10.7	11.2	11.7		16.8	17.3	17.8	18.3	18.8		AVG
4.8	111	110	112	112	112		117	121	122	115	110		113	101	100	108	94		111
4.3	116	106	111	106	118		119	116	122	116	115		98	100	95	98	82		108
3.8	114	113	99	104	113		113	113	111	106	110		107	103	92	102	79		105
3.3	104	100	102	96	107		115	99	106	114	101		97	90	80	89	78		99
2.8	96	101	99	95	104		110	100	92	109	103		91	96	100	99	95		99
2.3	97	94	100	108	86		96	96	100	102	95		75	96	92	99	78		94
1.8	85	95	89	94	88		101	96	101	100	89		78	100	93	91	84		92
1.3	79	93	89	82	79		95	86	97	92	88		82	86	78	87	75		86
0.8	81	93	68	73	68		92	79	82	86	78		87	94	76	84	68		81
0.3	140	112	75	78	108		140	101	70	71	78		120	73	73	84	74		
AVG	98	100	97	97	97		106	101	104	105	99		92	96	90	95	81		

WINDOW WALL

Fig. 29. Final char depth [mm] measurements of CLT ceiling elements. X and Y represent compartment coordinates. The measurements at 0.3 *m* height were not included in the average. Dark green marks the lowest char depths, and dark red marks the largest. (For interpretation of the references to colour in this figure legend, the reader is referred to the Web version of this article.)

temperatures were in about the same range but slightly lower in this experiment. In addition, the duration of the exposure was about three times longer in Test 2. Summarised, the facade exposure in this experiment was for a short period, almost as severe as Test 2, which had a 60% higher fuel load density and was a strongly under-ventilated fire.

4.5. Comparison between #FRIC-01 (exposed ceiling) and #FRIC-02 (exposed ceiling and wall)

The fire developed completely differently in #FRIC-01 and #FRIC-02. These differences can be explained by the three changes in the experimental setup: 1) Exposed CLT on the back wall. 2) Different wind conditions. 3) A different ignition source, as detailed below.

The differences in the ignition source are highlighted in Table 6 and shown in Fig. 35. The increase in the heptane amount was because the wood crib fire in #FRIC-01 almost extinguished after 4 min when the heptane fire burned out. We were afraid that the wood crib fire in #FRIC-02 could extinguish completely if no changes were made to the ignition source. Hence, to avoid the risk of extinguishment of the wood crib fire in #FRIC-02, the ignition method was changed to ensure the wood crib fire was well established when the heptane fire burned out.

In #FRIC-01, the initial heptane and wood crib fire did not ignite the ceiling, and the ceiling was ignited first after 32.5 min when the CLT

ceiling had been heated sufficiently to auto-ignite. By changing the ignition source in #FRIC-02, the heptane fuel surface increased by 40%, and the setup also exposed a larger portion of the wood crib to the fire. This change turned out to be sufficient to ignite the ceiling early.

From the point the ceiling was ignited in the two experiments, the fire development was completely different. In #FRIC-01, the ceiling had been preheated for about half an hour, and the ignition of it caused a rapid flash fire over a large area of the ceiling. In #FRIC-02, the ceiling had not been preheated, and the fire spread across the ceiling developed slower. While the ceiling fire in #FRIC-01 retracted quickly, the ceiling fire in #FRIC-02 continued to spread and developed into a full flashover 1.5 min after the ceiling was ignited. In #FRIC-01, on the other hand, the fire spread across the room in 13 min, where the leading edge of the fire travelled back and forth in three flashing waves before flashover was reached after the fourth wave. This difference is believed to be directly linked to the exposed back wall in this experiment. From video analysis, and also shown in Fig. 26, it is evident that the wall worked as a bridge between the ceiling and the wood crib. The CLT wall contributed to emissions of combustible gases before ignition and after ignition to increased radiation to the wood crib and the ceiling. This re-radiation between three burning surfaces was here sufficient to maintain burning in all of them, and no retraction of the flames was observed.

That the top of the wall ignited about the same time as the ceiling

BACK WALL SIDE

WINDOW SIDE

Fig. 30. Visualization of non-uniform charring for one CLT ceiling element based on a photo. Black is the 3rd layer, yellow is the 4th, and red is the 5th layer. The holes at the right and left lower corners of the window side were caused by smouldering and reignition after the end of the experiment, as this part was hard to reach with water due to safety precautions. (For interpretation of the references to colour in this figure legend, the reader is referred to the Web version of this article.)

with flame spread downwards was expected based on the measured heat fluxes at the wall in #FRIC-01, which was 10–40 kW/m^2 between the 1st and 2nd flashing wave. This level is well above what is needed for piloted ignition of a wooden surface [38].

In addition to the increased spread rate in this experiment, the temperatures, the HRR and the external flames were also higher. The temperatures were during the most intense period 1010–1172 °C in the whole compartment, while in #FRIC-01, they were 785–1038 °C. The more extreme temperatures were caused by a higher HRR, which was estimated to be 32 MW (78%) higher at maximum for #FRIC-02, of

which 13 MW was directly caused by the combustion of the CLT wall. The comparison indicates that the contribution of the exposed wall resulted in an increased combustion rate of the wood crib and the CLT ceiling. The maximum HRR of the wood crib was determined to be 15 MW (75%) higher in this experiment. From these 15 MW, 5 MW was due to the higher HRR per unit length caused by higher temperatures and more considerable heat fluxes towards the wood crib [39]. The remaining 10 MW was due to faster fire spread across the wood crib, which caused a larger part of the crib to burn simultaneously at maximum HRR per unit length.

The average charring rates in this experiment were 21% and 28% faster than in #FRIC-01 for 0–10 mm and 10–20 mm depth, respectively. This increase corresponds to an estimated HRR increase for the ceiling of 3.5 MW.

The external flames were highly non-symmetrical in this experiment, whereas in #FRIC-01, they were more symmetrical. This was likely caused by different wind conditions. In #FRIC-01, there was no measurement of the wind, but the smoke was going almost straight up, indicating a very low wind velocity. In #FRIC-02, the wind was coming diagonally from behind, and smoke and flames were going away from the compartment. Despite relatively low winds, the wind conditions in #FRIC-02 are still expected to have caused an underpressure outside of Window 4, leading to the particularly large external flames from this window, as explained in Section 4.4.

The extinction of flames at the CLT occurred in both experiments but at a higher incident heat flux in #FRIC-02 (see Section 4.3). The following decay phase was nearly linear in both experiments, with an average temperature reduction of 7.1 °C/min in #FRIC-01 and 5.7 °C/min in this experiment. The 20% slower decay rate was likely related to the re-radiation between the wall and the ceiling and more heat stored in the CLT wall than in the gypsum boards. After 65 min in #FRIC-02, the wood crib was completely consumed. The decay phase seemed to follow the behaviour of #FRIC-01, in which temperatures were continuously decaying until ambient conditions were reached, with no re-ignition. However, despite using the same CLT materials and variable fuel load, #FRIC-01 did not exhibit a re-ignition or second flashover, while #FRIC-02 did. This difference was likely due to the higher gas temperature in #FRIC-02 when delamination occurred, 430–445 °C in #FRIC-02 vs. approx. 220 °C in #FRIC-01. Furthermore, the fact that delamination in #FRIC-02 occurred simultaneously in multiple locations certainly contributed to the transition of larger flames and, eventually, the second flashover.

5. Conclusion

- The article describes the second of two compartment fire experiments where the aim was to study the effect of exposed CLT, ventilation conditions and room geometry on fire spread and fire dynamics. The setup was designed as a 95 m^2 open-plan compartment, and this is, to our knowledge, the largest experiment to date

Fig. 31. The fire burned through the intersection between the back wall and the bottom plank at approximately 60 min. The image is taken at a later point when the gap had become larger. The lack of a fire sealant between the bottom plank and the CLT wall enabled this and highlights that connection details are crucial to fire safety.
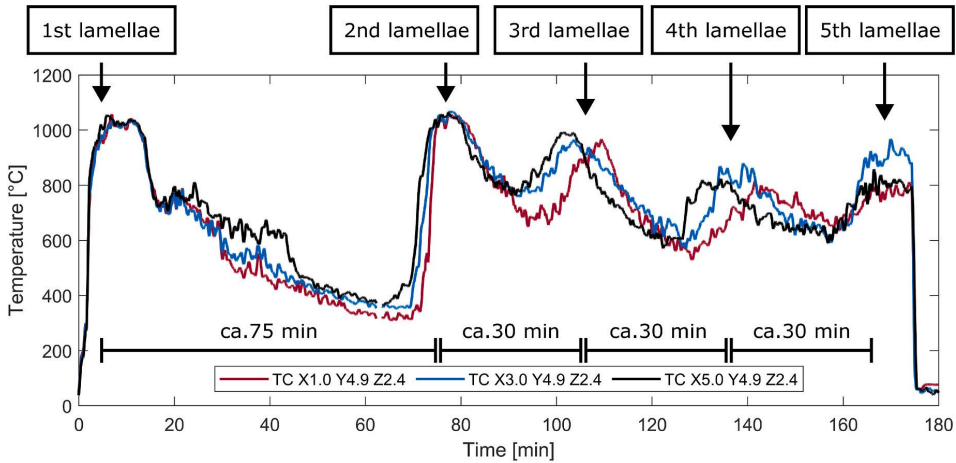
Fig. 32. Temperature of three TCs located next to the back wall. The peaks correspond to the burning of the different layers in the CLT wall.

Table 5
Estimated time for the char front to reach the different layers, based on a charring rate of 0.52 mm/min for the ceiling (Table 3) and 0.67 mm/min for the back wall (Table 4).

	Estimated time [min] for char front to reach			
	2nd layer (40 mm)	3rd layer (60 mm)	4th layer (80 mm)	5th layer (100 mm)
Ceiling	76	114	153	191
Wall	76	106	136	166

with both an exposed CLT wall and ceiling. The fire spread across the room in less than 3.5 min from ignition (5.5 m/min) and in 1.5 min from ignition of the ceiling (11.7 m/min), which is significantly faster than most values found in the literature. The fast fire spread also led to a fire growth rate considerably faster than the fastest fire growth rate in Eurocode 1.

- The accelerating flame spread rate indicates that significantly larger compartments would not necessarily take significantly more time to ignite.
- During the most intense burning phase of the fire, large asymmetrical external flames were observed. The flames were particularly large from one window and reached 3–6 m above the window soffit for several minutes after flashover. This result highlights that large

external flames might also occur in compartments with large window openings.
- After an intense burning phase, the flames at the CLT extinguished, and the wood crib burned out. However, 60 min after the extinction of flames at the CLT, a second flashover occurred. The fire varied in intensity but burned with temperatures up to 800 °C when manually extinguished after 3 h. The ongoing fire resulted from the thin (20 mm) intermediate layers in the CLT and the use of an adhesive that resulted in glue-line integrity failure.
- The charring of the CLT was strongly non-uniform, with an increasing char depth of the ceiling from the window opening to the back wall and increased charring of the wall compared to the ceiling.
- Self-extinction of flames at the CLT was observed at temperatures 805–845 °C and incident heat flux 70–84 kW/m². This is higher than reported earlier and is assumed to be caused by the low oxygen content and thick char layer.

These results should be considered together with the results of #FRIC-01 [9] for the complete picture of the research and background information. From comparisons between #FRIC-01 (exposed ceiling) and #FRIC-02 (exposed ceiling and wall), the following is concluded.
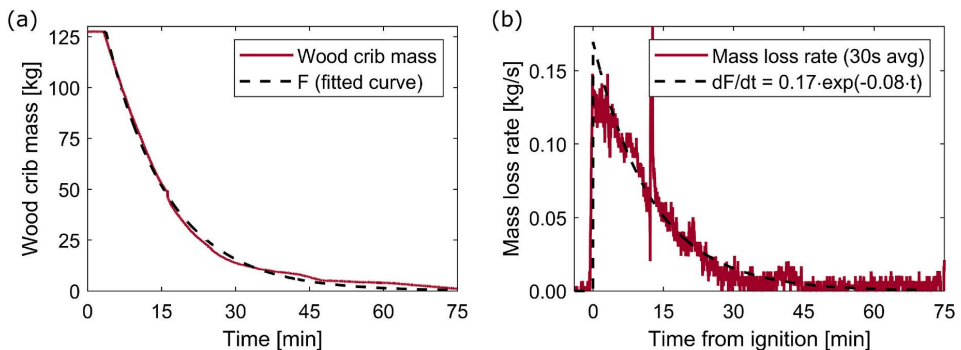
Fig. 33. (a) Mass loss of the small wood crib (1.0 m × 2.8 m) put on a scale. (b) Mass loss rate of the small wood crib.
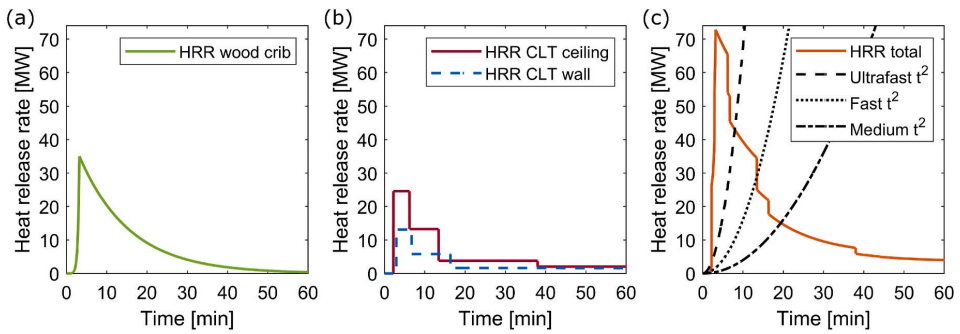
Fig. 34. Heat release rate of the wood crib (a), CLT (b) and total (c). The total HRR of the experiment is compared against the medium, fast and ultrafast fire growth rates [6].
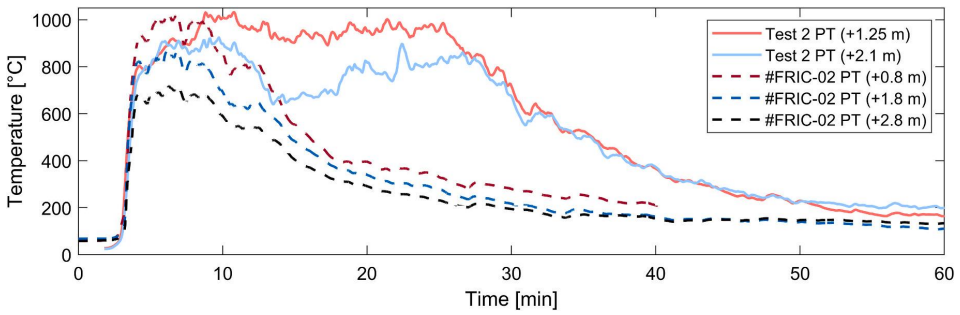
Fig. 35. Comparison of PT temperatures above Window 4 to Test 2 of Sjöström et al. [37]. The x-axis of Test 2 is shifted +1.8 min to synchronise the times for easier comparison.
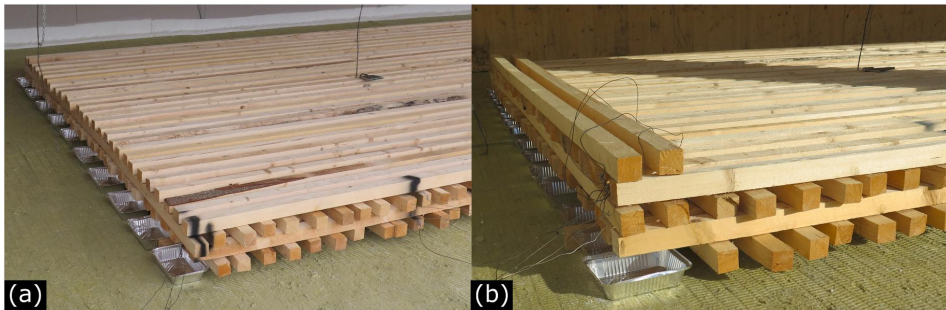

Fig. 36. Comparison of ignition method of #FRIC-01 (a) and #FRIC-02 (b). The wires shown in (b) are thermocouples from different loggers to synchronise the data.

Table 6
Differences in ignition source between #FRIC-01 and #FRIC-02.

	#FRIC-01	#FRIC-02
No. Of heptane trays	10	14
Heptane amount in each tray	0.5 L	0.7 L
Total amount of heptane	5.0 L	9.8 L
Rotation of trays	0°	90°
Part of tray below the wood crib	5 cm	15 cm

- Despite minor changes in the ignition source, the comparison indicates that the presence of an exposed wall can significantly accelerate the fire development.
- In #FRIC-02, the fire spread rate was faster, and temperatures, charring rates, heat release rates and external flames were higher.
- In #FRIC-02, a second flashover and subsequent fluctuations of fire intensity occurred, while #FRIC-01 did not exhibit a secondary flashover. This was likely caused by the increased fire exposure due to the additional fuel by the wall and increased HRR from the wood crib and CLT ceiling. This combination caused a higher gas temperature next to the CLT when delamination occurred, sufficient to ignite the fresh wood of the second layer.

Sample CRediT author statement

Andreas Sæter Bøe: Conceptualization, Methodology, Investigation, Formal Analysis, Data Curation, Writing - Original Draft, Writing - Review & Editing, Visualization.

Kathinka Leikanger Friquin: Conceptualization, Methodology, Writing - Review & Editing.

Daniel Brandon: Conceptualization, Methodology, Writing - Review & Editing.

Anne Steen-Hansen: Conceptualization, Writing - Review & Editing.

Ivar S. Ertesvåg: Conceptualization, Writing - Review & Editing.

Declaration of competing interest

The authors declare that they have no known competing financial interests or personal relationships that could have appeared to influence the work reported in this paper.

Data availability

Data will be made available on request.

Appendix A. Supplementary data

Supplementary data to this article can be found online at https://doi.org/10.1016/j.firesaf.2023.103986.

References

[1] G. Ronquillo, D. Hopkin, M. Spearpoint, Review of large-scale fire tests on cross-laminated timber, J. Fire Sci. 39 (5) (2021) 327–369, https://doi.org/10.1177/07349041211034460.

[2] J. Liu, E.C. Fischer, Review of large-scale CLT compartment fire tests, Construct. Build. Mater. 318 (2022), 126099, https://doi.org/10.1016/j.conbuildmat.2021.126099.

[3] H. Mitchell, P. Kotsovinos, F. Richter, D. Thomson, D. Barber, G. Rein, Review of fire experiments in mass timber compartments: current understanding, limitations, and research gaps, Fire Mater. 47 (4) (2023) 415–432, https://doi.org/10.1002/fam.3121.

[4] P. Kotsovinos, et al., Fire dynamics inside a large and open-plan compartment with exposed timber ceiling and columns: CodeRed #01, Fire Mater. 47 (4) (2023) 542–568, https://doi.org/10.1002/fam.3049.

[5] P. Kotsovinos, et al., Impact of ventilation on the fire dynamics of an open-plan compartment with exposed timber ceiling and columns: CodeRed #02, Fire Mater. 47 (4) (2023) 569–596, https://doi.org/10.1002/fam.3082.

[6] EN 1991 1-2 (2002) Eurocode 1: Actions on Structures - Part 1-2: General Actions - Actions on Structures Exposed to Fire, CEN, Brussels, Belgium, 2002.

[7] E. Rackauskaite, et al., Fire experiment inside a very large and open-plan compartment: x-ONE, Fire Technol. 58 (2022) 905–939, https://doi.org/10.1007/s10694-021-01162-6.

[8] M. Heidari, et al., Fire experiments inside a very large and open-plan compartment: x-TWO, in: Presented at the Proceedings of the 11th International Conference on Structures in Fire (SiF2020), The University of Queensland, Brisbane, Australia, 2020.

[9] A.S. Bøe, K.L. Friquin, D. Brandon, A. Steen-Hansen, I.S. Ertesvåg, Fire spread in a large compartment with exposed cross-laminated timber and open ventilation

[10] A. Nadjai, et al., Large scale fire test: the development of a travelling fire in open ventilation conditions and its influence on the surrounding steel structure, Fire Saf. J. 130 (2022), 103575, https://doi.org/10.1016/j.firesaf.2022.103575, 2022/06/01/.

[11] J.P. Hidalgo, et al., The Malveira fire test: full-scale demonstration of fire modes in open-plan compartments, Fire Saf. J. 108 (2019), https://doi.org/10.1016/j.firesaf.2019.102827.

[12] R.M. Hadden, et al., Effects of exposed cross laminated timber on compartment fire dynamics, Fire Saf. J. 91 (2017) 480–489, https://doi.org/10.1016/j.firesaf.2017.03.074.

[13] X. Li, X. Zhang, G. Hadjisophocleous, C. McGregor, Experimental study of combustible and non-combustible construction in a natural fire, Fire Technol. 51 (6) (2015) 1447–1474, https://doi.org/10.1007/s10694-014-0407-4.

[14] J. Su, P.-S. Lafrance, M.S. Hoehler, M.F. Bundy, Fire Safety Challenges of Tall Wood Buildings–phase 2: Task 3-Cross Laminated Timber Compartment Fire Tests. Report No. FPRF-2018-01-REV, NFPA (National Fire Protection Association), Quincy, Massachusetts, USA, 2018. March 28, 2023. [Online], https://tsapps.nist.gov/publication/get_pdf.cfm?pub_id=925297.

[15] D. Brandon, J. Sjöström, A. Temple, E. Hallberg, F. Kahl, RISE report - final Project Report - fire Safe implementation of visible mass timber in tall buildings - compartment fire testing (2021:40), RISE Fire Res, 2021, p. 40 [Online], http://urn.kb.se/resolve?urn=urn:nbn:se:ri:diva-58153. RISE Report 2021.

[16] A.R. Medina Hevia, Fire Resistance of Partially Protected Cross-Laminated Timber Rooms, Carleton University, Ottawa, Ontario, 2014. Master thesis.

[17] C. Dagenais, L. Ranger, N. Benichou, J. Su, "Improved fire performance of cross-laminated timber," presented at the World Conference on Timber Engineering, Santiago, Chile (2021) 9–12. August.

[18] D. Hopkin, et al., Large-scale enclosure fire experiments adopting CLT slabs with different types of polyurethane adhesives: genesis and preliminary findings, Fire 5 (2) (2022), https://doi.org/10.3390/fire5020039.

[19] R. Emberley, et al., Description of small and large-scale cross laminated timber fire tests, Fire Saf. J. 91 (2017) 327–335, https://doi.org/10.1016/j.firesaf.2017.03.024.

[20] R. Emberley, T. Do, J. Yim, J.L. Torero, Critical heat flux and mass loss rate for extinction of flaming combustion of timber, Fire Saf. J. 91 (2017) 252–258, https://doi.org/10.1016/j.firesaf.2017.03.008.

[21] R. Crielaard, J.-W. van de Kuilen, K. Terwel, G. Ravenshorst, P. Steenbakkers, Self-extinguishment of cross-laminated timber, Fire Saf. J. 105 (2019) 244–260, https://doi.org/10.1016/j.firesaf.2019.01.008, 2019/04/01/.

[22] EN 520:2004+A1:2009, Gypsum Plasterboards - Definitions, Requirements and Test Methods, CEN, Brussels, Belgium, 2004.

[23] EN 1995-1-2 (Eurocode 5): Design of Timber Structures - Part 1-2: General - Structural Fire Design, CEN, Brussels, Belgium, 2004.

[24] U. Wickström, Temperature Calculation in Fire Safety Engineering, Springer, 2016.

[25] B.J. McCaffrey, G. Heskestad, A robust bidirectional low-velocity probe for flame and fire application, Combust. Flame 26 (1976) 125–127, https://doi.org/10.1016/0010-2180(76)90062-6.

[26] M. Aniszewska, A. Gendek, Comparison of heat of combustion and calorific value of the cones and wood of selected forest trees species, For. Res. Pap. 75 (3) (2014) 231–236 [Online], https://depot.ceon.pl/handle/123456789/5332.

[27] ISO 12570:2000, Hygrothermal Performance of Building Materials and Products- Determination of Moisture Content by Drying at Elevated Temperature, ISO, Brussels, Belgium, 2000, 2000.

[28] M. Bonner, W. Węgrzyński, G. Rein, Visual fire power: an algorithm for measuring heat release rate of visible flames in camera footage, with applications in facade fire experiments, Fire Technol. 59 (2023) 191–215, https://doi.org/10.1007/s10694-022-01341-z.

[29] R.G. Gann, et al., Reconstruction of the fires and thermal environment in World Trade Center buildings 1, 2, and 7, Fire Technol. 49 (2013) 679–707.

[30] H.E. Nelson, Engineering View of the Fire of May 4, 1988 in the First Interstate Bank Building, 1989. Los Angeles, California (NIST IR 89-4061).

[31] B.R. Kirby, D.E. Wainman, L.N. Tomlinson, T.R. Kay, B.N. Peacock, Natural fires in large scale compartments, Int. J. Eng. Performance-Bases Fire Codes 1 (2) (1999) 43–58.

[32] D.C.O. Marney, L.J. Russell, R. Mann, Fire performance of wood (Pinus radiata) treated with fire retardants and a wood preservative, Fire Mater. 32 (6) (2008) 357–370, https://doi.org/10.1002/fam.973.

[33] F. Richter, F.X. Jervis, X. Huang, G. Rein, Effect of oxygen on the burning rate of wood, Combust. Flame 234 (2021), 111591, https://doi.org/10.1016/j.combustflame.2021.111591.

[34] H. Mitchell, R. Amin, M. Heidari, P. Kotsovinos, G. Rein, Structural hazards of smouldering fires in timber buildings, Fire Safe. J. 140 (2023) 103861, https://doi.org/10.1016/j.firesaf.2023.103861, 10/01/2023.

[35] J. Cuevas, J.L. Torero, C. Maluk, Flame extinction and burning behaviour of timber under varied oxygen concentrations, Fire Saf. J. 120 (2021), 103087, https://doi.org/10.1016/j.firesaf.2020.103087.

[36] A. Bartlett, A. Law, Influence of excess fuel from timber lined compartments, Construct. Build. Mater. 235 (2020), 117355, https://doi.org/10.1016/j.conbuildmat.2019.117355.

[37] J. Sjöström, D. Brandon, A. Temple, J. Anderson, R. McNamee, External fire plumes from mass timber compartment fires—comparison to test methods for regulatory

conditions: #FRIC-01 - exposed ceiling, Fire Saf. J. (2023), 103869, https://doi.org/10.1016/j.firesaf.2023.103869.

compliance of façades, Fire Mater. 47 (4) (2023) 433–444, https://doi.org/10.1002/fam.3129.

[38] A.I. Bartlett, R.M. Hadden, L.A. Bisby, A Review of factors affecting the burning behaviour of wood for application to tall timber construction, Fire Technol. 55 (1) (2019/01/01 2019) 1–49, https://doi.org/10.1007/s10694-018-0787-y.

[39] V. Gupta, J.L. Torero, J.P. Hidalgo, Burning dynamics and in-depth flame spread of wood cribs in large compartment fires, Combust. Flame 228 (2021) 42–56, https://doi.org/10.1016/j.combustflame.2021.01.031.

Paper III

Numerical simulation of fire spread in large-scale open CLT compartment

Lei Jiang, Andreas Sæter Bøe, Tian Li

Submitted manuscript

2023

This paper is submitted for publication and is therefore not included

Paper IV

Experimental Study of the Charring of I-Joists and Recession of
Combustible Insulation in Light Timber Frame Assemblies with
Comparison to Eurocode 5

Andreas Sæter Bøe

Katrin Nele Mäger, Kathinka Leikanger Friquin, Alar Just

Experimental Study of the Charring of I-Joists and Recession of Combustible Insulation in Light Timber Frame Assemblies with Comparison to Eurocode 5

Andreas Sæter Bøe *, Norwegian University of Science and Technology (NTNU), Trondheim, Norway

Katrin Nele Mäger , Tallinn University of Technology (TalTech), Tallinn, Estonia

Kathinka Leikanger Friquin , SINTEF Research Institute, Trondheim, Norway

Alar Just , Tallinn University of Technology (TalTech), Tallinn, Estonia

Abstract. Design models are commonly used in fire safety design of light timber frame assemblies. Parameters for use in the models are available for rectangular members with mineral wool, wood fibre or cellulose insulation and for assemblies with I-joists and mineral wool. For assemblies where I-joists and combustible insulations are combined, design parameters are missing. Five fire experiments with two I-joist types and four combustible insulation products have been conducted. The aim was to study charring of I-joist flanges and recession rates of combustible insulations and in addition, to compare their behaviour to the new and existing models of Eurocode 5. Charring rates for the flanges were 0.40–0.76 mm/min and 0.54–1.72 mm/min for the protected and post-protected phase, respectively. Rates decreased with increasing flange size. Charring rates for flanges of solid wood and LVL were comparable. The results show that lateral charring of I-joist flanges can be significant in the protected phase. The tested insulation products showed a lower recession rate than values reported for glass wool insulation, with a more pronounced difference for wood fibre and cellulose insulations. The low recession rates compared to previously reported generic values can possibly be explained by better product-specific properties, negligible shrinking and slightly different test set-up. The insulation stayed well in place after gypsum board fall-off and best-practice for keeping the insulation in place is given. The results, completed with future loaded full-scale tests, can give basis for further development of design models for assemblies with I-joists and combustible insulations.

---

*Correspondence should be addressed to: Andreas Sæter Bøe, E-mail: andreas.s.boe@ntnu.no

1. Introduction

Wood has been used extensively in buildings for centuries and the fire performance of traditional structural members has been studied for decades. Simplified design models for predicting char depths and load-bearing capacities for rectangular timber members have been developed earlier.

Design of the fire resistance of timber structures generally consists of two parts: calculation of the charring depth and, thereafter, determination of the mechanical resistance [1–5]. The charring depth is determined based on the charring rate of the wood and will be a function of the wood species, density, moisture, etc. [6, 7].

In fire-resistant design, the primary protection for timber members is offered by claddings. Several methods are developed to determine the residual load-bearing capacity and separating function of timber frame assemblies based on furnace tests with standard fire exposure [8, 9], for example, in Europe [1, 10], USA [2], Canada [5], Australia [11] and New Zealand [11]. The methods are similar, where determination of the char depth is the main principle, but the charring rates vary. In some of the methods, the residual load-bearing capacity for the remaining cross-section will thereafter be determined based on reduced strength and stiffness properties of the wood. In other methods, a layer is deducted from the cross-section due to reduced strength and stiffness properties caused by increased temperature. The residual load-bearing capacity is then determined for the remaining cross-section with strength and stiffness properties at normal temperature. The protection given by claddings or insulation in the cavities is included in different ways. For further comparison, see Buchanan and Östman [12] and LaMalva and Hopkin [3].

In Europe, the methods given in EN 1995-1-2:2004 [1] (EN 1995-1-2) are commonly used for rectangular cross-sections. The main model of EN 1995-1-2 was developed by König and Walleij [13] and considers one-dimensional heat transfer, where the charring rate is treated as a constant. The model transfers the residual cross-section to a rectangular one and accounts for corner rounding by multiplying the one-dimensional charring rate with coefficients.

In the design methods described in EN 1995-1-2 [1], the charring behaviour of the wood is considered in three phases, see Figure 1. In Phase 1, no charring occurs as the cladding protects the timber from direct heat exposure and the temperature on the timber surface has not reached 300°C. Phase 2, also known as the protected phase, begins when the timber has started to char, i.e., the surface of the timber has reached 300°C, but is still protected by the cladding. Phase 3, the post-protected phase, starts when the cladding falls off and the timber members become directly exposed to the fire. To calculate the charring depth of the different phases, additional coefficients for the protected and post-protected phase are added.

For timber frame assemblies with insulated cavities, the charring is also affected by the cavity insulation. A design model for timber members with rectangular cross-sections to include the effect of stone wool insulation in timber frame assemblies is available in Annex C of EN 1995-1-2. Charring is considered to occur only
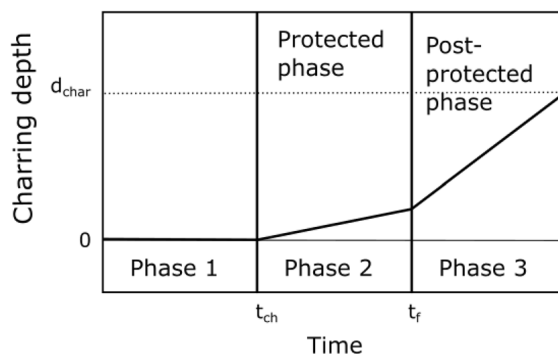
Figure 1. Charring of timber protected by a cladding material. d_{char} represents the final charring depth, while t_{ch} and t_f indicate the start of charring and fall-off of cladding, respectively. Figure based on EN 1995-1-2 [1].

from the fire-exposed side of the cross-section. The lateral sides are considered protected by stone wool. The model is valid also for assemblies with glass wool, but only until fall-off of the cladding.

Improved models that also include glass wool insulation were later developed by Just [14] and published in the handbooks *Brandsäkra trähus* [15] and *Fire safety in timber buildings—Technical Guideline for Europe* [10]. The models are applicable to light timber frame assemblies with rectangular cross-sections of solid timber and cavity insulation of mineral wool. In the COST Action network FP1404 *Fire Safe Use of Bio-Based Building Products* [16], new models were developed based on the previous. Protection levels of insulation were included, protection time of fire protective cladding was improved and the thickness of the zero-strength layer was differentiated for tension, compression and bending in the cross-section. The zero-strength layer is here defined as a layer where the strength and stiffness properties of the wood material are assumed to be zero due to the increased temperatures caused by the fire. This layer is directly behind the charred wood and it is assumed that the strength and stiffness properties of the wood behind the layer are unchanged.

In the last years, the popularity of lightweight engineered wood products has increased. One example is the I-joist, an I-shaped timber member consisting of a top and bottom flange with a web in between. They have become increasingly popular [17], among others, due to their great strength-to-weight ratio. Timber frame assemblies with I-joists are not included in any of the mentioned models [1, 14, 16] and only briefly mentioned in handbooks [10, 15].

König [18] investigated the fire resistance of I-joists and developed models to analyse the load-bearing capacity of I-joists exposed to fire. The assumption for charring calculations was a cavity completely filled with stone or glass wool insulation. Moreover, the model is only valid for glass wool until the failure of the cladding on the fire side.

In addition to new engineered wood products, there is now also a range of different insulation materials available, including combustible insulations. As introduction of combustible insulations might change the fire dynamics of a compartment fire, it is important to understand the contribution of the insulation [19].

The above-mentioned models [1, 10, 14–16, 18] are applicable to assemblies insulated with stone wool and glass wool. Hence, none of the combustible insulation products that have entered the market in the past years, like wood fibre, cellulose and phenolic foam insulations, are included in the models.

However, recently several experiments were carried out on combustible insulations. Tiso [20] conducted 36 furnace tests with a solid wood timber frame and several different cavity insulations. The work resulted in the description of protection levels (PLs) to characterise different insulation materials. The PLs are described in detail later in this section.

Based on the experiments of Tiso [20], Tiso and Just [21–23] developed a design model for timber frame assemblies with rectangular cross-sections and cavities filled with different combustible insulation (wood fibre, cellulose, EPS, PUR and PIR).

Mäger and Just [24, 25] further developed the model of Tiso and Just [21–23] by adding a proposed design model for assemblies with I-joists and mineral wool insulations.

This model includes four different charring phases, see Figure 2. In Phase 1, no charring occurs, while Phase 2 considers charring behind the cladding. Phase 3 is after fall-off of the cladding and an increased charring rate is seen. Phase 3 is followed by Phase 4, which is recognised by a reduced charring rate compared to Phase 3. The reduced charring rate is caused by formation of a sufficiently thick char layer to slow down the heat transport into the char front, approximately 25 mm. Phase 2 is neglected if fall-off of the cladding occurs before charring of the protected wood has started. Similarly, if a sufficiently thick char layer forms in
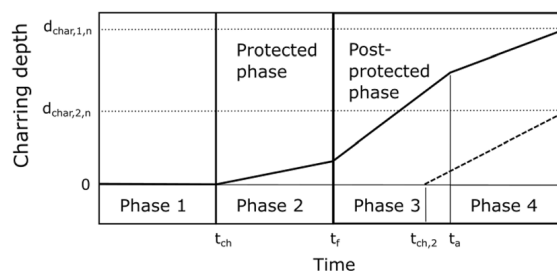
Figure 2.   Charring of timber protected by a combustible cavity insulation. t_{ch} and $t_{ch,2}$ represents the start of charring of the exposed and lateral side, respectively. t_f is the time for fall-off of cladding, and t_a is the time when charring is reduced due to a sufficiently thick char layer. $d_{char,1,n}$ and $d_{char,2,n}$ represents the final charring depth for the exposed side and the lateral side, respectively. Figure based on EN 1995-1-2 [1].

Phase 2, Phase 3 is neglected. On the other hand, if the final charring depth does not reach a sufficiently thick layer to reduce charring, Phase 4 is not considered. The start time of charring from the lateral sides may occur in Phase 2, 3 or 4, depending on the insulation properties and the fall-off time for the cladding.

However, design parameters for assemblies of I-joists in combination with combustible cavity insulation have not yet been established. Therefore, predicting the charring of I-joists in these assemblies is not possible based on the currently available design parameters.

A new version of Eurocode 5 is being developed, the final draft of prEN 1995-1-2:2021 [26] (prEN 1995-1-2) is referred to here. It includes a design model for charring of I-joists based on the work of Mäger and Just [24, 25]. The model includes more possibilities for variations of materials and the calculation of the charring depth includes coefficients considering the protection of the timber member, grain direction, thickness, density etc. The design method for I-joists is largely similar to the effective cross-section method (ECSM) [1] for rectangular timber members. The effective cross-section is what remains after the charred material and the layer with reduced strength and stiffness (zero-strength layer) are removed from the timber member.

The prEN 1995-1-2 also provides guidance on how to assess new insulation products based on the work of Tiso [20]. A test method to determine the Protection Levels for insulation products is described. In the test, a small timber frame assembly consisting of solid timber elements with dimensions 45 mm × 145 mm is used. The insulation product is placed in the cavities on each side of the centre beam. The wood frame is closed with a gypsum board on the fire-exposed side and a particleboard on the unexposed side. Thermocouples (TC) are positioned at the intersection between the gypsum board and the wood surface and on the lateral sides of the beams at 100 mm depth. The test specimen is then exposed to the standard fire temperature curve according to EN 1363-1 [27]. The gypsum board is provoked to fall off after 45 min by manual intervention and the test is terminated after 60 min. The Protection Level classification is based on the temperature of the beams at 100 mm depth at 45 and 60 min, with the following classification scheme:

- PL1 if the temperature is lower than 300°C at 60 min.
- PL2 if the temperature is lower than 300°C at 45 min and higher than 300°C at 60 min.
- PL3 if the temperature is higher than 300°C at 45 min.

The recession rate is determined based on the time it takes for the TC at 100 mm depth to reach 300°C. This method presumes that no lateral charring has occurred before fall-off of the gypsum board.

In prEN 1995-1-2, the recession rate for cavity insulation in PL2 made of glass wool is 30 mm/min, based on Just [14]. The rate for wood fibre and cellulose-based insulation in PL2 is 14 mm/min [20]. These values are considered to be on the conservative side.

Winter et al. [28] performed furnace tests of rectangular solid wood members similar to the tests of Tiso [20, 23]. For cellulose insulation, a much lower recession rate was obtained compared to the values of Tiso [20, 23]. The cellulose insulation was classified as PL1 (together with stone wool), while Tiso's measurements put this insulation in PL2 (together with traditional glass wool). Wood fibre insulations were classified as PL2 in both studies [20, 28]. The low recession rates for cellulose insulation were explained by how the insulation was installed, blown-in loose-fill insulation [28] versus manually packed batts [20, 23]. Winter et al. also found large differences in recession rates between insulations installed in a wall configuration compared to a floor configuration.

Although the design model is applicable to I-joists, all known recession rates are derived from tests with solid wood and not I-joists. Hence, design parameters for combustible insulations derived from tests with I-joists are still missing.

To develop a design model for light timber frame assemblies with I-joists and combustible cavity insulation, design parameters for the I-joists and insulation must be determined. The parameters can be determined based on the charring rate of the I-joists on the fire-exposed and lateral sides. The charring on the lateral sides will be influenced by the recession rate of the different types of insulation which, therefore, must be known. The parameters required for calculating the charring depth of the I-joists may be determined by testing, with supplement from thermal finite element simulations. Testing is recommended to gain input for simulations and to verify the results.

The aim of this study was, therefore, to establish the charring rate of I-joists in light timber frame assemblies with combustible cavity insulation. The recession behaviour of different combustible insulation products was also studied. A series of five fire experiments with assemblies with I-joists and combustible insulation was conducted. Two types of I-joists and four different insulation products were used in the experiments.

2. Methods

The experimental method and methods for calculating the charring rates of the I-joists and recession rates of the insulations are described here.

2.1. Experimental Method

2.1.1. Test Specimens In total, five furnace tests were carried out at RISE Fire Research in Trondheim, Norway. The test specimens were built up with various combinations of two different I-joist types and four different insulation products. Details on the I-joists and insulations are given in Sect. 2.1.2 and summarised in Tables 1 and 2. The I-joists were installed in a timber frame. A centre beam divided the frame into two similar-sized rectangular spaces, Space A and B. In each space, three I-joists of the same type but with different flange sizes were installed. The cavities between the I-joists and the frame were completely filled with insulation. The build-up and dimensions are shown in Figure 3. All joints between the solid timber elements in the frame were covered with aluminium tape, see Figure 4

Table 1
Details of the I-Joists Used in the Tests

Name used in the report	Hunton I-joist	Masonite I-joist
Produced by	Steico	Masonite beams
Flange	Laminated veneer lumber—3 mm layer thickness	Solid wood, spruce or pine
Web	8 mm hard fibreboards	10 mm particleboards
Flange height[a]	39 mm	47 mm
Flange width—Small	45 mm	47 mm
Flange width—Medium	60 mm	70 mm
Flange width—Large	90 mm	97 mm

[a]The measured flange height varied slightly between the different I-joists. Hunton: 40–41 mm, Masonite: 47–47.5 mm

Table 2
Insulation Products

Insulation product name	Type	Density	R-value[a] for 200 mm thickness	Material information
CBI isocell evolution	Cellulose fibre, Loose-fill–blown in	$\sim$ 57 kg/m^3	5.41 m^{2}K/W	92% mass weight of unused newspapers, 8% mineral salts without Boron
Hunton Nativo® Wood Fibre	Wood fibre, Loose-fill–manually packed	$\sim$ 40 kg/m^3	5.26 m^{2}K/W	Natural wood fibre from spruce with addition of the fire-retardant ammonium phosphate
Hunton Nativo® Wood Fibre	Wood fibre Batt	$\sim$ 51 kg/m^3	5.26 m^{2}K/W	Natural wood fibre from spruce with addition of the fire-retardant ammonium phosphate
Kingspan Kooltherm K12	Thermoset phenolic Batt	$\sim$ 36 kg/m^3	9.52 m^{2}K/W	Thermoset phenolic foam insulation

[a]R-value is insulation thickness [m] divided by the conductivity [W/mK] and is the reciprocal of the U-value

and the joints between the timber elements and the boards were sealed with a fire sealant to reduce smoke and heat leakage during the fire tests.

In Test 1, the same I-joist type was used in both Space A and B, but the cavities in the two spaces were filled with two different insulations. In Tests 2, 3 and 4, the I-joists in Spaces A and B were different, while the insulation was the same type in both spaces. In Test 5, both the I-joist and the insulation were the same in both spaces, but at one side, only the two largest flange sizes were tested. The distance between the I-joists in Test 5 with only two I-joist sizes was 600 mm instead
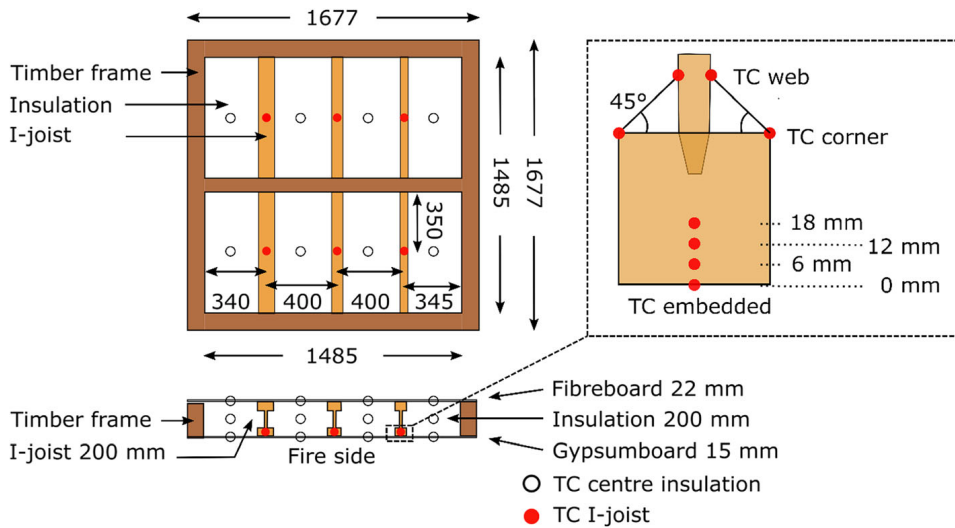
Figure 3. **Build-up of test specimen in plan and cross-section, and position of thermocouples. Dimensions in mm.**

Figure 4. **Left: Test specimen filled with wood fibre batt on the left half side and phenolic foam batt on the right half side. Right: Test specimen filled with wood fibre loose-fill insulation (manually packed) between the Hunton I-joists (left) and Masonite I-joists (right). The fibreboard is not installed.**

of 400 mm, which was used in the other tests. The increased centre-centre distance on one side was chosen to study the effect of the insulation width. An overview of all tests is given in Table 3, whereas an explanation for the test ID is given in Figure 5.

The test specimen was protected by a 15.4 mm gypsum board type F, according to the classification of EN 520 [29], on the fire exposed side and covered with a 22 mm fibreboard on the non-exposed side. The screw distance for both the gypsum board and the fibreboard was ca. 300 mm. Each of the two equally sized spaces was completely covered by one separate gypsum board, with no joints on the I-joists or the insulation. The two gypsum boards were cut slightly smaller than the furnace opening, so they could freely fall down into the furnace when the boards or their fasteners failed. The gypsum boards were fastened with 41 mm

Table 3
Test Matrix

TEST ID	Test no	I-joist	Flange width	Insulation
T1MaSKb	1	Masonite	S47 mm	Kingspan Kooltherm phenolic foam batt (Kb)
T1MaMKb		(Ma)	M70 mm	
T1MaLKb			L97 mm	
T1MaSHb			S47 mm	Hunton Nativo® Wood Fibre Insulation batt
T1MaMHb			M70 mm	(Hb)
T1MaLHb			L97 mm	
T2HuSClf	2	Hunton	S45 mm	CBI Isocell Evolution cellulose (Clf)
T2HuMClf		(Hu)	M60 mm	
T2HuLClf			L90 mm	
T2MaSClf		Masonite	S47 mm	
T2MaMClf		(Ma)	M70 mm	
T2MaLClf			L97 mm	
T3HuSHlf	3	Hunton	S45 mm	Hunton Nativo® Wood Fibre loose-fill insula-
T3HuMHlf		(Hu)	M60 mm	tion (Hlf)
T3HuLHlf			L90 mm	
T3MaSHlf		Masonite	S47 mm	
T3MaMHlf		(Ma)	M70 mm	
T3MaLHlf			L97 mm	
T4HuSHb	4	Hunton	S45 mm	Hunton Nativo® Wood Fibre Insulation batt
T4HuMHb		(Hu)	M60 mm	(Hb)
T4HuLHb			L90 mm	
T4MaSHb		Masonite	S47 mm	
T4MaMHb		(Ma)	M70 mm	
T4MaLHb			L97 mm	
T5HuSHb	5	Hunton	S45 mm	Hunton Nativo® Wood Fibre Insulation batt
T5HuMHb		(Hu)	M60 mm	(Hb)
T5HuLHb			L90 mm	
T5HuMHbcc60[a]			M60 mm	
T5HuLHbcc60[a]			L90 mm	

[a]Flange centre-to-centre distance was 600 mm instead of 400 mm
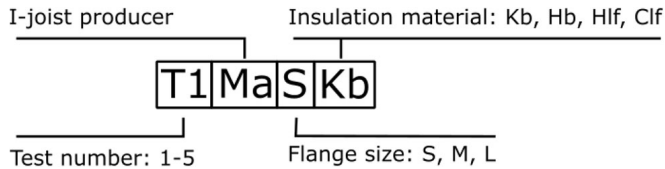
Figure 5. Explanation for the given test IDs.

gypsum screws in Tests 1, 2 and 3, but was reduced to screws with 30 mm length in Test 4 and 5 to reduce the fall-off time.

2.1.2. I-Joist and Insulation Types I-joists from two different manufacturers, Masonite and Hunton, were used. They had different materials in the flange and
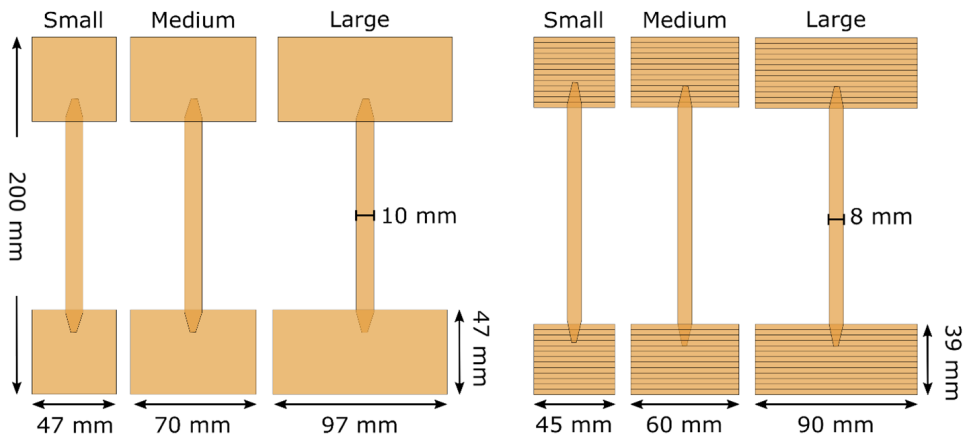
Figure 6. Left: I-joists from Masonite with solid flanges. Right: I-joists from Hunton with LVL flanges.

web and different dimensions, see Figure 6 and Table 1. All tested I-joists had a total depth of 200 mm. The moisture content was measured for all I-joists using a calibrated moisture meter and varied from 11.7% to 13.3%. Two different I-joist products were used as the charring of wood can vary with the wood species, density, moisture or type of engineered timber used in the flange [6].

Four different insulation products were used; Hunton Nativo® Wood Fibre insulation, batt (Hunton batt, wood fibre batt), Hunton Nativo® Wood Fibre insulation, loose-fill (Hunton LF, wood fibre LF), CBI Isocell Evolution insulation of cellulose fibre, loose-fill (Isocell LF, cellulose LF) and Kingspan Kooltherm K12 insulation of thermoset phenolic, batt (phenolic foam batt). See Table 2 for description of the insulation products. The products are produced according to the relevant product standards [30–32].

The wood fibre batts were cut to match the profiles of the I-joists to get an optimised fit. The insulation was cut with a slight overshoot of 15–20 mm to increase the likelihood of the insulation staying in place after the gypsum board fall-off. Due to less elasticity of the phenolic insulation, it was cut to exactly fit the flange-to-flange distance without a profile. The small space between the web and the insulation batts was filled with pieces of phenolic batts as tight as possible. The loose-fill insulation cellulose LF was blown in, while the wood fibre LF was manually packed.

The phenolic insulation consisted of two 100 mm layers. In Tests 1 and 4, the wood fibre batts were 200 mm thick but had to be cut in half (ca. 100 mm) to be installed. In Test 5, 2 × 100 mm thick batts were used.

Except for the blown-in loose-fill insulation, all insulation products were conditioned inside the test hall (ca. 22°C) at least 24 h before installation in the test frame and testing.

2.1.3. Instrumentation The specimens were instrumented with several thermocouples (TC) to measure the temperature development in the assemblies, I-joists and
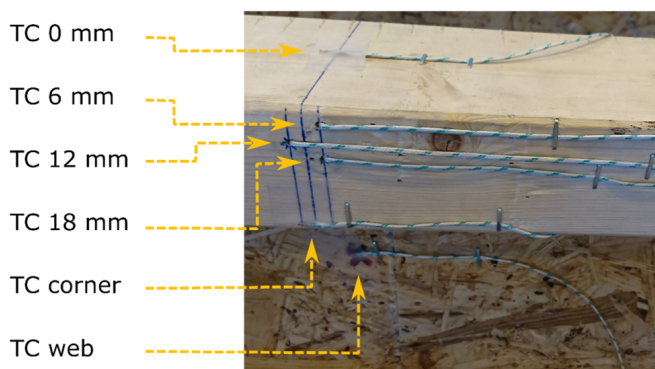
Figure 7.   The bottom flanges of the I-joists (fire-exposed side) are instrumented by eight TCs, where six of them are shown in the image. View from the fire exposed side.

insulations. All TCs were of type K (Chromel and Alumel conductors [33]), with an exposed twisted junction of ca. 1.5 mm. Each I-joist was instrumented with eight TCs, see Figures 3 and 7. Four TCs were used to measure the temperature at 0 mm, 6 mm, 12 mm and 18 mm into the bottom flange from the fire exposed side. The embedded TCs were inserted into the side of the flange in 2 mm large holes, drilled in a drill press stand. The depth of the holes reached to the centre of the flange width. In addition, the surface temperature on the top corners of the bottom flange and on the web was monitored. The TCs on the web were attached to the surface by staples and was located at a 45° angle from the corner. The TCs on the corner of the flange were positioned at the top corner of the bottom of the flange, i.e., at 40.5 mm and 47 mm depth for Hunton and Masonite I-joists, respectively. The reason why 40.5 mm was used instead of 39 mm was a small deviation between the measured flange height and the height given by the Hunton I-joist datasheet, see Table 1.

Thermocouples were also installed in the centre between the I-joists. One at the intersection between the gypsum board and insulation, one at the centre of the insulation at 100 mm depth into the insulation and one at the intersection between the fibreboard and the insulation.

All TCs were installed at ∼ 350 mm distance from the centre beam and in general, installed to follow the isotherm for at least 50 mm before stretching them from hot to cold temperatures. Stretching them directly from the measurement point to the cold side of the specimen, air gaps around the thermocouples and the thermocouples themselves can lead to errors in the temperature measurements [34–36]. However, in Tests 1–4, the TCs in the centre of the insulation were inserted from the unexposed side of the insulation perpendicular to the predicted isotherms, as no practical method was found to install the TCs parallel to the isotherm. The measurements gave rough indications of temperatures inside the insulation and were only used to support other data. In Test 5, the insulation batts were 2 × 100 mm thick instead of 1 × 200 mm and the TCs were, therefore, installed parallel to the isotherm.

2.1.4. Test Procedure The test specimens were mounted horizontally on top of a furnace. The inner dimension of the furnace was 1560 mm × 1560 mm × 1560 mm. The test specimen was aligned symmetrically above the opening with an exposed area of 1560 mm × 1560 mm. The furnace was heated according to the standard time–temperature curve [8, 9]. The aim was to run the tests as long as possible to collect as much data as possible but without a complete charring of the flanges or the web. The tests were planned to be terminated when both the temperature at the web and the flange corner had reached 300°C. However, due to some unforeseen events, like gypsum board failure, insulation fall-down and large temperature differences between the different I-joist sizes, the termination plan was not perfectly followed.

Termination of the test was executed by first turning off the furnace heaters, then cutting the TC wires, lifting the test specimen by a crane and cooling down the test specimen with water from a fire hose. This process lasted about two minutes.

2.1.5. Determination of Residual Height and Cross-Section When the test specimen had cooled down, a sample (∼ 50 mm wide) was sawn out of each I-joist close to where the TCs were installed. The char layer of each sample was then physically removed with a steel brush. The remaining height of the I-joist was measured on both sides of the cut sample by a calliper, with an accuracy of 0.5 mm.

To determine the remaining cross-section, the outline of the I-joist samples was drawn on a mm-paper. The remaining area was then calculated using a measurement tool in the vector graphic editing software *Inkscape*, using the mm-paper as reference scale. To verify the calculated area, the remaining height was also calculated and compared with the height measured by the calliper. This method was preferred instead of drawing the outline in a software based on an image because the scaling against a reference turned out to be less accurate.

2.2. Determination of Charring Rates

Two different charring rates have been calculated, before and after fall-off of the gypsum board, i.e., for the protected and post-protected phase.

2.2.1. Protected Phase The charring rate in the protected phase was based on a best-fit regression analysis of the time the embedded TCs reached 300°C before fall-off. The obtained charring rate for this phase was named a1.

In Test 1 with phenolic insulation, the fall-off happened early and the time of start charring happened right after this. Therefore, no protected phase was present with phenolic insulation. In Tests 4 and 5, there was a short protected phase, but not long enough for any of the embedded TCs to reach 300°C. Hence, a charring rate for the protected phase for these tests was not found.

2.2.2. Post-protected Phase The charring rate in the post-protected phase was calculated based on two data points, the charring depth at fall-off of the gypsum board and the final charring depth at the end of test, as explained below:

Experimental Study of the Charring of I-Joists and Recession

1. Determination of the charring depth at fall-off of the gypsum board
(a) Fall-off time was defined as the time at which the TC-readings at the non-ex-posed side of the gypsum board made a significant jump and TC readings reached about the same temperature as the furnace.
(b) The charring depth at fall-off time was then predicted based on extrapolation of the calculated charring rate before fall-off of the same test. In Tests 4 and 5, the data were insufficient to calculate a charring rate before fall-off and predict the charring depth at fall-off. The charring rate for the same type of insulation from Test 1 was, therefore, used.

The uncertainty of this method was based on how accurate the calculated charring rate before char fall-off was.

2. Determination of charring depth at the end of the test
(a) The time for the end of the test was set equal to when the furnace burners were turned off.
(b) The charring depth at the end of the test was determined as the difference between the initial height and the measured residual height.

The obtained charring rates for this phase were named a2.

The uncertainty of (2a) was related to the mismatch between the defined end of the test and the actual end of charring. The end of the test was still set to the time when the furnace was turned off due to the following reasons: (I) it would not be possible to determine precisely when charring stopped as there might have been residual heat and smouldering in the insulation, causing charring until the specimen was cooled down with water and (II) after the burners were turned off, the specimen was no longer exposed to the standard time–temperature curve.

The uncertainty of determining the charring depth (2b) was due to some variation in the initial height of the I-joists. A minimum and maximum height was therefore defined for the I-joists, 40/41 mm for Hunton I-joists and 47/47.5 mm for Masonite I-joists. Also, for the measured residual height, for some I-joists there was a slight difference in the measured charring depth of the front and the back side of the I-joist. The difference in initial height and residual height was expressed as a minimum and maximum charring rate for the post-protected phase.

The reason why only two data points were used to find the charring rate after fall-off is explained below:

1. For Tests 1, 2 and 3, the charring front had reached the deepest embedded TC, at 18 mm depth, at the time of fall-off. In other words, there were no more measurements to include for the calculation of the charring rate.
2. For Tests 4 and 5, the fall-off happened before charring reached 18 mm, but the TC readings were after fall-off affected by the direct flame impingement on the wire and could not be used. In Test 5, the charring rate was found by combining the charring depth for the two similar-sized flanges in the same test. The I-joists were positioned in different spaces in the specimen, where the only difference between them was the centre distance between the flanges. Since they

were exposed to direct flames at different times, i.e., different fall-off times of the gypsum board, they were aligned in a graph where the time axis starts at fall-off.

2.2.3. Lateral Charring Lateral charring could not be determined in the same way as charring from the exposed side, as the start of charring along the side happened at different times corresponding to the recession of the insulation on the side. Hence, results on lateral charring in this paper were therefore based on visual inspection of the remaining cross-section area.

2.3. Method to Compare Charring Rates—Experimental Versus Design Methods

Charring rates from the experiments were compared to charring rates determined using the methods given for rectangular cross-sections in Annex C in EN 1995-1-2 [1] and for I-joists in Annex I of prEN 1995-1-2 [26].

According to EN 1995-1-2, the notional charring rate during the protected phase can be determined by Equation 1:

$$\beta_n = k_n \cdot k_s \cdot k_2 \cdot \beta_0 \tag{1}$$

where k_2 is the insulation factor of the gypsum board thickness in mm (h_p) and is given by Equation 2:

$$k_2 = 1.05 - 0.0073 \cdot h_p \tag{2}$$

For a gypsum board thickness of 15.4 mm used in these experiments, k_2 becomes 0.938. β_0 is the one-dimensional charring rate of 0.65 mm/min [1]. k_n converts the actual charring depth ($d_{char,1}$) to a notional charring depth ($d_{char,1,n}$) and converts the residual cross-section to a rectangular shape, as seen in Figure 8. k_s is the
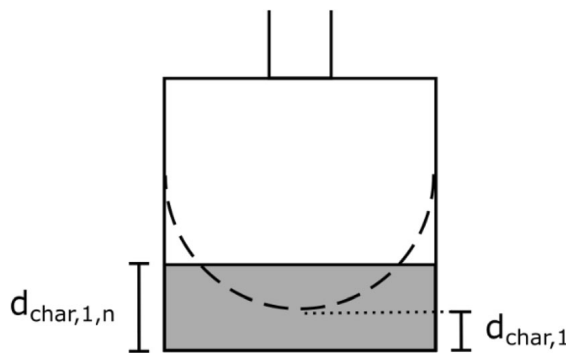
Figure 8. The remaining measured height in the experiment corresponds to the natural charring depth $d_{char,1}$, while the charring depth of the design models corresponds to $d_{char,1,n}$.

cross-section factor to account for different widths of the timber frame member, see Table 4.

The obtained charring rates from the experiments measured the actual charring depth, while the design methods use the notional charring depth. To compare the experimental charring rates with the design methods, the conversion factor for the corner roundings (k_n) is not taken into account (i.e., = 1).

This modified version of the charring rate will be called β_m, as given in Equation 3:

$$\beta_m = k_2 \cdot k_s \cdot \beta_0 \tag{3}$$

In prEN 1995-1-2, the notional charring rate for I-joists in the protected phase can be determined by Equation 4:

$$\beta_n = k_2 \cdot k_{s,n,1} \cdot \beta_0 \tag{4}$$

The factor k_2 is still the insulation factor for the gypsum board, but here calculated by Equation 5:

$$k_2 = 1 - \frac{h_p}{55} \tag{5}$$

For a gypsum board thickness of 15.4 mm, k_2 becomes 0.72. The one-dimensional charring rate $\beta_0 = 0.65$ mm/min [26]. The $k_{s,n,1}$ parameter is a combined conversion (k_n) and section factor (k_s) for the insulation types used in these experiments and gives the notional charring depth (Figure 8). Because we need the actual charring depth, $k_{s,n,1}$ is in this study replaced by k_s, which changes Equation 4 to be similar to Equation 3, but with different parameter values. The k_s parameter was

Table 4
Parameters for Calculation of Charring Rates for the Protected Phase, from EN 1995-1-2:2004 (Current Eurocode 5) [1] and prEN 1995-1-2:2021 (Final Draft of New Eurocode 5) [26]

Method	β_0 [mm/min]	k_n [–]	k_2 [–]	Flange width [mm]	k_s [–]	β_m [mm/min]
EN 1995-1-2	0.65	1	0.938	45	1.3	0.79
				47	1.3	0.67
				≥ 60	1.1	0.67
prEN 1995-1-2			0.72	45	1.49	0.70
				60	1.35	0.63
				90	1.18	0.55
				47	1.47	0.69
				70	1.28	0.60
				97	1.15	0.54

extracted based on the work of Mäger and Just [25] when defining the $k_{s,n,1}$ parameter and is given by Equation 6:

$$k_s = 5.43 \cdot w_f^{-0.34} \tag{6}$$

where w_f is the flange width in mm.

A comparison will reveal how both the existing model in EN 1995-1-2 [1] and the new model in prEN 1995-1-2 [26] could predict the experimental results. Such comparisons are important as they contribute to validate and improve the models.

All parameter values used in the comparison are given in Table 4.

2.4. Determination of Insulation Recession Rate

The insulation recession rate in this study was defined as the rate at which the 300°C isotherm was propagating through the insulation material, similar to the charring rate of wood and similar to other experiments studying the recession of combustible insulations [20, 28].

As the purpose of the insulation in case of fire is to protect the timber members from charring and the charring temperature of wood is approximately 300°C, the recession temperature for the insulation was also defined as 300°C.

TCs used for the determination of the recession rate were located at the interface between the gypsum board and insulation, at the centre of the insulation 100 mm into the insulation and at the upper corners of the bottom flange at depths 40.5 mm and 47 mm into the insulation for Hunton and Masonite I-joists, respectively. Figures 3 and 7 show the position of the TCs. Two different recession rates could, therefore, be calculated for each combination of I-joist type and insulation type: the recession rate at 40.5/47 mm depth and at 100 mm depth.

The recession rates were then found by Equation 7.

$$recession\,rate\,[mm/min] = \frac{distance\ between\ surface\ TC\ and\ embedded\ TC}{time\ to\ reach\ 300°C\ for\ (embedded\ TC - surface\ TC)} \tag{7}$$
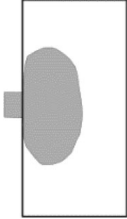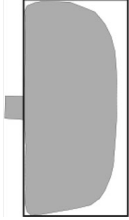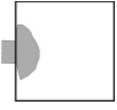
In each test specimen, there was a total of 12 corner-TCs and 8 centre insulation-TCs. The recession rates were calculated as an average of the measured rates to reduce the effect of mounting uncertainty.
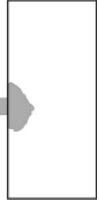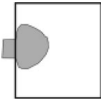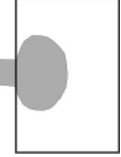
3. Results

3.1. Residual Cross-Section Profiles and Measured Charring Depths

The remaining height, area and cross-section profile of the bottom flanges from all tests are presented in Tables 5 and 6. The measured charring depths for the I-joists as a function of time are presented in Figures 9, 10, 11, 12. The symbols in the figures represent the time when the TCs reached 300°C at different depths into the flanges. The time to reach fall-off of the gypsum board and the end of the tests, are marked with lines in the graphs. For some I-joists, the entire flange was
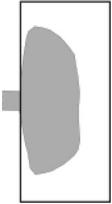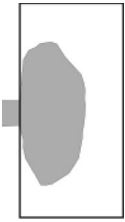
Table 5
Residual Height, Area, and Cross-Section of Flanges of Tests 1, 2 and 3

Test ID	Residual[a] Height min/max [mm]	Area min/max [%][b]	Cross-section (grey colour)	Test ID	Residual[a] Height min/max [mm]	Area min/max [%][b]	Cross-section (grey colour)
Test 1							
T1MaSKb	0.0	0.0		T1MaSHb	37.5/38.5	68.5/69.2	
T1MaMKb	24.5/29.0	23.8/29.0		T1MaMHb	39.0/39.5	71.6/72.4	
T1MaLKb	24.5/25.0	25.0/25.0		T1MaLHb	41.0/41.0	77.0/77.1	
Test 2							
T2HuSClf	0.0	0.0		T2MaSClf	8.5/10.5	6.8/9.2	

Table 5
continued

Test ID	Residual[a]			Test ID	Residual[a]		
	Height min/max [mm]	Area min/max [%][b]	Cross-section (grey colour)		Height min/max [mm]	Area min/max [%][b]	Cross-section (grey colour)
T2HuMClf	0.0	0.0		T2MaMClf	13.5/15.5	14.9/17.6	
T2HuLClf	8.5/10.5	2.3/3.0		T2MaLClf	20.0/21.0	30.8/32.3	
Test 3				T3MaSHlf	0.0	0.0	
T3HuSHlf	15.0/16.5	13.2/13.4		T3MaMHlf	22.0/23.5	19.2/18.5	
T3HuMHlf	19.0/20.0	20.3/22.4					
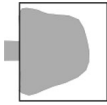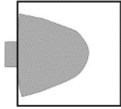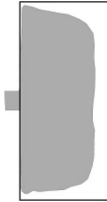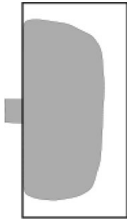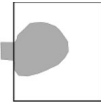
Table 5 continued

Test ID	Residual[a]			Test ID	Residual[a]		
	Height min/max [mm]	Area min/max [%][b]	Cross-section (grey colour)		Height min/max [mm]	Area min/max [%][b]	Cross-section (grey colour)
T3HuLHlf	26.0/27.5	39.2/40.1		T3MaLHlf	27.5/30.0	27.5/32.7	

[a]The minimum and maximum height are measured on both ends of the ~ 50 mm piece cut from the I-joist after the test
[b]Percent of the original area

Table 6
Residual Height, Area, and Cross-Section (grey colour) of Flanges of Tests 4 and 5

Test ID	Height min/max [mm]	Area min/max [%][b]	Cross-section (grey colour)	Test ID	Height min/max [mm]	Area min/max [%][b]	Cross-section (grey colour)
		Residual[a]				Residual[a]	
Test 4							
T4HuSHb	30.0/30.5	54.3/54.6		T4MaSHb	32.5/34.0	45.4/52.6	
T4HuMHb	30.0/30.5	56.7/58.9		T4MaMHb	33.0/34.5	50.3/53.1	
T4HuLHb	32.5/32.5	67.8/70.5		T4MaLHb	35.5/36.0	57.3/57.6	
Test 5							
T5HuSHb	24.5/24.5	24.6/28.0		Not tested			

Table 6
continued

Test ID	Residual[a]			Test ID	Residual[a]		
	Height min/max [mm]	Area min/max [%][b]	Cross-section (grey colour)		Height min/max [mm]	Area min/max [%][b]	Cross-section (grey colour)
T5HuMHb	23.5/24.5	29.8/32.7		T5HuMHbcc60	21.0/21.0	26.1/26.9	
T5HuLHb	25.0/25.5	41.9/45.1		T5HuLHbcc60	22.5/23.5	35.4 38.3	

[a]The minimum and maximum height are measured on both ends of the ~ 50 mm piece cut from the I-joist after the test
[b]Percent of the original area
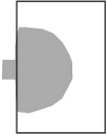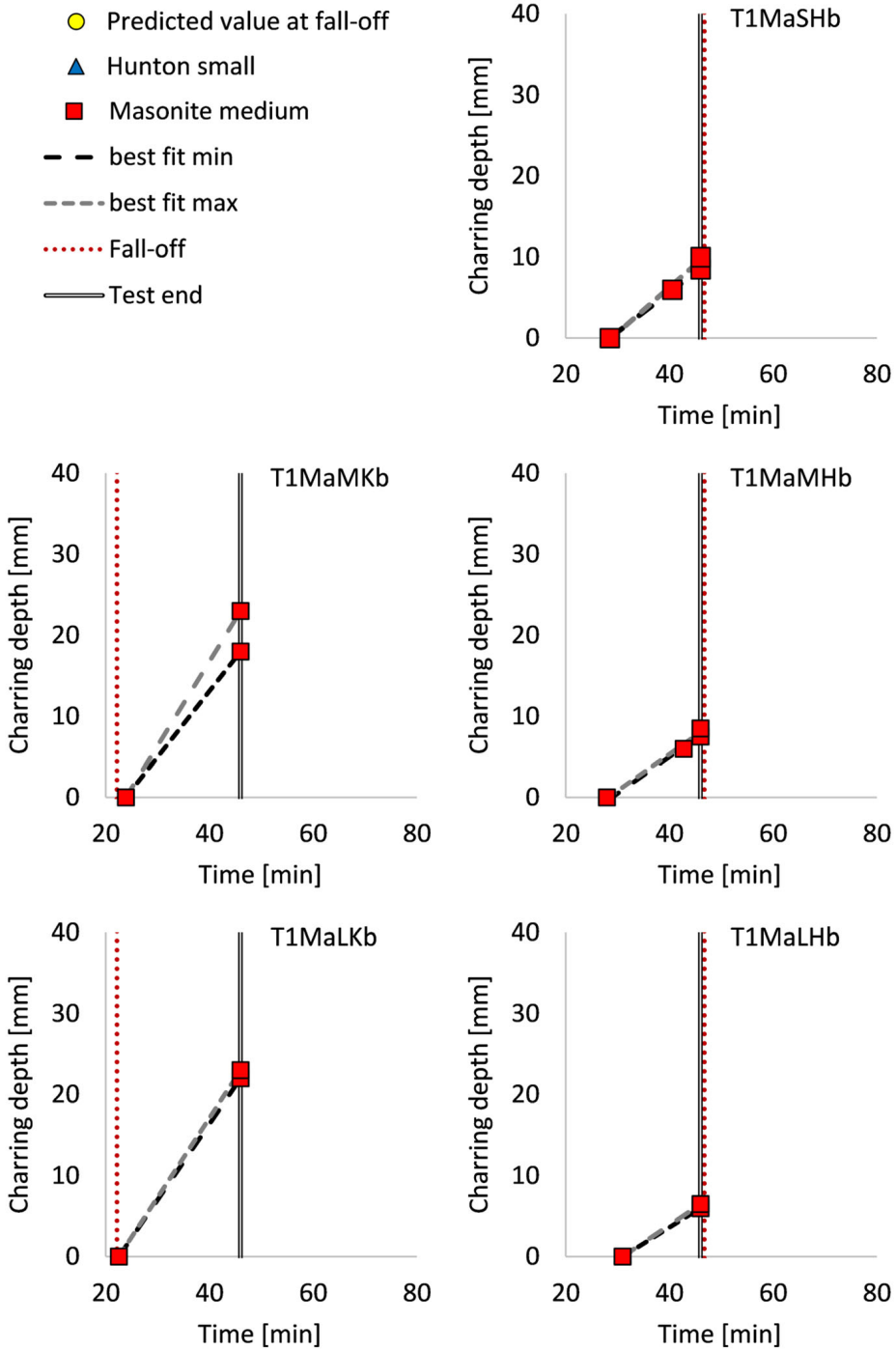
Figure 9. Test 1—Charring of flange from the exposed side.
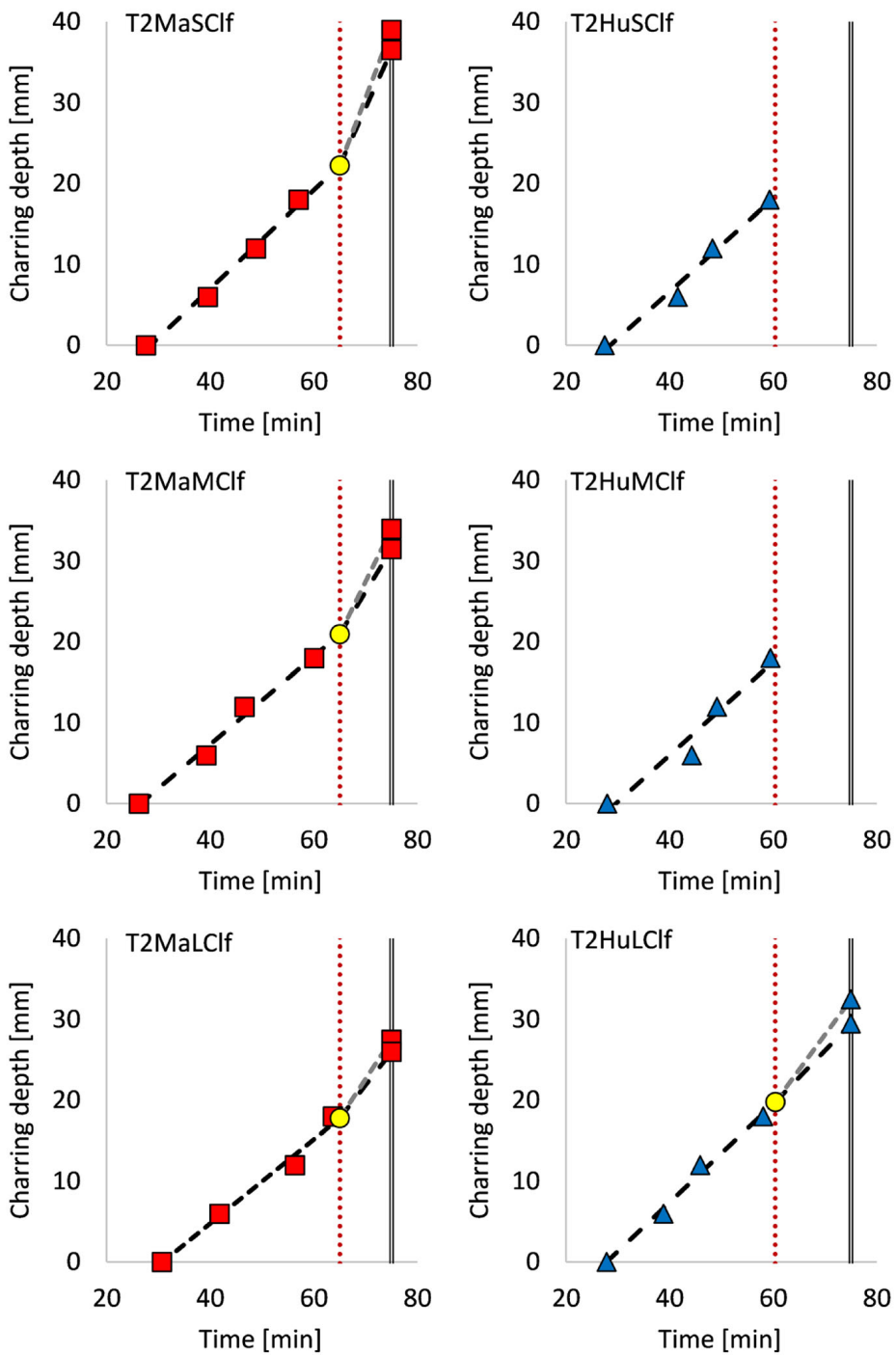
Figure 10. Test 2—Charring of flange from the exposed side.
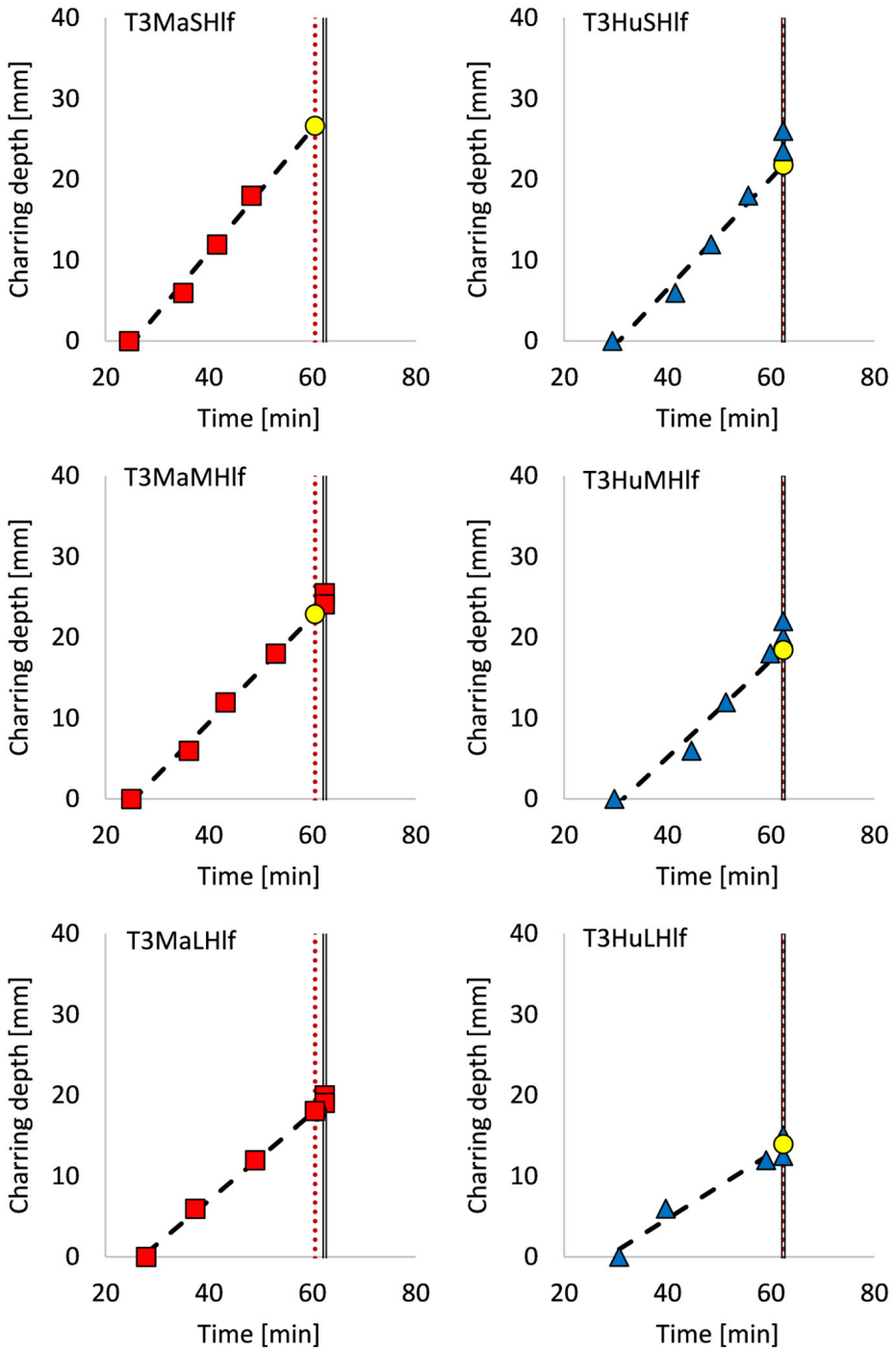
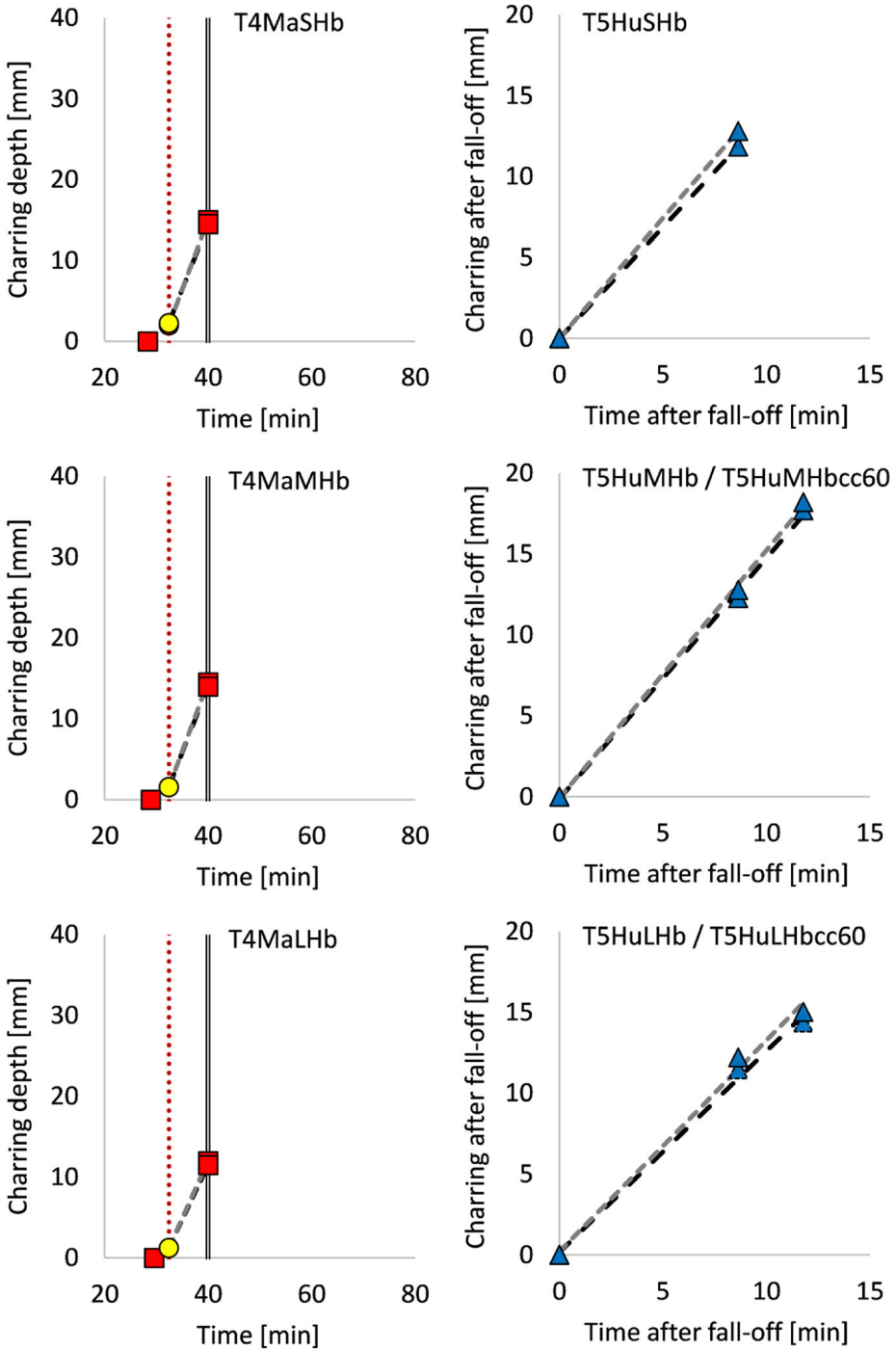**Figure 11. Test 3—Charring of flange from the exposed side.**

Figure 12. **Test 4 (left) and Test 5 (right)—Charring of flange from the exposed side.**

charred through at the end of the test. It is not known precisely at which time the flange was completely charred. The final charring depth for those flanges is, therefore, not included in the figures.

In Figure 13, the reduction of cross-section area influenced by different fall-off times of gypsum plasterboards is shown. In Figure 14, the reduction of cross-section area influenced by insulation fall-down is shown.

3.2. Charring Rates for I-joists

The calculated charring rates are given in Table 7 and are based on the procedure described in Sect. 2.2. The results with Hunton I-joists from Test 4 are not included in the table due to the short duration of the post-protection phase, which caused too large uncertainties in the calculation.

A few of the flanges were totally charred. In test T1MaSKb, the entire flange and about 25 mm of the web were charred. In test T2HuMClf, the entire flange and about 5 mm of the web were charred. For T2HuSCl,f the entire flange was charred, but the web had not been charred. The charring rates for these three tests were calculated based on charring of the full flange height and is set to larger or equal ($\geq$) to the calculated charring rate.

Start of charring on the flanges of the I-joists is given as t_{ch} in Table 7. $a1_{max}$ is the calculated maximum charring rate and $a1_{min}$ is the calculated minimum charring rate in the protected phase. While $a2_{max}$ and $a2_{min}$ are the calculated charring rates in the post-protected phase.

3.3. Comparison of Charring Rates Against Design Methods

A comparison between the experimental charring rates and the calculated values based on EN 1995-1-2 and prEN 1995-1-2 was made. This was performed according to the method in Sect. 2.3.
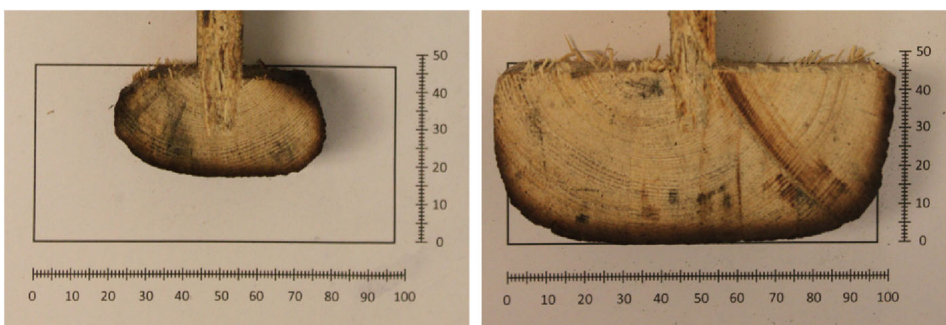

Figure 13. The protective effect given by the gypsum board is shown by comparing two flanges from Test 1, where the left flange experienced a gypsum board fall-off at 22 min, while the right flange was protected by the gypsum board throughout the test (to 45 min). The rectangular shape is the original flange size. Numbers are in mm.
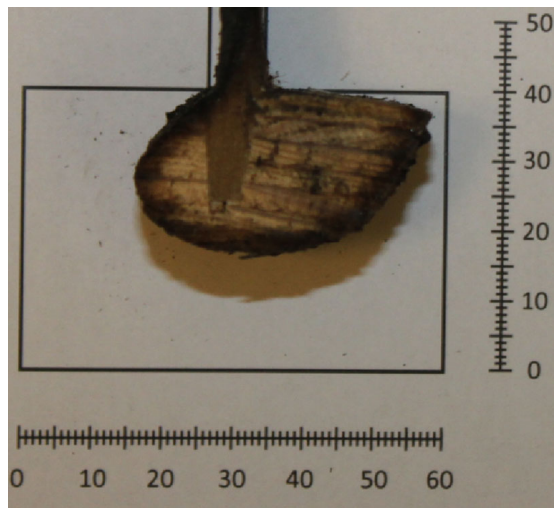
Figure 14.   Example of a medium-sized Hunton flange in Test 5 with a highly irregular shape. The flange experienced insulation fall-down during the test on one side, resulting in the irregular shape. The rectangular shape is the original flange size. Numbers are in mm.

The values of all design parameters and the corresponding charring rates are summarised in Table 4, while the comparison is given in Table 8. Due to the short protected phase of Test 1 with phenolic insulation and Test 4 and 5 with wood fibre batts, it was not possible to calculate a charring rate in the protected phase for those tests. Hence, the table does not include values for those tests.

3.4. Recession Rates for Combustible Insulation

The average time for the 300°C isotherm to reach the TCs in the insulation and on the interface between the insulation and I-joist flange was measured in the tests. Recession rates for the different insulations have been calculated based on the procedure in Sect. 2.4 and are given in Table 9.

In all tests, the TCs at the corners reached 300°C and the recession rate of the insulation next to the flange could therefore be determined. However, in only one test, the centre TCs at 100 mm depth into the insulation reached 300°C. The recession rate for the other tests not reaching 300°C was therefore set to "less than" (<).

The results show that the recession rate was lower, close to the flange, than between two I-joists.

In most tests, the recession rate was obtained for exposure mainly in the protected phase. However, recession of the phenolic batt was only measured in the post-protected phase because the gypsum board fell down early.

The wood fibre batts were used in several tests and the average recession rate at the corner for all tests was 3.3 ± 0.7 mm/min, based on 26 values.

Table 7
Calculated Charring Rates on the Fire Exposed Side of the I-Joists from the Experiments

Test ID	t_{ch} [min]	Gypsum board fall-off [min]	End of test [min]	Protected phase Charring rate $a1_{min}$ [mm/min]	$a1_{max}$	Post-protected phase Charring rate $a2_{min}$ [mm/min]	$a2_{max}$
Test 1							
T1MaSKb	23.7	22.2	45	–	–	≥ 2.13[a]	
T1MaMKb	23.9			–	–	0.81	1.04
T1MaLKb	22.5			–	–	0.94	0.98
T1MaSHb	28.5	46.5		0.49	0.56	–	–
T1MaMHb	28.0			0.45	0.45	–	–
T1MaLHb	31.0			0.40	0.43	–	–
Test 2							
T2HuSClf	27.5	60.4	75	0.58		≥ 1.55[a]	
T2HuMClf	28.0			0.58		≥ 1.59[a]	
T2HuLClf	27.9			0.61		0.67	0.87
T2MaSClf	27.6	65.0		0.61		1.43	1.68
T2MaMClf	26.2			0.54		1.05	1.30
T2MaLClf	30.7			0.52		0.82	0.97
Test 3							
T3HuSHlf	29.4	62.4	62.5	0.69		–	–
T3HuMHlf	29.8			0.60		–	–
T3HuLHlf	30.7			0.40		–	–
T3MaSHlf	24.6	60.5		0.76		–	–
T3MaMHlf	25.0			0.65		0.65	1.39
T3MaLHlf	27.8			0.54		0.54	1.03
Test 4							
T4HuSHb	30.2	38.3	40	–		–	–
T4HuMHb	30.2			–		–	–
T4HuLHb	31.5			–		–	–
T4MaSHb	28.4	32.4		–		1.61	1.72
T4MaMHb	28.9			–		1.64	1.71
T4MaLHb	29.6			–		1.36	1.44
Test 5							
T5HuSHb	30.0	36.5	45	–		1.37	1.49
T5HuMHb + T5HuMHbcc60	27.1	36.5		–		1.49	1.53
	30.5	33.3					
T5HuLHb + T5HuLHbcc60	29.5	36.5		–		1.24	1.31
	28.4	33.3					

[a]The flange was completely charred at the test end
[b]No R^2 value is given when only two data points are present

Table 8
Charring Rates Calculated Based on Results from the Experiments During the Protected Phase Compared to Calculated Charring Rates Based on EN 1995-1-2:2004 (Current Eurocode 5) [1] and prEN 1995-1-2:2021 (Final Draft of the New Eurocode 5) [26]

	Experimental	EN 1995-1-2:2004		prEN 1995-1-2:2021	
Test ID	$a1_{max}$ [mm/min]	β_m [mm/min]	$\beta_m - a1_{max}$ [mm/min]	β_m [mm/min]	$\beta_m - a1_{max}$ [mm/min]
Test 1					
T1MaSHb	0.56	0.79	0.23	0.69	0.13
T1MaMHb	0.45	0.67	0.22	0.60	0.15
T1MaLHb	0.43	0.67	0.24	0.54	0.10
Test 2					
T2HuSClf	0.58	0.79	0.22	0.70	0.12
T2HuMClf	0.58	0.67	0.09	0.63	0.05
T2HuLClf	0.61	0.67	0.06	0.55	− 0.06
T2MaSClf	0.61	0.79	0.18	0.69	0.08
T2MaMClf	0.54	0.67	0.13	0.60	0.05
T2MaLClf	0.52	0.67	0.15	0.54	0.02
Test 3					
T3HuSHlf	0.69	0.79	0.11	0.70	0.01
T3HuMHlf	0.60	0.67	0.07	0.63	0.03
T3HuLHlf	0.40	0.67	0.27	0.55	0.15
T3MaSHlf	0.76	0.79	0.03	0.69	− 0.08
T3MaMHlf	0.65	0.67	0.02	0.60	− 0.06
T3MaLHlf	0.54	0.67	0.13	0.54	0.00

4. Discussion

4.1. Charring of I-Joists

4.1.1. Charring Rates on Fire Exposed Side 4.1.1.1. Protected Phase For the protected phase, a best-fit analysis was used, including several data points ranging over a relatively long time span (up to 38 min) (Table 7). The calculated charring rates of the protected phase are therefore considered to be quite accurate. This is supported by the good linear match of the data points.

Although the Masonite (solid) and Hunton (LVL) I-joists were manufactured with different components, their charring rates were in the same range in comparable tests. The charring rates varied from 0.40–0.76 mm/min to 0.40–0.69 mm/min for Masonite and Hunton I-joists, respectively. In most of the comparable tests, the Hunton I-joists had a slightly lower charring rate than the Masonite I-joists, see Table 7. In general, the charring rate decreased with increasing flange width, which is as expected [1]. The reason being that for wider flanges, less heat from the lateral sides reaches the centre of the flange, where the TCs to monitor charring are located. And the effect of the corner rounding is smaller for wider flanges.

Table 9
Recession Rates for the Different Insulation Products

Test no	Insulation	Recession rate ± std. deviation [mm/min]	Average time to reach 300°C after start charring		Based on (at depth)
			Protected [min]	Post-protected [min]	
1	Wood fibre batt	2.7 ± 0.3	18	0	6 corner TCs (47 mm)
		< 4.9[a]	21	0	4 insulation centre TCs (100 mm)
1	Phenolic foam batt	5.7 ± 2.3	0	9	6 corner TCs (47 mm)
		6.8 ± 1.2	0	15	4 insulation centre TCs (100 mm)
2	Cellulose loose-fill	1.1 ± 0.04	39	3	12 corner TCs (40.5/ 47 mm)
		≤ 2.2[b]	39	12	8 insulation centre TCs (100 mm)
3	Wood fibre loose-fill	2.3 ± 0.5	20	0	12 corner TCs (40.5/ 47 mm)
		4.1 ± 0.7	25	0	8 insulation centre TCs (100 mm)
4	Wood fibre batt	3.6 ± 0.9	11	2	12 corner TCs (40.5/ 47 mm)
		< 7.0[a]	11	5	8 insulation centre TCs (100 mm)
5	Wood fibre batt	3.1 ± 0.4	12	1	10 corner TCs (40.5 mm)
		< 7.9[a]	12	5	7 insulation centre TCs (100 mm)

[a]None of the centre TCs had reached 300°C when the test was ended. The actual recession rate is likely to be slower than the value in the table
[b]Only 2 of 8 centre TCs reached 300°C. 2.2 mm/min was the maximum of those two values

4.1.1.2. Post-protected Phase The charring rates in the post-protected phase ranged from 0.54 mm/min to 1.72 mm/min when excluding the I-joists where the flange was fully charred. This was higher than charring rates in the protected phase, as expected. The charring rates were obtained from only two data points with some related uncertainties (see Sect. 2.2.2). In addition, this phase had a shorter duration. These effects combined imply that there was a higher degree of uncertainty related to the charring rates in the post-protected phase and no comparison is made with the design models.

Although the charring rates have some uncertainties, the maximum charring rate for this phase is believed to be on the conservative side due to the following reasons:

- Measurement uncertainties, e.g., measured remaining height of the flange, were included in the calculation.
- The end of the test was defined as when the furnace burners were shut off since the fire exposure would no longer be according to the standard time–temperature curve. However, the pyrolysis process of the I-joists continued for a short period ($\sim$ 2 min) between the burner shut-off and extinguishment.

The measured charring depth is, therefore, probably a bit larger than it was at the end of the test. The consequence is that the calculated charring rates after fall-off are somewhat higher than the actual rate in the fire test. For the tests where the post-protection phase was short, this effect becomes more prominent.

The design model for I-joists developed by Mäger and Just [24, 25] consists of four phases, where Phases 3 and 4 occur after gypsum board fall-off and Phase 4 is recognised by a reduced slope as the charring layer reaches 25 mm, see Figure 2. In this case, observing such a slope reduction has not been possible for several reasons. To observe the change from Phase 3 to Phase 4, the post-protected phase must be sufficiently long for a 25 mm char layer to be formed and a sufficient number of TCs to measure the charring depth must be present. In this test series, the TCs were either malfunctioned (Test 4 and Test 5) after fall-off, or the deepest embedded TC had already reached 300°C at the time of fall-off. These two effects caused the charring rate of the post-protected phase to be based on the measurements at two charring points only, i.e., the charring depth at fall-off and the final charring depth at the test end. This is described in detail in Sect. 2.2.2. In addition, several flanges were charred less than 25 mm during the whole test.

A learning outcome of these experiments is to use sheathed TCs for future tests, as they can better withstand direct flame exposure to the wire without affecting the TC readings at the junction. Related to this test series, such a change would have provided more data points for the analysis of Test 4 and Test 5, thereby reducing the uncertainty of the charring rate for the post-protected phase. Sheathed TCs would also have allowed for smaller drilled holes which had reduced any convective heat transfer through the holes.

4.1.2. Lateral Charring and Remaining Cross-section Area As seen in Tables 5 and 6, the remaining cross-section of the flanges had the characteristic trapezoid-like shape for short exposures (Test 1 and 4) and a more rounded shape for longer exposures (Test 2 and Test 3). These characteristic shapes were due to the lateral charring, which became more dominant when the insulation degraded as the lateral sides were more and more exposed.

In Test 1 with wood fibre batt insulation and Test 3 with wood fibre LF insulation, several flanges were heavily charred on the lateral side, although there was barely any post-protected phase. This highlights that lateral charring of the flanges of an I-joist should not be neglected in the protected phase. I-joists are vulnerable to charring due to the thin cross-section, while rectangular beams are more resilient. Therefore, even limited charring of the lateral sides of the flanges must be considered. This is a difference compared to charring of rectangular beams, where lateral charring, in general, is not considered in the protected phase [20].

In Test 1, due to the early fall-off of the gypsum board (Table 7), the flanges protected by the phenolic insulation experienced only a post-protected phase. The gypsum board on the other half remained until the end of the test and the flanges protected with wood fibre batt insulation were only exposed in the protected phase. The difference between them was clearly visible (Figure 13). The flanges only experiencing the protected phase were barely charred on the lateral side and charred only 6–9 mm on the fire-exposed side. The flanges only experiencing the post-protected phase were heavily charred from the lateral sides, had more rounded corners and charred approx. 22 mm on the fire-exposed side on the two largest flange sizes.

It is obvious that this difference was related to the tougher thermal exposure for the I-joists and insulation on the phenolic foam side when not protected by the gypsum board. Based on video analysis and TC readings, the insulation was present in both Spaces A and B at the end of the test. This can rule out that insulation fall-down contributed to the difference seen.

Since two different insulation types were used, the recession speed of the two would also contribute to the different char depths. Based on the available data, the recession speed for the wood fibre batt was 2.7 mm/min (protected phase) and 5.7 mm/min (post-protected) for the phenolic foam batt. The latter corresponds to 4.1 mm/min with a conversion to the protected phase (see Sect. 4.2.1), which is about 50% higher than the wood fibre insulation. A different charring would therefore have been expected also with similar heating exposure.

In this test, it is unclear what triggered the early fall-off on one side of the test specimen. However, early fall-off has been related to both the insulation type and the screw distance from the edge of the board [37].

In this test, there was no temperature difference on the back side of the two gypsum boards until 18 min. After this point, the temperature on the side with phenolic foam insulation increased faster than on the other side, probably due to the higher R-value (Table 2). Gypsum board fall-off happened at around 340°C, which was considerably lower than the backside temperature of the other gypsum boards in the other tests. It, therefore, seems unlikely that the gypsum board fell off due to heat alone, but probably with contribution from a crack.

Test 2 had the longest exposure, with a total test time of 75 min. The small and medium flanges of the Hunton I-joists were fully charred, while a small fraction of the large flange was remaining. Compared to the Masonite I-joists of the same test, none of the flanges was fully charred, although these also were heavily charred. The difference in charring between the Hunton and Masonite I-joists can be explained by two reasons: (a) The Hunton I-joists had a 5 min longer post-protected phase. (b) The Hunton flange height was initially 7 mm shorter and the small and medium Hunton flange widths were 2 mm and 10 mm smaller than the Masonite small and medium flange, respectively.

The shorter flange height influences the maximum time a flange can be exposed before it is fully charred from the exposed side. It also influences the time until the lateral side of the flange becomes fully exposed due to insulation recession. As the recession rate of the insulation was about 1.1 mm/min in this test, this means

that the lateral side of the Hunton I-joists became fully exposed about 7 min before the lateral side of the Masonite I-joists.

The reduced flange width influenced the charring in several ways: Firstly, by the time until the flange was fully charred due to lateral charring. Secondly, the smaller width contributed to a faster charring from the exposed side [1]. Thirdly, it affected the time until the flange was charred from three sides, as explained above.

As Test 2 had both a protected and post-protected phase, it was not straightforward to assess how much of the lateral charring that happened in each of the two phases.

When comparing the remaining cross-section area of Masonite I-joists of Test 2 and Test 3, it was seen that the corners of the exposed flanges (marked as "TC corner" in Figure 3) were less rounded in Test 2, although this test had a longer exposure. The reason for this was the particularly low recession rate, 1.1 mm/min, of the cellulose LF insulation in Test 2. In comparison, the recession rate of the wood fibre LF insulation in Test 3 was 2.3 mm/min. In Test 2, the lateral sides of the Masonite flanges were fully exposed due to insulation recession at 69 min on average, while in Test 3, the lateral sides were fully exposed at 43 min on average.

For T3MaSHlf, there was a good linear fit for the data points in the protected phase, see Figure 11. However, the predicted charring depth at fall-off does not correspond with the fact that the flange was fully charred, see Figure 11 and Table 5. Based on the linear prediction, the charring depth of the flange at fall-off should have been about 27 mm, with 20 mm left to be charred. As the post-protected phase only lasted for about two minutes, to get the flange fully charred, the charring rate must have been about 10 mm/min. This is many times higher than typical charring rates in the post-protected phase and is not realistic. Another effect must have been present.

The most likely explanation is related to the effect of the lateral charring. Compared with a similar test, T3HuSHlf, with the same insulation and approximately the same flange size, see Table 5, it is clear that the lateral charring has played a significant role in the protected phase of this test. There were just a few millimetres left on the lateral sides of the flange before the integrated web was reached. As the start of charring occurred earlier for T3MaSHlf and it was exposed to direct flames longer than T3HuSHlf, it is likely that the flange was totally charred due to lateral charring.

In Test 3, the lateral sides of the flange were totally exposed at about 43 min, i.e., no insulation remained covering the originally 47 mm wide flange. To reach complete charring of the flange in this test, the average lateral charring rate must have been larger than 1.2 mm/min, which seems likely.

At the beginning of the charring process, the charring on the exposed and lateral sides can almost be treated as two independent processes. However, as the charring proceeded, the solid volume of the flange decreased. The ability to transport heat away from the charring zone and further into the wood was thereby reduced. This resulted in an increased heat accumulation in the remaining flange with a corresponding increased heat propagation rate through the material. It is likely that the flange at one point reached a critical remaining volume where the charring on the exposed and the lateral side could no longer be treated as inde-

pendent processes. Instead, they must be treated as interdependent processes. The charring rate in this phase was naturally higher than at the beginning of the charring process. The smaller the original flange was, the more prone the flange was to get affected by this effect. The large difference in charring rate between the small and medium-sized flange in test 1 with phenolic batt insulation was likely caused by this effect. This effect should be studied more and possibly added to the design method.

For Test 4, the Masonite I-joists had a smaller remaining cross-section area than the Hunton I-joists. This was likely caused by the duration of the post-protected phase, which was 6 min longer for the Masonite I-joists.

In Test 5, several flanges had a non-symmetrical remaining area, particularly the top corners of the flange (Figure 14). This can be explained by the fact that three of seven insulation batts fell down during the test. However, none of the flanges lost both adjacent insulation batts. The fall-down happened after the lateral side had been fully exposed, so the fall-down did not affect the calculated recession rate of the insulation. However, the fall-down caused the inner side flange, where the web was attached, to be exposed. This caused an increased charring of the upper corner area, as seen in Table 6 and Figure 14.

In several tests, there were large differences in remaining cross-sections between the flange sizes (Table 5). The corner rounding due to charring had a larger effect on the narrow flanges than the wider ones. The height of the residual cross-section was, therefore, smaller. In addition, the wider flanges provided longer protection of the web because it took more time to char through from the lateral sides.

In general, insulation that is adapted to the I-joist profiles protects the web and flange on two sides (lateral and inner side of the flange). Without this insulation, the flange is exposed from three sides (exposed, lateral and inner) and the web becomes directly exposed to fire. Charring from these sides and the web will quickly reduce the load-bearing capacity [38].

As explained in Sect. 2.2, it was not possible to retrieve TC readings throughout the whole test duration from all tests. This resulted in different quality of charring and recession data for the different combinations of I-joists and insulation types. Further work is, therefore, needed to fill the gaps in this study and should also include other insulation types.

4.1.3. Comparison with Calculation Methods The experimental results for the charring rate in the protected phase, see Table 8, were lower than the predicted charring rate of EN 1995-1-2 [1] for rectangular cross-sections. The difference was on average 0.14 ± 0.08 mm/min lower.

The experimental charring rates were also compared with rates calculated based on the proposed new design method for I-joists in prEN 1995-1-2 [26], see Table 8. The experimental charring rate was on average 0.05 ± 0.08 mm/min lower than calculated. The minimum value was 0.15 mm/min lower than the calculated and the maximum value 0.08 mm/min higher. Related to this data set, the charring rates predicted by the new design method in prEN 1995-1-2 were more accurate than the predicted charring rate of the current design method in EN 1995-1-2.

4.2. Recession of Combustible Insulation

4.2.1. Recession Rates Both the wood fibre and cellulose loose-fill insulations degraded slowly, with an average recession rate measured at the corners of the flanges of about 1.1 mm/min (protected phase) and 2.3 mm/min (protected phase), respectively. The wood fibre batt and the phenolic foam had a slightly higher recession rate, with 3.3 mm/min (protected phase) for the wood fibre batt and 5.7 mm/min (post-protected phase) for the phenolic foam batt. See Table 9.

Due to an early fall-off of the gypsum board (Table 7), the phenolic insulation had its whole exposure in the post-protected phase. To compare the recession rate with the other insulation products, which mainly were exposed in the protected phase, one can multiply it with the insulation factor k_2 for the protected phase (see Sect. 2.3). This gives a recession rate of 4.1 mm/min, which is closer to the other values but still higher.

An overview of recession rates for wood fibre, cellulose, glass wool and stone wool is presented in Table 10. Most of them were obtained in the post-protected phase. Therefore, to compare the results to the other values, the recession rate must be divided by a factor of 0.72, the k_2 value for type F gypsum board used in the tests, see Equation 5. Still, with this correction, all the insulation types had a recession rate lower than typical values found for glass wool (5–28 mm/min) [14, 39].

The values of both loose-fill insulations in this test series had about the same recession rate as the value given for stone wool [39]. However, further testing is needed to confirm this.

Regarding wood fibre and cellulose insulation, the recession rates obtained in this test series are in line with the lowest obtained values previously reported [23, 28] (Table 10).

Another reason for the large difference in recession rates might be different shrinking properties of the insulations and the use of rectangular cross-sections and not I-joists, as discussed in Sect. 4.2.2.

Table 10
Overview of Recession Rates for Different Insulation Types

Research	Insulation type	Recession rate	Phase
Winter et al. [28]	Cellulose, loose-fill	1–2 mm/min	Protected
Winter et al. [28]	Cellulose, loose-fill	2–5 mm/min	Post-protected
Tiso and Just [23]	Cellulose, batt	13.4 mm/min	Post-protected
Winter et al. [28]	Wood fibre, batt	2–4 mm/min	Protected
Winter et al. [28]	Wood fibre, batt	4–16 mm/min	Post-protected
Manguse [39]	Stone wool, batt	2.7 mm/min	Mix of protected and post-protected
Just [14]	Glass wool, batt	15–28 mm/min	Post-protected
Manguse [39]	Glass wool, batt	4.6–11.1 mm/min	Post-protected

Further testing is needed to confirm the large variation of recession rates seen for glass wool and the values of both loose-fill insulations, which were lower than observed values for stone wool (Table 10).

In most of the tests performed in our study, the TCs at 100 mm depth in the middle of the insulation did not reach 300°C during the test and the recession rates in those tests could only be set to a "less than" value, based on the test duration. These rates could, therefore, not be compared with the recession rates determined based on the measurements from the TCs on the corner of the flanges.

For the few tests where the TCs in the insulation reached 300°C, the recession rates were higher than those of the same tests measured close to the flanges, see Table 9. This is probably due to the thermal properties of the I-joist compared to the insulation. The heat conduction coefficient of wood is many times higher than for the insulation materials. Hence, in the interface between insulation and I-joist, heat will be transported from the insulation to the flange as a heat sink. This reduces the heating of the insulation close to the flange compared to the bulk part of the insulation.

4.2.2. The Effect of Shrinking on the Recession Rate As discussed in Sect. 4.2.1, the recession rates in this test series were substantially lower than several of the previously reported values for similar insulation types. There are several reasons which could explain this difference. One reason is related to the reported values being measured in the post-protected phase, as discussed in Sect. 4.2.1. This effect, however, does not compensate for the whole difference. Regarding the recession rates of prEN 1995-1-2 [26], these are generic values, meaning that they are the highest measured in a sample, to be on the conservative side.

Another effect may be related to shrinking of the insulation. In general, the shrinking affects the ability of the insulation to protect the wood member in two ways: (a) shrinkage reduces the insulation height and thereby the lateral side of the wood member becomes more exposed, (b) when the insulation shrinks, a small gap between the wood member and the insulation occurs. This small gap allows for a convective heat transfer through this gap. The TCs on the lateral side of the wood member used to evaluate the recession rate are then heated up in correlation with the size of the gap and, thereby, the shrinking properties of the insulation.

Most reported recession rates were obtained in a different test setup, with rectangular members and not I-joists. The recession rate was measured at 100 mm depth, not 40.5 mm/47 mm, as in this test series.

As the insulation degraded past the flanges in all tests before the test was terminated, it was not possible to assess whether a gap had been formed between the flange and the insulation. However, for most of the tests with wood fibre batts, the insulation remained in the cavity after extinguishing and there was no visible gap between the insulation and the web, indicating negligible shrinking. In the tests with wood fibre batt, the batt had been cut larger than the cavity and compressed into the cavity. This compression affected the test result in two ways, the insulation was less prone to fall down and the oversizing compensated for any

shrinking. This is an advantage which may be utilised for compressible insulation types.

For the phenolic batt, the insulation was still in the cavity after the end of the test, although a small gap was observed a few places. However, as the insulation had been cut to match the flange-to-flange distance, this caused a gap between the insulation and the web, which was filled with small pieces of phenolic batt. The small observed gaps may then have been due to displacement of the small insulation pieces. However, the fact that the batts stayed in place after the test indicates little or negligible shrinking.

For the test where the insulation fell down during the extinguishing process (Test 2—cellulose LF), it was possible to locate precisely where the insulation had been due to a distinct division between charred and uncharred wood on the web. This division proves that shrinking had a negligible effect in this test series.

For the wood fibre LF insulation—Test 3, it was not possible to assess the shrinking property as the insulation fell down before the test ended. The recession rate, however, was not affected by this as the insulation had degraded past the flange at the time it fell down.

Another observation which influenced the recession rates was the time until the corner flanges had reached 300°C. This time could vary up to several minutes in the same test with the same flange height and the same insulation and is shown through the standard deviation in Table 9. No trend was seen related to the size of the flange. Instead, this was believed to be directly related to how tight the insulation was fitted to the flange. This explanation also matches the ability of the insulations to be compressed and oversized. The loose-fill insulations and the compressible wood fibre batt had all quite uniform recession rates, i.e., a low standard deviation. The phenolic foam, however, had a large standard deviation and was the only incompressible insulation.

4.2.3. Insulation Fall-Down In general, insulations not fastened to the timber frame are vulnerable to fall-down when the cladding falls off. The loadbearing capacity of floors made of I-joists is particularly vulnerable to insulation fall-down, as floors made of I-joists are likely to fail when the web is burned through, even if the bottom flanges are partly remaining [38].

Regarding the loose-fill insulations, wood fibre LF fell down almost immediately after fall-off of the gypsum board, while the cellulose LF stayed in place until the end of the test, more than 10 min after fall-off of the gypsum board. The different behaviour may have been caused by how the insulations were filled into the cavities, where the cellulose LF was blown-in and the wood fibre LF was manually packed. It is believed that blown-in insulation sticks better together and acts more like a batt than the loose-fill insulation that was manually packed. For future tests, the blown-in method would be recommended for loose-fill insulation types, as it is more realistic and seems to stay better in place.

In Test 4, the wood fibre batts did not fall down during the test. This is believed to be because the batts were cut larger than the cavity opening. The cut profile to match the flange probably also helped keeping them in place. However, in Test 5, three of seven batts fell out during the test. The most probable reason is

that the batts by accident were cut with a less oversize than in the other tests. The fall-down in Test 5 made it hard to compare the effect of the insulation width, 400 mm versus 600 mm. However, the fall-down gave a reminder of the importance of holding the insulation in place, see Figure 14. The flange side with no insulation had a more rounded shape and the remaining cross-section was effectively reduced compared to the flange side with insulation still in place. In addition, the lack of insulation also makes the web exposed to the fire and the I-joist more vulnerable to failure [38].

Most of the insulation products did not fall down during the test and this is likely due to how they were installed, like cut to match the I-joists profile and oversizing the insulation batts. However, such an installation procedure is time-consuming, hard to repeat precisely and most likely will not be followed each time in an actual building. Therefore, precise instruction details and adapted tools for cutting the flange profiles are needed if this oversizing should be implemented in actual installations.

However, the blown-in loose-fill insulation is different. Firstly, it fills the whole cavity without any need for tailor-made insulation batts and is less time-consuming. Secondly, the process is highly repeatable and since the blown-in method must be performed by a certified worker, this ensures that testing in a lab is realistic to how it will be in an actual building.

In this test series, cellulose LF had the lowest recession rate and showed a good ability to stay in place after gypsum board fall-down. This shows that it is possible to protect the I-joists well without time-consuming and less repeatable tailor-made solutions.

4.2.4. Classification of Insulation Products In prEN 1995-1-2 [26], insulations are given a classification, a so-called protection level (PL), due to how they degrade in a furnace test. That setup is similar to the setup used in the current tests but with the following differences:

- Rectangular cross-sections instead of I-joists
- The gypsum board is provoked to fall-off after 45 min by a manual intervention, while in this test series, the fall-off occurred naturally.
- The test is terminated at 60 min, while in this test series, the tests were terminated based on the charring progression in each test.

The determination of PL for an insulation product is then based on the temperature of a TC at 100 mm depth at the intersection between the insulation and the rectangular beam at 45 and 60 min.

As the setup in this test series is not performed according to the test setup in prEN 1995-1-2, the results cannot be used as documentation for the PL level for the tested insulation products.

An adjustment of the test method for determination of the PL level should be considered for insulations used to protect I-joists, as the obtained recession rate is much lower than previously reported values found through the PL test method.

4.3. Effect of Having a Non-loaded Test Specimen

Compared to a real floor, the test specimen in these experiments were not loaded. It is, therefore, relevant to consider what effect the lack of any load had on the charring rate and the recession rate.

One typical behaviour of loaded test specimens is deflections in the structural members when their cross-section is reduced. Deflections might cause increased distance between structural members, which might cause openings of gypsum board joints and cause extra stress to the screws and the boards, which ultimately might fall off or crack.

For a deflection to occur, a significant reduction in the cross-section of the I-joist flanges must be present. In this paper, it is shown that several flanges were heavily charred already in the protected phase, i.e., while the gypsum board was in place. It is, therefore, likely that gypsum board failure would have occurred earlier if the test specimen had been loaded. However, Figures 10, 11 show that the calculated charring rate in the protected phase would not have been much different, although failure of the gypsum board had occurred slightly earlier.

After the failure of the gypsum boards, the increased distance between structural members would increase the probability that insulation falls down. Fall-down of insulation will further enhance the lateral charring, as explained in Sect. 4.2.3. However, the insulation in these tests stayed in general well in place, supported by the profile of the joist. This effect is believed to compensate for a small increased distance between the I-joists in case of a deflection.

Another effect that would have changed the failure time of the gypsum board is if the test specimen had been built with I-joists of one size. As an example, the small flanges in Test 2 and Test 3 had charred more than the screw length at the time of gypsum board failure. In those tests, it is evident that the gypsum board had failed earlier if I-joists with only small flanges were used.

5. Conclusions

The experiments were performed to develop data for improvement of the design methods in EN 1995-1-2.

The results from the experiments show that the charring rates for an I-joist with flanges of solid wood and Laminated Veneer Lumber are comparable.

The charring rates in the protected phase varied between 0.40 mm/min and 0.76 mm/min and the charring rate decreased with increasing flange size.

The charring rate during the post-protected phase varied from 0.54 mm/min to 1.72 mm/min. The uncertainty of the measurements was highest for the post-protected phase.

All charring rates of the I-joists in the protected phase were lower than the calculated values of rectangular cross-sections in EN 1995-1-2:2004. Compared to the new design method for I-joists in the final draft of prEN 1995-1-2:2021, there was a better match between experimental and calculated charring rates and the discrepancies were mainly on the conservative side.

The remaining cross-section area of all I-joist flanges had a trapezoid-like or rounded shape, which is characteristic of lateral charring.

Several flanges were heavily charred on the lateral side, although there was barely any post-protected phase. This highlights that lateral charring of the flanges of an I-joist can be significant in the protected phase.

Overall, the insulation stayed well in place after gypsum board fall-off. In most tests, the insulation was still in its place at the end of the test. This is due to the I-joist profile, which has a positive impact on keeping the insulation in its place. This advantage could be exploited in practical installation of insulation. All four insulation products showed a lower recession rate than typical values reported for glass wool insulation. The difference was more pronounced for the wood fibre and cellulose insulations. The recession rates were at the lower end of previously reported values for these types of insulation. The cellulose loose-fill insulation had the lowest recession rate at 1.1 mm/min, which is lower than any value reported previously for combustible insulations.

The low values found can possibly be explained by a different test setup and negligible shrinking of the insulation. Further, the recession rates in this test series were mainly measured in the protected phase, while reported values are often reported for the post-protected phase.

These tests have provided new knowledge on the topic I-joists and combustible insulations. Due to few repetitions of the experiments, results should be considered as indicative and should be completed with instrumented full-scale loaded tests.

Further research is needed on the following topics: Advanced analysis of the lateral charring, more insulation products to be investigated as evidently there are large differences between them, fall-down time and shrinkage of the insulations as these parameters directly affect the calculated recession rates and verification of test method for determining the protection levels for insulations for assemblies with I-joists.

Acknowledgements

Funding

References

1. EN 1995-1-2:2004/AC:2009 (2004) Brussels, Belgium
2. National Forest Products Association (2018) National design specification for wood construction. A. W. Council, Worthing
3. LaMalva K, Hopkin D (2021) International handbook of structural fire engineering. Springer, Cham
4. Brandon D, Hopkin D, Emberley R, Wade C (2021) Timber structures. In: LaMalva K, Hopkin D (eds) International handbook of structural fire engineering Springer, Cham, pp 235–322
5. CSA O86:14 (R2019) Engineering design in wood, Canada
6. Friquin KL (2011) Material properties and external factors influencing the charring rate of solid wood and glue-laminated timber. Fire Mater 35(5):303
7. M. Klippel, J. Schmid, and A. Frangi, "Fire design of CLT. In: Proceedings of the Joint Conference of COST Actions FP1402 & FP1404 KTH Building Materials, Cross Laminated Timber–a Competitive Wood Product for Visionary and Fire Safe Buildings," in *Proceedings of the Joint Conference of COST Actions FP1402 & FP1404 KTH Building Materials, Cross Laminated Timber–a Competitive Wood Product for Visionary and Fire Safe Buildings*, 2016, pp. 101–122
8. EN 1991-1-2 (2002) Brussels, Belgium
9. ISO 834-1 (1999) Fire-resistance tests—elements of building construction—Part 1: general requirements, ISO
10. Östman B et al (2010) Fire safety in timber buildings—technical guideline for Europe. SP Rep 2010:19
11. AS/NZS 1720.4:2019 (2019) Timber structures—Part 4: Fire resistance of timber elements, Australia/New Zealand
12 Buchanan A, Östman B (2022) Fire safe use of wood in buildings: global design guide, 1st edn. CRC Press, Boca Raton
13. König J, Walleij L (2000) Timber frame assemblies exposed to standard and parametric fires. Part 2: a design model for standard fire exposure. Swedish Institute for Wood Technology Research, Stockholm
14. Just A (2010) Post protection behaviour of wooden wall and floor structures completely filled with glasswool. In 6th International conference on Structures in Fire, SiF Conferences

15. Östman B, König J, Schmid J, Just A (2012) Brandsäkra trähus 3: nordisk-baltisk kunskapsöversikt och vägledning. SP Rep 2012:18
16 Just A, Schmid J (2018) Improved fire design models for Timber Frame Assemblies—Guidance document. COST Action FP1404, Zürich
17. IMARC Group (2022) I-joist market: global industry trends, share, size, growth, opportunity and forecast 2023–2028. International Market Analysis Research and Consulting Group, Brooklyn
18. König J (2006) Fire exposed simply supported wooden I-joists in floor assemblies. SP Rep 2006:44
19 Hidalgo JP, Welch S, Torero JL (2015) Performance criteria for the fire safe use of thermal insulation in buildings. Constr Build Mater 100:285
20. Tiso M (2018) PhD-thesis: The contribution of cavity insulations to the load-bearing capacity of timber frame assemblies exposed to fire. Tallinn University of Technology, Tallinn
21. Tiso M, Just A (2018) Fire protection provided by insulation materials—a new design approach for timber frame assemblies. Struct Eng Int 27(2):231
22 Tiso M, Just A, Mäger KN (2016) Behavior of wooden based insulations at high temperatures. Energy Procedia 96:729
23. Tiso M, Just A (2017) Design criteria for insulation materials applied in timber frame assemblies. J Struct Fire Eng 9(3):252
24 Mäger KN, Tiso M, Just A (2020) Fire design model for timber frame assemblies with rectangular and i-shaped members. International scientific conference on wood & fire safety Springer, Cham
25. Mäger KN, Just A (2019) 52-16-1 Preliminary design model for wooden I-joists in Fire presented at the International Network on Timber Engineering Reserach (INTER) Meeting 52
26. Final draft of prEN 1995-1-2 (2021) Eurocode 5: design of timber structures Part 1–2: general-structural fire design
27. EN 1363-1:2020 (2020) Brussels, Belgium
28. Winter S, Werther N, Hoffmann V, Kammerer E, Rauch M (2019) Standardisierung der brandschutztechnischen Leistungsfähigkeit von Holztafelkonstruktionen mit biogenen Dämmstoffen. Technical University Munich (TUM), Munich
29. EN 520:2004 + A1:2009 (2004) Brussels, Belgium
30. EN 13171:2012 + A1:2015 (2012) Belgium, Brussels
31. EN 15101-1:2013 + A1:2019 (2013) Brussels, Belgium
32. EN 13166:2012 + A2:2016 (2012) Brussels, Belgium
33. IEC 60584-1:2013 (2013) Thermocouples—Part 1: EMF specifications and tolerances, IEC, Brussels
34. Fahrni R, Schmid J, Klippel M, Frangi A. (2018) Correct temperature measurements in fire exposed wood. In Proceedings of the 2018 World conference on timber engineering, World Conference on Timber Engineering (WCTE)
35 Pope I, Hidalgo JP, Hadden RM, Torero JL (2022) A simplified correction method for thermocouple disturbance errors in solids. Int J Therm Sci 172:107324
36. Beck JV (1962) Thermocouple temperature disturbances in low conductivity materials. J Heat Transf 84(2):124
37 Sultan MA (2008) Fire resistance of wood joist floor assemblies. Fire Technol 44(4):383
38. Kodur V, Stein J, Fike R, Tabbador M (2017) Comparative fire performance of traditional lumber and engineered wood joists. J Struct Fire Eng 8(1):2–13
39. Manguse H (2020) Master thesis: charring analysis of wooden I-joists in standard fire. Tallinn University of Technology, Tallinn

Experimental Study of the Charring of I-Joists and Recession

Part III – Appendixes

Appendix A - MATLAB code for 2D temperature map

Matlab code to make 2D temperature plot

This is a complete code to make a 2D temperature plot of a TC pattern

```matlab
clear all
close all
clc

%Import your data, here the data is an Excel-file with Time (min)
% in the first column,and temperature data in the consecutive columns
T = readtable('Test2_CLT.xlsx','ReadRowNames',false,...
    'VariableNamingRule','preserve',ReadVariableNames=true);
C = table2array(T); % converts the table to a matrix without headers

%Set your coordinates for the TC pattern
x1 = 1;
x2 = 3;
x3 = 5;
x4 = 7;
x5 = 9;
x6 = 11.5;
x7 = 14.0;
x8 = 16.5;
x9 = 18.8;


z1 = 0.3;
z2 = 1.1;
z3 = 1.8;
z4 = 2.1;
z5 = 2.4;

% Use linspace to generate evenly spaced values over the range of your
% unevenly sampled data.
xlin = linspace(1,18.8,188);
zlin = linspace(0.3,2.4,21);

% Use meshgrid to generate the plotting grid with the output of linspace.
[X,Z] = meshgrid(xlin,zlin);

%Set up your X, Z coordinates
x = [x1 x2 x3 x4 x5 x6 x7 x8 x9...
    x1 x2 x3 x4 x5 x6 x7 x8 x9 ...
    x1 x2 x3 x4 x5 x6 x7 x8 x9 ...
    x1 x2 x3 x4 x5 x6 x7 x8 x9 ...
    x1 x2 x3 x4 x5 x6 x7 x8 x9 ];

z = [z1 z1 z1 z1 z1 z1 z1 z1 z1 ...
    z2 z2 z2 z2 z2 z2 z2 z2 z2 ...
    z3 z3 z3 z3 z3 z3 z3 z3 z3 ...
    z4 z4 z4 z4 z4 z4 z4 z4 z4 ...
    z5 z5 z5 z5 z5 z5 z5 z5 z5 ];
```

```
%Insert the times you want to plot. Here, the numbers represent row-numbers
% of the excel sheet
TestTimes = [161 191]; %

j=1;%counts the number of figures

%produce a temperature map for each of the chosen times in TestTimes
for m= 1:length(TestTimes)
        k = TestTimes(m); %finds the row-number for this specific time

    % C1 to C9 represent a unique name for each TC tree, while the numbering
    % indicate the height of the TC location for each TC tree
        C1_0_3 = C(k,2);
        C1_1_1 = C(k,3);
        C1_1_8 = C(k,4);
        C1_2_1 = C(k,5);
        C1_2_4 = C(k,6);

        C2_0_3 = C(k,7);
        C2_1_1 = C(k,8);
        C2_1_8 = C(k,9);
        C2_2_1 = C(k,10);
        C2_2_4 = C(k,11);

        C3_0_3 = C(k,12);
        C3_1_1 = C(k,13);
        C3_1_8 = C(k,14);
        C3_2_1 = C(k,15);
        C3_2_4 = C(k,16);

        C4_0_3 = C(k,17);
        C4_1_1 = C(k,18);
        C4_1_8 = C(k,19);
        C4_2_1 = C(k,20);
        C4_2_4 = C(k,21);

        C5_0_3 = C(k,22);
        C5_1_1 = C(k,23);
        C5_1_8 = C(k,24);
        C5_2_1 = C(k,25);
        C5_2_4 = C(k,26);

        C6_0_3 = C(k,27);
        C6_1_1 = C(k,28);
        C6_1_8 = C(k,29);
        C6_2_1 = C(k,30);
        C6_2_4 = C(k,31);

        C7_0_3 = C(k,32);
        C7_1_1 = C(k,33);
        C7_1_8 = C(k,34);
        C7_2_1 = C(k,35);
        C7_2_4 = C(k,36);
```

```matlab
        C8_0_3 = C(k,37);
        C8_1_1 = C(k,38);
        C8_1_8 = C(k,39);
        C8_2_1 = C(k,40);
        C8_2_4 = C(k,41);

        C9_0_3 = C(k,42);
        C9_1_1 = C(k,43);
        C9_1_8 = C(k,44);
        C9_2_1 = C(k,45);
        C9_2_4 = C(k,46);

TC = [C1_0_3 C2_0_3 C3_0_3 C4_0_3 C5_0_3 C6_0_3 C7_0_3 C8_0_3 C9_0_3 ...
      C1_1_1 C2_1_1 C3_1_1 C4_1_1 C5_1_1 C6_1_1 C7_1_1 C8_1_1 C9_1_1 ...
      C1_1_8 C2_1_8 C3_1_8 C4_1_8 C5_1_8 C6_1_8 C7_1_8 C8_1_8 C9_1_8...
      C1_2_1 C2_2_1 C3_2_1 C4_2_1 C5_2_1 C6_2_1 C7_2_1 C8_2_1 C9_2_1 ...
      C1_2_4 C2_2_4 C3_2_4 C4_2_4 C5_2_4 C6_2_4 C7_2_4 C8_2_4 C9_2_4 ];

        % x, z and TC are now row-vectors, need to be transposed in the
        % scatteredInterpolant, i.e. x.' transpose x etc.

        %The TC data are interpolated before the contourplot is made
            f = scatteredInterpolant(x.',z.',TC.','linear','linear');
            %
            TC2 = f(X,Z); %TC2 now contains the interpolated values

            sz=10; % size of scatter plot points
            fsz = 12; % font size in plots

        figure
        [A1,B1] = contourf(X,Z,TC2,'ShowText','on'); %produce the temperature
map as a contour plot
        hold on


            % the temperature contours that should be marked
            v =[100,200,300,400, 500,600, 700,800, 900,1000, 1100,1200];
            clabel(A1,B1,v,'FontSize',11); %font size of label

         colormap jet %chooses the colormap color
         caxis([0 1200]) %sets the colorbar limits
         colorbar('Ticks',[0, 200, 400, 600,800, 1000, 1200],...
             'TickLabels',[0, 200, 400, 600,800, 1000, 1200])

        %Finding the minutes and seconds to be displayed as mm:ss
                seconds_total= round(C(k,1)*60,0);
                seconds = mod(seconds_total,60);
                minutes = (seconds_total-seconds)/60;

    if seconds <10 %adding a 0 after the seconds

        if minutes <10 %adding a 0 before the minute
            title(strcat('Time [mm:ss] = ',num2str(0),num2str(minutes),...
                ':',num2str(seconds),num2str(0)))
```

```matlab
        else
            title(strcat('Time [mm:ss] = ',num2str(minutes),...
                ':',num2str(seconds),num2str(0)))
        end
    else
        if minutes <10
            title(strcat('Time [mm:ss] = ',num2str(0),num2str(minutes),...
                ':',num2str(seconds)))
        else
            title(strcat('Time [mm:ss] = ',num2str(minutes),...
                ':',num2str(seconds)))
        end
    end


scatter(x,z,sz,'filled','black') % add black dots for each TC position

xlim([0 18.9]) % X-axis range
ylim([0 2.5]) % Y-axis range
ytickformat('%.1f') % one digit after comma for numbers on the Y-axis
ylabel('height [m]')
xlabel('x-distance [m]')

   %figure dimension in cm
 x0 = 10; %distance from left display edge to inner left edge
 y0 = 10;
 width =30; %distance between inner edges of the figure
 height = 6.4; %distance between top an bottom inner edges of the window

 %set the dimension of the figure
 set(gcf,'units','centimeters','innerposition',[x0,y0,width,height])
 % set the font size and the color of the X and Y axis
 set(gca,'FontSize',fsz, 'XColor',[0 0 0],'YColor',[0 0 0])

%****** WOOD CRIB **************************************************
% for easier visualisation a wood crib could be added to the plot

%first layer of crib
    CRIB_x1 = 1.1;
    CRIB_x2 = 18.2;
    CRIB_y1 = 0.09;
    CRIB_y2 = 0.18;

    CRIB_X = [CRIB_x1,CRIB_x2, CRIB_x2, CRIB_x1, CRIB_x1];
    CRIB_Y = [CRIB_y1,CRIB_y1, CRIB_y2, CRIB_y2, CRIB_y1];
    fill (CRIB_X, CRIB_Y, [0.8500 0.3250 0.0980],...
        'Edgecolor','k', 'LineWidth',0.6)

    %second layer of crib
    for w = 1:2:122
        CRIB_x1 = 1.1 +(w-1)*0.14;
        CRIB_x2 = 1.1 + w*0.14;
        CRIB_y1 = 0.0;
        CRIB_y2 = 0.09;
```

```
        CRIB_X = [CRIB_x1,CRIB_x2, CRIB_x2, CRIB_x1, CRIB_x1];
        CRIB_Y = [CRIB_y1,CRIB_y1, CRIB_y2, CRIB_y2, CRIB_y1];
        fill (CRIB_X, CRIB_Y, [0.8500 0.3250 0.0980],...
            'Edgecolor','k', 'LineWidth',0.6)
    end

    %third layer of crib
    for w = 1:2:122
        CRIB_x1 = 1.1 +(w-1)*0.14;
        CRIB_x2 = 1.1 + w*0.14;
        CRIB_y1 = 0.18;
        CRIB_y2 = 0.27;

        CRIB_X = [CRIB_x1,CRIB_x2, CRIB_x2, CRIB_x1, CRIB_x1];
        CRIB_Y = [CRIB_y1,CRIB_y1, CRIB_y2, CRIB_y2, CRIB_y1];
        fill (CRIB_X, CRIB_Y, [0.8500 0.3250 0.0980],...
            'Edgecolor','k', 'LineWidth',0.6)
    end

    %***** SAVE FIGURES
 *************************************************************

    %Tiff
    print(strcat('TIFF/Test2_XZ',num2str(minutes),'_',num2str(seconds)),...
        '-dtiff','-r600')
  %png
    figsaver_CLT(strcat('PNG/Test2_XZ_CLT',num2str(minutes),...
        '_',num2str(seconds)))

    j=j+1; %updates number of plots
end
```
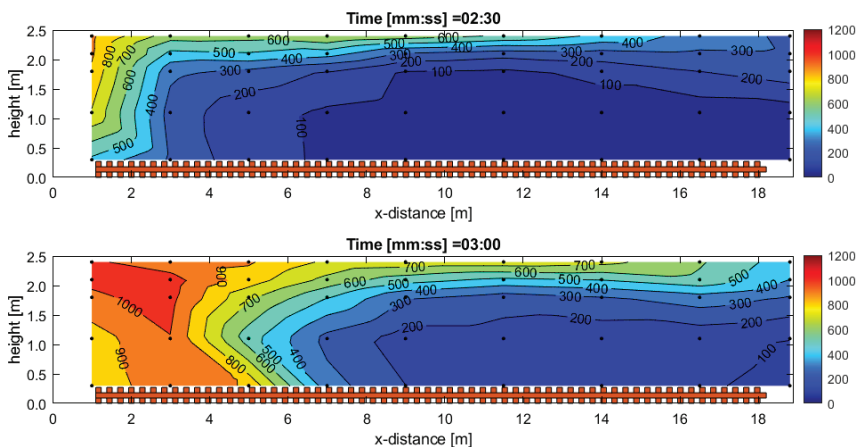

Published with MATLAB® R2021b

NTNU

Norwegian University of
Science and Technology